Proceedings of the First International Conference on Flavor Physics and CP Violation

May 16-18, 2002

University of Pennsylvania, Philadelphia

Editor
R. G. C. Oldeman

Organized by the University of Pennsylvania

Foreword

The First International Symposium on Flavor Physics and CP Violation was held on the University of Pennsylvania campus on May 16–18, 2002.

This conference is a merging of two physics conferences, the Heavy Flavor Physics Conference, most recently held at Caltech (David Hitlin, Caltech, 9th conference) and begun at Heidelberg (Klaus Schubert, Dresden) with the biannual International Conference on B Physics and CP Violation, most recently held at Ise, Japan (A.I. (Tony) Sanda, Nagoya, BCP4) and begun at Nagoya (A.I. (Tony) Sanda). The new conference will be called Flavor Physics and CP Violation (FPCP). The second in the series will be held in 2003 and will be located in Paris.

Conference Organization

International Organizing Committee

A. Ali	(Desy)	J. Appel	(Fermilab)
G. Bonneaud	(Ecole Polytechnique)	A. Buras	(Munich)
P. Dornan	(Imperial College)	H. Evans	(Columbia)
F. Gilman	(Carnegie-Mellon)	M. Giorgi	(Pisa)
B. Grinstein	(UC San Diego)	M. Gronau	(Technion)
D. Hitlin	(Caltech)	G. Hou	(Taiwan)
C. Jarlskog	(Stockholm)	D. London	(Montreal)
T. Nakada	(CERN/Lausanne)	S. Olsen	(Hawaii)
R. Patterson	(Cornell)	K. Pitts	(Illinois)
H. Quinn	(SLAC)	J. Rosner	(Chicago)
A. I. Sanda	(Nagoya)	K. Schubert	(Dresden)
M. Shapiro	(Berkeley)	S. Stone	(Syracuse)
H. Sugawara	(KEK)	F. Takasaki	(KEK)

Local Organizing Committee

L. D. Gladney	(Penn)	D. Marlow	(Princeton)
J. Kroll	(Penn)	A.J.S. Smith	(Princeton)
P. Langacker	(Penn)	M. Strassler	(Penn)
N. S. Lockyer	(Penn)	H. H. Williams	(Penn)

CONTENTS

Recent Results in Theories of Hadronic B decay

Experimental Results from the Tevatron and LEP

Cosmology

New Ideas About CP in B Decays and CKM Determination

Recent Hot Results from B Factories

Charm Physics I

Future Experiments in Heavy Flavor Physics

Neutrino and Kaon Physics

Theoretical Developments in V_{cb} and V_{ub}

B Decays

Radiative B Decays

Charm Physics II

May 16, session 1.

Session Chair: S. Smith

Conference Introduction

Opening address

K.R. Schubert

Present status of CKM parameters

The CKM Matrix in the Era of the B Factories

A. Höcker

Indirect CP violation

Measurement of CP-Violating Asymmetry $\sin 2\beta$ with the *BABAR* Detector

Sh. Rahatlou

$\sin 2\phi_1$ with 45 Million $B\overline{B}$ Pairs at Belle

M. Hazumi

New Physics in $B \to J/\psi K^*$

R. Sinha

New Physics Effects in $B \to J/\Psi K$

T. Mannel

Opening Address

Klaus R. Schubert
Technische Universität Dresden
D-01062 Dresden, Germany

One Conference less is better than one Conference more. So, the decision last September to combine two series of Conferences with very similar scope was not too difficult. The two roots of this combination are the International Symposia on Heavy Flavour Physics, with HF9 last year, and the Conferences on B Meson Physics and CP violation with BCP4 also last year.

The Heavy Flavour Series included CP Violation from the beginning, the first Symposium took place in 1986 at Heidelberg. The idea was born in a ski lift at the Rencontres de Moriond when Berthold Stech and me went uphill together. Before we skied down again, we agreed to organize a Symposium on c, b, and t quarks, τ leptons, and CP violation in the Kaon system. This was one of about 50 symposia in Sciences and Letters for celebrating the 600th Anniversary of Heidelberg University. We had about 100 participants, among them half the ARGUS group, Klaus Wille – who presented his first design for a B Meson Factory –, and Freddy Fridman and Elliot Bloom who wanted to organize a follow-up 1987 in California.

In this second Symposium, at Stanford University, ARGUS had to defend the $B^0\overline{B}^0$ mixing discovery against attacks from CLEO, that was fun. Because of its clear focus on flavour physics, production mechanisms as well as decays, we decided at Stanford to continue in a bi-annual sequence, and Karl Berkelman offered to organize number 3 in 1989 at Cornell. The next Symposia were in 1991 at Orsay, organized by Michel Davier, then the 5th in 1993 at McGill Montreal, run by David MacFarlane, the 6th in 1995 at Pisa, organized by Marcello Giorgi, the 7th in 1997 at Santa Barbara with Mike Witherell as host, the 8th in 1999 organized by Chris Sachrajda at Southampton, where BABAR showed its first result, a scan over the $\Upsilon(4S)$ resonance, and finally HF9 last September at Caltech organized by David Hitlin.

Speaking for all nine previous hosts, organizing committees and participants, I would like to wish good luck for the marriage of the two series and fruitful continuation of discussing, attacking, and defending results in our field of Flavour Physics.

Especially best wishes for our meeting here! I like very much that it takes place in the city of Benjamin Franklin who started here, after a successful career as printer, editor, and writer at the age of 37 with his experiments and models on electricity. Three years later he was a "full time electrician" and had found that there are two types of sparks, he called them male and female fires, later positive and negative fire, electric fire, electric matter. He also formulated charge conservation, but here I better stop. Charge is still conserved, Franklin was right. It's a great place for our Conference, we thank Nigel Lockyer for bringing us here and wish him and us best success.

The CKM Matrix in the Era of the B Factories

Andreas Höcker
Laboratoire de l'Accélérateur Linéaire
IN2P3-CNRS et Université de Paris-Sud
BP 34
F-91898 Orsay Cedex, France

1 Introduction

Until the establishment of *CP* violation (CPV) in the B sector by *BABAR* [1] and Belle [2] in Summer 2001, global CKM analyses [9] primarily attempted to predict yet unmeasured observables like, *e.g.*, the three angles of the unitary triangle of the B sector. Indeed, as pointed out by Bigi [3]: "in '98 courageous souls predicted $\sin 2\beta \sim 0.73 \pm 0.06$ [4]", which turned out to be in excellent agreement with the direct measurement (the present world average reads $\sin 2\beta = 0.78 \pm 0.08$ [5]). Since then more and more measurements of *CP* asymmetries and rare decays emerge from the breathlessly operating B factories. They qualify us to significantly probe the Standard Model (SM) and to search for contributions from new physics. Obviously, predictions are still valuable in the sectors of rare K and B decays in order to assess the necessary sensitivities experiments have to provide in order to perform meaningful measurements. Both goals require a robust and sufficiently conservative approach to accommodate a global fit of observables the theoretical predictions of which are often dominated by hardly accountable systematic uncertainties of theoretical origin.

2 *CP* Violation in the Standard Model

In the Standard Model of three quark generations, CPV is generated by a single phase in the unitary CKM matrix [8], governing flavor changing charged currents. Throughout this review, the Wolfenstein parameterization [10] of the CKM matrix is used. It expands the matrix elements in terms of powers of $\lambda = V_{us} \sim 0.2$ so that one finds for the diagonal elements $|V_{ud}| \sim |V_{cs}| \sim |V_{tb}| \sim 1$, and for the off-diagonal elements $|V_{us}| \sim |V_{cd}| \sim \lambda$, $|V_{cb}| \sim |V_{ts}| \sim \lambda^2$, $|V_{ub}| \sim |V_{td}| \sim \lambda^3$. The CKM phase is given by $\tan^{-1}(\overline{\eta}/\overline{\rho})$, with $\overline{\rho}(\overline{\eta}) = \rho(\eta)(1 - \lambda^2/2)$ [11] so that one can elegantly display the available constraints in the complex $\overline{\rho} - \overline{\eta}$ plane, representing the (rescaled) *Unitarity Triangle* (UT):

$$\frac{V_{ud}V_{ub}^*}{V_{cd}V_{cb}^*} + 1 + \frac{V_{td}V_{tb}^*}{V_{cd}V_{cb}^*} = 0 \; . \tag{1}$$

It is interesting to note that multiplying the $\overline{\rho} - \overline{\eta}$ plane by a phase, rotates the UT while leaving its surface invariant. Hence, the surface of the UT represents a phase-convention invariant quantity which measures CPV. A more general form of this has been given by C. Jarlskog [12]:

$$\mathrm{Im}\left[V_{ij}V_{kl}V_{il}^{*}V_{kj}^{*}\right] = J\sum_{m,n=1}^{3}\epsilon_{ikm}\epsilon_{jln}\ , \tag{2}$$

(with ϵ_{ikm} being the total antisymmetric tensor) corresponding to twice the (*non-rescaled*) UT (1). The empirical value of J is small compared to its geometrical maximum of $1/(6\sqrt{3}) \simeq 0.1$, showing that CP violation is suppressed as a consequence of the strong hierarchy exhibited by the CKM matrix elements. It is the remarkable outcome of the derivation of J, involving the commutator of the up-type and down-type unitary mass matrices, that CPV requires not only J to be non-zero, but also the existence of a non-degenerated mass hierarchy. Equal masses between at least two generations of up-type or down-type quarks would remove the CKM phase.

Over-determining the CKM phase with the ambition to discover new physics represents the primary motivation to study B decays in the era of the B factories. Direct or indirect constraints on the CKM phase are collected from the following sources:

- CPV in the B and the K systems. Studied are three types: (i), CPV in interference of decays with and without mixing, (ii), CPV in mixing and (iii), CPV in the interference between decay amplitudes (often called *direct* CPV).

- $B_d^0\overline{B}_d^0$ and $B_s^0\overline{B}_s^0$ mixing.

- direct determination of the matrix element $|V_{ub}|$ (and $|V_{cb}|$) by means of exclusive and inclusive rate measurements.

- detection of rare K and B decays.

A graphical compilation of the most relevant present and future constraints, sensitive to the *CP*-violating phase, is displayed in Fig. 1. The UT (1) is indicated by the hatched area. Its three angles α, β and γ (or, in the trigonometric order: $\phi_1 \equiv \beta$, $\phi_2 \equiv \alpha$, $\phi_3 \equiv \gamma$) and two non-trivial sides are determined by the processes described above. More precisely, the sides and the angle γ are measured by tree level processes, while α and β are determined from loop induced processes. Only the latter are believed to be sensitive to new physics so that the comparison with the former effectively probes the SM.

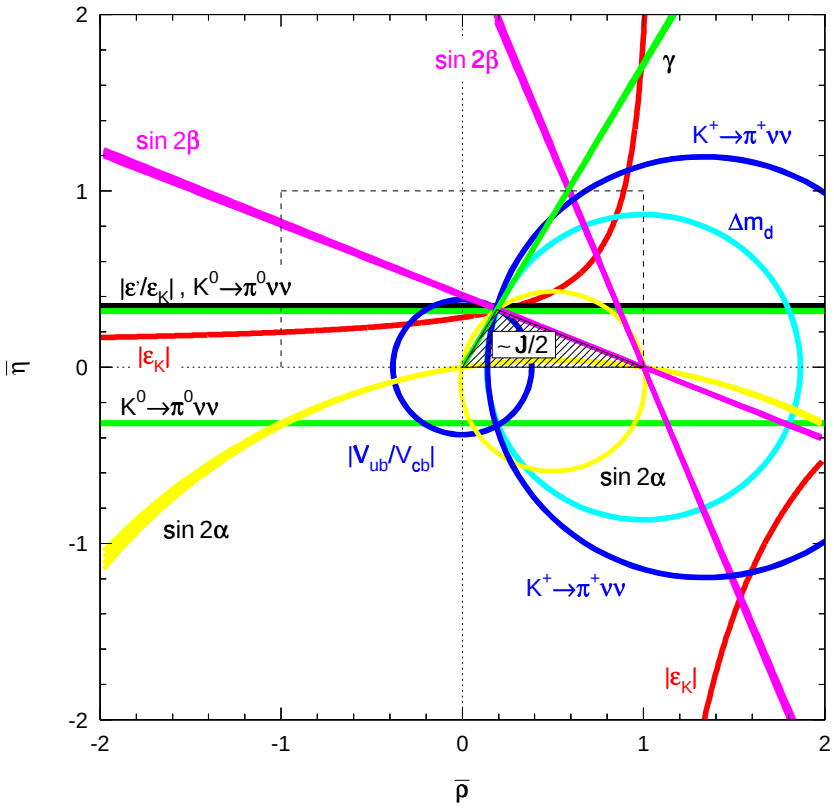

Figure 1: What is the value of J in our world? Constraints in the $\overline{\rho} - \overline{\eta}$ plane for the most relevant observables. The theoretical parameters used correspond to some "standard" set chosen to reproduce compatibility. The unitarity triangle on which we concentrate in the following for the global fit is indicated by the hatched area. It's surface is proportional to the Jarlskog parameter J (*c.f.*, Eq. (2)).

3 The Standard CKM Analysis

Table 1 represents an attempt to categorize the abundance of the constraints that can be (or will in the near future be) used in a global CKM determination[1]. The "star" system qualifies mainly the concern of theoretical uncertainties in the SM prediction of a given observable. At present, the only measurements to which three stars shall be attributed are the determination of λ from rates of $u \to d$ and $u \to s$

[1]The most promising measurements on B_s decays that will be performed at the hadron colliders TEVATRON and LHC are not yet taken into account.

Observables	CKM Parameters	Experimental Sources	Theoretical Uncertainties	Quality
$\lvert V_{ud}\rvert$	λ	nuclear β decay	small	$\star\star\star$
$\lvert V_{us}\rvert$		$K \to \pi e \nu_e$		
ϵ_K	$\overline{\eta} \propto (1-\overline{\rho})^{-1}$	$K^0 \to \pi^+\pi^-,\ \pi^0\pi^0$	B_K, η_{cc}	$\star$
ϵ'/ϵ_K	$\overline{\eta}$	$K^0 \to \pi^+\pi^-,\ \pi^0\pi^0$	B_6, B_8	?
$\mathrm{Im}^2[V_{ts}^* V_{td} \ldots]$	$(\lambda^2 A)^4 \overline{\eta}^2$	$K_L^0 \to \pi^0 \nu\overline{\nu}$	small [but: $\propto (\lambda^2 A)^4$]	$\star\star\,(\star)$
$\lvert V_{td}\rvert$	$(1-\overline{\rho})^2 + \overline{\eta}^2$	$K^+ \to \pi^+ \nu\overline{\nu}$	charm loop, [$\propto (\lambda^2 A)^4$]	$\star\,(\star)$
Δm_d ($\lvert V_{td}\rvert$)	$(1-\overline{\rho})^2 + \overline{\eta}^2$	$B_d^0\overline{B}_d^0$ mixing	$f_{B_d}\sqrt{B_d}$	$\star$
Δm_s ($\lvert V_{ts}\rvert$, ξ)	A	$B_s^0\overline{B}_s^0$ mixing	$\xi = f_{B_s}\sqrt{B_s}/f_{B_d}\sqrt{B_d}$	$\star\star$
$\sin 2\beta$	$\overline{\rho}$, $\overline{\eta}$	$(\overline{b}d) \to (\overline{c}c,\ \overline{s}s)(\overline{s}d)$	small	$\star\star\star$
$\sin 2\alpha$	$\overline{\rho}$, $\overline{\eta}$	$(\overline{b}d) \to (u\overline{d})(\overline{u}d)$	penguins	?
γ	$\overline{\rho}$, $\overline{\eta}$	$B \to DK$	small (statistics?)	$\star\star$
		$b \to u$, direct CPV	penguins	?
$\lvert V_{cb}\rvert$	A	$b \to c\ell\nu$ (excl./incl.)	$F_{D^*}(1)$/OPE	$\star\star$
$\lvert V_{ub}\rvert$	$\overline{\rho}^2 + \overline{\eta}^2$	$b \to u\ell\nu$ (excl./incl.)	model/OPE	$\star\star$
$\lvert V_{td}\rvert$	$(1-\overline{\rho})^2 + \overline{\eta}^2$	$B_d \to \rho\gamma$	model	?
$\lvert V_{ts}\rvert$	A (new phys.)	$B_d \to X_s(\mathrm{or}: K^{(*)})\gamma$	model	?
		$B_d \to K^{(*)}\ell^+\ell^-$ (FCNC)		
$\lvert V_{ub}\rvert$ (f_{B_d})	$\overline{\rho}^2 + \overline{\eta}^2$	$B^+ \to \tau^+\nu_\tau$	f_{B_d}	$\star\star$

Table 1: Observables sensitive to the CKM matrix elements.

transitions[2], and the prominent $\sin 2\beta$ measured in of a time-dependent analysis using $(\overline{b}d) \to (\overline{c}c,\ \overline{s}s)(\overline{s}d)$ CP eigenstates. The charmonium modes being tree dominated and the $\overline{s}s$ modes being penguin dominated (for which larger scales are involved), the independent measurements of both modes represent a powerful probe of new physics. A number of observables suffer from significant theoretical uncertainties mainly due to long distance QCD of non-perturbative origin. Some of them will be discussed below.

3.1 Fit technique

This review heavily employs the framework package *CKMfitter* [6], featuring the statistical approach *R*fit [7], which is based on a frequentist understanding of systematic theoretical uncertainties. No probability distributions are assumed for theoretical

[2]The apparent up to 3σ incompatibility between the determination of λ from $|V_{ud}|$ and $|V_{us}|$, respectively, is not limiting the determination of the CKM phase, as far as one can assume that only large scale phenomena are responsible for physics beyond the SM (see also Ref. [14]).

parameters. The CKM analysis is performed in three stages:

1. *Probing the SM*: the overall consistency between data and the theoretical framework, here the SM, is tested by means of a Monte Carlo simulation.

2. *Metrology*: if the agreement between data and the SM is found to be acceptable, confidence levels (CL) in parameter subspaces are determined.

3. *Probing new physics*: extensions of the SM are tested and limits on new physics parameters are determined.

Since the CL obtained for the SM in the first step of the CKM analysis is found to be sufficient (57%), we will concentrate on the metrology phase (step 2) in this review. Due to the lack of space, tests of new physics are not discussed. The reader is referred to Ref. [13] for an example application to $B^0_d\overline{B}^0_d$ mixing using *R*fit. If the hypothesis "the CKM picture of the SM is correct" is accepted, CLs in parameter subspaces (*e.g.*, $\overline{\rho}-\overline{\eta}$) are evaluated by means of fine granular scans. For a given point in a subspace, one determines the best agreement between data and theory. One obtains the quantity $\Delta\chi^2$ by varying freely all model parameters with the exception of those that are scanned in the subspace. After fitting, the corresponding CL is obtained from $\mathrm{CL} = \mathrm{Prob}(\Delta\chi^2, N_{\mathrm{dof}})$, where N_{dof} is the number of degrees of freedom, which in general coincides with the dimension of the subspace.

3.2 Fit inputs

The input observables and parameters used for the standard CKM fit are listed in Table 2.

A precise knowledge of $|V_{ub}|$ is required for a comparison with the loop-induced $\sin 2\beta$ (search for new physics). The element $|V_{cb}|$ is an important ingredient of the SM predictions of observables from kaon physics, in particular the rates of rare kaon decays. Theoretical uncertainties are sizeable for the determination of $|V_{ub}|$ and $|V_{cb}|$ from exclusive and inclusive semileptonic $b \to u$ and $b \to c$ transitions, respectively. The theoretical analyses intensively employ *Heavy Quark Symmetry*[3]. The computation tools are *Heavy Quark Effective Theory* and the *Operator Product Expansion* (OPE), where the latter organizes short and long-distance contributions in a power series of $\lambda_{\mathrm{QCD}}/m_b$ and $\alpha_s(m_b)$. On the exclusive side, the knowledge of the corresponding weak transition form factor is crucial, the prediction of which is model-dependent [23]. In principle, fully inclusive decays do not suffer from this drawback. This is however no longer true once experimental cuts are involved [24]. In particular, $b \to u$ transitions

[3] In the $m_Q \to \infty$ limit, the heavy quark represents a static color source with fixed four-momentum so that the light degrees of freedom become insensitive to spin and flavor of the heavy quark.

Observable/Parameter	Value ± error	Source
$\|V_{ub}\|$	$(3.25\,^{+0.25}_{-0.32} \pm 0.55) \times 10^{-3}$	CLEO exclusive [17]
$\|V_{ub}\|$	$(4.08 \pm 0.56 \pm 0.40) \times 10^{-3}$	CLEO inclusive & moments [15]
$\|V_{ub}\|$	$(4.09 \pm 0.61 \pm 0.42) \times 10^{-3}$	LEP inclusive [16]
$F_{D^\star}(1)\|V_{cb}\|$	$(35.4 \pm 1.9 \pm 1.8) \times 10^{-3}$	Belle exclusive [18]
$F_{D^\star}(1)\|V_{cb}\|$	$(43.1 \pm 1.3 \pm 1.8) \times 10^{-3}$	CLEO exclusive [19]
$F_{D^\star}(1)\|V_{cb}\|$	$(38.2 \pm 1.1) \times 10^{-3}$	LEP exclusive [21]
$\|V_{cb}\|$	$(40.4 \pm 1.0 \pm 0.8) \times 10^{-3}$	CLEO inclusive & moments [20]
Δm_d	(0.496 ± 0.007) ps^{-1}	WA
Δm_s	Amplitude Spectrum	WA [22]
$\sin 2\beta$	0.78 ± 0.08	WA [5]
$m_t(\overline{\rm MS})$	(166 ± 5) GeV/c^2	PDG'00
$f_{B_d}\sqrt{B_d}$	$(230 \pm 28 \pm 28)$ MeV	Lattice 2000
ξ	$(1.16 \pm 0.03 \pm 0.05)$ MeV	Lattice 2000
B_K	$(0.87 \pm 0.06 \pm 0.13)$ MeV	Lattice 2000

Table 2: Values and errors of some of the most relevant CKM fit input observables and parameters. Averages of uncorrelated determinations of the same observables are obtained in a natural way using the product of the corresponding likelihoods. For $|V_{ub}|$ and $|V_{cb}|$, the first errors are experimental and the second theoretical. For $F_{D^\star}(1)|V_{cb}|$, the first errors are statistical and the second systematic. The relevant $B \to D^*\ell\nu$ form factor is $F_{D^\star}(1) \simeq 0.91 \pm 0.04$ (see refs. and discussion in [7]). We use the averaged amplitude spectrum to incorporate the $B^0_s\overline{B}^0_s$ oscillation results [22]. The standard CKM analysis is theoretically limited (with the exception of $\sin 2\beta$).

are largely overcast by $b \to c$ background events. Kinematic cuts allow to reduce this background to the cost of a loss of inclusiveness and thus a rise of the theoretical uncertainty. A precise measurement of the *shape function* representing the Fermi motion of the b quark within the B meson (the light quark (*light degrees of freedom*) "knocks" at the heavy quark) could significantly reduce the theoretical uncertainties on the cuts applied. A useful shape function can be extracted from $B \to s\gamma$ decays, using some theoretical input for higher order corrections of the transfer function [15, 24].

The combined use of Δm_d and Δm_s improves the theoretically limited prediction of the individual $B^0\overline{B}^0$ mixing frequencies by a factor of about 3.6, since only the relative frequencies are involved (see Ref. [25] for recent criticism concerning the precision of ξ). The experimental information on $B^0_s\overline{B}^0_s$ mixing is yet insufficient to claim a signal. We use the averaged amplitude spectrum [22] and compute from it the expected

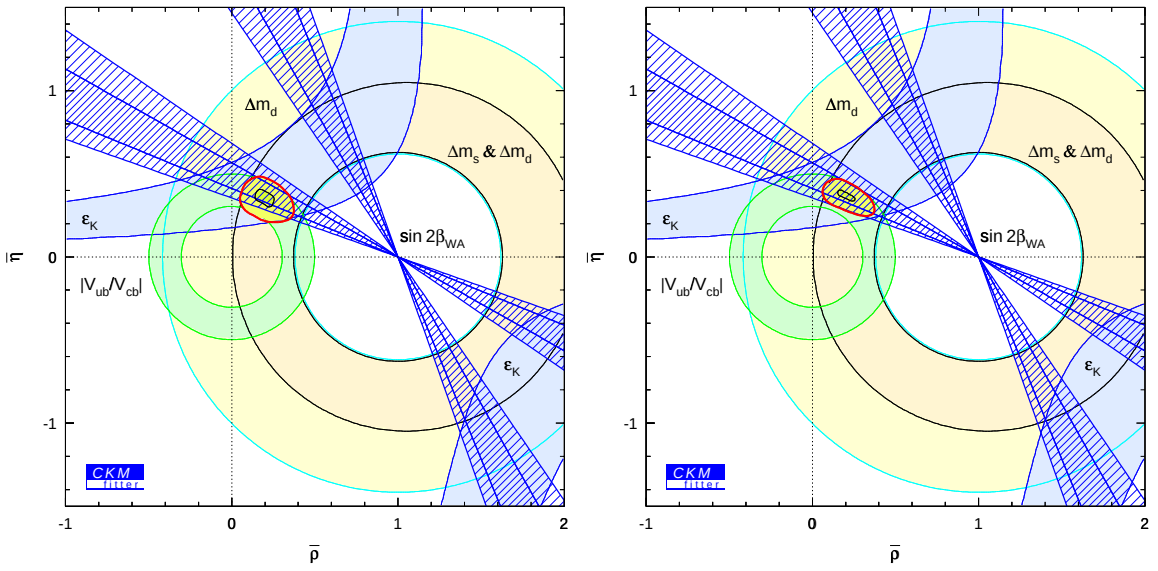

Figure 2: The standard CKM fit in the $\overline{\rho}-\overline{\eta}$ plane. Left: $> 5\%$ CL individual domains (the $\sin 2\beta$ WA is shown with its 1σ and 2σ bands) and the global fit without using the world average of $\sin 2\beta$. Right: including $\sin 2\beta$ in the combined fit. The inner zone indicates the importance of theoretical uncertainties, which is greatly reduced when including $\sin 2\beta$ in the fit.

confidence level as a function of Δm_s, to be used in the global fit [26].

The matrix elements of the effective four fermion couplings used to compute the box diagrams that mediate K and B mixing, are obtained from lattice QCD. Model-independent unquenched calculations are undertaken, but not yet precise enough for the needs in the global fit. In effect, with the exception of $\sin 2\beta$ and the inclusive determinations of $|V_{u(c)b}|$, the standard CKM fit is now in the hand of the Lattice community!

3.3 Fit results

The resulting confidence levels of the standard fit are displayed in the $\overline{\rho}-\overline{\eta}$ plane in Fig. 2. Also shown are the $> 5\%$ CL bands of the individual constraints, including the 4-fold ambiguity of the $\sin 2\beta$ measurement. *Its agreement with the indirect determination represents a triumph for the Standard Model and the KM paradigm [8]. It establishes the KM mechanism as the dominant source of CPV at the electroweak scale.* The inclusion of $\sin 2\beta$ (right hand plot in Fig. 2) into the standard fit significantly reduces the allowed region.

Parameter	95% CL region	Parameter	95% CL region
λ	0.2221 ± 0.0041	$\lvert V_{ud}\rvert$	0.97504 ± 0.00094
A	0.76 - 0.90	$\lvert V_{ub}\rvert$ $[10^{-3}]$	3.15 - 4.37
$\overline{\rho}$	0.08 - 0.35	$\lvert V_{cb}\rvert$ $[10^{-3}]$	36.9 - 43.6
$\overline{\eta}$	0.28 - 0.45	$\lvert V_{td}\rvert$ $[10^{-3}]$	6.3 - 9.1
J $[10^{-5}]$	2.2 - 3.5	$\lvert V_{ts}\rvert$ $[10^{-3}]$	36.4 - 43.0
$\sin 2\alpha$	-0.81 - 0.43	$\lvert V_{tb}\rvert$	0.99905 - 0.99932
$\sin 2\beta$	0.64 - 0.84	BR$(K_{\rm L}^0 \to \pi^0\nu\overline{\nu})$ $[10^{-11}]$	1.6 - 4.2
α	77° - 117°	BR$(K^+ \to \pi^+\nu\overline{\nu})$ $[10^{-11}]$	5.1 - 8.4
β	19.9° - 28.6°	BR$(B^+ \to \tau^+\nu_\tau)$ $[10^{-5}]$	7.2 - 22.1
$\gamma = \delta_{CP}$	40° - 78°	BR$(B^+ \to \mu^+\nu_\mu)$ $[10^{-7}]$	2.9 - 8.7

Table 3: Fit results for the unitary CKM parameters, the CKM matrix elements and branching ratios of some rare K and B meson decays *including the world average* $\sin 2\beta$ *in the fit*. Ranges are given for the quantities that are limited by systematic theoretical errors.

Table 3 lists 95% CL allowed domains of some relevant parameters, obtained from one-dimensional scans equivalent to those performed in the $\overline{\rho} - \overline{\eta}$ plane. The world average of $\sin 2\beta$ is always included in the fits. The procedure ensures the consistency of all numbers among each other and with the combined fit.

4 Beyond the Standard Fit

A precise measurement of rare K and B decays can greatly augment the available information on the CKM phase.

4.1 Rare K decays

The detection of a second $K^+ \to \pi^+\nu\overline{\nu}$ event has been announced early 2002 by the E787 Collaboration at Brookhaven [27], leading to a branching fraction of $(1.57^{+1.75}_{-0.82}) \times 10^{-10}$, which is compatible with the SM prediction [28] given in Table 3. A total of 5 to 10 SM events is expected to be detected at the successor experiment E949 at BNL [29], so that this channel becomes an interesting ingredient of the CKM fit. It should be noted that the translation of results on rare kaon decay into a measurement of $|V_{td}|$ and $\overline{\eta}$, respectively, requires a good knowledge of the matrix element $|V_{cb}|$ entering with its fourth power the SM predictions.

4.2 Rare B decays

The high luminosity B factories provide a detailed picture of rare, charmless B decays. We shall distinguish in the following two categories:

1. Semileptonic (FCNC) and radiative B decays, mediated by box and penguin diagrams.

2. Hadronic $b \to u(d,s)$ decays, mainly mediated by tree and penguin diagrams.

Since large virtual scales are involved, the first class of decays provides sensitive probes for new physics (SUSY, right-handed couplings, etc) via the measurements of rates and direct CPV. In addition, they can be used to determine the matrix elements $|V_{td}|$ and $|V_{ts}|$ as well as HQET parameters. Of particular interest is the measurement of the ratio $\Gamma(B \to \rho\gamma)/\Gamma(B \to K^*\gamma)$ which can be theoretically predicted to some accuracy [30, 31]. The present experimental upper limit is close to the the prediction obtained from the standard CKM fit so that a signal of the Cabibbo suppressed mode $B \to \rho\gamma$ is expected to be "just around the corner".

We will concentrate in the following on the second class of charmless B decays, allowing to measure CPV in the interference between decays with and without mixing and thus the determination of the UT angle α. The measurement of direct CP asymmetries and total rates provides information on the UT angle γ. Moreover, powerful tests of the factorization hypothesis can be performed.

Tge amplitudes of rare hadronic $B \to \pi\pi'$ decays into two pions are generally parameterized by:

$$A(B \to \pi\pi') = R_u e^{i\gamma} T + R_t e^{-i\beta} P \ , \tag{3}$$

$$A(\overline{B} \to \pi\pi') = R_u e^{-i\gamma} T + R_t e^{i\beta} P \ , \tag{4}$$

where T and P denote (complex) tree and penguin amplitudes, respectively. The CP transformation alters the sign of the weak phase only, since the strong interaction is assumed to be CP conserving. The parameters $R_u = |V_{ud}V_{ub}^*|$ and $R_t = |V_{td}V_{tb}^*|$ represent the sides of the UT. For decay modes into two pions the tree and penguin amplitudes are of the same order λ^3, while the tree is λ^4-suppressed and the penguin λ^2-enhanced in decays into one kaon and one pion. Interference of tree and penguin amplitudes of similar size can lead to significant rate differences between CP conjugated amplitudes, *i.e.*, may exhibit direct CPV in the experiment.

Bounds on γ

Pioneered by the work of Fleischer-Mannel [32], it has been shown by many authors that CP-averaged branching fractions of B decays into two pseudoscalers can be used

to infer constraints on the UT angle γ. The theoretical analysis deals among others with $SU(3)$ breaking, rescattering contributions (FSI) and electroweak penguins. One can define the following CP-averaged ratios [41]:

$$R \equiv \frac{\tau_{B^+}}{\tau_{B^0}} \frac{\Gamma(B^0 \to K^\pm \pi^\mp)}{\Gamma(B^\pm \to K^0 \pi^\pm)} = 1.07^{+0.15}_{-0.12} \quad (< 1\ ?)\ , \tag{5}$$

$$R_n \equiv \frac{1}{2} \frac{\Gamma(B^0 \to K^\pm \pi^\mp)}{\Gamma(B^0 \to K^0 \pi^0)} = 1.04^{+0.37}_{-0.22} \quad (\neq 1\ ?)\ , \tag{6}$$

$$R_c \equiv 2 \frac{\Gamma(B^\pm \to K^\pm \pi^0)}{\Gamma(B^\pm \to K^0 \pi^\pm)} = 1.24^{+0.24}_{-0.21} \quad (\neq 1\ ?)\ , \tag{7}$$

known as Fleischer-Mannel [32], Buras-Fleischer [33] and Neubert-Rosner (NR) [34] bounds, respectively. While Eq. (5) is required to be smaller than 1 to obtain non-trivial bounds on γ, the other two can lead to constraints once they significantly depart from 1 (see Ref. [35] for a further going analysis of these ratios). At present, only the addition of phenomenological or theoretical estimates on the size of the penguin amplitudes and/or the strong phases involved leads to significant information: Figure 3 shows on the left hand plot the NR bound (7) in the $\overline{\rho} - \overline{\eta}$ plane[4], when constraining the size of the tree-over-penguin ratio using the experimental values of $\Gamma(B^\pm \to \pi^\pm \pi^0)/\Gamma(B^\pm \to K^0 \pi^\pm)$ (tree-only over penguin-only ratio) together with a correction for $SU(3)$ breaking (and using naive factorization[5]). The constraints are weak compared to the current knowledge from the standard fit. Using in addition *QCD Factorization* (QCD FA) [36], which predicts small relative strong phases between tree and penguin amplitudes, does lead to a significant constraint (right hand plot in Fig. 3).

4.3 CPV in $B^0 \to \pi^+\pi^-$ decays

On the contrary to the golden mode $B^0 \to J/\psi K^0$, where penguin contributions with different weak phases are doubly-Cabibbo suppressed, the time-dependent CP-asymmetry analysis of $B^0 \to \pi^+\pi^-$ decays suffers from significant penguin pollution. As a consequence, both the sine and the cosine terms in the time evolution are unknown:

$$a_{CP}(t) = S_{\pi\pi} \sin(\Delta m_d \Delta t) - C_{\pi\pi} \cos(\Delta m_d \Delta t)\ , \tag{8}$$

with the time difference, Δt, between the CP and the tag side decay vertices, and the coefficients

$$S_{\pi\pi} = \frac{2\mathrm{Im}\lambda_{\pi\pi}}{1 + |\lambda_{\pi\pi}|^2} \quad \text{and} \quad C_{\pi\pi} = \frac{1 - |\lambda_{\pi\pi}|^2}{1 + |\lambda_{\pi\pi}|^2}\ . \tag{9}$$

[4]The R&D logo labels plots for which the discussion of theoretical uncertainties is not settled.

[5]Factorization is based on the concept of *color transparency*: since the energy release of the heavy-to-light transition is large, soft gluons do not interact with the small $q\overline{q}$ color dipole of the emitted meson.

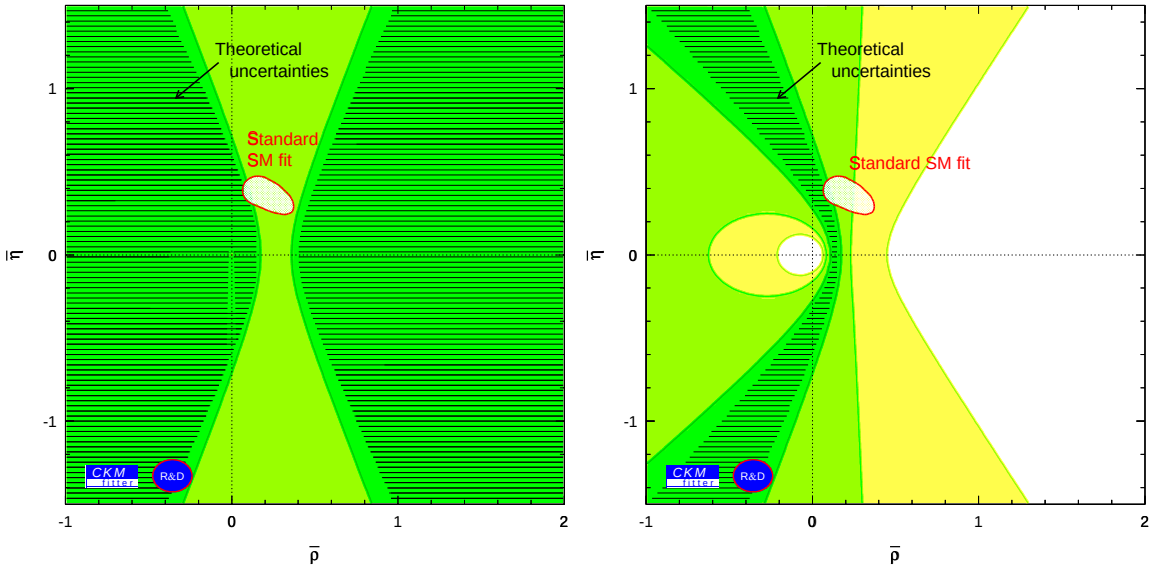

Figure 3: The Neubert-Rosner bound in the $\overline{\rho} - \overline{\eta}$ plane. Left: using a phenomenological constraint on the $|P/T|$ ratio and right: using in addition QCD FA, predicting small relative strong phases [36]. The shaded regions indicate the $\geq 5\%$, $\geq 32\%$ and $\geq 90\%$ CL domains. Also shown is the $> 5\%$ CL region of the standard CKM fit (including $\sin 2\beta$).

The CP parameter $\lambda_{\pi\pi}$ is given by the standard expression

$$\lambda_{\pi\pi} = e^{-2i\beta} \frac{A(\overline{B}^0 \to \pi^+\pi^-)}{A(B^0 \to \pi^+\pi^-)} = e^{2i\alpha} \frac{1 - (R_t/R_u)|P/T|e^{-i(\alpha-\delta)}}{1 - (R_t/R_u)|P/T|e^{+i(\alpha+\delta)}} \equiv |\lambda_{\pi\pi}| e^{2i\alpha_{\rm eff}} \ , \qquad (10)$$

where the phase $e^{-2i\beta}$ arises due to $B^0_d \overline{B}^0_d$ mixing and $R_{t(u)}$ are the sides of the UT (1), not to be confounded with the ratios (5-7). Note that $\pi^+\pi^-$ is a CP eigenstate with eigenvalue $+1$. In the presence of penguin contributions, the UT angle α is modified by the relative strong phase $\delta \equiv \arg(PT^*)$ between the penguin and the tree amplitudes. As a consequence, a measurement of the parameters $S_{\pi\pi}$ and $C_{\pi\pi}$ cannot be translated into $\sin 2\alpha$ without prior information on the strong phase difference δ and the ratio $|P/T|$. In principle, the Gronau-London isospin analysis [37] allows one to recover the missing pieces using the relations

$$\begin{aligned} A(B^+ \to \pi^+\pi^0) &= \frac{1}{\sqrt{2}} A(B^0 \to \pi^+\pi^-) + A(B^0 \to \pi^0\pi^0) \ , \qquad (11) \\ |A(B^+ \to \pi^+\pi^0)| &= |A(B^- \to \pi^-\pi^0)| \ , \end{aligned}$$

where electroweak penguins have been neglected. However, the unknown tagged rates for $B^0(\overline{B}^0) \to \pi^0\pi^0$, precludes from a complete application and only permits to

Observable	Value	Source
$\mathcal{B}(B^0 \to \pi^+\pi^-)$	$(5.2 \pm 0.6) \times 10^{-6}$	WA [41]
$\mathcal{B}(B^\pm \to \pi^\pm\pi^0)$	$(4.9 \pm 1.1) \times 10^{-6}$	WA [41]
$\mathcal{B}(B^0 \to \pi^0\pi^0)$	$< 3.4 \times 10^{-6}$ (90% CL)	*BABAR* [41]
$S_{\pi\pi}$	-0.01 ± 0.38	*BABAR* [42]
	$-1.21^{+0.41}_{-0.30}$	Belle [43]
$C_{\pi\pi}$	-0.02 ± 0.30	*BABAR* [42]
	$-0.94^{+0.32}_{-0.27}$	Belle [43] [sign convention reversed]

Table 4: Experimental results on $B \to \pi\pi$ decays used for the Gronau-London isospin analysis [37]. Statistical and systematic errors have been added in quadrature.

derive bounds on the difference $|\alpha - \alpha_{\text{eff}}|$. This has been first exploited by Grossman-Quinn [38] and Charles [39] and was further improved by Gronau-London-Sinha-Sinha [40]. While the evaluation of the above bounds gives an interesting insight into the structure of the isospin relations, it is by no means a necessary exercise. Indeed, since no additional input is used it merely represents a reformulation of Eqs. (11). Numerical analysis tools like *CKMfitter* automatically exploit the information from the bounds once they dispose of the input observables and the isospin relations. Moreover, it guarantees the optimal use of the totality of the constraints provided.

It is instructive to follow a hierarchy of approaches, using more and more theoretical input to constrain the CKM phase:

(A) using as input $C_{\pi\pi}$ and $S_{\pi\pi}$ as well the branching fractions $B \to \pi\pi$ ($\pi \in \{\pi^+, \pi^0\}$) and strong isospin.

(B) using (A) and $B^0 \to K^+\pi^-$ together with $SU(3)$ (neglecting OZI-suppressed penguin annihilation topologies [39]).

(C) using (B) and the determination of $|P/T|$ by means of the rates of the decays $B^+ \to \pi^+\pi^0$ and $B^+ \to K^0\pi^+$ and $SU(3)$ and naive factorization, but leaving the relative strong phase unconstrained.

(D) using (B) and the prediction of the complex P/T ratio (absolute value and phase) by means of QCD Factorization.

We will only show results for the items (A) and (D) in these proceedings. The experimental measurements used are given in Table 4. We consider the *CP* asymmetry results obtained by *BABAR* and Belle to be incompatible at present and thus treat

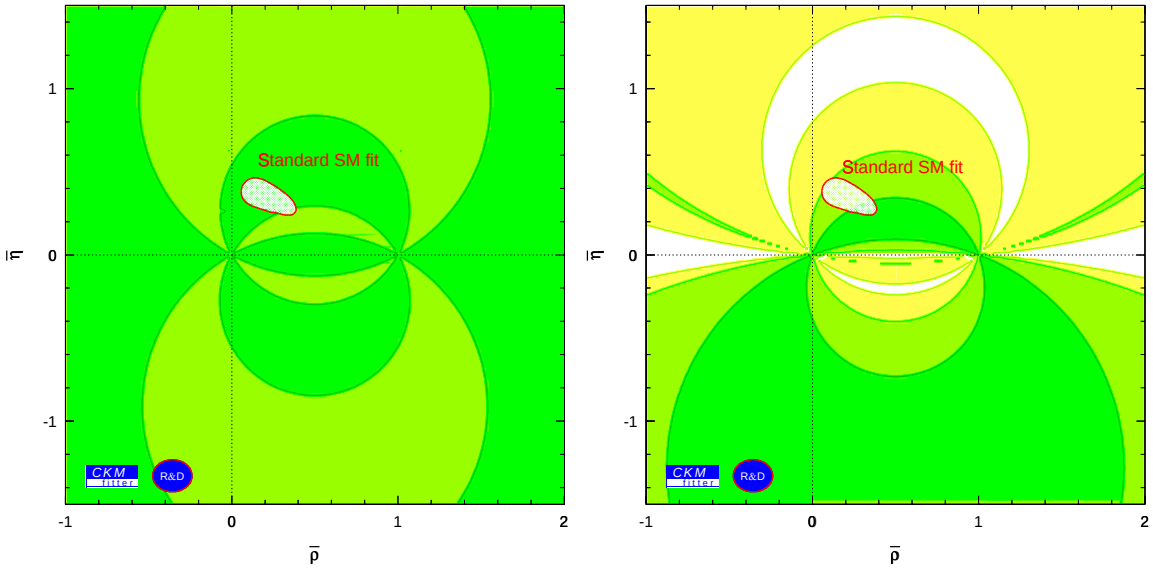

Figure 4: Results on $\pi\pi$ in the $\overline{\rho}-\overline{\eta}$ plane using the Gronau-London isospin analysis. Left: using $S_{\pi\pi}$ and $C_{\pi\pi}$ from *BABAR*, right: Belle. The shaded regions indicate the $\geq 5\%$, $\geq 32\%$ and $\geq 90\%$ CL domains. Also shown is the $> 5\%$ CL region of the standard CKM fit (including $\sin 2\beta$).

them independently. Figure 4 shows the constraints obtained by the isospin analysis applying the experimental limit on the rate of $B^0 \to \pi^0\pi^0$ (*BABAR*) and using time-dependent CP asymmetry results from *BABAR* (left) and Belle (right). Both experiments agree with the standard fit within the large uncertainties from the weak bound on the penguin contribution. To turn this approach into a competitive method, either the branching fraction of $B^0 \to \pi^0\pi^0$ has to be significantly lower than 10^{-6}, or very large luminosity is required to precisely measure their tagged rates.

As a subsequent, more promising but also less robust approach, we shall apply the full QCD FA [36] prediction of the complex P/T ratio to constrain α via Eq. (9). The resulting constraints in the $\overline{\rho}-\overline{\eta}$ plane are plotted in Fig. 5. We find that the *BABAR* result is well within the expected range, whereas—not surprisingly—the Belle numbers prefer a larger phase and $|P/T|$ ratio. The agreement of the latter with the standard fit is on the 10% level. The upper right hand plot shows the *BABAR* results on $S_{\pi\pi}$ and $C_{\pi\pi}$ together with the world average of $\sin 2\beta$. It visualizes the impressive constraint already obtained from the time-dependent analyses of the B factories alone.

One may reverse Eq. (9) and inject the result of the standard fit on α in order to probe the relative strong phase and the $|P/T|$ ratio in a model-independent matter.

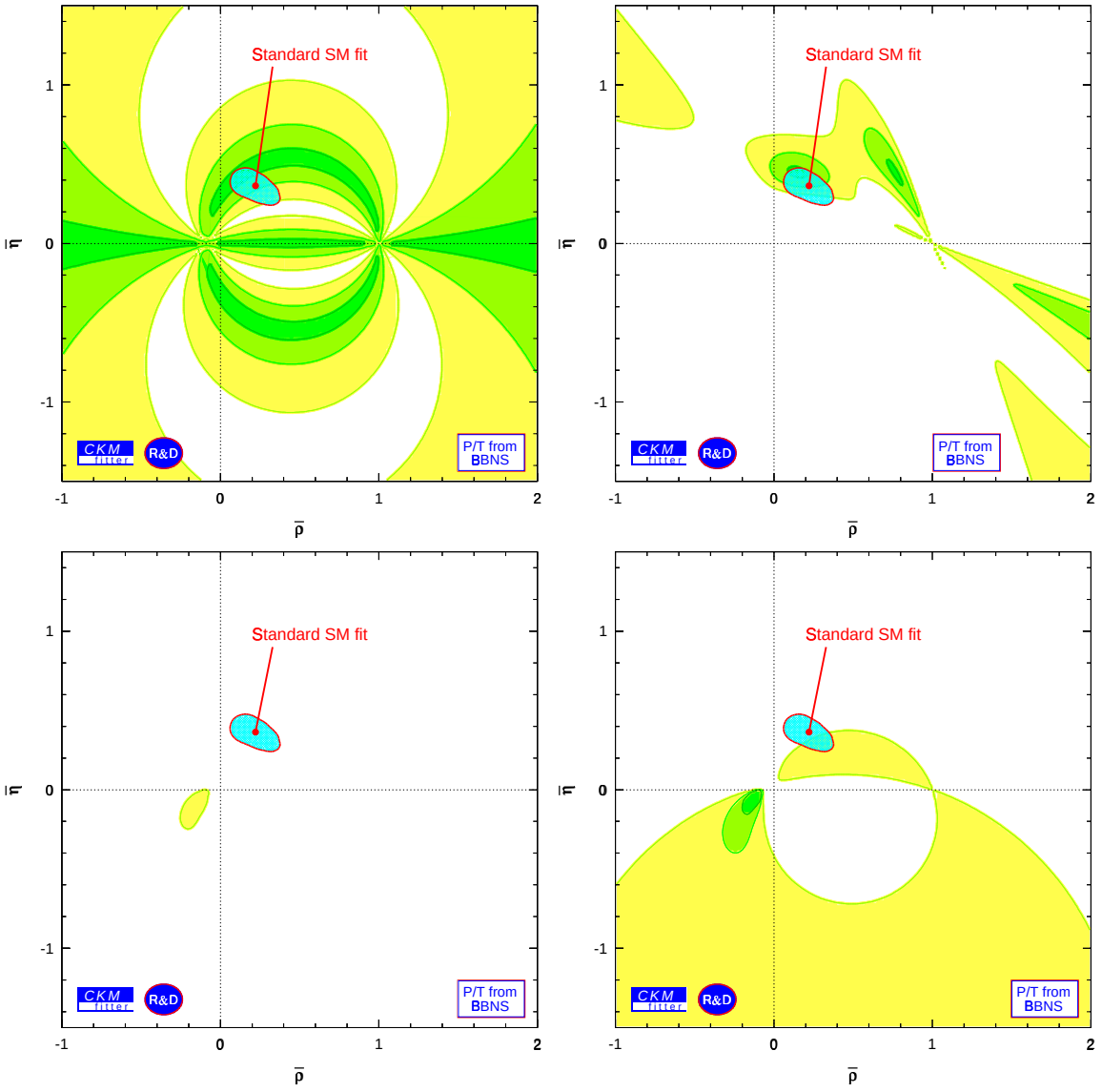

Figure 5: Upper plot: *BABAR* results on $\pi^+\pi^-$ in the $\overline{\rho} - \overline{\eta}$ plane using the QCD FA [36] prediction of the penguin contribution and strong phase difference. The upper right hand plot shows the combined results for the CP asymmetry measurements using charmonium modes and $\pi^+\pi^-$ (*BABAR*). Lower plots: the corresponding results from Belle. The right hand plot zooms the CLs between 0 and 10%. Also shown in all plots is the $> 5\%$ CL region of the standard CKM fit (including $\sin 2\beta$).

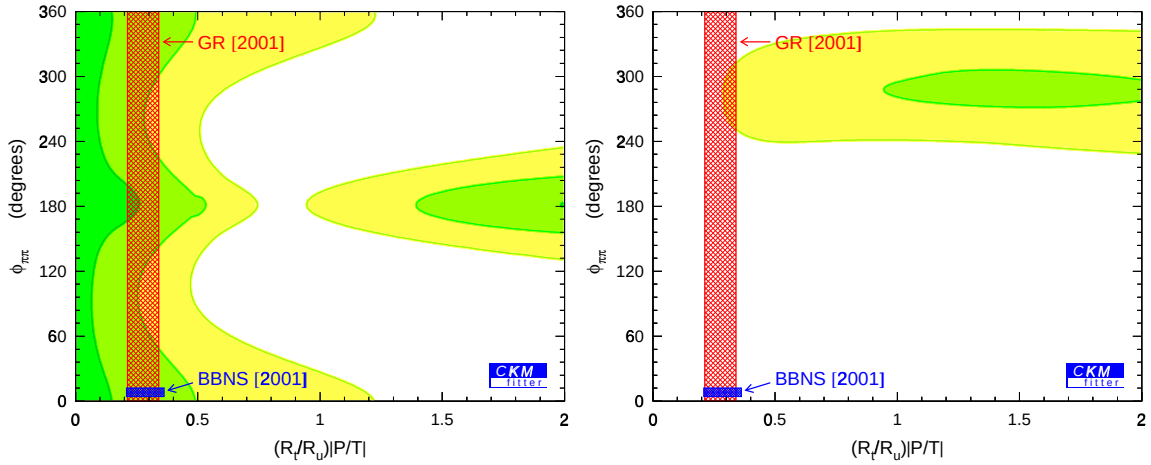

Figure 6: The $S_{\pi\pi}$ and $C_{\pi\pi}$ measurements of *BABAR* (left) and Belle (right) are used to determine the relative strong phase (ordinate) and the penguin-to-tree ratio (abscissa). The value of the UT angle α of the standard CKM fit is injected with its uncertainties. The allowed regions are compared to theoretical predictions [36, 44].

The resulting confidence levels are given in Fig. 6. As expected, the *BABAR* result (left) agrees with QCD FA while Belle prefers larger phases. However, it is important to note that these observations are tendencies only, not yet supported by statistically significant results.

5 Conclusions

The successful operation of the B factories at SLAC and KEK has provided a flood of new results that can be used to obtain information on the CP-violating phase of the CKM matrix. The extraordinary agreement of the world average of $\sin 2\beta$ with the indirect determination represents a triumph for the Standard Model and the KM paradigm. It establishes the KM mechanism as the dominant source of CPV at the electroweak scale. While the inclusion of $\sin 2\beta$ into the global CKM fit is a grateful task, exploiting rare B decays requires some theoretical digestion in order to lead to meaningful constraints at present.

We now constrain the center of the $\overline{\rho}-\overline{\eta}$ plane to quite some accuracy, albeit it is still too large to seriously challenge the Standard Model at the percent level. Obviously, a better understanding of long distance QCD opens the shrine to a full exploitation of the huge data samples currently produced at KEK-B and PEP-II, and the tremendous data quantities that will be produced at the TEVATRON and the LHC. Much hope is sent towards the Lattice community in this respect. Will we be able to discover

signs of new physics before the advent of the LHC?

This conference was a true pleasure: for it's scientific program and the attendance as well as for the smooth organization. My sincere thanks are dedicated to the local organization committee. I am indebted to the fruitful and pleasant collaboration with Heiko Lacker, Sandrine Laplace, Franccois Le Diberder, José Ocariz and Muriel Pivk.

References

[1] *BABAR* Collaboration (B. Aubert *et. al.*), Phys. Rev. Lett. **86**, 2515 (2001)

[2] Belle Collaboration (A. Abashian *et. al.*)), Phys. Rev. Lett. **86**, 2509 (2001)

[3] I.I. Bigi, Talk given at Meson 2002, Cracow, Poland, 24-28 May 2002, UND-HEP-02-BIG-05, TTP-02-10, [hep-ph/0206261]

[4] F. Parodi, P. Roudeau and A. Stocchi, Nuovo Cim. **A112** 833 (1999)

[5] M. Hazumi (Belle) and S. Rahatlou (*BABAR*), *these proceedings*

[6] For a description of *CKMfitter* and the source code as well as links to the newest plots and presentations, consult the web site:
http://ckmfitter.in2p3.fr/

[7] A. Höcker, H. Lacker, S. Laplace and F. Le Diberder, Eur. Phys. J. **C21**, 225 (2001), [hep-ph/0104062]

[8] M. Kobayashi and T. Maskawa, *Prog. Theor. Phys.* **49** (1973) 652; N. Cabibbo, *Phys. Rev. Lett.* **10** (1963) 351

[9] Several groups have pioneered global CKM fits in the past. For the attempt of an exhaustive list, please see Ref. [8] of [7]

[10] L. Wolfenstein, Phys. Rev. Lett. **51**, 1945 (1983)

[11] A.J. Buras, M.E. Lautenbacher and G. Ostermaier, Phys. Rev. **D50**, 3433 (1994)

[12] C. Jarlskog, Phys. Rev. Lett. **55**, 1039 (1985)

[13] S. Laplace, Z. Ligeti, Y. Nir and G. Perez, Phys. Rev. **D65**, 094040 (2002)

[14] H. Abele et al., Phys. Rev. Lett. **88**, 211801 (2002)

[15] CLEO Collaboration (A. Bornheim *et. al.*), Phys. Rev. Lett. **88**, 231803 (2002); (D. Cronin-Hennessy *et. al.*), Phys. Rev. Lett. **87**, 251808 (2001);

[16] LEP $|V_{ub}|$ Working Group (2001),
http://battagl.home.cern.ch/battagl/vub/vub.html

[17] CLEO Collaboration (B.H. Behrens *et. al.*), Phys. Rev. **D61**, 052001 (2000)

[18] Belle Collaboration (K. Abe et al.), Phys. Rev. Lett. **88**, 231803 (2002

[19] CLEO Collaboration (R.A. Briere *et. al.*), CLNS-01-1773, CLEO-01-26 (2002), [hep-ex/0203032]

[20] CLEO Collaboration Phys Rev lett **87**, 251808 (2001)

[21] LEP $|V_{cb}|$ Working Group (Winter 2002),
http://lepvcb.web.cern.ch/LEPVCB/

[22] LEP B Oscillation Working Group (Moriond 2002),
http://lepbosc.web.cern.ch/LEPBOSC/

[23] A. Kronfeld, *these proceedings*

[24] M. Luke, *these proceedings*

[25] A.S. Kronfeld, S.M. Ryan, FERMILAB-PUB-02-109-T (2002), [hep-ph/0206058]

[26] F. Le Diberder, contribution to WG II of the CERN CKM Workshop (2002),
http://ckm-workshop.web.cern.ch/ckm-workshop/

[27] E787 Collaboration (S. Adler *et. al.*), Phys. Rev. Lett. **88**, 041803 (2002)

[28] G. Buchalla and A. Buras, Nucl. Phys. **B398**, 285 (1993); Nucl. Phys. **B400**, 225 (1993); Nucl. Phys. **B548**, 309 (1999)

[29] The E949 web site:
http://www.phy.bnl.gov/e949/

[30] A. Ali, A.Y. Parkhomenko, Eur. Phys. J. **C23**, 89 (2002)

[31] S.W. Bosch, G. Buchalla, Nucl. Phys. **B621**, 459, 2002

[32] R. Fleischer and T. Mannel, Phys. Rev. **D57**, 2752 (1998)

[33] A. Buras and R. Fleischer, Eur. Phys. J. **C11**, 93 (1998)

[34] M. Neubert and J.L. Rosner, Phys. Lett. **B441**, 403 (1998)

[35] M. Bargiotti *et. al.*, Eur. Phys. J. **C24**, 361 (2002)

[36] M. Beneke, G. Buchalla, M. Neubert and C.T. Sachrajda, Nucl. Phys. **B606**, 24 (2001)

[37] M. Gronau and D. London, Phys. Rev. Lett. **65**, 3381 (1990)

[38] Y. Grossman and H.R. Quinn, Phys. Rev. **D58**, 017504 (1998)

[39] J. Charles, Phys. Rev. **D59**, 054007 (1999)

[40] M. Gronau, D. London, N. Sinha, R. Sinha, TECHNION-PH-2001-27, UdeM-GPP-TH-01-89, IMSc-2001/05/27 (2001), [hep-ph/0105308]

[41] R. Bartoldus, *these proceedings*

[42] P. Dauncey (*BABAR*), *these proceedings*

[43] E. Won (Belle), *these proceedings*

[44] M. Gronau and J.L. Rosner, Phys. Rev. **D65**, 013004 (2002)

Measurement of CP-Violating Asymmetry $\sin 2\beta$ with the *BABAR* Detector

Shahram Rahatlou
Department of Physics
University of California, San Diego
9500 Gilman Drive
La Jolla, CA 92093
(for the BABAR Collaboration)

1 Introduction

The Standard Model of electroweak interactions describes CP violation in weak interactions as a consequence of a complex phase in the three-generation Cabibbo-Kobayashi-Maskawa (CKM) quark-mixing matrix [1]. In this framework, measurements of CP-violating asymmetries in the time distribution of neutral B decays to charmonium final states provide a direct measurement of $\sin 2\beta$ [2], where $\beta \equiv \arg\left[-V_{\rm cd}V_{\rm cb}^*/V_{\rm td}V_{\rm tb}^*\right]$.

We report an updated measurement of time-dependent CP-asymmetries in samples of fully reconstructed B decays to charmonium-containing CP eigenstates ($b \to c\bar{c}s$). The data for these studies were recorded at the $\Upsilon(4S)$ resonance with the *BABAR* detector at the PEP-II asymmetric-energy e^+e^- collider at the Stanford Linear Accelerator Center.

We fully reconstruct a sample of neutral B mesons, B_{CP}, decaying to several CP final states. Each event in the B_{CP} is examined for evidence that the recoiling neutral B meson decayed as a B^0 or $\overline{B}^0$ (flavor tag). The time distribution of B meson decays to a CP eigenstate with a B^0 or $\overline{B}^0$ tag can be expressed in terms of a complex parameter λ that depends on both the B^0-$\overline{B}^0$ oscillation amplitude and the amplitudes describing $\overline{B}^0$ and B^0 decays to this final state [3]. The decay rate $\mathrm{f}_+(\mathrm{f}_-)$ when the tagging meson is a $B^0(\overline{B}^0)$ is given by

$$\mathrm{f}_{\pm}(\,\Delta t) = \frac{\mathrm{e}^{-|\Delta t|/\tau_{B^0}}}{4\tau_{B^0}} \times \left[\, 1 \pm \frac{2\,\mathcal{I}m\lambda}{1+|\lambda|^2}\sin\left(\Delta m_d \Delta t\right) \mp \frac{1-|\lambda|^2}{1+|\lambda|^2}\cos\left(\Delta m_d \Delta t\right)\right], \qquad (1)$$

where $\Delta t = t_{\rm rec} - t_{\rm tag}$ is the difference between the proper decay times of the reconstructed B meson ($B_{\rm rec}$) and the tagging B meson ($B_{\rm tag}$), τ_{B^0} is the B^0 lifetime, and Δm_d is the B^0-$\overline{B}^0$ oscillation frequency.

In the Standard Model $\lambda = \eta_f e^{-2i\beta}$ for charmonium-containing $b \to c\bar{c}s$ decays and η_f is the CP eigenvalue of the state f. Thus, the time-dependent CP-violating asymmetry is

$$A_{CP}(\Delta t) \equiv \frac{\mathrm{f}_+(\Delta t) - \mathrm{f}_-(\Delta t)}{\mathrm{f}_+(\Delta t) + \mathrm{f}_-(\Delta t)} = -\eta_f \sin 2\beta \sin\left(\Delta m_{B^0}\,\Delta t\right), \qquad (2)$$

with $\eta_f = -1$ for $J/\psi\,K^0_S$, $\psi(2S)K^0_S$, and $\chi_{c1}K^0_S$, and $+1$ for $J/\psi\,K^0_L$.

The measurement of $\sin 2\beta$ with the decay mode $B \to J/\psi\,K^{*0}(K^{*0} \to K^0_S\pi^0)$ is experimentally complicated by the presence of both even (L=0, 2) and odd (L=1) orbital angular momenta in the final state. The decay rate $\mathrm{f}_+(\mathrm{f}_-)$ when the tagging meson is a $B^0(\overline{B}^0)$, in addition to Δt, is also a function of the angular distribution of the particles in the final state [4].

2 The *BABAR* detector

A detailed description of the *BABAR* detector can be found in Ref. [5]. Charged particles are detected and their momenta measured by a combination of a silicon vertex tracker (SVT) consisting of five double-sided layers and a central drift chamber (DCH), in a 1.5-T solenoidal field. The average vertex resolution in the z direction is $70\,\mu$m for a fully reconstructed B meson. We identify leptons and hadrons with measurements from all detector systems, including the energy loss ($\mathrm{d}E/\mathrm{d}x$) in the DCH and SVT. Electrons and photons are identified by a CsI electromagnetic calorimeter (EMC). Muons are identified in the instrumented flux return (IFR). A Cherenkov ring imaging detector (DIRC) covering the central region, together with the $\mathrm{d}E/\mathrm{d}x$ information, provides K-π separation of at least three standard deviations for B decay products with momentum greater than $250\,\mathrm{MeV}/c$ in the laboratory.

3 Data Sample

The data sample used in this analysis consists of approximately $56\,\mathrm{fb}^{-1}$, corresponding to about 62 million $B\overline{B}$ pairs, collected on the $\Upsilon(4S)$ resonance with the *BABAR* detector at the SLAC PEP-II storage ring between October 1999 and December 2001.

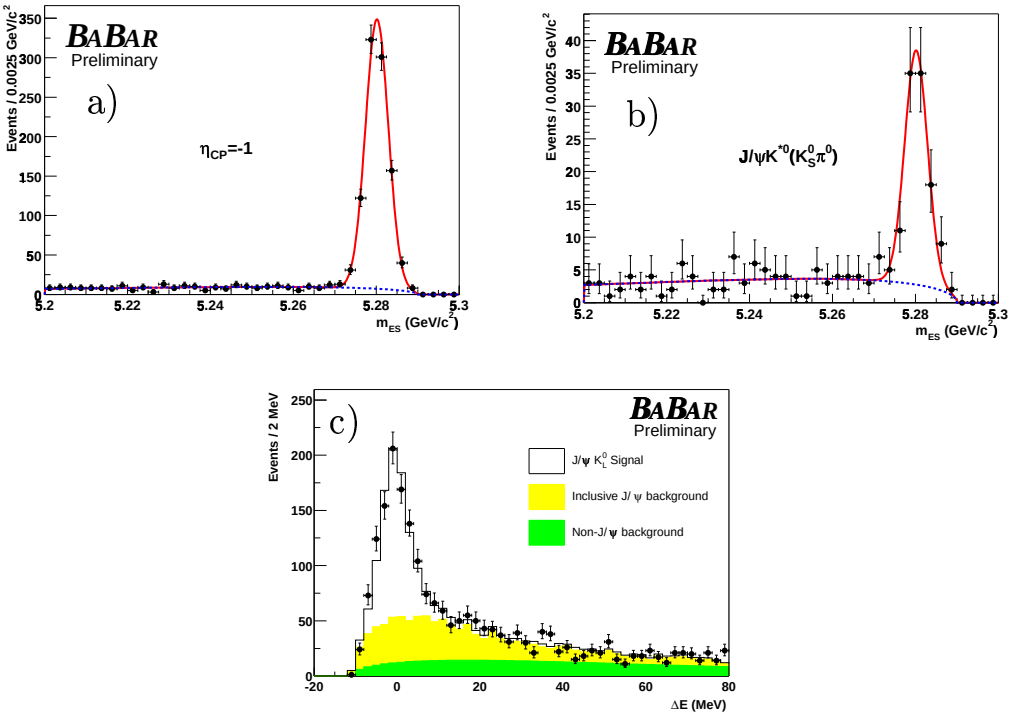

Figure 1: Distribution of $m_{\rm ES}$ for flavor tagged B_{CP} candidates selected in the final states a) $J/\psi K^0_S$ ($K^0_S \to \pi^+\pi^-$), $J/\psi K^0_S$ ($K^0_S \to \pi^0\pi^0$), $\psi(2S)K^0_S$, and $\chi_{c1}K^0_S$, b) $J/\psi K^{*0}(K^{*0} \to K^0_S\pi^0)$, and c) distribution of ΔE for flavor tagged $J/\psi\, K^0_L$ candidates.

We fully reconstruct B candidates in the final states $J/\psi\, K^0_S$ ($K^0_S \to \pi^+\pi^-$, $\pi^0\pi^0$), $\psi(2S)K^0_S$ ($K^0_S \to \pi^+\pi^-$), $\chi_{c1}K^0_S$ ($K^0_S \to \pi^+\pi^-$), $J/\psi\, K^{*0}$ ($K^{*0} \to K^0_S\pi^0$, $K^0_S \to \pi^+\pi^-$), and $J/\psi\, K^0_L$ as described in Ref. [4]. Figure 1 shows the distribution of the beam-energy substituted mass $m_{\rm ES} = \sqrt{(E^{\rm cm}_{\rm beam})^2 - (p^{\rm cm}_B)^2}$ for final states containing a K^0_S and ΔE for the $J/\psi\, K^0_L$ mode.

4 The Measurement Technique

A measurement of A_{CP} requires a determination of the experimental Δt resolution and the fraction w of events in which the tag assignment is incorrect. This mistag fraction reduces the observed CP asymmetry by a factor $(1-2w)$. Mistag fractions and Δt resolution functions are determined from a large sample $B_{\rm flav}$ of neutral B decays to flavor eigenstates consisting of the channels $D^{(*)-}h^+(h^+ = \pi^+, \rho^+$, and $a_1^+)$ and $J/\psi\, K^{*0}(K^{*0} \to K^+\pi^-)$. Figure 2 shows the distribution of the beam-energy substituted mass m_{ES} for this sample.

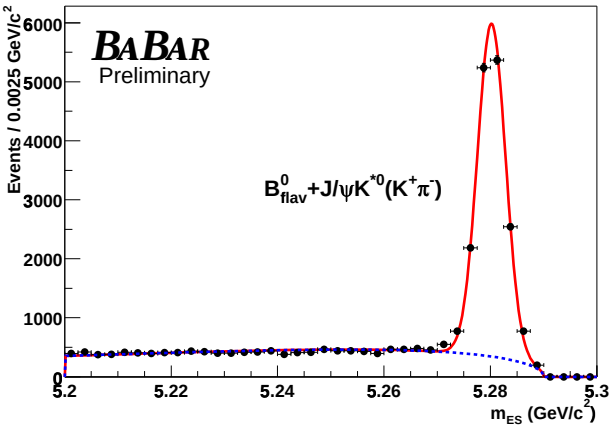

Figure 2: Beam-energy substituted mass distribution for the $B_{\rm flav}$ sample. In 56 fb^{-1}, we reconstruct about 17500 signal events. Average signal purity for $m_{\rm ES} > 5.27\,{\rm GeV}/c^2$ is 85 %.

4.1 B Flavor-Tagging Algorithm

The algorithm used to determine the flavor of the tagging B meson $B_{\rm tag}$ is described in Ref. [6]. The charges of energetic electrons and muons from semileptonic B decays, kaons, soft pions from D^* decays, and high momentum particles are correlated with the flavor of the decaying b quark. For example, a positive lepton indicates a B^0 tag.

Each event is assigned to one of four hierarchical, mutually exclusive tagging categories or has no flavor tag. A lepton tag requires an electron (muon) candidate with a center-of-mass momentum $p_{\rm cm} > 1.0$ (1.1) GeV/c. This efficiently selects primary leptons and reduces contamination due to oppositely-charged leptons from charm decays. Events meeting these criteria are assigned to the `Lepton` category unless the lepton charge and the net charge of all kaon candidates indicate opposite tags. Events without a lepton tag but with a non-zero net kaon charge are assigned to the `Kaon` category. All remaining events are passed to a neural network algorithm whose main inputs are the momentum and charge of the track with the highest center-of-mass momentum, and the outputs of secondary networks, trained with Monte Carlo samples to identify primary leptons, kaons, and soft pions. Based on the output of the neural network algorithm, events are tagged as B^0 or $\overline{B}^0$ and assigned to the `NT1` (more certain tags) or `NT2` (less certain tags) category, or not tagged at all. The tagging power of the `NT1` and `NT2` categories arises primarily from soft pions and from recovering unidentified isolated primary electrons and muons.

The tagging efficiencies ε_i and mistag fractions w_i for the four tagging categories are measured from data and summarized in Table 1.

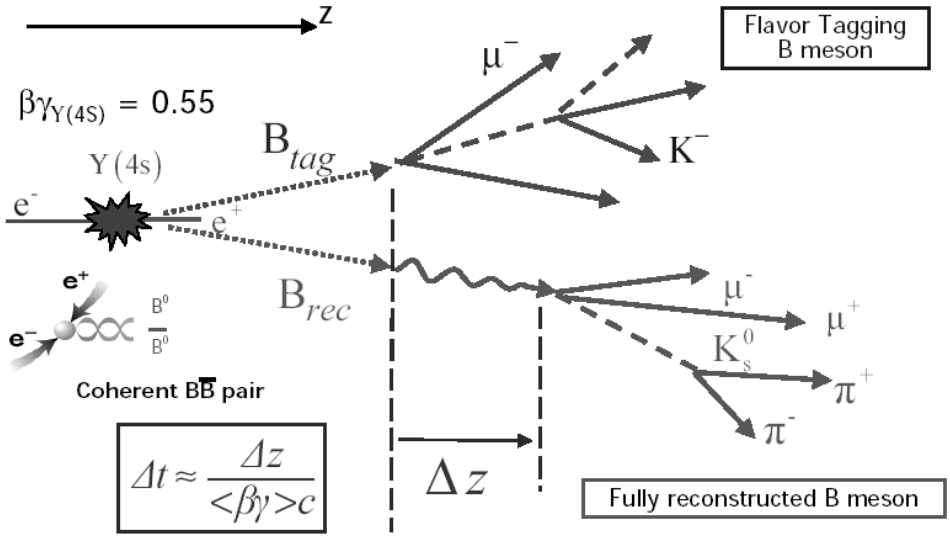

Figure 3: Topology of an event where one B meson is fully reconstructed in a CP eigenstate and the flavor of the other B meson is determined from its decay products.

4.2 Δt Measurement and Resolution Function

The topology of a typical CP event is shown in Figure 3. The time interval Δt between the two B decays is calculated from the measured separation Δz between the decay vertices of $B_{\rm rec}$ and $B_{\rm tag}$ along the collision (z) axis [6]. We determine the z position of the $B_{\rm rec}$ vertex from its charged tracks. The $B_{\rm tag}$ decay vertex is determined by fitting tracks not belonging to the $B_{\rm rec}$ candidate to a common vertex, employing constraints from the beam spot location and the $B_{\rm rec}$ momentum [6]. We accept events with a Δt uncertainty of less than 2.5 ps and $|\Delta t| < 20$ ps. The fraction of events satisfying these requirements is 93%. The r.m.s. Δt resolution for 99.5% of

Table 1: Efficiencies ϵ_i, average mistag fractions w_i, and mistag fraction differences $\Delta w_i = w_i(B^0) - w_i(\overline{B}^0)$, for the four tagging categories, determined from the likelihood fit to the time distribution of the $B_{\rm flav}$ sample.

Category	Efficiency (%)	w	Δw
`Lepton`	11.1 ± 0.2	8.6 ± 0.9	0.6 ± 0.5
`Kaon`	34.7 ± 0.4	18.1 ± 0.7	-0.9 ± 0.1
`NT1`	7.7 ± 0.2	22.0 ± 1.5	1.4 ± 0.3
`NT2`	14.0 ± 0.3	37.3 ± 1.3	-4.7 ± 0.9
All	67.5 ± 0.5		

these events is 1.1 ps.

The Δt resolution function for the signal is represented in terms of $\delta_t \equiv \Delta t - \Delta t_{\rm true}$ by a sum of three Gaussian distributions with different means and widths:

$$\mathcal{R}(\delta_{\rm t}) \;=\; \sum_{k=\rm core,tail} \frac{f_k}{S_k\sigma_{\Delta t}\sqrt{2\pi}} \exp\left(-\frac{(\delta_{\rm t}-b_k\sigma_{\Delta t})^2}{2(S_k\sigma_{\Delta t})^2}\right) + \frac{f_{\rm outlier}}{\sigma_{\rm outlier}\sqrt{2\pi}} \exp\left(-\frac{\delta_{\rm t}^2}{2{\sigma_{\rm outlier}}^2}\right).$$

For the core and tail Gaussians, we use two separate scale factors S_k to multiply the measured uncertainty $\sigma_{\Delta t}$ that is derived from the vertex fit for each event. The scale factor for the tail component is fixed to the value found in simulated data since it is strongly correlated with the other resolution function parameters. The core and tail Gaussian distributions are allowed to have non-zero means to account for any daughters of long-lived charm particles included in the $B_{\rm tag}$ vertex. The mean of the core Gaussian is allowed to be different for each tagging category, but only one common mean is used for the tail component. These offsets are computed from the event-by-event $\sigma_{\Delta t}$ multiplied by a scale factor b_k which accounts for a correlation between the mean of the $\delta_{\rm t}$ distribution and $\sigma_{\Delta t}$ observed in simulated events. The outlier Gaussian has a fixed width of 8 ps and no offset; it accounts for less than 0.5% of events with incorrectly reconstructed vertices. In simulated events we find no significant difference between the Δt resolution function of the B_{CP} and the $B_{\rm flav}$ samples, hence the same resolution function is used for both.

5 Results

We determine sin2β with a simultaneous unbinned maximum likelihood fit to the Δt distributions of the tagged B_{CP} and $B_{\rm flav}$ samples. In this fit the Δt distributions of the B_{CP} sample are described by Eq. 1 with $|\lambda| = 1$. The Δt distributions of the $B_{\rm flav}$ sample evolve according to the known frequency for flavor oscillation in B^0 mesons. The observed amplitudes for the CP asymmetry in the B_{CP} sample and for flavor oscillation in the $B_{\rm flav}$ sample are reduced by the same factor $1-2w$ due to flavor mistags. Events are assigned signal and background probabilities based on the $m_{\rm ES}$ (all modes except $J/\psi K^{*0}$ and $J/\psi K^0_L$) or ΔE ($J/\psi K^0_L$) distributions. The Δt distributions for the signal are convolved with the resolution function described in Section 4.2. Backgrounds are incorporated with an empirical description of their Δt spectrum, containing prompt and non-prompt components convolved with a resolution function [6] distinct from that of the signal.

There are 35 free parameters in the fit: sin2β (1), the average mistag fractions w and the differences Δw between B^0 and $\overline{B}^0$ mistag fractions for each tagging category (8), parameters for the signal Δt resolution (8), and parameters for background time dependence (6), Δt resolution (3), and mistag fractions (8). In addition, we allow cos2β (1), which is determined from the $J/\psi K^{*0}$ events, to vary in the fit [4]. We

fix τ_{B^0} and Δm_d [7]. The determination of the mistag fractions and Δt resolution function parameters for the signal is dominated by the high-statistics $B_{\rm flav}$ sample. The largest correlation between sin2β and any linear combination of the other free parameters is 0.14.

Figure 4 shows the Δt distributions and A_{CP} as a function of Δt overlaid with the likelihood fit result for the $\eta_f = -1$ and $\eta_f = +1$ samples. The fit to the B_{CP} and $B_{\rm flav}$ samples yields

$$\sin 2\beta = 0.75 \pm 0.09 \text{ (stat)} \pm 0.04 \text{ (syst)}.$$

The dominant sources of systematic error are the uncertainties in the level, composition, and *CP* asymmetry of the background in the selected *CP* events (0.022), limited Monte Carlo simulation statistics (0.014), and the assumed parameterization of the Δt resolution function (0.013), due in part to residual uncertainties in the internal alignment of the vertex detector. Uncertainties in Δm_d and τ_{B^0} each contribute 0.010 to the systematic error. The large sample of reconstructed events allows a number of consistency checks, including separation of the data by decay mode, tagging category and $B_{\rm tag}$ flavor. The results of fits to some subsamples and to the samples of non-*CP* decay modes are shown in Table 2. For the latter, no statistically significant asymmetry is found.

With the theoretically preferred choice of the strong phases, consistent with the hypothesis of the s-quark helicity conservation in the decay [8], the parameter cos2β is measured to be $+3.3^{+0.6}_{-1.0}$ (stat)$^{+0.6}_{-0.7}$ (syst) [4].

If the parameter $|\lambda|$ in Eq. 1 is allowed to float in the fit to the $\eta_f = -1$ sample, which has high purity and requires minimal assumptions on the effect of backgrounds, the value obtained is $|\lambda| = 0.92 \pm 0.06$ (stat) ± 0.02 (syst). The sources of the systematic error are the same as for the sin2β measurement with an additional contribution in quadrature of 0.012 from the uncertainty on the difference in the tagging efficien-

Table 2: Number of tagged events, signal purity and observed *CP* asymmetries in the *CP* samples and control samples. Errors are statistical only.

Sample	$N_{\rm tag}$	Purity (%)	sin2β
$J/\psi\, K^0_S$,$\psi(2S)K^0_S$,$\chi_{c1}K^0_S$	995	94	0.76 ± 0.10
$J/\psi\, K^0_L$	742	57	0.73 ± 0.19
$J/\psi\, K^{*0}$, $K^{*0} \to K^0_S\pi^0$	113	83	0.62 ± 0.56
Full *CP* sample	1850	79	0.75 ± 0.09
$B_{\rm flav}$ non-*CP* sample	17546	85	0.00 ± 0.03
Charged B non-*CP* sample	14768	89	-0.02 ± 0.03

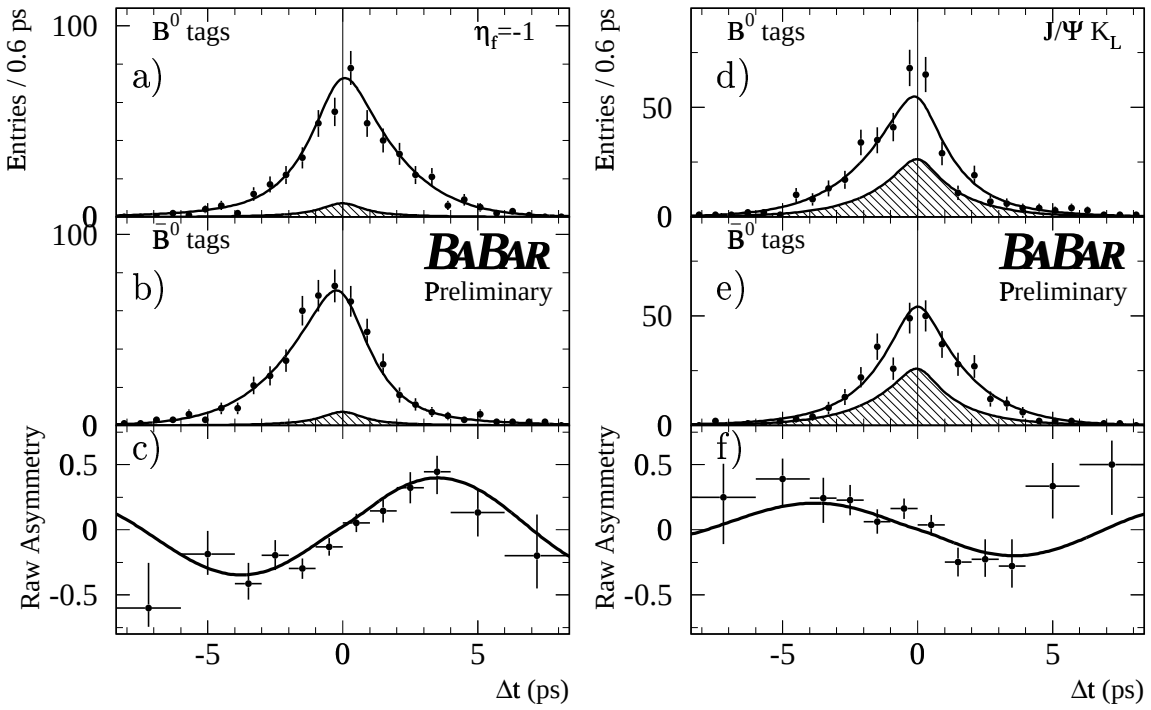

Figure 4: Number of $\eta_f = -1$ candidates ($J/\psi K^0_s$, $\psi(2S)K^0_s$, $\chi_{c1}K^0_s$) in the signal region a) with a B^0 tag N_{B^0} and b) with a $\overline{B}^0$ tag $N_{\overline{B}^0}$, and c) the raw asymmetry $(N_{B^0} - N_{\overline{B}^0})/(N_{B^0} + N_{\overline{B}^0})$, as functions of Δt. The solid curves represent the result of the combined fit to the full $B_{\rm CP}$ sample. The shaded regions represent the background contributions. Figures d) – f) contain the corresponding information for the $\eta_f = +1$ mode $J/\psi K^0_L$.

cies for B^0 and $\overline{B}^0$ tagged events. In this fit, the coefficient of the $\sin(\Delta m_d \Delta t)$ term in Eq. 1 is measured to be 0.76 ± 0.10 (stat) in agreement with Table 1.

6 Summary

We have presented a new preliminary measurement of *CP*-violating asymmetry $\sin 2\beta$ using a sample of fully reconstructed B mesons decaying into *CP* final states.

Ever since this Conference we have further improved the analysis and updated our measurement [10]. Changes in the analysis with respect to the result presented here include a new flavor-tagging algorithm and the addition of the decay mode $B^0 \to \eta_c K^0_s$. The new result $\sin 2\beta = 0.741 \pm 0.067$ (stat) ± 0.033 (syst) improves upon and supersedes the result presented at this Conference and provides the most precise

measurement of sin2β currently available. It is consistent with the range implied by measurements and theoretical estimates of the magnitudes of CKM matrix elements in the context of the Standard Model [11].

References

[1] N. Cabibbo, Phys. Rev. Lett. **10**, 531 (1963); M. Kobayashi and T. Maskawa, Prog. Th. Phys. **49**, 652 (1973).

[2] A.B. Carter and A.I. Sanda, Phys. Rev. **D23**, 1567 (1981); I.I. Bigi and A.I. Sanda, Nucl. Phys. **B193**, 85 (1981).

[3] See, for example, L. Wolfenstein, Phys. Rev. **D66**, 010001 (2002).

[4] *BABAR* Collaboration, B. Aubert *et al.*, SLAC-PUB-9153, hep-ex/0203007.

[5] *BABAR* Collaboration, B. Aubert *et al.*, Nucl. Instr. and Methods **A479**, 1 (2002).

[6] *BABAR* Collaboration, B. Aubert *et al.*, SLAC-PUB-9060, hep-ex/0201020, to appear in Phys. Rev. D **.**

[7] Particle Data Group, D.E. Groom *et al.*, Eur. Phys. Jour. C **15**, 1 (2000).

[8] M. Suzuki, Phys. Rev. **D64**, 117503 (2001).

[9] *BABAR* Collaboration, B. Aubert *et al.*, Phys. Rev. Lett. **87**, 091801 (2001).

[10] *BABAR* Collaboration, B. Aubert *et al.*, SLAC-PUB-9293, hep-ex/0207042, submitted to Phys. Rev. Lett. **.**

[11] See, for example, F.J. Gilman, K. Kleinknecht and B. Renk, Eur. Phys. Jour. C **15**, 110 (2000).

$\sin 2\phi_1$ with 45 Million $B\overline{B}$ Pairs at Belle

Masashi Hazumi
Institute of Particle and Nuclear Studies
High Energy Accelerator Research Organization (KEK)
1-1 Oho, Tsukuba-shi, Ibaraki-kun 305-0801, Japan

Abstract

We present an improved measurement of the standard model CP violation parameter $\sin 2\phi_1$ (also known as $\sin 2\beta$) based on a sample of 45×10^6 $B\overline{B}$ pairs collected at the $\Upsilon(4S)$ resonance with the Belle detector at the KEKB asymmetric-energy e^+e^- collider. One neutral B meson is reconstructed in a $J/\psi K^0_S$, $\psi(2S)K^0_S$, $\chi_{c1}K^0_S$, $\eta_c K^0_S$, $J/\psi K^{*0}$, or $J/\psi K^0_L$ CP-eigenstate decay channel and the flavor of accompanying B meson is identified from its decay products. From the asymmetry in the distribution of the time intervals between the two B meson decay points, we obtain $\sin 2\phi_1 = 0.82 \pm 0.12(\mathrm{stat}) \pm 0.05(\mathrm{syst})$.

In the Standard Model (SM), CP violation arises from an irreducible complex phase in the weak interaction quark-mixing matrix (CKM matrix) [1]. In particular, the SM predicts a CP-violating asymmetry in the time-dependent rates for B^0 and $\overline{B}^0$ decays to a common CP eigenstate, f_{CP}, with negligible corrections from strong interactions[2]:

$$A(t) \equiv \frac{\Gamma(\overline{B}^0 \to f_{CP}) - \Gamma(B^0 \to f_{CP})}{\Gamma(\overline{B}^0 \to f_{CP}) + \Gamma(B^0 \to f_{CP})} = -\xi_f \sin 2\phi_1 \sin(\Delta m_d t), \qquad (1)$$

where $\Gamma(B^0, \overline{B}^0 \to f_{CP})$ is the decay rate for a B^0 or $\overline{B}^0$ to f_{CP} dominated by a $b \to c\bar{c}s$ transition at a proper time t after production, ξ_f is the CP eigenvalue of f_{CP}, Δm_d is the mass difference between the two B^0 mass eigenstates, and ϕ_1 is one of the three interior angles of the CKM unitarity triangle, defined as $\phi_1 \equiv \pi - \arg(-V^*_{tb}V_{td}/-V^*_{cb}V_{cd})$. Non-zero values for $\sin 2\phi_1$ were reported by the Belle and BaBar groups[3, 4].

Belle's published measurement of $\sin 2\phi_1$ is based on a 29.1 fb^{-1} data sample containing 31.3×10^6 $B\overline{B}$ pairs produced at the $\Upsilon(4S)$ resonance. In this paper, we report an improved measurement that uses 45×10^6 $B\overline{B}$ pairs (42 fb^{-1}). The data were collected with the Belle detector [5] at the KEKB asymmetric collider [6], which

collides 8.0 GeV e^- on 3.5 GeV e^+ at a small ($\pm$11 mrad) crossing angle. We use events where one of the B mesons decays to f_{CP} at time t_{CP}, and the other decays to a self-tagging state, $f_{\rm tag}$, *i.e.*, a final state that distinguishes B^0 and $\overline{B}^0$, at time $t_{\rm tag}$. The CP violation manifests itself as an asymmetry $A(\Delta t)$, where Δt is the proper time interval between the two decays: $\Delta t \equiv t_{CP} - t_{\rm tag}$. At KEKB, the $\Upsilon(4S)$ resonance is produced with a boost of $\beta\gamma = 0.425$ nearly along the electron beam direction (z direction), and Δt can be determined as $\Delta t \simeq \Delta z/(\beta\gamma)c$, where Δz is the z distance between the f_{CP} and $f_{\rm tag}$ decay vertices, $\Delta z \equiv z_{CP} - z_{\rm tag}$. The Δz average value is approximately 200 μm.

The Belle detector [5] is a large-solid-angle spectrometer that consists of a silicon vertex detector (SVD), a central drift chamber (CDC), an array of aerogel threshold Čerenkov counters (ACC), time-of-flight scintillation counters (TOF), and an electromagnetic calorimeter comprised of CsI(Tl) crystals (ECL) located inside a superconducting solenoid coil that provides a 1.5 T magnetic field. An iron flux-return located outside of the coil is instrumented to detect K^0_L mesons and to identify muons (KLM).

We reconstruct B^0 decays to the following CP eigenstates [1] $J/\psi K^0_S$, $\psi(2S)K^0_S$, $\chi_{c1}K^0_S$, $\eta_c K^0_S$ for $\xi_f = -1$ and $J/\psi K^0_L$ for $\xi_f = +1$. We also use $B^0 \to J/\psi K^{*0}$ decays where $K^{*0} \to K^0_S\pi^0$. Here the final state is a mixture of even and odd CP, depending on the relative orbital angular momentum of the J/ψ and K^{*0}. We find that the final state is primarily $\xi_f = +1$; the $\xi_f = -1$ fraction is $0.19 \pm 0.02({\rm stat}) \pm 0.03({\rm syst})$[7]. For reconstructed $B \to f_{CP}$ candidates other than $J/\psi K^0_L$, we identify B decays using the energy difference $\Delta E \equiv E_B^{\rm cms} - E_{\rm beam}^{\rm cms}$ and the beam-energy constrained mass $M_{\rm bc} \equiv \sqrt{(E_{\rm beam}^{\rm cms})^2 - (p_B^{\rm cms})^2}$, where $E_{\rm beam}^{\rm cms}$ is the beam energy in the center-of-mass system (cms), and $E_B^{\rm cms}$ and $p_B^{\rm cms}$ are the cms energy and momentum of the reconstructed B candidate, respectively. Figure 1 (left) shows the $M_{\rm bc}$ distributions for all B^0 candidates except for $B^0 \to J/\psi K^0_L$ that have ΔE values in the signal region. Table 1 lists the numbers of observed candidates ($N_{\rm rec}$).

Candidate $B^0 \to J/\psi K^0_L$ decays are selected by requiring ECL and/or KLM hit patterns that are consistent with the presence of a shower induced by a neutral hadron. The centroid of the shower is required to be in a 45° cone centered on the K^0_L direction that is inferred from two-body decay kinematics and the measured four-momentum of the J/ψ. Figure 1 (right) shows the $p_B^{\rm cms}$ distribution, calculated with the $B^0 \to J/\psi K^0_L$ two-body decay hypothesis. The histograms are the results of a fit to the signal and background distributions. There are 767 entries in total in the $0.20 \le p_B^{\rm cms} \le 0.45$ GeV/c signal region [2]; the fit indicates a signal purity of 60%. The reconstruction and selection criteria for all of f_{CP} channels used in the measurement

[1] Throughout this paper, when a decay mode is quoted, the inclusion of the charge conjugation mode is implied.

[2] When the K^0_L is identified with the ECL only, the signal region is defined to be $0.20 \le p_B^{\rm cms} \le 0.40$ GeV/c.

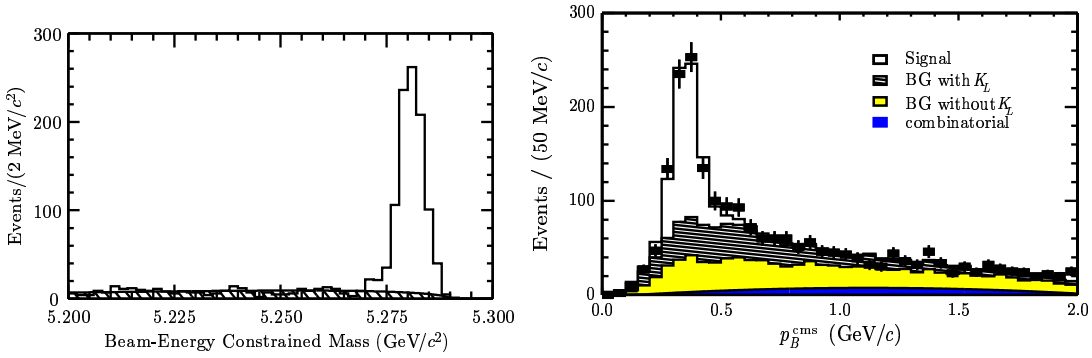

Figure 1: The beam-energy constrained mass distribution for all decay modes combined other than $J/\psi K^0_L$ (left). The $p_B^{\rm cms}$ distribution for $B^0 \to J/\psi K^0_L$ candidates with the results of the fit (right).

are described in more detail elsewhere [3].

Leptons, charged pions, kaons, and Λ baryons that are not associated with a reconstructed CP eigenstate decay are used to identify the b-flavor of the accompanying B meson: high momentum leptons from $b \to c\ell^-\overline{\nu}$; lower momentum leptons from $c \to s\ell^+\nu$; charged kaons and Λ baryons from $b \to c \to s$; fast pions from $B^0 \to D^{(*)-}(\pi^+, \rho^+, a_1^+,$ etc.); and slow pions from $D^{*-} \to \overline{D}^0\pi^-$. Based on the measured properties of these tracks, two parameters, q and r, are assigned to an event. The first, q, has the discrete values $q = \pm 1$ that is $+1$ (-1) when $B_{\rm tag}$ is likely to be a B^0 $(\overline{B}^0)$, and the parameter r is an event-by-event Monte-Carlo-determined flavor-tagging dilution factor that ranges from $r = 0$ for no flavor discrimination to $r = 1$ for an unambiguous flavor assignment. It is used only to sort data into six intervals of r, according to flavor purity; the wrong-tag probabilities, w_l $(l = 1, 6)$, that are used in the final fit are determined directly from data. Samples of B^0 decays to exclusively reconstructed self-tagged channels are utilized to obtain w_l using time-dependent B^0-$\overline{B}^0$ mixing oscillation: $(N_{\rm OF} - N_{\rm SF})/(N_{\rm OF} + N_{\rm SF}) = (1-2w_l)\cos(\Delta m_d \Delta t)$, where $N_{\rm OF}$ and $N_{\rm SF}$ are the numbers of opposite and same flavor events. The total effective tagging efficiency is determined to be $\sum_{l=1}^{6} f_l(1-2w_l)^2 = 0.270 \pm 0.008({\rm stat})^{+0.006}_{-0.009}({\rm syst})$, where f_l is the event fraction for each r interval.

The vertex position for the f_{CP} decay is reconstructed using leptons from J/ψ decays or kaons and pions from η_c and that for $f_{\rm tag}$ is obtained with well reconstructed tracks that are not assigned to f_{CP}. Tracks that are consistent with coming from a $K^0_S \to \pi^+\pi^-$ decay are not used. Each vertex position is required to be consistent with a run-by-run-determined interaction region profile that is smeared in the r-ϕ plane by the B meson decay length. With these requirements, we are able to determine a vertex even with a single track; the fraction of single-track vertices is about 10%

for z_{CP} and 30% for $z_{\rm tag}$. The proper-time interval resolution function, $R_{\rm sig}(\Delta t)$, is formed by convolving four components: the detector resolutions for z_{CP} and $z_{\rm tag}$, the shift in the $z_{\rm tag}$ vertex position due to secondary tracks originating from charmed particle decays, and smearing due to the kinematic approximation used to convert Δz to Δt. A small component of broad outliers in the Δz distribution, caused by misreconstruction, is represented by a Gaussian function. We determine ten resolution parameters from the data from fits to the neutral and charged B meson lifetimes [8] and obtain an average Δt resolution of ~ 1.56 ps (rms). The width of the outlier component is determined to be (36^{+5}_{-4}) ps; the fractional areas are $(6^{+3}_{-2}) \times 10^{-4}$ and $(3.1 \pm 0.4) \times 10^{-2}$ for the multiple- and single-track cases, respectively.

After flavor tagging and vertexing, we find 766 events with $q = +1$ flavor tags and 784 events with $q = -1$. Figure 2 shows the observed Δt distributions for the $q\xi_f = +1$ (solid points) and $q\xi_f = -1$ (open points) event samples. The asymmetry between the two distributions demonstrates the violation of CP symmetry. We determine

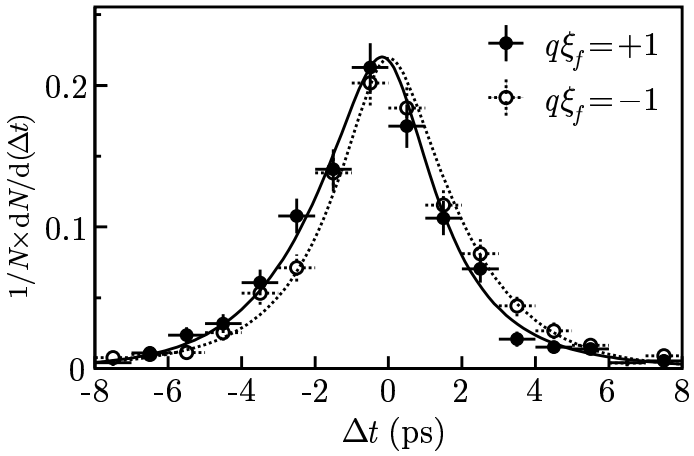

Figure 2: Δt distributions for the events with $q\xi_f = +1$ (solid points) and $q\xi_f = -1$ (open points). The results of the global fit with $\sin 2\phi_1 = 0.82$ are shown as solid and dashed curves, respectively.

$\sin 2\phi_1$ from an unbinned maximum-likelihood fit to the observed Δt distributions. The probability density function (pdf) expected for the signal distribution is given by

$$\mathcal{P}_{\rm sig}(\Delta t, q, w_l, \xi_f) = \frac{e^{-|\Delta t|/\tau_{B^0}}}{4\tau_{B^0}}[1 - q\xi_f(1-2w_l)\sin 2\phi_1 \sin(\Delta m_d \Delta t)], \qquad (2)$$

where we fix the B^0 lifetime (τ_{B^0}) and mass difference at their world average values[9]. Each pdf is convolved with the appropriate $R_{\rm sig}(\Delta t)$ to determine the likelihood value

for each event as a function of $\sin 2\phi_1$:

$$P_i = (1-f_{\rm ol})\int\Big[f_{\rm sig}\mathcal{P}_{\rm sig}(\Delta t',q,w_l,\xi_f)R_{\rm sig}(\Delta t-\Delta t') + (1-f_{\rm sig})\mathcal{P}_{\rm bkg}(\Delta t')R_{\rm bkg}(\Delta t-\Delta t')\Big]d\Delta t' + f_{\rm ol}P_{\rm ol}(\Delta t), \quad (3)$$

where $f_{\rm sig}$ is the signal probability calculated as a function of $p_B^{\rm cms}$ for $J/\psi K_L^0$ and of ΔE and $M_{\rm bc}$ for other modes. $\mathcal{P}_{\rm bkg}(\Delta t)$ is the pdf for combinatorial background events, which is modeled as a sum of exponential and prompt components. It is convolved with a sum of two Gaussians, $R_{\rm bkg}$, which is regarded as a resolution function for the background. To account for a small number of events that give large Δt in both the signal and background, we introduce the pdf, $P_{\rm ol}$, and the fractional area, $f_{\rm ol}$, of the outlier component. The only free parameter in the final fit is $\sin 2\phi_1$, which is determined by maximizing the likelihood function $L = \prod_i P_i$, where the product is over all events. The result of the fit is

$$\sin 2\phi_1 = 0.82 \pm 0.12({\rm stat}) \pm 0.05({\rm syst}).$$

The sources of the systematic error are listed in Table 2. The systematic error is dominated by uncertainties in the vertex reconstruction. Other significant contributions come from uncertainties in the wrong tag fractions, the resolution function parameters and the $J/\psi K_L^0$ background fraction.

A number of checks on the measurement are performed. Table 3 lists the results obtained by applying the same analysis to various subsamples. All values are statistically consistent with each other. Figure 3(a), (b), and (c) show the raw asymmetries and the fit results for all modes combined, $(c\overline{c})K_S^0$, and $J/\psi K_L^0$, respectively. A fit to the non-CP eigenstate self-tagged modes $B^0 \to D^{(*)-}\pi^+$, $D^{*-}\rho^+$ and $J/\psi K^{*0}(K^+\pi^-)$, where no asymmetry is expected, yields $0.05 \pm 0.04({\rm stat})$. Figure 3(d) shows the raw asymmetry for these non-CP control samples.

Finally we comment on the possibility of direct CP violation. The signal pdf for a neutral B meson decaying into a CP eigenstate (Eq. (2)) can be expressed in a more general form as

$$\mathcal{P}_{\rm sig}(\Delta t,q,w_l,\xi_f) = \frac{e^{-|\Delta t|/\tau_{B^0}}}{4\tau_{B^0}}\Big\{1+q(1-2w_l)\Big[\frac{2|\lambda|(-\xi_f)a_{CP}}{|\lambda|^2+1}\sin(\Delta m_d\Delta t) + \frac{|\lambda|^2-1}{|\lambda|^2+1}\cos(\Delta m_d\Delta t)\Big]\Big\}, \quad (4)$$

where λ is a complex parameter that depends on both B^0-$\overline{B}^0$ mixing and on the amplitudes for B^0 and $\overline{B}^0$ decay to a CP eigenstate. The parameter a_{CP} in the coefficient of $\sin(\Delta m_d\Delta t)$ is given by $a_{CP} = -\xi_f Im\lambda/|\lambda|$ and is equal to $\sin 2\phi_1$ in the SM. The presence of the cosine term ($|\lambda| \neq 1$) would indicate direct CP violation;

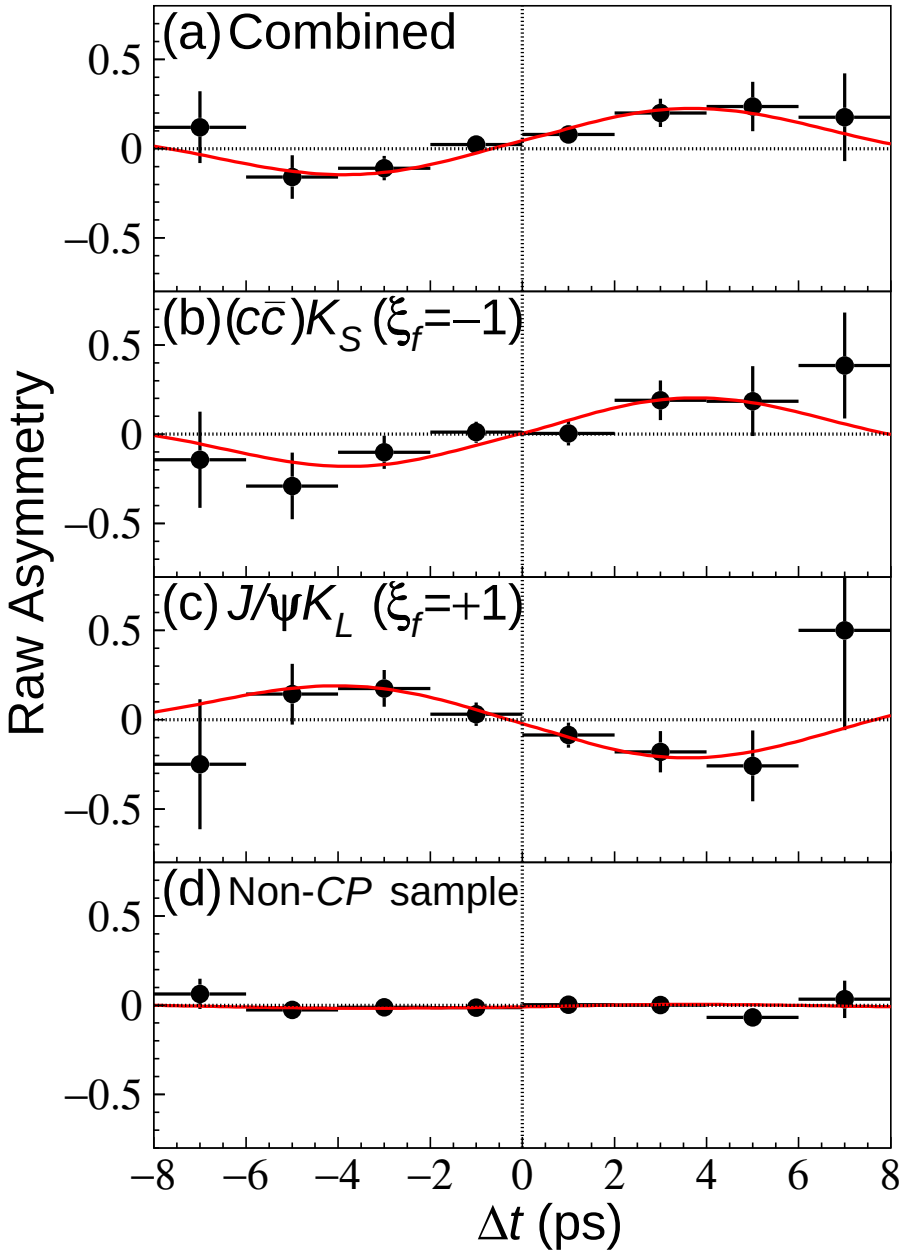

Figure 3: (a) The raw asymmetry for all modes combined. The asymmetry for $J/\psi K^0_L$ and $J/\psi K^{*0}$ is inverted to account for the opposite CP eigenvalue. The corresponding plots for (b) $(c\overline{c})K^0_S$, (c) $J/\psi K^0_L$, and (d) non-CP control samples are also shown. The curves are the results of the unbinned maximum likelihood fit applied separately to the individual data samples.

the value for $\sin 2\phi_1$ reported above is determined with the assumption $|\lambda| = 1$, as expected in the SM. In order to test this assumption, we also performed a fit using the above expression with a_{CP} and $|\lambda|$ as free parameters, keeping everything else the same. We obtain $|\lambda| = 1.01^{+0.08}_{-0.07}(\text{stat})$ and $a_{CP} = 0.82 \pm 0.12(\text{stat})$ for all CP modes combined. This result confirms the assumption used in our analysis.

We wish to thank the KEKB accelerator group for the excellent operation of the KEKB accelerator. We acknowledge support from the Ministry of Education, Culture, Sports, Science, and Technology of Japan and the Japan Society for the Promotion of Science; the Australian Research Council and the Australian Department of Industry, Science and Resources; the National Science Foundation of China under contract No. 10175071; the Department of Science and Technology of India; the BK21 program of the Ministry of Education of Korea and the CHEP SRC program of the Korea Science and Engineering Foundation; the Polish State Committee for Scientific Research under contract No. 2P03B 17017; the Ministry of Science and Technology of the Russian Federation; the Ministry of Education, Science and Sport of the Republic of Slovenia; the National Science Council and the Ministry of Education of Taiwan; and the U.S. Department of Energy.

References

[1] M. Kobayashi and T. Maskawa, Prog. Theor. Phys. **49**, 652 (1973).

[2] A. B. Carter and A. I. Sanda, Phys. Rev. D **23**, 1567 (1981); I. I. Bigi and A. I. Sanda, Nucl. Phys. **B193**, 85 (1981).

[3] K. Abe *et al.* (Belle Collab.), Phys. Rev. Lett. **87**, 091802 (2001); K. Abe *et al.* (Belle Collab.), hep-ex/0202027, accepted for publication in Phys. Rev. D.

[4] B. Aubert *et al.* (BaBar Collab.), Phys. Rev. Lett. **87**, 091801 (2001); B. Aubert *et al.* (BaBar Collab.), hep-ex/0201020, submitted to Phys. Rev. D.

[5] A. Abashian *et al.* (Belle Collab.), Nucl. Instr. and Meth. A **479**, 117 (2002).

[6] E. Kikutani ed., KEK Preprint 2001-157 (2001), to appear in Nucl. Instr. and Meth. A.

[7] K. Abe *et al.* (Belle Collab.), Phys. Lett. B **538**, 11 (2002).

[8] K. Abe *et al.* (Belle Collab.), Phys. Rev. Lett. **88**, 171801 (2002).

[9] K. Hagiwara *et al.*, Particle Data Group, Phys. Rev. D **66**, 010001 (2002).

Mode	$N_{\rm rec}$	$N_{\rm bkg}$
$J/\psi(\ell^+\ell^-)K^0_S(\pi^+\pi^-)$	636	31.2
$J/\psi(\ell^+\ell^-)K^0_S(\pi^0\pi^0)$	102	20.8
$\psi(2S)(\ell^+\ell^-)K^0_S(\pi^+\pi^-)$	49	2.4
$\psi(2S)(J/\psi\pi^+\pi^-)K^0_S(\pi^+\pi^-)$	57	4.3
$\chi_{c1}(J/\psi\gamma)K^0_S(\pi^+\pi^-)$	34	2.3
$\eta_c(K^+K^-\pi^0)K^0_S(\pi^+\pi^-)$	39	11.1
$\eta_c(K^0_SK^-\pi^+)K^0_S(\pi^+\pi^-)$	33	8.9
$J/\psi(\ell^+\ell^-)K^{*0}(K^0_S\pi^0)$	55	6.0
$J/\psi(\ell^+\ell^-)K^0_L$	767	307

Table 1: The numbers of observed candidates ($N_{\rm rec}$) and the estimated background ($N_{\rm bkg}$) in the signal region for each f_{CP} mode.

source	+error	−error
vertex reconstruction	+0.030	−0.030
wrong tag fraction	+0.024	−0.026
resolution function	+0.022	−0.019
background fraction ($J/\psi K^0_L$)	+0.014	−0.015
background fraction (except for $J/\psi K^0_L$)	+0.007	−0.006
τ_{B^0} and Δm_d	+0.007	−0.006
total	+0.048	−0.048

Table 2: List of systematic errors on $\sin 2\phi_1$.

Sample	$\sin 2\phi_1$
$f_{\rm tag} = B^0$ $(q = +1)$	0.60 ± 0.19
$f_{\rm tag} = \overline{B}^0$ $(q = -1)$	0.99 ± 0.16
$J/\psi K^0_S(\pi^+\pi^-)$	0.67 ± 0.18
$(c\overline{c})K^0_S$ except $J/\psi K^0_S(\pi^+\pi^-)$	0.88 ± 0.31
$J/\psi K^0_L$	1.14 ± 0.23
$J/\psi K^{*0}(K^0_S\pi^0)$	1.62 ± 1.10
All	0.82 ± 0.12

Table 3: The values of $\sin 2\phi_1$ for various subsamples (statistical errors only).

New Physics in $B \to J/\psi K^*$[1]

David London
Laboratoire René J.-A. Lévesque
Université de Montréal
C.P. 6128, succ. centre-ville
Montréal, QC, CANADA H3C 3J7

Nita Sinha and Rahul Sinha
The Institute of Mathematical Sciences
Taramani, Chennai 600113 INDIA

CP violation in the B system [1] has been established by the recent measurements of $\sin 2\beta$, with a world average of $\sin 2\beta = 0.78 \pm 0.08$ [2]. The main B decay used to probe the weak phase β is the so-called "gold-plated" mode $B^0_d(t) \to J/\psi K_S$. In order to extract weak-phase information cleanly, i.e. with no hadronic uncertainties, a given B decay must be dominated by a single weak decay amplitude. However, even within the SM, $B^0_d \to J/\psi K_S$ receives contributions from two weak amplitudes: the tree amplitude and the $b \to s$ penguin amplitude. Nevertheless, this decay mode is very clean for the following two reasons. First, the $c\bar{c}$ quark pair must be produced in a color-singlet state, requiring three gluons in the penguin amplitude. Consequently, the penguin contribution is expected to be considerably smaller than the tree contribution. Second, in the Wolfenstein parameterization [3] the CKM matrix elements involved in the $b \to s$ penguin amplitude ($V^*_{tb}V_{ts}$) and in the tree amplitude ($V^*_{cb}V_{cs}$) are both real. Thus, the weak phases of these two amplitudes are the same, so that effectively only a single weak amplitude contributes to $B^0_d \to J/\psi K_S$. The extraction of the CP phase β from this decay mode is therefore extremely clean.

The decay $B^0_d(t) \to J/\psi K^*$ is also a clean mode, for exactly the same reasons as above. The complication, in comparison to $B^0_d(t) \to \psi K_S$, is that the final state now consists of two vector particles, so that the CP-even and CP-odd components must be distinguished by performing an angular analysis [1]. Each component can then be treated separately, and β can be obtained cleanly.

In the presence of new physics, the extraction of the weak phase β may not be clean. If the new physics contributes only to B^0_d–$\overline{B}^0_d$ mixing, the measurement of β remains clean, though the measured value is not the true SM value, but rather one which is shifted by a new-physics phase. On the other hand, if new physics affects the decay amplitude, then the extraction of β is no longer clean – it may be contaminated by hadronic uncertainties. It is this situation which interests us.

[1] Talk given by Rahul Sinha

How can new physics affect the decay amplitude? This can occur if there are new contributions to the $b \to s$ penguin amplitude[4], so that this amplitude no longer has the same weak phase as the tree amplitude. There are a variety of new-physics models in which this can occur. These include, for example, supersymmetric models with R-parity breaking, Z- and Z'-mediated flavor-changing neutral currents [5], and the Top-Higgs doublet model [6].

An obvious question is then: how does one see new-physics contributions to the decay amplitudes if they are present? The standard method is to search for direct CP violation. In the presence of two decay amplitudes, the full amplitude for the decay $B \to f$ can be written as

$$A(B \to f) = ae^{i\phi_a}e^{i\delta^a} + be^{i\phi_b}e^{i\delta^b} \ . \tag{1}$$

Here, $\phi_{a,b}$ and $\delta^{a,b}$ are, respectively, the weak and strong phases of the two contributing amplitudes. The amplitude for the CP-conjugate decay $\overline{B} \to \overline{f}$ can be obtained from the above by changing the signs of the weak phases. The direct CP asymmetry a_{dir}^{CP} is then given by

$$a_{dir}^{CP} = \frac{\Gamma(B \to f) - \Gamma(\overline{B} \to \overline{f})}{\Gamma(B \to f) + \Gamma(\overline{B} \to \overline{f})} = -\frac{2ab\sin(\phi_a - \phi_b)\sin(\delta^a - \delta^b)}{a^2 + b^2 + 2ab\cos(\phi_a - \phi_b)\cos(\delta^a - \delta^b)} \ . \tag{2}$$

This expression holds for both neutral and charged B decays. Thus, if new physics is present, we can expect to see direct CP violation in both $\overset{(-)}{B}{}_d^0 \to J/\psi K_s$ and $B^\pm \to J/\psi K^\pm$ decays.

It is obvious from Eq. (2) that an observable direct asymmetry requires not only a nonzero weak-phase difference between the two decay amplitudes, but also a strong-phase difference. However, it has been argued that since the b-quark is rather heavy, all strong phases in B decays should be quite small. If the strong phases of the two amplitudes happen to be almost equal, there will be no observable signal of direct CP violation, even though new physics is present. Hence new physics may be hard to find using direct asymmetries.

One is therefore led to the question: *if the strong-phase differences vanish, is there any way of detecting the presence of new physics?* As we show below, the answer to this question is *yes*, if one uses the final state $J/\psi K^*$ rather than $J/\psi K$. As above, we assume that there are two contributions to the decay amplitude, coming from the SM and from new physics. The weak phase of the SM contribution is zero, while the new physics contribution has a nonzero weak phase. Since the final state consists of two vector mesons, there are three helicity amplitudes. These take the form

$$\begin{aligned} A_\lambda \equiv Amp(B \to J/\psi K^*)_\lambda &= a_\lambda e^{i\delta_\lambda^a} + b_\lambda e^{i\phi}e^{i\delta_\lambda^b} \ , \\ \overline{A}_\lambda \equiv Amp(\overline{B} \to J/\psi \overline{K}^*)_\lambda &= a_\lambda e^{i\delta_\lambda^a} + b_\lambda e^{-i\phi}e^{i\delta_\lambda^b} \ , \end{aligned} \tag{3}$$

where the a_λ and b_λ represent the SM and new physics amplitudes, ϕ is the new-physics weak phase, the $\delta_\lambda^{a,b}$ are the strong phases, and the helicity index λ takes the values $\{0, \|, \perp\}$. Using CPT invariance, the full decay amplitudes can be written as

$$\mathcal{A} = Amp(B \to J/\psi K^*) = A_0 g_0 + A_\| g_\| + i\, A_\perp g_\perp \quad , \tag{4}$$

$$\overline{\mathcal{A}} = Amp(\overline{B} \to J/\psi \overline{K}^*) = \overline{A}_0 g_0 + \overline{A}_\| g_\| - i\, \overline{A}_\perp g_\perp \quad , \tag{5}$$

where the g_λ are the coefficients of the helicity amplitudes written in the linear polarization basis. The g_λ depend only on the angles describing the kinematics [7, 8].

We first consider neutral B decays and assume that the $\overset{(-)}{K}{}^*$ is detected through its decay to $K_s\pi^0$, so that both B_d^0 and $\overline{B}_d^0$ decay to the same final state. With the above equations, the time-dependent decay rates for $\overset{(-)}{B}_d(t) \to J/\psi \overset{(-)}{K}{}^*$ can be written as

$$\Gamma\big(\overset{(-)}{B}_d(t) \to J/\psi K^*\big) = e^{-\Gamma t} \sum_{\lambda \le \sigma} \Big(\Lambda_{\lambda\sigma} \pm \Sigma_{\lambda\sigma} \cos(\Delta M t) \mp \rho_{\lambda\sigma} \sin(\Delta M t) \Big) g_\lambda g_\sigma \ . \tag{6}$$

By performing a time-dependent study and angular analysis of the decays $\overset{(-)}{B}_d(t) \to J/\psi \overset{(-)}{K}{}^*$, one can measure the observables $\Lambda_{\lambda\sigma}$, $\Sigma_{\lambda\sigma}$ and $\rho_{\lambda\sigma}$. In terms of the helicity amplitudes $A_0, A_\|, A_\perp$, these can be expressed as follows:

$$\Lambda_{\lambda\lambda} = \frac{|A_\lambda|^2 + |\overline{A}_\lambda|^2}{2} \ , \qquad \Sigma_{\lambda\lambda} = \frac{|A_\lambda|^2 - |\overline{A}_\lambda|^2}{2} \ ,$$

$$\Lambda_{\perp i} = -\mathrm{Im}(A_\perp A_i^* - \overline{A}_\perp \overline{A}_i{}^*) \ , \quad \Lambda_{\|0} = \mathrm{Re}(A_\| A_0^* + \overline{A}_\| \overline{A}_0{}^*) \ ,$$

$$\Sigma_{\perp i} = -\mathrm{Im}(A_\perp A_i^* + \overline{A}_\perp \overline{A}_i{}^*) \ , \quad \Sigma_{\|0} = \mathrm{Re}(A_\| A_0^* - \overline{A}_\| \overline{A}_0{}^*) \ ,$$

$$\rho_{\perp i} = -\mathrm{Re}\Big(\tfrac{q}{p}[A_\perp^* \overline{A}_i + A_i^* \overline{A}_\perp]\Big) \ , \quad \rho_{\perp\perp} = -\mathrm{Im}\Big(\frac{q}{p} A_\perp^* \overline{A}_\perp\Big) \ ,$$

$$\rho_{\|0} = \mathrm{Im}\Big(\tfrac{q}{p}[A_\|^* \overline{A}_0 + A_0^* \overline{A}_\|]\Big) \ , \quad \rho_{ii} = \mathrm{Im}\Big(\frac{q}{p} A_i^* \overline{A}_i\Big) \ , \tag{7}$$

where $i = \{0, \|\}$. In the above, $q/p = \exp(-2\,i\phi_M)$, where ϕ_M is the weak phase in B_d^0–$\overline{B}_d^0$ mixing (in the SM, $\phi_M = \beta$). Note that the direct CP asymmetry a_{dir}^{CP} is proportional to the $\Sigma_{\lambda\lambda}$ observables.

The key observable in the $B \to J/\Psi K^*$ mode is $\Lambda_{\perp i}$. Using the expressions for the amplitudes found in Eq. (3), this can be written as

$$\Lambda_{\perp i} = 2\left[a_\perp b_i \cos(\delta_\perp^a - \delta_i^b) - a_i b_\perp \cos(\delta_\perp^b - \delta_i^a)\right] \sin\phi \ . \tag{8}$$

Even if the strong-phase differences vanish, this observable is still nonzero in the presence of new physics ($\phi \neq 0$), in contrast to the direct CP asymmetry a_{dir}^{CP} given

in Eq. (2). Thus, a complete search for new physics should include the measurement of $\Lambda_{\perp i}$ in addition to a_{dir}^{CP}.

The reason that $\Lambda_{\perp i}$ is proportional to $\cos(\delta_\perp^{a,b} - \delta_i^{b,a})$, rather than $\sin(\delta_\perp^{a,b} - \delta_i^{b,a})$, is that the $\perp$ helicity is CP-odd, while the 0 and $\|$ helicities are CP-even. Thus, $\perp$–0 and $\perp$–$\|$ interferences are CP-odd and switch sign [7, 9, 10, 11] between process and conjugate process. This results in the $\cos(\delta_\perp^{a,b} - \delta_i^{b,a})$ term. Obviously, such interferences will not occur for final states such as $J/\psi K_S$, which have only one helicity state.

As can be seen from Eq. (6), the $\Lambda_{\perp i}$ term is common to both $B_d^0(t)$ and $\overline{B}_d^0(t)$ decay rates. Thus, if one does not distinguish between $B_d^0(t)$ and $\overline{B}_d^0(t)$ decays, and instead simply adds the two rates together, the $\Lambda_{\lambda\sigma}$ terms remain. Note also that these terms are time-independent (i.e. they are not proportional to $\cos\Delta Mt$ or $\sin\Delta Mt$). Therefore, *no tagging or time-dependent measurements are needed to extract* $\Lambda_{\perp i}$! It is only necessary to perform an angular analysis of the final state $J/\psi \overset{(-)}{K}{}^*$, with $\overset{(-)}{K}{}^* \to K_S\pi^0$. Thus, this measurement can even be made at a symmetric B-factory such as CLEO.

The decays $B^\pm \to J/\psi K^{*\pm}$ are even simpler to analyze since no mixing is involved. It is straightforward to see that it is not even necessary to distinguish between B^+ and B^- decays for this measurement. In light of this, one can in principle combine charged and neutral B decays to increase the sensitivity to new physics. One simply performs an angular analysis on all decays in which a J/ψ is produced accompanied by a charged or neutral K^*. A nonzero value of $\Lambda_{\perp i}$ is a smoking-gun signal for new physics.

Now, suppose that $\Lambda_{\perp i}$ is measured to be nonzero. This means that new physics is present, which in turn implies that the measured value of β as extracted from $B_d^0(t) \to J/\psi K_S$ or $B_d^0(t) \to \psi K^*$ is not the true SM value of β. This then raises the following questions. Is it nevertheless possible to obtain the true value of β from measurements of $B_d^0(t) \to \psi K^*$? If not, can one at least constrain the difference $|\beta - \beta^{meas}|$? We explore these questions below.

It is straightforward to show that one cannot extract the true value of β. There are a total of six amplitudes describing $B_d^0(t) \to \psi K^*$ [Eq. (3)]. Experimentally, at best one can measure the magnitudes and relative phases of these six amplitudes, giving 11 measurements. However, there are a total of 13 theoretical parameters describing these amplitudes: 3 a_λ's, 3 b_λ's, 5 strong phase differences, ϕ and β. Since there are more unknown parameters than there are measurements, one cannot obtain any of the unknowns. In particular, it is impossible to extract β.

However, it is still possible to constrain the theoretical parameters. For example, with a bit of algebra one can express b_λ as follows:

$$b_\lambda^2 = \frac{1}{2\sin^2\phi}\left[\Lambda_{\lambda\lambda} - \sqrt{\Lambda_{\lambda\lambda}^2 - \Sigma_{\lambda\lambda}^2}\cos(2\beta_\lambda^{meas} - 2\beta)\right]. \qquad (9)$$

The minimum value of b_λ^2 is easy to find:

$$b_\lambda^2 \geq \frac{1}{2}\left[\Lambda_{\lambda\lambda} - \sqrt{\Lambda_{\lambda\lambda}^2 - \Sigma_{\lambda\lambda}^2}\right]. \tag{10}$$

Thus, if direct CP violation is observed ($\Sigma_{\lambda\lambda} \neq 0$), one can place a lower bound on the new-physics amplitude b_λ, and consequently the scale of new physics. The above bound becomes trivial, i.e. $b_\lambda \geq 0$, if all strong phases are quite small, leading to a vanishing value of $\Sigma_{\lambda\lambda}$. However, even if the strong phases vanish, it is still possible to obtain lower bounds on b_λ and $|\beta - \beta^{meas}|$ using measurements of $\Lambda_{\perp i}$ [12].

R.S. thanks the organizers of FPCP2002 for a wonderful conference. N.S. and R.S. thank D.L. for the hospitality of the Université de Montréal, where part of this work was done. The work of D.L. was financially supported by NSERC of Canada. The work of Nita Sinha was financially supported by a young scientist award of the Department of Science and Technology, India.

References

[1] For a review, see, for example, *The BaBar Physics Book*, eds. P.F. Harrison and H.R. Quinn, SLAC Report 504, October 1998.

[2] R. Patterson, *Conference Summary* talk in this proceedings.

[3] L. Wolfenstein, *Phys. Rev. Lett.* **51** (1983) 1945.

[4] See, for example, M. Gronau and D. London, *Phys. Rev.* **D55** (1997) 2845; Y. Grossman and M.P. Worah, *Phys. Lett.* **395B** (1997) 241.

[5] For a discussion, see K. Leroux and D. London, *Phys. Lett.* **526B** (192002) 97.

[6] G. H. Wu and A. Soni, Phys. Rev. D **62**, 056005 (2000) [arXiv:hep-ph/9911419].

[7] N. Sinha and R. Sinha, *Phys. Rev. Lett.* **80** (1998) 3706.

[8] A.S. Dighe I. Dunietz and R. Fleischer, *Eur. Phys. J.* **C6** (1999) 647.

[9] G. Valencia, Phys. Rev. D **39**, 3339 (1989);

[10] G. Burdman and J. F. Donoghue, Phys. Rev. D **45**, 187 (1992).

[11] X. G. He and W. S. Hou, Phys. Rev. D **58**, 117502 (1998). Our conclusions differ significantly from those drawn in this reference. We do not find new physics models contributing to $\Lambda_{\perp i}$ as discussed in this reference. We also find that there is no need to flavor tag B.

[12] David London, Nita Sinha and Rahul Sinha, in preparation.

New Physics Effects in $B \to J/\Psi K$

Thomas Mannel
Institut für Theoretische Teilchenphysik
University of Karlsruhe
D-76128 Karlsruhe, GERMANY

1 Introduction

At present, we are at the beginning of the B-factory era in particle physics, which will provide valuable insights into CP violation and various tests of the CKM picture of this phenomenon. Among the most interesting B-decay channels is the "gold-plated" mode $B_d \to J/\psi K_S$ [1], which allows the determination of the angle β of the unitarity triangle of the Cabibbo–Kobayashi–Maskawa (CKM) matrix. The present status of these measurements is summarized in other contributions to this conference [2, 3].

In this talk, which is based on a collaboration with Robert Fleischer [4], I consider the neutral mode $B_d \to J/\psi K_S$ together with its charged counterpart $B^\pm \to J/\psi K^\pm$. Making use of the isospin symmetry of strong interactions, we derive a model-independent parametrization of the corresponding decay amplitudes. After a careful analysis of the standard-model contributions, we consider possible new-physics amplitudes and introduce a set of observables, which allows us a general analysis of new-physics effects in the $B \to J/\psi K$ system.

There is a large variety of possible new physics scenarios. One of the most popular one is a supersymmetric extension of the standard model, which has in its most general form a very complicated flavour sector. Other models, like large extra dimension or left-right symmetric models, have similar disadvantages, and a general feature of all these models is an unacceptably large CP violation. It is fair to say that currently there is no generally accepted way to model new physics effects in the flavour sector.

The standard model is the most general renormalizable theory with the desired particle spectrum and interactions, and a generic parametrization of new-physics effects can in principle be obtained by adding "non-renormalizable" dimension-6 operators $\mathcal{O}_i$ [5]

$$\mathcal{L} = \mathcal{L}_{SM} + \frac{1}{\Lambda^2} \sum_i C_i \mathcal{O}_i \tag{1}$$

where the C_i are their coefficients and Λ^2 is the scale of new physics. The problem with this parametrization is that the number of possible operators $\mathcal{O}_i$ is $\mathcal{O}(100)$, such

that this parametrization in its full generality is useless for practical applications. Still it is useful to get an estimate of the size of a possible new physics contribution.

Once we have added the new contributions given by the dimension-6 operators, we proceed in the same way as before and consider a low-energy effective theory by integrating out the top quark and the heavy gauge bosons. The result of this step are four-fermion operators with couplings proportional to

$$G_F = \frac{g^2}{M_W^2} = \frac{1}{< v >^2} \tag{2}$$

while contributions from new physics effects enter with coefficients of order $1/\Lambda^2$. Furthermore, in the standard model we have in addition also CKM factors, such that certain transitions in this model are small and a possible new physics contribution could be observable even for large scales Λ.

However, focussing on $\Delta B = \pm 2$ transition operators the number of possible dimension-6 operators is not very large. Generically these are given by

$$\mathcal{L}_{new}^{\Delta B=2} = \frac{1}{\Lambda^2} \sum C_i \left[(\bar{b}\Gamma_i S_i d_1)(\bar{b}\Gamma_i S_i d_2) \right] \tag{3}$$

where Γ_i is an arbitrary Dirac matrix and S_i indicates the color structure ($S_i \times S_i = 1 \times 1$ or $T^a \times T^a$). Such a contribution will not only change the frequency of the $B - \overline{B}$ oscillations, but can also contribute to the mixing phase, which in the standard model is simply $\sin(2\beta)$.

The interesting point about the $\Delta B = \pm 2$ contribution is that the standard model contribution is very small. The only non-vanishing coefficient in the standard model is the one for $\Gamma_i \times \Gamma_i = \gamma_\mu(1-\gamma_5) \times \gamma^\mu(1-\gamma_5)$ and $S_i \times S_i = 1 \times 1$. This coefficient is of the order

$$C_{SM} = \frac{G_{\rm F}}{\sqrt{2}} \left(\frac{G_{\rm F} M_W^2}{\sqrt{128}\pi^2} \right) (V_{td} V_{tb}^*)^2 \tag{4}$$

which is small due to the CKM suppression by two powers of $|V_{td}|$. Furthermore, the standard model diagramms are at least one-loop, in which case one finds another suppression by a loop factor $1/(16\pi^2)$. It has already been pointed out some time ago [6] that this leads to a significant sensitivity to new physics in the $\Delta B = \pm 2$ sector. Furthermore, an ansatz of this type is the B-physics analogue of the superweak model invented in the context of kaon-CP violation.

To get a rough idea of possible new physics effects in $B - \overline{B}$ mixing, we assume the same coupling strenght (including the loop factor) as in the standard model and find

$$C_{NP} = \frac{G_{\rm F}}{\sqrt{2}} \left(\frac{G_{\rm F} M_W^2}{\sqrt{128}\pi^2} \right) \frac{M_W^2}{\Lambda^2} \tag{5}$$

where ψ is an additional weak phase induced by new physics. Adding this new piece to the standard-model contribution we get an estimate for the phase $\phi_{\rm M}$ of $B - \overline{B}$

mixing

$$\tan\phi_{\rm M} = \frac{\sin(2\beta) + \varrho^2\sin(2\psi)}{\cos(2\beta) + \varrho^2\cos(2\psi)}, \tag{6}$$

with

$$\varrho = \left(\frac{1}{\lambda^3 A R_t}\right)\left(\frac{M_W}{\Lambda}\right) \tag{7}$$

where λ is the Wolfenstein parameter and R_t is the length of side opposite to γ of the unitarity triangle. Note that ϱ could be $\mathcal{O}(1)$ due to the presence of the CKM factors, yielding a significant deviation. In turn, this yields a sensitivity up to very high scale, roughly $\Lambda \sim 8$ TeV.

2 Analysis of $B \to J/\Psi K$

The analysis of the $\Delta B = \pm 1$ transitions is much more involved than the $\Delta B = \pm 2$ case, since the number of possible operators is much larger. For that reason it is more convenient to study a particular decay.

For the class of decays $B \to J/\Psi K$ it is convenient to first perform an isospin analysis. The initial as well as the final state carry $I = 1/2$, consequently the effective interaction has either $I = 0$ or $I = 1$. Taking into account the neutral and the charged decay modes we have the following isospin doublets

$$\begin{pmatrix} |+1/2\rangle \\ |-1/2\rangle \end{pmatrix}: \quad \underbrace{\begin{pmatrix} |B^+\rangle \\ |B_d^0\rangle \end{pmatrix}, \begin{pmatrix} |\overline{B_d^0}\rangle \\ -|B^-\rangle \end{pmatrix}}_{CP}, \underbrace{\begin{pmatrix} |J/\psi K^+\rangle \\ |J/\psi K^0\rangle \end{pmatrix}, \begin{pmatrix} |J/\psi \overline{K^0}\rangle \\ -|J/\psi K^-\rangle \end{pmatrix}}_{CP} \tag{8}$$

where we indicated their relation through the CP tranformation.

Purely from isospin we find the relations

$$\langle J/\psi K^+|\mathcal{H}_{\rm eff}^{I=0}|B^+\rangle = +\langle J/\psi K^0|\mathcal{H}_{\rm eff}^{I=0}|B_d^0\rangle \tag{9}$$

$$\langle J/\psi K^+|\mathcal{H}_{\rm eff}^{I=1}|B^+\rangle = -\langle J/\psi K^0|\mathcal{H}_{\rm eff}^{I=1}|B_d^0\rangle \tag{10}$$

where $\mathcal{H}_{\rm eff}^I$ indicates the different isospin components of the effective interaction. Note that these relations are completely general and thus hold even in the presence of new physics.

In the standard model we can write the amplitudes for the decays as

$$A(B^+ \to J/\psi K^+) = \frac{G_{\rm F}}{\sqrt{2}}\left[V_{cs}V_{cb}^*\left\{A_c^{(0)} - A_c^{(1)}\right\} + V_{us}V_{ub}^*\left\{A_u^{(0)} - A_u^{(1)}\right\}\right] \tag{11}$$

$$A(B_d^0 \to J/\psi K^0) = \frac{G_{\rm F}}{\sqrt{2}}\left[V_{cs}V_{cb}^*\left\{A_c^{(0)} + A_c^{(1)}\right\} + V_{us}V_{ub}^*\left\{A_u^{(0)} + A_u^{(1)}\right\}\right], \tag{12}$$

where

$$A_c^{(0)} = A_{\rm CC}^c - A_{\rm QCD}^{\rm pen} - A_{\rm EW}^{(0)}, \quad A_c^{(1)} = -A_{\rm EW}^{(1)} \tag{13}$$

$$A_u^{(0)} = A_{\rm CC}^{u(0)} - A_{\rm QCD}^{\rm pen} - A_{\rm EW}^{(0)}, \quad A_u^{(1)} = A_{\rm CC}^{u(1)} - A_{\rm EW}^{(1)} \tag{14}$$

where CC indicates the contribution from the current-current operators, $QCD-pen$ the one from the QCD penguin operators and EW the one from the electroweak penguins, while the superscript index denotes the isospin of the contribution.

Relations (11) yield an idea about the sizes of the various terms. The explicit CKM factors show a suppression of the terms carrying a weak phase by a factor λ^2. Furthermore, all these contributions correspond to penguin topologies and hence one expects a further, dynamical suppression. It is commonly believed that this is of the order of the Wolfenstein parameter λ, and we shall asusme for the sake of "power counting" that this suppression factor is just λ. Due to the fact that the electroweak penguin contributions are also strongly suppressed by the dynamics and CKM factors, we get the well-known standard-model result

$$A(B^+ \to J/\psi K^+) = A(B_d^0 \to J/\psi K^0) = \frac{G_{\rm F}}{\sqrt{2}} \left(1 - \frac{\lambda^2}{2}\right) \lambda^2 A\, A_c^{(0)} + \mathcal{O}(\lambda^3) \tag{15}$$

A possible new physics contribution can enter this decay mode in various ways. Firstly, there could be an additional weak phase from new physics in the $\Delta B = \pm 2$ which has been discussed above. Secondly, there could be new contributions in both the $I = 0$ and $I = 1$ pieces of the effective Hamiltonian. These contributions are parametrized as

$$A(B^+ \to J/\psi K^+) = A_{\rm SM}^{(0)} \left[1 + \sum_k r_0^{(k)} e^{i\delta_0^{(k)}} e^{i\varphi_0^{(k)}} - \sum_j r_1^{(j)} e^{i\delta_1^{(j)}} e^{i\varphi_1^{(j)}}\right] \tag{16}$$

$$A(B_d^0 \to J/\psi K^0) = A_{\rm SM}^{(0)} \left[1 + \sum_k r_0^{(k)} e^{i\delta_0^{(k)}} e^{i\varphi_0^{(k)}} + \sum_j r_1^{(j)} e^{i\delta_1^{(j)}} e^{i\varphi_1^{(j)}}\right] \tag{17}$$

where $A_{\rm SM}^{(0)}$ is the standard model amplitude, $r_I^{(l)}$ is the Modulus, $\delta_I^{(l)}$ is the strong and $\varphi_I^{(l)}$ the weak phase of the l^{th} contribution with isospin I. Note that according to the above discussion we have $r_I^{(l)} \sim \mathcal{O}(M_W^2/\Lambda^2)$

In order to test for these additional contributions, we look at the observables in the $B \to j/\Psi K$ system. Aside from the information gathered from the measurement of the time-dependent asymmetry in the neutral modes

$$a_{\rm CP}(t) = \mathcal{A}_{\rm CP}^{\rm dir} \cos(\Delta M_d t) + \mathcal{A}_{\rm CP}^{\rm mix} \sin(\Delta M_d t) \tag{18}$$

we suggest to also measure the direct CP asymmetry in the charged modes

$$\mathcal{A}_{\rm CP}^{(+)} = \frac{|A(B^+ \to J/\psi K^+)|^2 - |A(B^- \to J/\psi K^-)|^2}{|A(B^+ \to J/\psi K^+)|^2 + |A(B^- \to J/\psi K^-)|^2} \tag{19}$$

as well as the difference of the CP averaged rates of the charged and the neutral modes ($\langle ... \rangle$ denotes the CP average)

$$B = \frac{\langle |A(B_d \to J/\psi K)|^2 \rangle - \langle |A(B^\pm \to J/\psi K^\pm)|^2 \rangle}{\langle |A(B_d \to J/\psi K)|^2 \rangle + \langle |A(B^\pm \to J/\psi K^\pm)|^2 \rangle} \tag{20}$$

Given the parametrization (16) of new-physics effects, we suggest a slightly different set of observables which is

$$S = \frac{1}{2}\left[\mathcal{A}_{\rm CP}^{\rm dir} + \mathcal{A}_{\rm CP}^{(+)}\right], \quad D = \frac{1}{2}\left[\mathcal{A}_{\rm CP}^{\rm dir} - \mathcal{A}_{\rm CP}^{(+)}\right] \tag{21}$$

and B as given before.

In terms of the parameters introdued in (16) we see that S measures the $I = 0$ new physics contribution

$$S = -2\left[\sum_k r_0^{(k)} \sin\delta_0^{(k)} \sin\varphi_0^{(k)}\right]\left[1 - 2\sum_l r_0^{(l)} \cos\delta_0^{(l)} \cos\varphi_0^{(l)}\right], \tag{22}$$

B is sensitive to a CP conserving $I = 1$ new-physics contribution, while D is sensitive to a CP violating new physics contribution

$$B = +2\sum_j r_1^{(j)} \cos\delta_1^{(j)} \cos\varphi_1^{(j)} \quad D = -2\sum_j r_1^{(j)} \sin\delta_1^{(j)} \sin\varphi_1^{(j)} \tag{23}$$

However, one has to keep in mind the limitations of this approach. The size of the standard-model contributions which are under poor theoretical control is $\mathcal{O}(\lambda^3)$ which means that a possible new physics contributions has to be larger than this.

This work was supported by the DFG Forschergruppe "Quantenfeldtheorie, Computeralgebra und Monte Carlo Simulationen" and by the German Ministry for Education and Research (BMBF).

References

[1] A.B. Carter and A.I. Sanda, *Phys. Rev. Lett.* **45** (1980) 952; *Phys. Rev.* **D23** (1981) 1567; I.I. Bigi and A.I. Sanda, *Nucl. Phys.* **B193** (1981) 85.

[2] S. Rahatlou (BaBar Collaboration), talk at this conference.

[3] M. Hazumi (Belle Collaboration), talk at this conference.

[4] R. Fleischer and T. Mannel, Phys. Lett. B **506**, 311 (2001).

[5] W. Buchmüller and D. Wyler, *Nucl. Phys.* **B268** (1986) 621.

[6] A review is given in: Y. Grossman, Y. Nir and R. Rattazzi, Adv. Ser. Direct. High Energy Phys. **15**, 755 (1998)

May 16, session 2.

Session Chair: A. I. Sanda

Indirect CP violation

$\sin 2\phi_2 (= \alpha)$ from Belle

E. Won

$\sin 2\alpha$ from BABAR

P. Dauncey

Penguin Pollution in $B_d^0 \to \pi\pi$

N. Sinha

Recent Results in Theories of Hadronic B Decays

Recent results from the QCD factorization approach to non-leptonic B decays

M. Beneke

Charming Penguins Saga

M. Ciuchini

$\sin 2\phi_2(=\alpha)$ from Belle

Won, Eunil (representing the Belle Collaboration)
Department of Physics
Korea University
Seoul 136-701 Korea

1 Introduction

Recent measurements of the CP-violating parameter $\sin 2\phi_1$ by Belle [1] and BaBar [2] collaborations established CP violation in the neutral B meson system that is consistent with Kobayashi and Maskawa (KM) expectations [3]. Therefore, measurements of other CP-violating parameters such as ϕ_2 and ϕ_3 provide important tests of the KM model. In this note we describe a measurement of CP-violating asymmetries in the mode $B^0 \to \pi^+\pi^-$ which are sensitive to the parameter $\sin 2\phi_2$.

The KM model predicts CP-violating asymmetries in the time-dependent rates for B^0 and $\overline{B}^0$ decays to a common CP eigenstates, f_{CP} [4]. When the $\Upsilon(4S)$ decays into a $B^0\overline{B}^0$ meson pair, the two mesons remain in a coherent p-wave state until one of them decays. The decay of one of the B mesons at time t_{tag} to a final state, f_{tag}, which distinguishes between B^0 and $\overline{B}^0$, projects the accompanying B meson onto the opposite b-flavor at τ_{tag}; this meson decays to $\pi^+\pi^-$ at time t_{CP}. The decay rate has a time dependence given by [5]

$$P^q_{\pi\pi}(\Delta t) = \frac{e^{-|\Delta t|/\tau_{B^0}}}{4\tau_{B^0}}[1 + q\cdot\{S_{\pi\pi}\sin(\Delta m_d\Delta t) + A_{\pi\pi}\cos(\Delta m_d\Delta t)\}], \quad (1)$$

where τ_{B^0} is the B^0 lifetime, Δm_d is the mass difference between the two B^0 mass eigenstates, $\Delta t = t_{CP} - t_{tag}$, and the b-flavor charge $q = +1$ (-1) when the tagging B meson is a B^0 ($\overline{B}^0$). The CP-violating parameters $S_{\pi\pi}$ and $A_{\pi\pi}$ defined in Eq. (1) are expressed by

$$S_{\pi\pi} = \frac{2Im\lambda}{|\lambda|^2+1} \text{ and } A_{\pi\pi} = \frac{|\lambda|^2-1}{|\lambda|^2+1} \quad (2)$$

where λ is a complex parameter that depends on both $B^0\overline{B}^0$ mixing and on the amplitudes for B^0 and $\overline{B}^0$ decays to $\pi^+\pi^-$. In the Standard Model, to a good approximation, $|\lambda|$ is equal to the absolute value of the ratio of the $\overline{B}^0$ to B^0 decay amplitudes. Therefore $|\lambda| \neq 1$, or equivalently $A_{\pi\pi} \neq 0$, indicates direct CP violation.

In the case of $B^0 \to (c\overline{c})K^0_s$ CP eigenstate decays, the CP-violating parameters are rather precisely expressed as $S_{(c\bar{c})K^0_s} = \sin 2\phi_1$ and $A_{(c\bar{c})K^0_s} = 0$. This is due to the fact that the tree amplitude with W emission dominates the $b \to s$ penguin amplitude with associated $c\overline{c}$ production, which is small and has the same weak phase. For the $B^0 \to \pi^+\pi^-$ decay, we would have $S_{\pi\pi} = \sin 2\phi_2$ and $A_{\pi\pi} = 0$ if the $b \to u$ tree amplitude were dominant. The situation is complicated by the possibility of significant contributions from gluonic $b \to d$ penguin amplitudes that have a different weak phase and additional strong phases [6]. As a result, $S_{\pi\pi}$ may not be equal to $\sin 2\phi_2$ and direct CP violation, $A_{\pi\pi} \neq 0$, may occur. One can quantify the contributions from penguin amplitude as $\sin 2(\phi_2 + \theta)$ and determine θ using other decays. However, it requires measurements of branching fractions of $B^0 \to \pi^0\pi^0$ and $\overline{B}^0 \to \pi^0\pi^0$ separately, which is experimentally not within reach at this moment [7].

This measurement of CP-violating parameters in $B^0 \to \pi^+\pi^-$ is based on a 41.8 fb^{-1} data sample, which contains 44.1 million $B\overline{B}$ pairs, collected with the Belle detector at the KEKB asymmetric-energy e^+e^- (3.5 on 8 GeV) collider operating at the $\Upsilon(4S)$ resonance.

2 Event Selection

We use oppositely charged pairs of well measured tracks that are positively identified as pions according to the combined information from the ACC and the CDC dE/dx measurement. Candidate B mesons are reconstructed using the energy difference $\Delta E \equiv E_B^{cms} - E_{beam}^{cms}$ and the beam energy constrained mass $M_{bc} \equiv \sqrt{(E_{beam}^{cms})^2 - (p_B^{cms})^2}$, where E_{beam}^{cms} is the cms beam energy, and E_B^{cms} and p_B^{cms} are the cms energy and momentum of the B candidate. The signal region is defined as $5.271\ \mathrm{GeV}/c^2 < M_{bc} < 5.287\ \mathrm{GeV}/c^2$ and $|\Delta E| < 0.067$ GeV, corresponding to $\pm 3\sigma$ from the central values. In order to suppress background from the $e^+e^- \to q\overline{q}$ continuum ($q = u, d, s, c$), we form signal and background likelihood functions, $\mathcal{L}_S$ and $\mathcal{L}_{BG}$, from two variables. One is a Fisher discriminant determined from six modified Fox-Wolfram moments [8] and the other is the B flight direction in the cms, with respect to the z axis ($\cos\theta_B$). We determine $\mathcal{L}_S$ from Monte Carlo (MC) and $\mathcal{L}_{BG}$ from data. The likelihood ratio $\mathcal{L}_S/\ (\mathcal{L}_S + \mathcal{L}_{BG})$ for candidate events is required to be greater than 0.825. Figure 1 shows the ΔE distribution for $\pi^+\pi^-$ candidates. The signal yield is extracted by fitting the ΔE distribution with a Gaussian $\pi^+\pi^-$ signal function, plus contributions from misidentified $B^0 \to K^+\pi^-$ events, three-body B-decays, and continuum back-

ground. From the fit, we obtain 73.5 $\pm$ 13.8 events, 28.4 $\pm$ 12.5 $K^+\pi^-$ events, and 98.7 $\pm$ 7.0 continuum background events in the signal region, where errors are statistical only. The $K^+\pi^-$ contamination level is consistent with the $K \to \pi$ misidentification probability measured independently, and the contribution from three-body B-decays is little in the signal region.

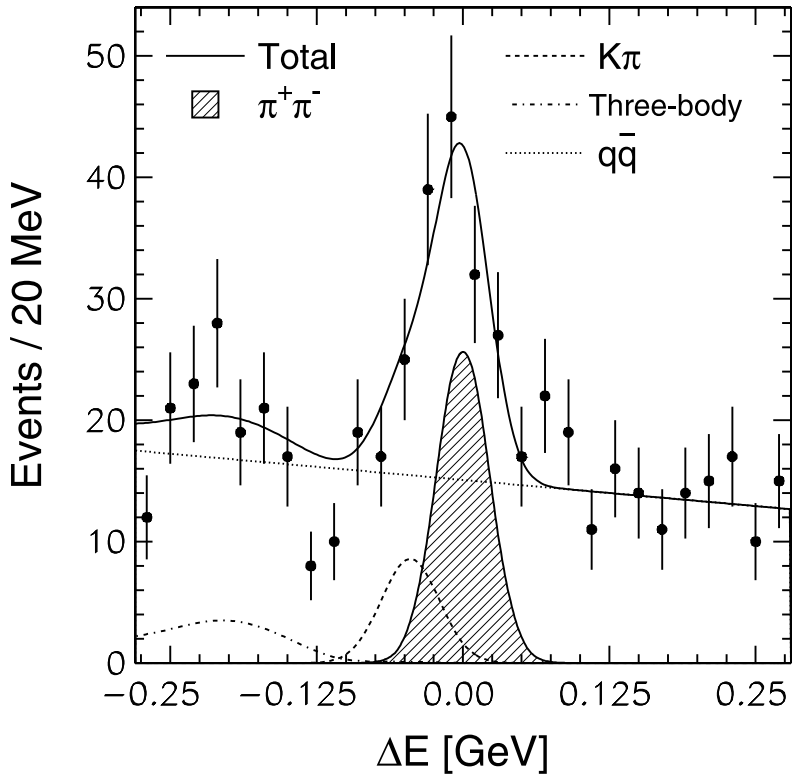

Figure 1: ΔE distribution for $\pi^+\pi^-$ event candidates that are in the M_{bc} signal region. Closed circles with error bars are the data, and individual curves are results of fits using various components indicated in the figure.

Leptons, charged pions, and kaons that are not associated with the reconstructed $B^0 \to \pi^+\pi^-$ decay are used to identify the flavor of the accompanying B meson. We apply the same method used for the $\sin 2\phi_1$ measurement [1]. We use two parameters, q and r, to represent the tagging information. The first, q, corresponds to the sign of the b quark charge where $q = +1$ for $\bar{b}$ and hence B^0, and $q = -1$ for b and $\overline{B}^0$. The parameter r is an event-by-event, MC-determined flavor-tagging dilution factor that ranges from $r = 0$ for no flavor discrimination to $r = 1$ for unambiguous flavor assignment. It is used only to sort data into six intervals of r, according to flavor purity.

The wrong tag fractions, w_l (l=1,6), are determined directly from the data for the six r intervals using exclusively reconstructed, self-tagged $B^0 \to D^{*-}l^+\nu$,$D^{(*)}\pi^+$, and $D^{*-}\rho^+$ decays. The b-flavor of the accompanying B meson is assigned according to the flavor-tagging algorithm described above. The decay vertices are reconstructed using the same algorithm used for the accompanying B mesons of $B^0 \to \pi^+\pi^-$ candidates. The values of w_l are obtained from the time evolution of neutral B meson pairs with opposite flavor (OF) or same flavor (SF), which is given by $P_{OF[SF]}(\Delta t) = e^{-|\Delta t|/\tau_{B^0}}/4\tau_{B^0}\ \{1+[-](1-2w_l)\cos(\Delta m_d \Delta t)\}$. For the fits, we fix Δm_d at the world average value [9].

The vertex positions for the $\pi^+\pi^-$ and f_{tag} decays are reconstructed using tracks that have at least one three-dimensional coordinate determined from associated $r-\phi$ and z hits in the same SVD layer and one or more additional z hits in the other layers. Each vertex position is required to be consistent with the interaction point profile smeared in the $r-\phi$ plane by the average transverse B meson decay length. The f_{tag} vertex is determined from all well reconstructed tracks, excluding the $B^0 \to \pi^+\pi^-$ candidate. Tracks that form a K^0_s candidate are not used. The MC simulation indicates that the typical vertex-finding efficiency is 92% and 91% for $\pi^+\pi^-$ and f_{tag}, respectively, while the typical vertex rms resolution in the z coordinate is 75 μm for $B^0 \to \pi^+\pi^-$ decays and 140 μm for f_{tag} decays.

The proper-time interval resolution for the signal, $R_{sig}(\Delta t)$, is obtained by convolving a sum of two Gaussians with a function that takes into account the cms motion of the B mesons. The fraction in the main Gaussian is determined to be 0.97 $\pm$ 0.02 from a study of $B^0 \to D^{*-}\pi^+$, $D^{*-}\rho^+$, $D^-\pi^+$, $J/\psi K^{*0}$, $J/\psi K^0_S$ and $B^+ \to \overline{D}^0\pi^+$, $J/\psi K^+$ events. The means ($\mu_{\rm main}$, $\mu_{\rm tail}$) and widths ($\sigma_{\rm main}$, $\sigma_{\rm tail}$) of the Gaussians are calculated event-by-event from the f_{CP} and $f_{\rm tag}$ vertex fit error matrices and the χ^2 values of the fit; typical values are $\mu_{\rm main} = -0.24$ ps, $\mu_{\rm tail} = 0.18$ ps and $\sigma_{\rm main} = 1.49$ ps, $\sigma_{\rm tail} = 3.85$ ps. The background resolution function $R_{q\bar{q}}(\Delta t)$, which is dominated by continuum background, has the same functional form but the parameters are obtained from a sideband region in M_{bc} and ΔE.

3 CP Fit Results

We determine CP violation parameters by performing an unbinned maximum-likelihood fit of a CP-violating probability density function (pdf) to the observed Δt distributions. We define the likelihood value for each event as a function of $S_{\pi\pi}$ and $A_{\pi\pi}$:

$$P_i = \int [\{f^l_{\pi\pi}P^q_{\pi\pi}(\Delta t', w_l; S_{\pi\pi}, A_{\pi\pi}) + f^l_{K\pi}P^q_{K\pi}(\Delta t', w_l)\} \cdot R_{sig}(\Delta t_i - \Delta t') + f^l_{q\bar{q}}P_{q\bar{q}}(\Delta t') \cdot R_{q\bar{q}}(\Delta t_i - \Delta t')] d\Delta t'. \quad (3)$$

Here $f^l_{\pi\pi}$, $f^l_{K\pi}$, and $f^l_{q\bar{q}}$ ($= 1 - f^l_{\pi\pi} - f^l_{K\pi}$) are the fractions of $\pi^+\pi^-$ signal, $K^+\pi^-$ background, and continuum background in flavor-tagging interval l, respectively. These fractions are determined on an event-by-event basis as a function of ΔE and $M_{\rm bc}$, properly normalized by the average signal and background fractions in the signal region. For higher r values where we are more sensitive to the asymmetry, the fraction of continuum background decreases; the ratio of $\pi^+\pi^-$ signal events to background $K^+\pi^-$ events is the same for all r bins. The pdfs for $\pi^+\pi^-$ ($P^q_{\pi\pi}$), $K^+\pi^-$ ($P^q_{K\pi}$), and continuum background ($P_{q\bar{q}}$), are convolved with their respective resolution functions. We use the same vertex resolution function for $\pi^+\pi^-$ and $K^+\pi^-$ candidates. For the $\pi^+\pi^-$ signal, the pdf is given by Eq. (1) with q replaced by $q(1-2w_l)$, to account for the dilution due to wrong flavor tagging. The pdf for the $K^+\pi^-$ background is $P^q_{K\pi}(\Delta t, w_l) = e^{-|\Delta t|/\tau_{B^0}}/4\tau_{B^0}\{1 + q\cdot(1-2w_l)A_{K\pi}\cos(\Delta m_d \Delta t)\}$, where $A_{K\pi}$ is the $\overline{B}^0 \to K^-\pi^+$ and $B^0 \to K^+\pi^-$ decay rate asymmetry. We fix $A_{K\pi} = 0$ and τ_{B^0} and Δm_d to their world average values [9]. Although the $K^+\pi^-$ background contamination is low, a possible deviation of $A_{K\pi}$ from zero is included in the systematic error. The pdf used for the $q\overline{q}$ background distribution is $P_{q\bar{q}}(\Delta t) = \{f_\tau\, e^{-|\Delta t|/\tau_{bkg}}/2\tau_{bkg} + (1\text{-}f_\tau)\delta(\Delta t)\}/2$, where f_τ is the background fraction with an effective lifetime τ_{bkg} and δ is the Dirac delta function. We determine $f_\tau = 0.011 \pm 0.004$ and $\tau_{bkg} = 2.7^{+1.0}_{-0.7}$ ps from the sideband data. In function $\mathcal{L} = \Pi P_i$, where the product is over all $B^0 \to \pi^+\pi^-$ candidates.

The result of the fit to the 162 candidates (92 B^0- and 70 $\overline{B}^0$-tags) that remain after flavor tagging and vertex reconstruction is:

$$\begin{aligned} S_{\pi\pi} &= -1.21\ ^{+0.38}_{-0.27}(\text{stat})\ ^{+0.16}_{-0.13}(\text{syst}); \\ A_{\pi\pi} &= +0.94\ ^{+0.25}_{-0.31}(\text{stat})\ \pm 0.09(\text{syst}). \end{aligned}$$

In Figs. 2(a) and (b), we show the Δt distributions for B^0- and $\overline{B}^0$-tagged events together with the fit curves; the background-subtracted Δt distributions are shown in Fig. 2(c). It appears that there are more B^0 tags than $\overline{B}^0$ tags. Figure 2(d) shows the background-subtracted CP asymmetry between the B^0- and $\overline{B}^0$-tagged events as a function of Δt, with the result of the fit superimposed.

4 Systematic Uncertainties

The systematic error on $S_{\pi\pi}$ is primarily due to uncertainties in the background fractions (± 0.09) and from the fit bias near the physical boundary ($^{+0.11}_{-0.02}$). For $A_{\pi\pi}$, the background fractions (± 0.06) and the wrong-tag fractions (± 0.06) are the two leading components. Other sources of systematic error are uncertainties in the resolution function, physics parameters (Δm_d, τ_{B^0}, and $A_{K\pi}$) and the background modeling. A value of $A_{K\pi} = -0.06 \pm 0.08$ is obtained from the self-tagged $B^0 \to K^+\pi^-$ sample. This introduces a systematic error of < 0.01 for $S_{\pi\pi}$ and $^{+0.02}_{-0.01}$ for $A_{\pi\pi}$.

We perform a number of cross checks. We examine the event yields and Δt distributions for B^0- and $\overline{B}^0$-tagged events in the sideband region and find no significant difference between the two samples. Figure 2(e) shows the observed raw asymmetry in the side band region. We select $B^0 \to K^+\pi^-$ candidates, which have the same track topology as $B^0 \to \pi^+\pi^-$, by positively identifying charged kaons. A fit to 309 events yields $A_{K\pi} = 0.07 \pm 0.17$, consistent with the value mentioned above, and $S_{K\pi}$ 0.15 ± 0.24. We also select $B^0 \to D^-\pi^+$, $D^{*-}\pi^+$ and $D^-\rho^+$ candidates using the same event shape criteria. These are non-CP eigenstate self-tagged modes, where neither mixing-induced nor direct CP-violating asymmetry is expected. We find no asymmetry in these modes. As an additional test of the consistency of the background treatment, we add events from the $B^0 \to \pi^+\pi^-$ sideband and adjust their ΔE and M_{bc} values. A fit to this background-enriched control sample, which has a similar background fraction as the $B^0 \to \pi^+\pi^-$ sample, yields $S = 0.08 \pm 0.06$ and $A = 0.03$ $\pm$ 0.04, both consistent with a null asymmetry. We measured τ_{B^0} from $B^0 \to \pi^+\pi-$ and $K^+\pi^-$ decays and obtained 1.49 ± 0.21 ps and 1.73 ± 0.15 ps, respectively (The world average value is 1.548 ± 0.032 ps [9]). We measured Δm_d from $B^0 \to K^+\pi^-$ and found Δm_d to be 0.57 ± 0.08 ps^{-1}, which is consistent with the current world average value (0.472 ± 0.017 ps^{-1} [9]).

Our central values of $S_{\pi\pi}$ and $A_{\pi\pi}$ are 1.2σ away from the physical boundary ($S^2_{\pi\pi}$ + $A^2_{\pi\pi} < 1$). However, the components of the present analysis are the same as those used to measure $\sin 2\phi_1$, τ_B, and Δm_d, which are all in good agreement with the world average values and we performed ensemble tests and found no indication of bias in the procedure and the likelihood fit errors are in reasonable agreement with expected from ensemble tests. Therefore, we attribute our central values of $S_{\pi\pi}$ and $A_{\pi\pi}$ being outside of the physical boundary as a statistical fluctuation.

5 Conclusions

In summary, we have measured the CP violation parameters in $B^0 \to \pi^+\pi^-$ decay. Our results for $S_{\pi\pi}$ indicates that mixing-induced CP violation is large. The large $A_{\pi\pi}$ term is an indication of direct CP violation in B meson decay, and suggests that there is a large hardronic phase and interference between the tree and penguin amplitudes. In this case, the precise determination of $\sin 2\phi_2$ from $S_{\pi\pi}$ requires additional measurements including the branching fractions for the decays $B^0 \to \pi^0\pi^0$ and $\overline{B}^0 \to$ $\pi^0\pi^0$ [7], which will be performed in the near future at B factories.

References

[1] K. Abe *et al.* (Belle Collab.), Phys. Rev. Lett. **87**, 091802 (2001).

[2] B. Aubert *et al.* (BaBar Collab.), Phys. Rev. Lett. **87**, 091801 (2001).

[3] M. Kobayashi and T. Maskawa, Prog. Theor. Phys. **49**, 652 (1973).

[4] A.B. Carter and A. I. Sanda, Phys. Rev. Lett. **45**, 952 (1980); A.B. Carter and A. I. Sanda, Phys. Rev. D **23**, 1567 (1981); I.I. Bigi and A. I. Sanda, Nucl. Phys. D **193**, 85 (1981).

[5] II. Bigi *et al.* "CP Violation" 175, ed. C. Jarlskog, World Scientific, Singapore (1989).

[6] M. Beneki *et al.* Nucl. Phys. B **606**, 245 (2001).

[7] M. Gronau *et al.* Phys. Lett. B **514**, 315 (2001).

[8] The Fox-Wolfram moments were introduced in G.C. Fox and S. Wolfram, Phys. Rev. Lett. **41**, 1581 (1978). The Fisher discriminant used by Belle is described in K. Abe *et al.* (Belle Collab.), Phys. Rev. Lett. **87**, 101801 (2001).

[9] D. E. Groom *et al.* (Particle Data Group), Eur. Phys. J. **C15**, 1 (2000).

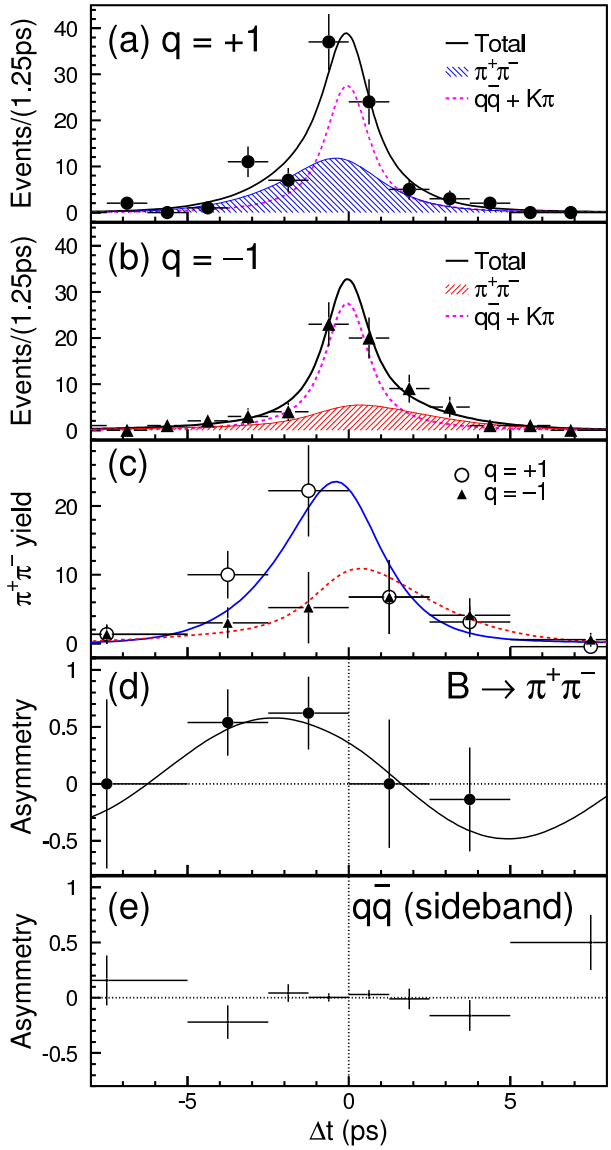

Figure 2: The Δt distributions for the $B^0 \to \pi^+\pi^-$ candidates in the signal region: (a) candidates with $q = +1$, i.e. the tag side is identified as B^0; (b) candidates with $q = -1$; (c) $\pi^+\pi^-$ yields after background subtraction. The rightmost (leftmost) bin ranges from 5 to 10 ps (-5 to -10 ps); (d) the CP asymmetry for $B^0 \to \pi^+\pi^-$ after background subtraction. The point in the rightmost bin has a large negative value that is outside of the range of the histogram; (e) the raw asymmetry for $B^0 \to \pi^+\pi^-$ sideband events. In Figs. (a) through (d), the curves show the results of the unbinned maximum likelihood fit.

Measurements of branching fractions and *CP*-violating asymmetries in $B^0 \to \pi^+\pi^-$, $K^+\pi^-$, K^+K^- decays

Paul D. Dauncey (representing the BABAR Collaboration)
Blackett Laboratory
Imperial College
Prince Consort Road
London SW7 2BW, UK

1 Introduction

Recent measurements of the *CP*-violating asymmetry parameter $\sin 2\beta$ by the *BABAR* [1] and BELLE [2] collaborations established *CP* violation in the B^0 system. These measurements, as well as updated preliminary results [3, 4], are consistent with the Standard Model expectation based on measurements and theoretical estimates of the elements of the Cabibbo-Kobayashi-Maskawa [5] (CKM) quark-mixing matrix.

The study of B decays to charmless hadronic two-body final states will yield important information about the remaining angles (α and γ) of the Unitarity Triangle. In the Standard Model, the time-dependent *CP*-violating asymmetry in the decay $B^0 \to \pi^+\pi^-$ is related to the angle α, nd ratios of branching fractions for various $\pi\pi$ and $K\pi$ decay modes are sensitive to the angle γ. We previously reported measurements of branching fractions [6] and *CP*-violating asymmetries [7] n $B^0 \to \pi^+\pi^-$, $K^+\pi^-$, and K^+K^- decays. (Unless explicitly stated, charge conjugate decay modes are assumed throughout this paper.) In this paper, we present a preliminary update of these results using a sample of 60 million $B\overline{B}$ pairs.

We reconstruct a sample of B mesons ($B_{\rm rec}$) decaying to the $h^+h'^-$ final state, where h and h' refer to π or K, and examine the remaining charged particles in each event to "tag" the flavor of the other B meson ($B_{\rm tag}$). The decay rate distribution f_+ (f_-) when $h^+h'^- = \pi^+\pi^-$ and $B_{\rm tag} = B^0$ ($\overline{B}^0$) is given by

$$f_\pm(\Delta t) = \frac{e^{-|\Delta t|/\tau}}{4\tau}\left[1 \pm S_{\pi\pi}\sin(\Delta m_d \Delta t) \mp C_{\pi\pi}\cos(\Delta m_d \Delta t)\right], \qquad (1)$$

where τ is the mean B^0 lifetime, Δm_d is the eigenstate mass difference, and $\Delta t = t_{\rm rec} - t_{\rm tag}$ is the time between the $B_{\rm rec}$ and $B_{\rm tag}$ decays. The *CP*-violating parameters $S_{\pi\pi}$ and $C_{\pi\pi}$ are defined in terms of a complex parameter λ as

$$S_{\pi\pi} = \frac{2\,\mathcal{I}m\lambda}{1+|\lambda|^2} \qquad \text{and} \qquad C_{\pi\pi} = \frac{1-|\lambda|^2}{1+|\lambda|^2}. \qquad (2)$$

If the decay proceeds purely through the $b \to uW^-$ tree process, then λ is given in terms of the CKM elements $V_{\rm ij}$ by

$$\lambda(B \to \pi^+\pi^-) = \left(\frac{V_{\rm tb}^* V_{\rm td}}{V_{\rm tb} V_{\rm td}^*}\right)\left(\frac{V_{\rm ud}^* V_{\rm ub}}{V_{\rm ud} V_{\rm ub}^*}\right). \quad (3)$$

In this case, $C_{\pi\pi} = 0$ and $S_{\pi\pi} = \sin 2\alpha$, where $\alpha \equiv \arg\left[-V_{\rm td}V_{\rm tb}^*/V_{\rm ud}V_{\rm ub}^*\right]$. In general, the $b \to dg$ penguin amplitude modifies both the magnitude and phase of λ, so that $C_{\pi\pi} \neq 0$ and $S_{\pi\pi} = \sqrt{1 - C_{\pi\pi}^2}\sin 2\alpha_{\rm eff}$, where $\alpha_{\rm eff}$ depends on the magnitudes and relative strong and weak phases of the tree and penguin amplitudes. Several approaches have been proposed to obtain information on α in the presence of penguins [8].

2 The *BABAR* detector and dataset

The data sample used in this analysis consists of $55.6\,{\rm fb}^{-1}$, corresponding to 60.2 ± 0.7 million $B\overline{B}$ pairs, collected on the $\Upsilon(4S)$ resonance with the *BABAR* detector at the SLAC PEP-II storage ring between October 1999 and December 2001. Equal branching fractions for $\Upsilon(4S) \to B^0\overline{B}^0$ and B^+B^- are assumed.

A detailed description of the *BABAR* detector is presented in [9]. Charged particle (track) momenta are measured in a tracking system consisting of a 5-layer double-sided silicon vertex tracker (SVT) and a 40-layer drift chamber (DCH) filled with a gas mixture of helium and isobutane. The SVT and DCH operate within a 1.5 T superconducting solenoidal magnet. Photons are detected in an electromagnetic calorimeter (EMC) consisting of 6580 CsI(Tl) crystals arranged in barrel and forward endcap subdetectors. The flux return for the solenoid is composed of multiple layers of iron and resistive plate chambers for the identification of muons and long-lived neutral hadrons. Tracks from the $B_{\rm rec}$ decay are identified as pions or kaons by the Cherenkov angle θ_c measured with a detector of internally reflected Cherenkov light (DIRC).

3 Analysis method

Event selection is identical to that described in [7]. Candidate $B_{\rm rec}$ decays are reconstructed from pairs of oppositely-charged tracks forming a good quality vertex, where the $B_{\rm rec}$ four-vector is calculated assuming the pion mass for both tracks. We require each track to have an associated θ_c measurement with a minimum of six Cherenkov photons above background, where the average is approximately 30 for both pions and kaons. Protons are rejected based on θ_c and electrons are rejected based on dE/dx measurements in the tracking system, shower shape in the EMC, and the ratio of shower energy and track momentum. Background from the reaction $e^+e^- \to q\overline{q}$ ($q = u, d, s, c$) is suppressed by removing jet-like events from the sample:

we define the center-of-mass (CM) angle θ_S between the sphericity axes of the B candidate and the remaining tracks and photons in the event, and require $|\cos\theta_S| < 0.8$, which removes 83% of the background. The total efficiency for signal events of the above selection is approximately 38%.

Signal decays are identified kinematically using two variables. We define a beam-energy substituted mass $m_{\rm ES} = \sqrt{E_{\rm b}^2 - \mathbf{p}_B^2}$, where the B candidate energy is defined as $E_{\rm b} = (s/2 + \mathbf{p}_i \cdot \mathbf{p}_B)/E_i$, $\sqrt{s}$ and E_i are the total energies of the e^+e^- system in the CM and laboratory frames, respectively, and $\mathbf{p}_i$ and $\mathbf{p}_B$ are the momentum vectors in the laboratory frame of the e^+e^- system and the $B_{\rm rec}$ candidate, respectively. Signal events are Gaussian distributed in $m_{\rm ES}$ with a mean near the B mass and a resolution of $2.6\,{\rm MeV}/c^2$, dominated by the beam energy spread. The background shape is parameterized by a threshold function [10] with a fixed endpoint given by the average beam energy.

We define a second kinematic variable ΔE as the difference between the energy of the $B_{\rm rec}$ candidate in the CM frame and $\sqrt{s}/2$. Signal $\pi\pi$ decays are Gaussian distributed with a mean value near zero. For decays with one (two) kaons, the distribution is shifted relative to $\pi\pi$ on average by $-45\,{\rm MeV}$ ($-91\,{\rm MeV}$), respectively, where the exact separation depends on the laboratory momentum of the kaon(s). The resolution on ΔE is approximately 26 MeV and is validated in large samples of fully reconstructed B decays. The background is parameterized by a quadratic function.

Candidate $h^+h'^-$ pairs selected in the region $5.2 < m_{\rm ES} < 5.3\,{\rm GeV}/c^2$ and $|\Delta E| < 0.15\,{\rm GeV}$ are used to extract yields and *CP*-violating asymmetries with an unbinned maximum likelihood fit. The total number of events in the fit region satisfying all of the above criteria is 17585.

To determine the flavor of the $B_{\rm tag}$ meson we use the same B-tagging algorithm used in the *BABAR* sin2β analysis [11]. The algorithm relies on the correlation between the flavor of the b quark and the charge of the remaining tracks in the event after removal of the $B_{\rm rec}$ candidate. We define five mutually exclusive tagging categories: `Lepton`, `Kaon`, `NT1`, `NT2`, and `Untagged`. `Lepton` tags rely on primary electrons and muons from semileptonic B decays, while `Kaon` tags exploit the correlation in the process $b \to c \to s$ between the net kaon charge and the charge of the b quark. The `NT1` (more certain tags) and `NT2` (less certain tags) categories are derived from a neural network that is sensitive to charge correlations between the parent B and unidentified leptons and kaons, soft pions, or the charge and momentum of the track with the highest CM momentum. The addition of `Untagged` events improves the signal yield estimates and provides a larger sample for determining background shape parameters directly in the maximum likelihood fit.

The quality of tagging is expressed in terms of the effective efficiency $Q = \sum_c \epsilon_c D_c^2$, where ϵ_c is the fraction of events tagged in category c and the dilution $D_c = 1 - 2w_c$ is related to the mistag fraction w_c. Table 1 summarizes the tagging performance in a data sample $B_{\rm flav}$ of fully reconstructed neutral B decays into $D^{(*)-}h^+$ ($h^+ =$

Category	ϵ (%)	D (%)	ΔD (%)	Q (%)
`Lepton`	11.1 ± 0.2	82.8 ± 1.8	-1.2 ± 3.0	7.6 ± 0.4
`Kaon`	34.7 ± 0.4	63.8 ± 1.4	1.8 ± 2.1	14.1 ± 0.6
`NT1`	7.6 ± 0.2	56.0 ± 3.0	-2.7 ± 4.7	2.4 ± 0.3
`NT2`	14.0 ± 0.3	25.4 ± 2.6	9.4 ± 3.8	0.9 ± 0.2
`Untagged`	32.6 ± 0.5	–	–	–
Total Q				25.0 ± 0.8

Table 1: Tagging efficiency ϵ, average dilution $D = 1/2\,(D_{B^0} + D_{\bar{B}^0})$, dilution difference $\Delta D = D_{B^0} - D_{\bar{B}^0}$, and effective tagging efficiency Q for signal events in each tagging category. The values are measured in the $B_{\rm flav}$ sample.

π^+, ρ^+, a_1^+) and $J/\psi\,K^{*0}$ ($K^{*0} \to K^+\pi^-$) flavor eigenstates. We use the same tagging efficiencies and dilutions for signal $\pi\pi$, $K\pi$, and KK decays. Separate background efficiencies for each species are determined simultaneously with $S_{\pi\pi}$ and $C_{\pi\pi}$ in the maximum likelihood fit.

The time difference Δt is obtained from the measured distance between the z positions of the $B_{\rm rec}$ and $B_{\rm tag}$ decay vertices and the known boost of the e^+e^- system. The z position of the $B_{\rm tag}$ vertex is determined with an iterative procedure that removes tracks with a large contribution to the total χ^2. An additional constraint is constructed from the three-momentum and vertex position of the $B_{\rm rec}$ candidate, and the average e^+e^- interaction point and boost. For 99.5% of candidates with a reconstructed vertex, the rms Δz resolution is $180\,\mu$m (1.1 ps). We require $|\Delta t| < 20\,$ps and $\sigma_{\Delta t} < 2.5\,$ps, where $\sigma_{\Delta t}$ is the error on Δt. The resolution function for signal candidates is a sum of three Gaussians, identical to the one described in [3], with parameters determined from a fit to the $B_{\rm flav}$ sample (including events in all five tagging categories). The background Δt distribution is parameterized as the sum of an exponential convolved with a Gaussian, and two additional Gaussians to account for tails. A common parameterization is used for all tagging categories, and the parameters are determined simultaneously with the CP parameters in the maximum likelihood fit. We find that 86% of background events are described by an effective lifetime of about 0.6 ps, while tails are described by 12 (2)% of events with a resolution of approximately 2 (8) ps.

Discrimination of signal from light-quark background is enhanced by the use of a Fisher discriminant $\mathcal{F}$ [6]. The discriminating variables are constructed from the scalar sum of the CM momenta of all tracks and photons (excluding tracks from the $B_{\rm rec}$ candidate) entering nine two-sided 10-degree concentric cones centered on the thrust axis of the $B_{\rm rec}$ candidate. The distribution of $\mathcal{F}$ for signal events is parameterized as a single Gaussian, with parameters determined from Monte Carlo simulated decays and validated with $B^- \to D^0\pi^-$ decays reconstructed in data. The

background shape is parameterized as the sum of two Gaussians, with parameters determined directly in the maximum likelihood fit.

Identification of $h^+h'^-$ tracks as pions or kaons is accomplished with the Cherenkov angle measurement from the DIRC. We construct Gaussian probability density functions (PDFs) from the difference between measured and expected values of θ_c for the pion or kaon hypothesis, normalized by the resolution. The DIRC performance is parameterized using a sample of $D^{*+} \to D^0\pi^+$, $D^0 \to K^-\pi^+$ decays, reconstructed in data. Figure 1 shows the typical separation between pions and kaons, which varies from 8σ at momenta of $2\,\mathrm{GeV}/c$ to 2.5σ at $4\,\mathrm{GeV}/c$, where σ is the average resolution of θ_c.

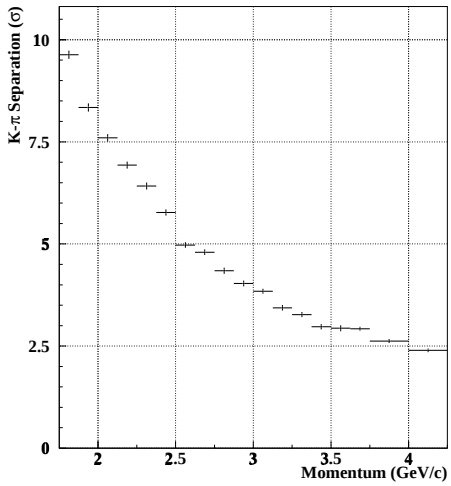

Figure 1: Variation of the separation between the kaon and pion Cherenkov angles with momentum, as obtained from a control sample of $D^{*+} \to D^0\pi^+$, $D^0 \to K^-\pi^+$ decays reconstructed in data.

4 Results

We use unbinned extended maximum likelihood fits to extract yields and *CP* parameters from the $B_{\rm rec}$ sample. The likelihood for candidate j tagged in category c is obtained by summing the product of event yield n_i, tagging efficiency $\epsilon_{i,c}$, and probability $\mathcal{P}_{i,c}$ over the eight possible signal and background hypotheses i (referring to $\pi\pi$, $K^+\pi^-$, $K^-\pi^+$, and KK decays),

$$\mathcal{L}_c = \exp\left(-\sum_i n_i\epsilon_{i,c}\right)\prod_j\left[\sum_i n_i\epsilon_{i,c}\mathcal{P}_{i,c}(\vec{x}_j;\vec{\alpha}_i)\right]. \qquad (4)$$

Mode	ϵ_T (%)	N_S (Events)	$\mathcal{B}$ (10^{-6})
$\pi^+\pi^-$	38.5 ± 0.7	$124^{+16\,+7}_{-15\,-9}$	$5.4 \pm 0.7 \pm 0.4$
$K^+\pi^-$	37.6 ± 0.7	$403 \pm 24 \pm 15$	$17.8 \pm 1.1 \pm 0.8$
K^+K^-	36.7 ± 0.7	< 16 (90% C.L.)	< 1.1 (90% C.L.)

Table 2: Summary of results for total detection efficiencies ϵ_T, fitted signal yields N_S and measured branching fractions $\mathcal{B}$.

For the $K^\mp\pi^\pm$ components, the yield is parameterized as $n_i = N_{K\pi}\,(1 \pm \mathcal{A}_{K\pi})\,/2$, where $N_{K\pi} = N_{K^-\pi^+} + N_{K^+\pi^-}$ and $\mathcal{A}_{K\pi} \equiv (N_{K^-\pi^+} - N_{K^+\pi^-})/(N_{K^-\pi^+} + N_{K^+\pi^-})$. The probabilities $\mathcal{P}_{i,c}$ are evaluated as the product of PDFs for each of the independent variables $\vec{x}_j = \{m_{\rm ES}, \Delta E, \mathcal{F}, \theta_c^+, \theta_c^-, \Delta t\}$, where θ_c^+ and θ_c^- are the Cherenkov angles for the positively and negatively charged tracks. We use identical PDFs for θ_c^+ and θ_c^-. The total likelihood $\mathcal{L}$ is the product of likelihoods for each tagging category and the free parameters are determined by minimizing the quantity $-\ln\mathcal{L}$.

4.1 Time-independent fit

In order to minimize the systematic error on the branching fraction measurements, we perform an initial fit without tagging or Δt information. A total of 16 parameters are varied in the fit, including signal and background yields (6 parameters) and asymmetries (2), and parameters for the background shapes in $m_{\rm ES}$ (1), ΔE (2), and $\mathcal{F}$ (5).

Table 2 summarizes results for total efficiencies, signal yields and branching fractions. The upper limit on the signal yield for $B^0 \to K^+K^-$ is given by the value of n^0 for which $\int_0^{n^0} \mathcal{L}_{\rm max}\,dn / \int_0^\infty \mathcal{L}_{\rm max}\,dn = 0.90$, where $\mathcal{L}_{\rm max}$ is the likelihood as a function of n, maximized with respect to the remaining fit parameters. The branching fraction upper limit is calculated by increasing the signal yield upper limit and reducing the efficiency by their respective systematic errors. The fit result for the $K\pi$ charge asymmetry $\mathcal{A}_{K\pi}$ is

$$\mathcal{A}_{K\pi} = -0.05 \pm 0.06 \pm 0.01, \qquad 90\%\ \text{C.L.}\ -0.14 < \mathcal{A}_{K\pi} < 0.05. \tag{5}$$

The statistical and systematic errors on $\mathcal{A}_{K\pi}$ are added in quadrature when calculating the 90% confidence level (C.L.).

The dominant systematic error on the branching fraction measurements is due to uncertainty in the shape of the θ_c PDF, while the dominant error on $\mathcal{A}_{K\pi}$ is due to possible charge bias in track and θ_c reconstruction. All measurements are consistent with our previous results reported in [6].

Figure 2 shows distributions of $m_{\rm ES}$ and ΔE after a cut on likelihood ratios. We define $\mathcal{R}_{\rm sig} = \sum_s n_s\mathcal{P}_s / \sum_i n_i\mathcal{P}_i$ and $\mathcal{R}_k = n_k\mathcal{P}_k / \sum_s n_s\mathcal{P}_s$, where $\sum_s\,(\sum_i)$ indicates

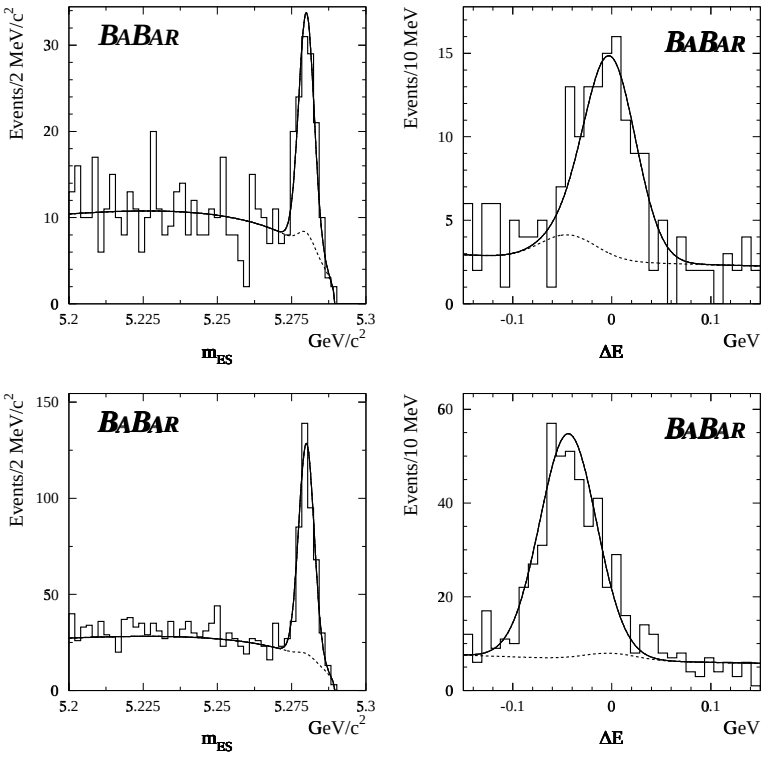

Figure 2: Distributions of $m_{\rm ES}$ (left) and ΔE (right) for events enhanced in signal $\pi\pi$ (top) and $K\pi$ (bottom) decays based on the likelihood ratio selection described in the text. Solid curves represent projections of the maximum likelihood fit result after accounting for the efficiency of the additional selection, while dashed curves represent $q\bar{q}$ and $\pi\pi \leftrightarrow K\pi$ cross-feed background.

a sum over signal (all) hypotheses, and $\mathcal{P}_k$ indicates the probability for signal hypothesis k. The probabilities include the PDFs for θ_c, $\mathcal{F}$, and $m_{\rm ES}$ (ΔE) when plotting ΔE ($m_{\rm ES}$). The selection is defined by optimizing the signal significance with respect to $\mathcal{R}_{\rm sig}$ and $\mathcal{R}_k$. The solid curve in each plot represents the fit projection after correcting for the efficiency of the additional selection (approximately 67% for $\pi\pi$ and 88% for $K\pi$).

4.2 Time-dependent fit

The time-dependent *CP* asymmetries $S_{\pi\pi}$ and $C_{\pi\pi}$ are determined from a second fit including tagging and Δt information, with the yields and $\mathcal{A}_{K\pi}$ fixed to the results of the first fit. The Δt PDF for signal $\pi^+\pi^-$ decays is given by Eq. (1), modified to include the dilution and dilution difference for each tagging category, and convolved

with the signal resolution function. The Δt PDF for signal $K\pi$ events takes into account B^0–$\overline{B}^0$ mixing, depending on the charge of the kaon and the flavor of $B_{\rm tag}$. We parameterize the Δt distribution in $B^0 \to K^+K^-$ decays as an exponential convolved with the resolution function.

A total of 34 parameters are varied in the fit, including the values of $S_{\pi\pi}$ and $C_{\pi\pi}$, separate background tagging efficiencies for $\pi\pi$, $K\pi$, and KK events (12), parameters for the background Δt resolution function (8), and parameters for the background shapes in $m_{\rm ES}$ (5), ΔE (2), and $\mathcal{F}$ (5). The signal tagging efficiencies and dilutions are fixed to the values in Table 1, while τ and Δm_d are fixed to their PDG values [12]. For each parameter, we also calculate the 90% C.L. interval taking into account the systematic error. The fit yields

$$\begin{aligned} S_{\pi\pi} &= -0.01 \pm 0.37 \pm 0.07, \qquad 90\%\ \text{C.L.}\ -0.66 < S_{\pi\pi} < 0.62, \\ C_{\pi\pi} &= -0.02 \pm 0.29 \pm 0.07, \qquad 90\%\ \text{C.L.}\ -0.54 < C_{\pi\pi} < 0.48, \end{aligned} \tag{6}$$

and the correlation between $S_{\pi\pi}$ and $C_{\pi\pi}$ is -13%.

Systematic uncertainties on $S_{\pi\pi}$ and $C_{\pi\pi}$ are dominated by the uncertainty on the shape of the θ_c PDF. Since we measure asymmetries near zero, multiplicative systematic errors have also been evaluated (0.05). We sum in quadrature multiplicative errors, evaluated at one standard deviation, with the additive systematic uncertainties.

To validate the analysis technique, we measure τ and Δm_d in the $B_{\rm rec}$ sample and find $\tau = (1.66 \pm 0.09)\,{\rm ps}$ and $\Delta m_d = (0.517 \pm 0.062)\hbar\,{\rm ps}^{-1}$. Figure 3 shows the asymmetry $\mathcal{A}_{\rm mix} = (N_{\rm unmixed} - N_{\rm mixed})/(N_{\rm unmixed} + N_{\rm mixed})$ in a sample of events enhanced in $B \to K\pi$ decays. The curve shows the expected oscillation given the value of Δm_d measured in the full sample.

For tagged events enhanced in signal $\pi\pi$ decays, Figure 4 shows the Δt distributions and the asymmetry $\mathcal{A}_{\pi\pi}(\Delta t) = [N_{B^0}(\Delta t) - N_{\overline{B}^0}(\Delta t)]/[N_{B^0}(\Delta t) + N_{\overline{B}^0}(\Delta t)]$. The selection procedure is the same as for Figure 2, with the likelihoods defined including the PDFs for θ_c, $\mathcal{F}$, $m_{\rm ES}$, and ΔE.

5 Summary

In summary, we have presented updated preliminary measurements of branching fractions and *CP*-violating asymmetries in $B^0 \to \pi^+\pi^-$, $K^+\pi^-$, and K^+K^- decays. All results are consistent with our previous measurements. No evidence for *CP* violation is observed and our measurement of $\mathcal{A}_{K\pi}$ disfavors theoretical models that predict a large asymmetry [13, 14].

We are grateful for the extraordinary contributions of our PEP-II colleagues in achieving the excellent luminosity and machine conditions that have made this work possible.

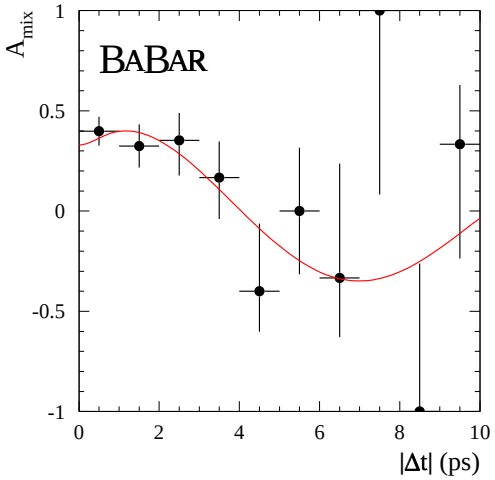

Figure 3: The asymmetry $\mathcal{A}_{\rm mix}$ between unmixed and mixed events in a sample enhanced in $K\pi$ decays. The curve indicates the expected oscillation corresponding to $\Delta m_d = 0.517\,\hbar\,\mathrm{ps}^{-1}$. The dilution from $q\overline{q}$ events is evident in the reduced amplitude near $|\Delta t| = 0$.

References

[1] *BABAR* Collaboration, B. Aubert *et al.*, Phys. Rev. Lett. **87**, 091801 (2001).

[2] BELLE Collaboration, K. Abe *et al.*, Phys. Rev. Lett. **87**, 091802 (2001).

[3] *BABAR* Collaboration, B. Aubert *et al.*, hep-ex/0203007 (2002).

[4] BELLE Collaboration, T. Higuchi, hep-ex/0205020 (2002).

[5] N. Cabibbo, Phys. Rev. Lett. **10**, 531 (1963); M. Kobayashi and T. Maskawa, Prog. Th. Phys. **49**, 652 (1973).

[6] *BABAR* Collaboration, B. Aubert *et al.*, Phys. Rev. Lett. **87**, 151802 (2001).

[7] *BABAR* Collaboration, B. Aubert *et al.*, Phys. Rev. D **65**, 051502 (2002).

[8] M. Gronau and D. London, Phys. Rev. Lett. **65**, 3381 (1990); Y. Grossman and H.R. Quinn, Phys. Rev. D **58**, 017504 (1998); J. Charles, Phys. Rev. D **59**, 054007 (1999); M. Gronau, D. London, N. Sinha, and R. Sinha, Phys. Lett. B **514**, 315 (2001); M. Beneke, G. Buchalla, M. Neubert, and C.T. Sachrajda, Nucl. Phys. B **606**, 245 (2001).

[9] *BABAR* Collaboration, B. Aubert *et al.*, Nucl. Instr. and Methods A **479**, 1 (2002).

[10] ARGUS Collaboration, H. Albrecht *et al.*, Z. Phys. C **48**, 543 (1990).

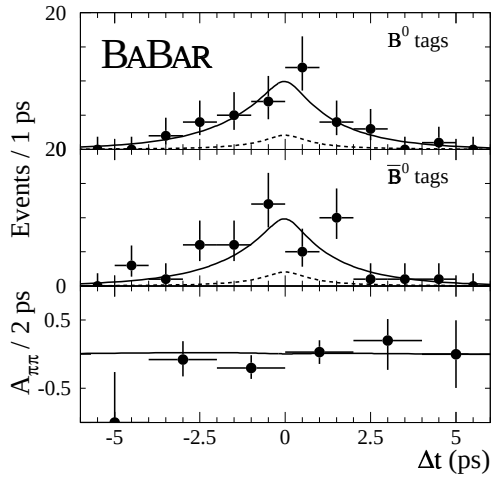

Figure 4: Distributions of Δt for events enhanced in signal $\pi\pi$ decays based on the likelihood ratio selection described in the text. The top two plots show events (points with errors) with $B_{\rm tag} = B^0$ or $\overline{B}^0$. Solid curves represent projections of the maximum likelihood fit, dashed curves represent the sum of $q\overline{q}$ and $K\pi$ background events. The bottom plot shows $\mathcal{A}_{\pi\pi}(\Delta t)$ for data (points with errors) and the fit projection.

[11] *BABAR* Collaboration, B. Aubert *et al.*, hep-ex/0201020, accepted by Phys. Rev. D.

[12] Particle Data Group, D.E. Groom *et al.*, Eur. Phys. Jour. C **15**, 1 (2000).

[13] Y.Y. Keum, H-n. Li, and A.I. Sanda, Phys. Rev. D **63**, 054008 (2001).

[14] M. Ciuchini *et al.*, Phys. Lett. B **515**, 33 (2001).

Penguin Pollution in $B_d^0 \to \pi\pi$[1]

Nita Sinha
The Institute of Mathematical Sciences
Taramani, Chennai 600113, INDIA

A principal decay mode considered for the measurement of the angle α, is $B_d^0(t) \to \pi^+\pi^-$. Unfortunately, this mode suffers from a well-known problem: penguin contributions may be large [2], and their presence will spoil the clean extraction of α. In the presence of penguin amplitudes, the CP asymmetry in $B_d^0(t) \to \pi^+\pi^-$ does not measure $\sin 2\alpha$, but rather some effective ("polluted") angle $2\alpha_{eff}$. We may write the time-dependent rate of $B_d^0(t) \to \pi^+\pi^-$ as,

$$\Gamma(B^0(t) \to \pi^+\pi^-) = e^{-\Gamma t} B^{+-} \left[1 + a_{dir}^{+-} \cos(\Delta m t) - y \sin 2\alpha_{eff} \sin(\Delta m t)\right] ,$$
$$\text{where,} \quad B^{+-} \equiv \frac{1}{2}\left(|A^{+-}|^2 + |\overline{A}^{+-}|^2\right) , \qquad a_{dir}^{+-} \equiv \frac{|A^{+-}|^2 - |\overline{A}^{+-}|^2}{|A^{+-}|^2 + |\overline{A}^{+-}|^2} , \qquad (1)$$

A^{+-} and $\overline{A}^{+-}$ are the amplitudes for $B_d^0 \to \pi^+\pi^-$ and $\overline{B}_d^0 \to \pi^+\pi^-$, respectively, and $y \equiv \sqrt{1 - (a_{dir}^{+-})^2}$. Writing the time dependent CP asymmetry as,

$$\mathcal{A} = C_{\pi\pi} \cos(\Delta m t) + S_{\pi\pi} \sin(\Delta m t) , \qquad (2)$$

we have, $C_{\pi\pi} = a_{dir}^{+-}$ and $S_{\pi\pi} = -y \sin 2\alpha_{eff}$. In Eq. (1), the coefficient of the $\sin(\Delta M t)$ term, probes the relative phase between the A^{+-} and $e^{-2i\beta}\overline{A}^{+-}$ amplitudes, and this phase, $2\alpha_{eff} = 2\alpha$, in absence of penguin contributions.

The problem of penguin pollution can be eliminated with the help of an isospin analysis [3]. By measuring the rates for $B^+ \to \pi^+\pi^0$ and $B_d^0/\overline{B}_d^0 \to \pi^0\pi^0$, in addition to $B_d^0(t) \to \pi^+\pi^-$, α can again be measured cleanly.

However, the isospin analysis requires separate measurement of $BR(B_d^0 \to \pi^0\pi^0)$ and $BR(\overline{B}_d^0 \to \pi^0\pi^0)$, and therefore suffers from potential practical complications: (i)The branching ratio for $B_d^0 \to \pi^0\pi^0$ is expected to be smaller than $B_d^0 \to \pi^+\pi^-$. (ii)The presence of two π^0's in the final state means that the reconstruction efficiency is smaller. (iii)It will be necessary to tag the decaying B_d^0 or $\overline{B}_d^0$ meson, which further reduces the measurement efficiency. Hence, we may only have, an actual measurement or an upper limit, on the sum of the branching ratios. In this case, a full isospin analysis cannot be carried out.

[1] major part of this talk is based on work done in collaboration with Michael Gronau, David London and Rahul Sinha [1].

Question: assuming that we have, at best, only partial knowledge of the sum, $(BR(B^0_d \to \pi^0\pi^0) + BR(\overline{B}^0_d \to \pi^0\pi^0))$, can we at least put bounds on the size of penguin pollution? In the presence of penguin amplitudes, the CP asymmetry in $B^0_d(t) \to \pi^+\pi^-$ measures $\sin 2\alpha_{eff}$. Writing $2\alpha_{eff} = 2\alpha + 2\theta$, where 2θ parametrizes the effect of the penguin contributions, the more precise question: is it possible to constrain θ? As demonstrated by Grossman and Quinn(GQ) [4] and later by Charles [5], the answer to this question is yes. They were able to show that $|2\theta|$ can be bounded even if we have only an upper limit on the sum of $BR(B^0_d \to \pi^0\pi^0)$ and $BR(\overline{B}^0_d \to \pi^0\pi^0)$:

$$\cos 2\theta \geq \frac{1 - 2B^{00}/B^{+0}}{y} \ , \qquad \cos 2\theta \geq \frac{1 - 4B^{00}/B^{+-}}{y} \ , \tag{3}$$

where, B^{00} and B^{+0} are defined analogous to the definition of B^{+-} in Eq. (1). Next question: does a more stringent bound exist? The answer to this is also yes; the most stringent bound possible on $|2\theta|$ was obtained by Gronau, London, Sinha and Sinha [1], by requiring that the two isospin triangles close and have a common base. We note, however, that neither of the bounds in Eq. (3) involves all three charge-averaged decay rates, B^{+-}, B^{+0} and B^{00}. Thus, a condition for the closure of the two isospin triangles is not included in these bounds.

We now present a geometrical derivation of this new bound on $|2\theta|$. We assume that the charge-averaged rates B^{+-} and B^{+0} have been measured, and that we have (at least) an upper bound on B^{00}. The $B \to \pi\pi$ decay amplitudes take the form

$$\frac{1}{\sqrt{2}}A^{+-} = Te^{i\gamma} + Pe^{-i\beta} \ , \qquad A^{00} = Ce^{i\gamma} - Pe^{-i\beta} \ , \qquad A^{+0} = (C+T)e^{i\gamma}, \tag{4}$$

where, the complex amplitudes T, C and P, which are sometimes referred to as "tree", "colour-suppressed" and "penguin" amplitudes, include strong phases. Note that we have implicitly imposed the isospin triangle relation,

$$\frac{1}{\sqrt{2}}A^{+-} + A^{00} = A^{+0} \ . \tag{5}$$

The $\overline{A}$ amplitudes can be obtained from the A amplitudes by reversing the signs of the weak phases. It is convenient to define the new amplitudes $\tilde{A}^{ij} \equiv e^{2i\gamma}\overline{A}^{ij}$. Then, $\tilde{A}^{-0} = A^{+0}$, so that the A and $\tilde{A}$ triangles have a common base. (A tiny electroweak penguin amplitude, forming a very small angle between A^{+0} and $\tilde{A}^{-0}$, will be neglected here.) In the absence of penguin contributions, $\tilde{A}^{+-} = A^{+-}$, thus, the relative phase 2θ between these two amplitudes is due to penguin pollution. Also, the relative phase between the penguin contributions in $\tilde{A}^{00}$ and A^{00} is $2(\beta+\gamma) \sim 2\alpha$. This information is encoded in Fig. 1. Note that the distance between the points X

and Y is $2\ell \equiv 2|P|\sin\alpha$. Now, $|P|$ can be expressed in terms of observables [5], and we can therefore write,

$$\ell = \frac{1}{2}\sqrt{B^{+-}}\sqrt{1 - y\cos 2\theta}\ . \tag{6}$$

Thus, a constraint on ℓ implies a bound on $\cos 2\theta$.

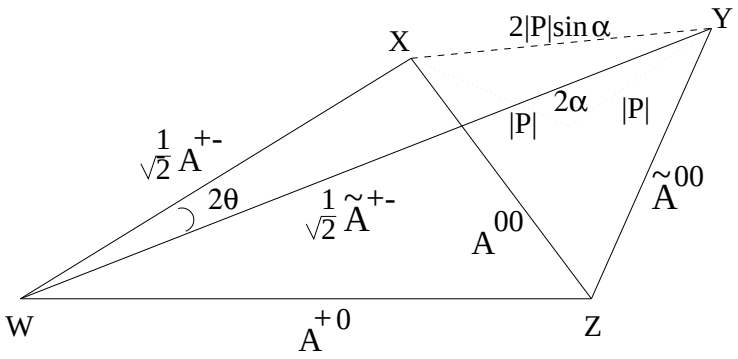

Figure 1: The A and $\tilde{A}$ isospin triangles.

In order to constrain ℓ, we proceed as follows. First, we assign a coordinate system to Fig. 1 such that the origin is at the midpoint of the points X and Y. The points X, Y, W and Z correspond respectively to the coordinates $(+\ell, 0)$, $(-\ell, 0)$, (x_1, y_1) and (x_2, y_2). The goal of the exercise is to find the values of the coordinates (x_1, y_1) and (x_2, y_2). We then note that

$$\begin{array}{ll} B^{+-} = 2(x_1^2 + y_1^2) + 2\ell^2, & B^{+-}a_{dir}^{+-} = -4x_1\ell\ , \\ B^{00} = (x_2^2 + y_2^2) + \ell^2, & B^{+0} = (x_1^2 + y_1^2) + (x_2^2 + y_2^2) - 2x_1x_2 - 2y_1y_2\ . \end{array} \tag{7}$$

We therefore have four (nonlinear) equations in four unknowns, and we can solve for these coordinates as a function of ℓ. However, we must obtain *only real solutions* for x_2 and y_2, otherwise the triangles do not close. This puts a constraint on ℓ, which in turn, gives the following bound,

$$\cos 2\theta \geq \frac{\left(\frac{1}{2}B^{+-} + B^{+0} - B^{00}\right)^2 - B^{+-}B^{+0}}{B^{+-}B^{+0}y}\ . \tag{8}$$

This is the new lower bound on $\cos 2\theta$ (or upper bound on $|2\theta|$).

The new bound contains the two previous bounds as limiting cases. We can rewrite this lower bound on $\cos 2\theta$ in two alternate forms [1], which involve a sum of two terms. In one form, the first term is simply the GQ bound and in the other, it is the Charles bound. The second terms in both forms are positive definite. Hence, the new bound is stronger than the GQ as well as the Charles bound, and since,

all isospin information has been used in obtaining Eq. (8), this is *the most stringent possible bound on* $\cos 2\theta$.

One would also like to know if it is possible to find a lower bound on $|2\theta|$? Unfortunately, the answer is no. This can be seen quite clearly in Fig. 1. Suppose that the two-triangle isospin construction can be made for some nonzero value of 2θ. It is then straightforward to show that one can always rotate A^{+-} and $\tilde{A}^{+-}$ continuously around W towards one another, without changing B^{00}, until they lie on one line corresponding to $\theta = 0$. Thus, without measuring separately $B^0_d \to \pi^0\pi^0$ and $\overline{B}^0_d \to \pi^0\pi^0$, one cannot put a lower bound on the penguin pollution parameter.

Using the world average values [7], $BR(B^0_d \to \pi^+\pi^-) = 5.2 \pm 0.6$ and $BR(B^0_d \to \pi^+\pi^0) = 4.9 \pm 1.1$ and Babar's value of $BR(B^0_d \to \pi^0\pi^0) = 0.9^{+0.9+0.8}_{-0.7-0.6}$, our bound yields, $\theta < 57^\circ$ or $\theta > 123^\circ$ at 90% CL, while the GQ bound gives $\theta < 61^\circ$ or $\theta > 119^\circ$ at 90% CL[2]. The Charles bound gives weaker constraints. Note that these values are obtained using zero direct asymmetry, the bounds will be stronger if direct asymmetry is non-vanishing.

The bound on $\cos 2\theta$ in Eq. (8) together with the condition that $\cos 2\theta \leq 1$, leads to a lower limit on B^{00}/B^{+-}. This lower limit, as well as an upper limit on the same quantity, follows directly from the closure of the two isospin triangles, which can be shown to imply that

$$\frac{1}{2} + \frac{B^{+0}}{B^{+-}} - \sqrt{\frac{B^{+0}}{B^{+-}}(1+y)} \leq \frac{B^{00}}{B^{+-}} \leq \frac{1}{2} + \frac{B^{+0}}{B^{+-}} + \sqrt{\frac{B^{+0}}{B^{+-}}(1+y)} \ . \tag{9}$$

The limits are weakest for $y = 1$. Using the central values of the world averages listed above, one finds $0.069 \leq B^{00}/B^{+-} \leq 2.815$, for $a^{+-}_{dir} = 0$; again, a non-zero value of the direct asymmetry will raise the lower limit. This lower limit on B^{00}/B^{+-} is useful, as it will give experimentalists some knowledge of the branching ratios for $B^0_d/\overline{B}^0_d \to \pi^0\pi^0$, and thus will help to anticipate the feasibility of the full isospin analysis. In addition, since the bound on B^{00}/B^{+-} relies only on the closure of the two triangles, it will hold even in the presence of isospin-violating electroweak-penguin contributions. However, it has been pointed out by Gardner [6] that the triangles will not close in the presence of other isospin-violating effects such as π^0–η, η' mixing. A comparison of the actual branching ratio B^{00} with this bound, may therefore give some information about the size of such isospin-violating effects.

Although no lower limit can be obtained on the penguin-pollution angle $|2\theta|$, we note that a lower bound can be derived for the magnitude of the penguin amplitude P from measurements of $B^0_d(t) \to \pi^+\pi^-$ alone,

$$|P|^2_{min} = \frac{B^{+-}(1-y^2)}{4(1 - y\cos 2\alpha_{eff})} \ . \tag{10}$$

[2]We thank Andreas Hoecker and Rainer Bartoldus for help in estimating the numerical values of our bound.

Recently Belle [8] and Babar [9] announced their results for the CP violating asymmetries $C_{\pi\pi}$ and $S_{\pi\pi}$. These asymmetries, may be written [10] in terms of the three parameters $|P/T|$, the strong phase difference of the penguin and tree amplitudes, $\delta = \delta_P - \delta_T$ and the weak phase α. If one assumes a value of $|P/T|$, one can determine α upto discrete ambiguities from the time dependent study of the $B_d^0(t) \to \pi^+\pi^-$ mode alone. There are discrete ambiguities associated with mapping the observables $(S_{\pi\pi}, C_{\pi\pi})$ with the parameters (α, δ). The ambiguities can be resolved by a measurement of $R_{\pi\pi}$, which is the ratio of the flavor-averaged $B_d^0 \to \pi^+\pi^-$ branching ratio to its predicted value due to the tree amplitude alone. If one averages over Belle and Babar asymmetry results, then a larger value of α is favored [10].

Concluding remark: By the end of this summer, with improved statistics ($\approx 100 fb^{-1}$), we hope to have a much clearer understanding about the amount of penguin pollution in $B_d^0 \to \pi^+\pi^-$.

N.S. would like to thank the organizers of FPCP for a great conference. She thanks David London for the hospitality of the Université de Montréal, where some of this work was done. This work is supported by the young scientist award from the Department of Science and Technology, India.

References

[1] M. Gronau, D. London, N. Sinha and R. Sinha, Phys. Lett. B **514**, 315 (2001).

[2] D. London and R. D. Peccei,Phys. Lett. B **223**, 257 (1989); M. Gronau,Phys. Rev. Lett. **63**, 1451 (1989), Phys. Lett. B **300**, 163 (1993); B. Grinstein, Phys. Lett. B **229**, 280 (1989).

[3] M. Gronau and D. London, Phys. Rev. Lett. **65**, 3381 (1990).

[4] Y. Grossman and H. R. Quinn,Phys. Rev. D **58**, 017504 (1998).

[5] J. Charles, Phys. Rev. D **59**, 054007 (1999).

[6] S. Gardner, Phys. Rev. D **59**, 077502 (1999).

[7] R. Bartoldus, talk given at this conference.

[8] Belle Collaboration, talk by K. Trabelsi at XXXVIIth Rencontres de Moriond on Electroweak Interactions and Unified Theories, les Arcs, France, March 9-16, 2002.

[9] Babar Collaboration, talk by A. Farbin at XXXVIIth Rencontres de Moriond on Electroweak Interactions and Unified Theories, les Arcs, France, March 9-16, 2002.

[10] M. Gronau and J. L. Rosner, Phys. Rev. D **65**, 093012 (2002).

Recent results from the QCD factorization approach to non-leptonic B decays

M. Beneke
Institut für Theoretische Physik E
RWTH Aachen
Sommerfeldstr. 28
D-52074 Aachen, GERMANY

1 Introduction

In this talk I report recent results on hadronic B decays obtained with the QCD factorization approach. In the first part I update the fit of the Wolfenstein parameters $(\overline{\rho},\overline{\eta})$ to CP-averaged $B\to\pi\pi,\pi K$ branching fractions performed in [1] to account for the new experimental data, and give the correlation between the time-dependent and direct CP asymmetry in $B_d\to\pi^+\pi^-$ decay, also based on the calculation of [1]. In the second part I present an investigation of B decays into final states containing an η or η' meson [2]. I discuss the new theoretical issues that arise for flavour singlet mesons and present preliminary numerical results that appear to reproduce the pattern of experimental data reasonably well.

The QCD factorization approach [3] uses heavy quark expansion methods ($m_b\gg\Lambda_{\rm QCD}$) and soft-collinear factorization (particle energies $\gg\Lambda_{\rm QCD}$) to compute the matrix elements $\langle f|O_i|\overline{B}\rangle$ relevant to hadronic B decays in an expansion in $1/m_b$ and α_s. Only the leading term in $1/m_b$ assumes a simple form. The basic formula is

$$\begin{aligned}\langle M_1M_2|O_i|\overline{B}\rangle \;=\; & F^{B\to M_1}(0)\int_0^1 du\,T^I(u)\Phi_{M_2}(u)\\ & +\int d\xi du dv\,T^{II}(\xi,u,v)\,\Phi_B(\xi)\Phi_{M_1}(v)\Phi_{M_2}(u),\end{aligned}\qquad(1)$$

where $F^{B\to M_1}$ is a (non-perturbative) form factor, Φ_{M_i} and Φ_B are light-cone distribution amplitudes and $T^{I,II}$ are perturbatively calculable hard scattering kernels.

Although not strictly proven to all orders in perturbation theory, the formula is presumed to be valid when both final state mesons are light. (M_1 is the meson that picks up the spectator quark from the B meson.) The formula shows that there is no long-distance interaction between the constituents of the meson M_2 and the (BM_1) system at leading order in $1/m_b$. This is the precise meaning of factorization. A summary of results that have been obtained in the QCD factorization approach is given in [4].

Factorization is not expected to hold at subleading order in $1/m_b$. Attempts to compute subleading power corrections to hard spectator-scattering in perturbation theory usually result in infrared divergences, which signal the breakdown of factorization. Some power corrections related to scalar currents are enhanced by factors such as $m_\pi^2/((m_u + m_d)\Lambda_{\rm QCD})$ [3]. At least these effects should be estimated and included into the error budget. All weak annihilation contributions belong to this class of effects.

2 CP-averaged $B \to \pi\pi, \pi K$ branching fractions

The possibility to determine the CP-violating angle γ by comparing the calculation of branching fractions into $\pi\pi$ and πK final states with the corresponding data has been investigated in detail [1] (see also [5]). The branching fractions for the modes $B^+ \to \pi^+\pi^0$ and $B^+ \to \pi^+ K^0$, which depend only on a single weak phase to very good approximation, are well described by the theory. This demonstrates that the magnitude of the tree and penguin amplitude is obtained correctly, where for the penguin amplitude the 1-loop radiative correction is important to reach this conclusion. There is, however, a relatively large normalization uncertainty for the πK final states, which are sensitive to weak annihilation and the strange quark mass through the scalar penguin amplitude. This uncertainty can be partially eliminated by taking ratios of branching fractions. The agreement is less good for branching fractions with significant interference of tree and penguin amplitudes, if γ is assumed to take values around 55° as favoured by indirect constraints.

In [1] a fit of the Wolfenstein parameters $(\overline{\rho}, \overline{\eta})$ to the six measured CP-averaged $B \to \pi\pi, \pi K$ branching fractions has been performed. The result of this fit is shown in the left panel of Figure 1. (The details of the fit procedure can be found in [1]). We now repeat this fit with the new world averages as presented at this conference [6], see Table 1. There are no dramatic changes in the data since spring 2001, but the small shifts of the various branching fractions (for instance, in the final state $\pi^0 K^0$) all work towards better agreement with the theoretical calculation, resulting in an improved fit. (The best fits with theory parameters in the allowed ranges have $\chi^2 \approx 0.5$.) On the theoretical side we changed the allowed values of the strange quark mass and the B meson decay constant to $[75, 125]$ MeV (from $[85, 135]$ MeV)

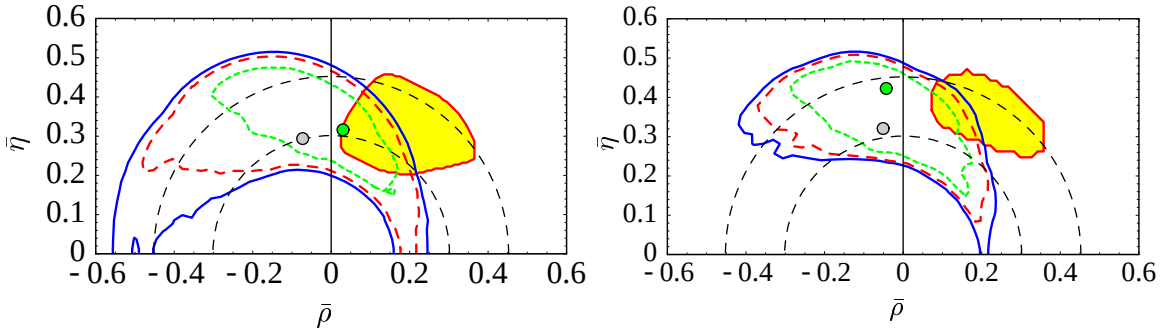

Figure 1: 95% (solid), 90% (dashed) and 68% (short-dashed) confidence level contours in the $(\overline{\rho}, \overline{\eta})$ plane obtained from a global fit to the CP averaged $B \to \pi K, \pi\pi$ branching fractions, using the scanning method as described in [7]. The darker dot shows the overall best fit, whereas the lighter dot indicates the best fit for the default hadronic parameter set. The left panel reproduces the fit of [1] reflecting the status of spring 2001; the right panel summarizes the current results. The light-shaded region indicates the region preferred by the standard global fit [7], excluding (including) the direct measurement of $\sin(2\beta)$ in the left (right) panel.

Decay Mode	Exp. Average	Default fit	Fit2
$B^0 \to \pi^+\pi^-$	5.15 ± 0.61	5.12	5.24
$B^\pm \to \pi^\pm\pi^0$	4.88 ± 1.06	5.00	4.57
$B^0 \to \pi^0\pi^0$	–	0.78	0.94
$B^0 \to \pi^\mp K^\pm$	18.56 ± 1.08	17.99	18.47
$B^\pm \to \pi^0 K^\pm$	11.49 ± 1.26	12.07	11.83
$B^\pm \to \pi^\pm K^0$	17.93 ± 1.70	15.65	17.88
$B^0 \to \pi^0 K^0$	8.82 ± 2.20	5.55	6.87

Table 1: CP-averaged $B \to \pi\pi, \pi K$ branching fractions (in units of 10^{-6}): data vs. results from the fit. The default fit to $(\overline{\rho}, \overline{\eta})$ (returning $|V_{ub}/V_{cb}| = 0.085$, $\gamma = 116^\circ$ with $\chi^2 = 4.5$) refers to the default theory parameter set as explained in the text. "Fit2" (returning $|V_{ub}/V_{cb}| = 0.079$, $\gamma = 97^\circ$, $\chi^2 = 1.0$) refers to a fit without annihilation contributions and chirally enhanced spectator corrections but with $m_s = 80\,\text{MeV}$ [100 MeV], $\lambda_B = 200\,\text{MeV}$ [350 MeV] and $R_{\pi K} = 0.8$ [0.9] (default values in square brackets). The experimental average is based on $9\,\text{fb}^{-1}$ from CLEO, $29.1\,\text{fb}^{-1}$ from Belle and $55.6\,\text{fb}^{-1}$ from Babar [6].

and $[170, 230]\,\text{MeV}$ (from $[140, 220]\,\text{MeV}$), respectively, to account for a change in the theoretically favoured ranges. The result of the current fit is shown in the right panel of Figure 1. The last two columns of Table 1 give the fitted branching fractions for the default theory parameter set (corresponding to the parameters used in [1] and the central values of the new ranges for m_s and f_B) and a second set, where all annihilation effects and chirally enhanced spectator interactions are switched off. The second set therefore shows that very good fits can also be obtained without these theoretically uncertain power-suppressed effects. While a large range of values of γ remains compatible with data, and the result of the fit is consistent with the standard fit based on meson mixing and $|V_{ub}|$, it shows a preference for γ near 90°, or, for smaller γ, smaller $|V_{ub}|$.

3 CP asymmetries in $B_d \to \pi^+\pi^-$ decay

The QCD factorization approach allows us to interpret directly the mixing-induced and direct CP asymmetry in $B_d \to \pi^+\pi^-$ decay without resort to other decay modes, since the tree and penguin amplitudes are both computed. The time-dependent asymmetry is defined by

$$\begin{aligned} A_{\rm CP}^{\pi\pi}(t) &= \frac{\text{Br}(B^0(t) \to \pi^+\pi^-) - \text{Br}(\overline{B}^0(t) \to \pi^+\pi^-)}{\text{Br}(B^0(t) \to \pi^+\pi^-) + \text{Br}(\overline{B}^0(t) \to \pi^+\pi^-)} \\ &= -S_{\pi\pi}\sin(\Delta m_B\, t) + C_{\pi\pi}\cos(\Delta m_B\, t), \end{aligned} \tag{2}$$

where $S_{\pi\pi} = \sin(2\alpha)$, if the penguin amplitude were zero, and $C_{\pi\pi}$ is the direct CP asymmetry. (This convention is related to those used by Babar and Belle by $S_{\pi\pi} = S_{\pi\pi}^{\rm Babar} = S_{\pi\pi}^{\rm Belle}$ and $C_{\pi\pi} = C_{\pi\pi}^{\rm Babar} = -A_{\pi\pi}^{\rm Belle}$.)

In [1] we have shown how a measurement of $S_{\pi\pi}$ translates into a determination of $\sin(2\alpha)$ and results in a stringent constraint in the $(\overline{\rho}, \overline{\eta})$ plane. In view of the new measurements of $S_{\pi\pi}$ and $C_{\pi\pi}$ from Babar [8] and Belle [9] (summarized in Table 2), it is also interesting to exhibit the correlation between the two observables. This is shown in Figure 2, where the $B\overline{B}$ mixing phase has been fixed such that $\sin(2\beta) = 0.78$. We assume this phase to be experimentally given and do not require that $B\overline{B}$ mixing is described by the Standard Model. Each closed curve is then

Experiment	$S_{\pi\pi}$	$C_{\pi\pi}$
Babar	$-0.01 \pm 0.37 \pm 0.17$	$-0.02 \pm 0.29 \pm 0.09$
Belle	$-1.21^{+0.38+0.16}_{-0.27-0.13}$	$-0.94^{+0.31}_{-0.25} \pm 0.09$

Table 2: CP asymmetries in $B_d \to \pi^+\pi^-$ from Babar and Belle [8, 9].

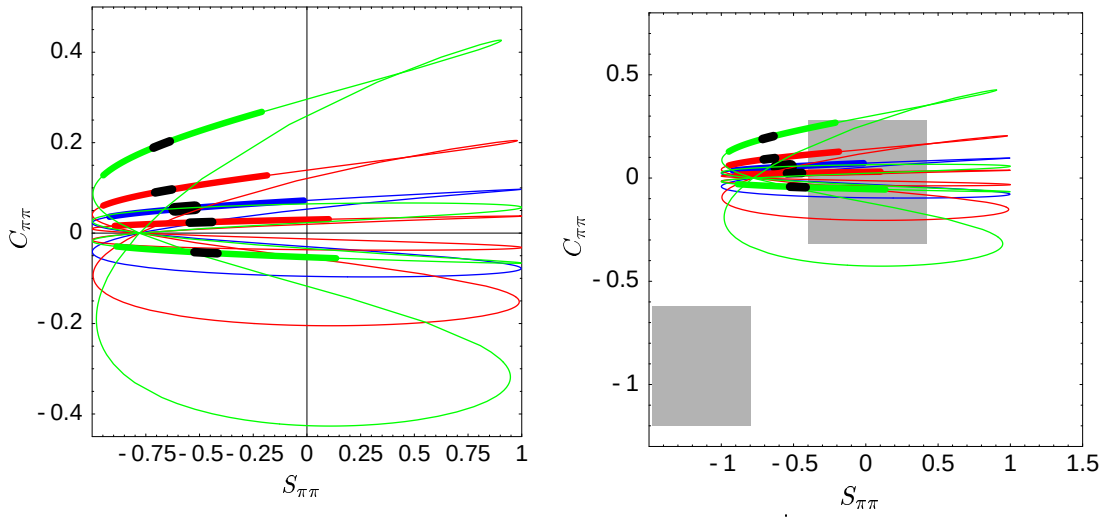

Figure 2: Predicted correlation between mixing-induced and direct CP asymmetry in $B_d \to \pi^+\pi^-$ decay. See text for explanation of the different curves. The right plot is a scaled version of the left plot, and includes the Belle result (upper left) and Babar result (center) with their 1σ errors (gray rectangles). (Note, however, that the physical range is $|S_{\pi\pi}|^2 + |C_{\pi\pi}|^2 \leq 1$.)

generated by specifying the theory input and letting γ vary from 0 to 360°. The central (dark) curve refers to the calculation of P/T, the penguin-to-tree ratio, with the default theory parameter set, the two neighboring (lighter) curves refer to P/T plus-minus its theoretical error without the error from weak annihilation (but including the one from $|V_{ub}|$), and the final (lightest) curves also include the error from weak annihilation. The black part on each curve marks the point $\gamma = 60°$; the fat line segment marks the range $[40°, 80°]$ favoured by the standard unitarity triangle fit with larger γ to the right of the black part. We can see from this that within the 1σ errors only the Babar result is compatible with the theoretical calculation, and it favours γ somewhat larger than the standard unitarity triangle fit, but consistent with the CP-averaged branching fraction data discussed above.

4 Final states containing $\eta^{(\prime)}$

These final states are interesting because the available data exhibit an interesting pattern in $\Delta S = 1$ decays (all branching fractions in units of 10^{-6}):

$$\mathrm{Br}(K\eta') \sim 70 \gg \mathrm{Br}(K\eta) \sim 5\,(?)$$

$$\mathrm{Br}(K^*\eta') \text{ not observed} < (?)\ \mathrm{Br}(K^*\eta) \sim 20 \tag{3}$$

These results are difficult to account for in the naive factorization approach [10] (see also Table 3).

The calculation of the flavour-singlet decay amplitude in QCD factorization involves several aspects specific to singlet mesons [2]. One of them is related to η-η' mixing for which we use the scheme advocated in [11], which amounts to assuming that mixing is described by a single mixing angle common to all matrix elements in the so-called quark-flavour basis. The other aspects are related to the pure gluon content of singlet mesons, which leads to the following new effects:

1. The CKM-enhanced $b \to c\bar{c}s$ transition can contribute to singlet mesons by closing the charm lines and attaching two gluons to them. This effect amounts to assigning a charm decay constant to $\eta^{(\prime)}$, which by explicit calculation of the diagrams is found to be

$$f_P^c = -\frac{m_P^2}{12 m_c^2}\,\frac{f_P^q}{\sqrt{2}} \approx -2.5\,\mathrm{MeV}\,[\eta'],\ -1\,\mathrm{MeV}\,[\eta], \tag{4}$$

   in agreement with [12]. Here f_P^q is the up-quark decay constant and the result is obtained for $m_c \gg \Lambda_{\mathrm{QCD}}$. Note the absence of any factors of α_s.

2. The singlet meson can be produced in a two-gluon state, where one gluon originates from a penguin $b \to s$ transition and the other from the spectator quark. We find a leading-power contribution from the configuration where the second gluon is soft, which implies that factorization breaks down in the conventional sense. Despite this, this non-perturbative contribution can be parameterized by a non-local $B \to K^{(*)}$ form factor, which introduces one new non-perturbative parameter. This effect is proportional to $\alpha_s C_{8g}$, where C_{8g} is the Wilson coefficient of the chromomagnetic dipole operator, and can amount to several percent of the amplitude for $\eta^{(\prime)}$ mesons.

3. There exists a singlet annihilation amplitude which is not power-suppressed in m_b, where two gluons radiate from the spectator quark and form an $\eta^{(\prime)}$ meson.

In Table 3 we present our (still preliminary) results for the CP-averaged $B \to K^{(*)}(\eta^{(\prime)}, \pi^0)$ branching fractions, not including effects 2. and 3. discussed above. We also used $|V_{ub}/V_{cb}| = 0.09$ and $\gamma = 60^\circ$ for the numerical evaluation. The dominant theoretical error is from the strange quark mass and weak annihilation and is correlated among the decay modes displayed in the Table.

Despite the shortcomings of the above analysis (some of which we hope to rectify in the final publication [2]), we see that the QCD factorization calculation appears to reproduce the pattern of the data reasonably well within the uncertainties of the calculation, which are very large for some of the decay modes. The basic features of

Mode	Naive Fact.	QCD Fact.	Exp. average
$B^- \to K^- \eta'$	13	47^{+40}_{-19}	75.1 ± 6.2
$\overline{B}^0 \to \overline{K}^0 \eta'$	14	47^{+38}_{-19}	61.0 ± 12.5
$B^- \to K^- \eta$	0.7	$1.3^{+1.4}_{-0.8}$	5.3 ± 1.8
$\overline{B}^0 \to \overline{K}^0 \eta$	0.1	$0.5^{+1.0}_{-0.5}$	< 9.3
$B^- \to K^- \pi^0$	4.4	$9.4^{+7.3}_{-3.4}$	11.5 ± 1.3
$\overline{B}^0 \to \overline{K}^0 \pi^0$	2.2	$6.4^{+6.1}_{-2.8}$	8.8 ± 2.2
$B^- \to K^{*-} \eta'$	2.9	$3.3^{+8.7}_{-3.3}$	< 35
$\overline{B}^0 \to \overline{K}^{*0} \eta'$	1.6	$2.1^{+7.4}_{-2.1}$	< 24
$B^- \to K^{*-} \eta$	3.8	$9.3^{+16.6}_{-6.1}$	25.4 ± 5.3
$\overline{B}^0 \to \overline{K}^{*0} \eta$	4.3	$10.4^{+17.3}_{-6.5}$	16.4 ± 3.0
$B^- \to K^{*-} \pi^0$	1.7	$3.0^{+4.0}_{-1.4}$	–
$\overline{B}^0 \to \overline{K}^{*0} \pi^0$	0.2	$0.8^{+2.5}_{-0.6}$	–

Table 3: CP-averaged $B \to K^{(*)}(\eta^{(\prime)}, \pi^0)$ branching fractions in units of 10^{-6} in naive factorization and QCD factorization compared to experimental averages. Theoretical results are preliminary as explained in the text. All theoretical errors are strongly correlated.

this pattern can be understood from the structure of the penguin contributions to the decay amplitudes:

$$\begin{aligned}
A(\overline{K}\pi^0) &\sim F^{B\to\pi}\frac{f_K}{\sqrt{2}}\left(a_4^c(\pi K) + r_\chi^K a_6^c(\pi K)\right), \\
A(\overline{K}P) &\sim F^{B\to P}\frac{f_K}{\sqrt{2}}\left(a_4^c(PK) + r_\chi^K a_6^c(PK)\right) \qquad \text{(I)} \\
&\quad + F^{B\to K}\Big(\left(\sqrt{2}f_P^q + f_P^s\right)\left(a_3^c(KP) - a_5^c(KP)\right) \qquad \text{(small)} \\
&\quad\quad + f_P^s\left(a_4^c(KP) + r_\chi^P a_6^c(KP)\right)\Big), \qquad \text{(II)} \qquad (5)
\end{aligned}$$

where $P = \eta, \eta'$ and $K = K, K^*$. For the $K\eta'$ decay the two penguin amplitudes I and II add constructively enhancing the branching fraction by a large factor compared to $K\pi^0$. For $K\eta$, on the other hand, the two amplitudes nearly cancel since the strange decay constant in the η satisfies $f_\eta^s/f_K \sim -2/3$. Replacing K by the vector meson K^* again changes the pattern, because the scalar penguin amplitude $r_\chi^{M_2} a_6^c(M_1M_2)$ changes sign for $M_1M_2 = K^*P$ (changing the sign of the term II) compared to KP and becomes small for $M_1M_2 = PK^*$. As a consequence the terms I and II interfere destructively for $K^*\eta'$ but constructively for $K^*\eta$, opposite to the

case of a pseudoscalar kaon. These features are not different from the expectation in naive factorization. However, radiative corrections in QCD factorization enhance the penguin amplitudes significantly and improve the comparison with data. While it appears unlikely that one can obtain an accurate theoretical description of final states with singlet mesons from first principles, the present results clearly demonstrate the relevance of factorization to this class of charmless B decays.

I am grateful to M. Neubert, G. Buchalla and C.T. Sachrajda for collaboration on the topics discussed in this talk. I thank U. Nierste for reading the manuscript.

References

[1] M. Beneke, G. Buchalla, M. Neubert and C. T. Sachrajda, Nucl. Phys. B **606**, 245 (2001).

[2] M. Beneke and M. Neubert, work in progress.

[3] M. Beneke, G. Buchalla, M. Neubert and C. T. Sachrajda, Phys. Rev. Lett. **83**, 1914 (1999); Nucl. Phys. B **591**, 313 (2000).

[4] M. Beneke, in: Proceedings of the 5th KEK Topical Conference: Frontiers in Flavor Physics (KEKTC5), Tsukuba, Ibaraki, Japan, 20-22 Nov 2001 [hep-ph/0202056].

[5] D. Du, H. Gong, J. Sun, D. Yang and G. Zhu, Phys. Rev. D **65**, 074001 (2002).

[6] R. Bartholdus, these proceedings.

[7] A. Höcker, H. Lacker, S. Laplace and F. Le Diberder, Eur. Phys. J. C **21**, 225 (2001).

[8] P.D. Dauncey [for the Babar Collaboration], these proceedings [hep-ex/0206064].

[9] E. Won [for the Belle Collaboration], these proceedings [hep-ex/0206066].

[10] A. Ali, J. Chay, C. Greub and P. Ko, Phys. Lett. B **424**, 161 (1998).

[11] T. Feldmann, P. Kroll and B. Stech, Phys. Rev. D **58**, 114006 (1998).

[12] M. Franz, M. V. Polyakov and K. Goeke, Phys. Rev. D **62**, 074024 (2000).

Charming Penguins Saga[1]

M. Ciuchini[⋆], *E. Franco*[‡], *G. Martinelli*[‡], *M. Pierini*[‡] *and L. Silvestrini*[‡]
[⋆] *Dip. di Fisica, Università di Roma Tre and I.N.F.N. Sezione di Roma III*
Via della Vasca Navale 84
I-00146 Roma, ITALY
[‡] *Dip. di Fisica, Università di Roma "La Sapienza" and I.N.F.N. Sezione di Roma*
P.le A. Moro 2
I-00185 Roma, ITALY

1 Introduction

"Charming penguins" started back in 1997, coming out of a study aimed to evaluate hadronic effects in non-leptonic two-body B decays. During the years, several episodes added to the saga:

1. *The penguin menace* [1, 2]. A lattice-inspired Wick-contraction parametrization of hadronic amplitudes was introduced and the observation was put forward that non-factorizable penguin contractions of current-current operators containing two c quarks (the charming penguins) could give large contributions in some B decay channels, notably $B \to K\pi$ (a similar idea was already present in ref. [3]).
2. *The neat hack of the clones* [4]. The original Wick-contraction parametrization was modified by Buras and Silvestrini. The hadronic matrix elements were expressed in terms of new renormalization-group invariant parameters given by suitable combinations of the old ones. Many B decay channels were classified according to the new parametrization. Charming penguins became a more complex object, containing further contractions (annihilations, penguin contractions of penguin operators) in addition to the original one.
3. *A new hope* [5, 6]. The one-loop proof that factorization of hadronic matrix elements holds in the limit $m_b \to \infty$ puts phenomenological approaches based on factorization on a firmer theoretical ground (other theoretical approaches to factorization in the infinite mass limit were already developed, although not at the same level of accuracy [7]). *In this limit*, non-factorizable corrections were shown to be computable using perturbation theory. Perturbative penguins turned out to give in general small contributions. Charming penguins seemed at loss.

[1] Talk given by M. Ciuchini.

4. *Charming penguins strike back* [8]. Using $B \to K\pi$ data, it was shown that the parameter accounting for charming penguins has the expected size of a Λ_{QCD}/m_b correction. Therefore, a sizable non-perturbative effect of charming penguins is not in disagreement with the results on factorization obtained in the infinite mass limit. In addition, it is preferred by the data.

5. *The return of factorization* [9, 10]. While everybody agrees that power-suppressed terms are in general non-perturbative and non-factorizable, it was argued that still the bulk of the Λ_{QCD}/m_b corrections can be either factorized or, failing that, accounted for by few parameters (this framework is called *improved* QCD factorization). In addition, these parameters, once properly defined, are claimed to have negligible effects on $B \to K\pi$ branching ratios. Under these assumptions, which were shown to be compatible with the present data, these branching ratios can be used to extract the CKM angle γ.

Is the saga arrived to its end? Theoretically, it is not clear whether a non-perturbative contribution such as charming penguins is large or small. A recent calculation using renormalons found no sign of it [11], while, on the contrary, it is present and effective in other approaches [12]. The $B \to K\pi$ data certainly call for power-suppressed terms and charming penguins are able to provide what is needed. Other approaches, such as the popular *improved* QCD factorization, are also compatible with the data, but none is able to make predictions based only on the theory, due to the presence of phenomenological parameters. Indeed, the presence of these parameters makes us very skeptical about the possibility of extracting the CKM angle γ from the measurement of the $B \to K\pi$ branching ratios.

2 Charming penguins at work

In this section we collect the main formulae for the amplitudes of $B \to K\pi, \pi\pi$, introducing the parametrization used in the analysis. We refer the reader to the literature for any detail on the origin and the properties of these parameters [1, 2, 4, 8]. From ref. [4], one reads

$$\begin{aligned}
A(B_d \to K^+\pi^-) &= \frac{G_F}{\sqrt{2}}\Big(\lambda_t^s P_1 - \lambda_u^s (E_1 - P_1^{GIM})\Big) \\
A(B^+ \to K^+\pi^0) &= \frac{G_F}{2}\Big(\lambda_t^s P_1 - \lambda_u^s (E_1 + E_2 - P_1^{GIM} + A_1)\Big) + \Delta A \\
A(B^+ \to K^0\pi^+) &= \frac{G_F}{\sqrt{2}}\Big(- \lambda_t^s P_1 + \lambda_u^s (A_1 - P_1^{GIM})\Big) + \Delta A \\
A(B_d \to K^0\pi^0) &= \frac{G_F}{2}\Big(- \lambda_t^s P_1 - \lambda_u^s (E_2 + P_1^{GIM})\Big) + \Delta A
\end{aligned} \tag{1}$$

$$
\begin{aligned}
A(B_d \to \pi^+\pi^-) &= \frac{G_F}{\sqrt{2}}\Big(\lambda_t^d(P_1+P_3) - \lambda_u^d(E_1+A_2-P_1^{GIM}) - P_3^{GIM}\Big) \\
A(B_d \to \pi^+\pi^0) &= \frac{G_F}{2}\Big(-\lambda_u^d(E_1+E_2)\Big) + \Delta A \\
A(B_d \to \pi^0\pi^0) &= \frac{G_F}{2}\Big(-\lambda_t^s(P_1+P_3) - \lambda_u^s(E_2+P_1^{GIM}+P_3^{GIM}-A_2)\Big) + \Delta A\,,
\end{aligned}
$$

where $\lambda_{q'}^q = V_{q'q}V_{q'b}^*$. Neglecting the A_i, these parameters can be rewritten as

$$
\begin{aligned}
&E_1 = a_1^c A_{\pi K}\,,\ E_2 = a_2^c A_{K\pi}\,,\ A_1 = A_2 = 0\,, \\
&P_1 = a_4^c A_{\pi K} + \tilde{P}_1\,,\ P_1^{GIM} = (a_4^c - a_4^u)A_{\pi K} + \tilde{P}_1^{GIM}\,.
\end{aligned} \tag{2}
$$

The terms proportional to a_i^q gives the parameters computed in the limit $m_b \to \infty$ using QCD factorization. Their definition, together with those of $A_{\pi K}$, $A_{K\pi}$, etc., can be found for instance in ref. [9], although power-suppressed terms included there, proportional to the chiral factors $r_{K,\pi}^\chi$, should be discarded in eqs. (2). In our case, in fact, terms of $O(\Lambda_{QCD}/m_b)$ are accounted for by two phenomenological parameters: the charming-penguin parameter $\tilde{P}_1$ and the GIM-penguin parameter $\tilde{P}_1^{GIM}$. In $B \to K\pi$ there are no other contributions, once flavour $SU(2)$ symmetry is used and few other doubly Cabibbo-suppressed terms, including corrections to emission parametes E_1 and E_2, some annihilations (A_1) and the Zweig-suppressed contactions (ΔA), are neglected [4]. On the contrary, further power-suppressed terms (A_2, P_3, P_3^{GIM}) enter the $B \to \pi\pi$ amplitudes, all with the same power of the Cabibbo angle. Therefore, these modes are subject to a larger uncertainty than the $B \to K\pi$ ones.

Using the inputs collected in Table 1, we fit the value of the complex parameter $\tilde{P}_1 = (0.13 \pm 0.02)\, e^{\pm i(114\pm 35)^o}$ in units of $f_\pi F_\pi(M_\pi)$. Notice that the sign of the phase is practically not constrained by the data. This result is almost independent of the inputs used for the CKM parameters ρ and η, namely whether these parameters are taken from the usual unitarity triangle analysis (UTA) [14, 15] or only the constraint from $|V_{ub}/V_{cb}|$ is used.

$\lvert V_{cb}\rvert \times 10^3$	$\lvert V_{ub}\rvert \times 10^3$	$\hat{B}_K$	$f_{B_d}\sqrt{B_d}$ (MeV)	ξ
40.9 ± 1.0	3.70 ± 0.42	$0.86 \pm 0.06 \pm 0.14$	$230 \pm 30 \pm 15$	$1.16 \pm 0.03 \pm 0.04$
$F_K(M_K^2)$	$\mathcal{B}(K^+\pi^-)\times 10^6$	$\mathcal{B}(K^+\pi^0)\times 10^6$	$\mathcal{B}(K^0\pi^+)\times 10^6$	$\mathcal{B}(K^0\pi^0)\times 10^6$
0.32 ± 0.12	18.6 ± 1.1	11.5 ± 1.3	17.9 ± 1.7	8.9 ± 2.3
$F_\pi(M_\pi^2)$	$\mathcal{B}(\pi^+\pi^-)\times 10^6$	$\mathcal{B}(\pi^+\pi^0)\times 10^6$	$\mathcal{B}(\pi^0\pi^0)\times 10^6$	
0.27 ± 0.08	5.2 ± 0.6	4.9 ± 1.1	< 3.4 *BaBar*	

Table 1: Values of the input parameters used in our analysis. The CP-averaged branching ratios $\mathcal{B}$ are taken from ref. [13].

Mode	UTA		$\lvert V_{ub}/V_{cb}\rvert$	
	$\mathcal{B}$ (10^{-6})	$\lvert\mathcal{A}_{CP}\rvert$	$\mathcal{B}$ (10^{-6})	$\lvert\mathcal{A}_{CP}\rvert$
$\pi^+\pi^-$	8.9 ± 3.3	0.37 ± 0.17	8.7 ± 3.6	0.39 ± 0.20
$\pi^+\pi^0$	5.4 ± 2.1	–	5.5 ± 2.2	–
$\pi^0\pi^0$	0.44 ± 0.13	0.61 ± 0.26	0.69 ± 0.27	0.45 ± 0.27
$K^+\pi^-$	18.4 ± 1.0	0.21 ± 0.10	18.8 ± 1.0	0.21 ± 0.12
$K^+\pi^0$	10.3 ± 0.9	0.22 ± 0.11	10.7 ± 1.0	0.22 ± 0.13
$K^0\pi^+$	19.3 ± 1.2	0.00 ± 0.00	18.1 ± 1.5	0.00 ± 0.00
$K^0\pi^0$	8.7 ± 0.8	0.04 ± 0.02	8.2 ± 1.2	0.04 ± 0.03

Table 2: Predictions for CP-averaged branching ratios $\mathcal{B}$ and absolute value of the CP asymmetries $|\mathcal{A}_{CP}|$. The left (right) columns show results obtained using constraints on the CKM parameters ρ and η obtained from the UTA (the measurement of $|V_{ub}/V_{cb}|$). The last four channels are those used for fitting the charming penguin parameter $\tilde{P}_1$.

For the sake of simplicity, we also neglect here the contribution of $\tilde{P}_1^{GIM}$. The $B \to K\pi$ data do not constrain this parameter very effectively, since its contribution is doubly Cabibbo suppressed with respect to $\tilde{P}_1$. The remaining $\pi^+\pi^-$ mode alone is not sufficient to fully determine the complex parameter $\tilde{P}_1^{GIM}$. It is interesting, however, to notice that the GIM-penguin contribution is potentially able to enhance the $\mathcal{B}(B \to \pi^0\pi^0)$ up to few $\times 10^{-6}$ [8].

Table 2 shows the predicted values of the CP-averaged branching ratios $\mathcal{B}$ and the absolute value of the CP-asymmetries $|\mathcal{A}_{CP}|$ for the $B \to K\pi$ and $B \to \pi\pi$ modes, since the data are not able to fix the sign of asymmetries. Charming penguins are able to reproduce the $K\pi$ data and are also consistent with the only $\pi\pi$ mode measured so far. It is interesting to notice that the latest measurements improve the consistency, for a comparison see refs. [2, 8].

3 Remarks on the different approaches

Since the different approaches aiming at evaluating power-suppressed terms contain phenomenological parameters, it is natural to ask whether, after all, they are equivalent or not, even if the physical mechanism invoked to introduce the parameters is not the same. To answer this question, it is useful to compute the parameters $\tilde{P}_1$ and $\tilde{P}_1^{GIM}$ within *improved* QCD factorization. They read

$$\tilde{P}_1 = r_K^\chi a_6^c A_{\pi K} + b_3 B_{\pi K}\,, \;\; \tilde{P}_1^{GIM} = r_K^\chi (a_6^c - a_6^u) A_{\pi K}\,, \tag{3}$$

where the functions a_i^q (b_i) contain the complex parameter ρ_H (ρ_A), see ref. [9] for the definitions. These two parameters account for chirally-enhanced terms, origi-

nating from hard-spectator interactions and annihilations respectively, which are not computable within the *improved* QCD factorization.

The functional dependence of the amplitudes on the phenomenological parameters in the two approaches is different. For instance, the GIM-penguin parameter is a pure short-distance correction in the *improved* QCD factorization, since the ρ_H dependence cancels out in the difference $a_6^c - a_6^u$. In practice, however, the main contribution of the phenomenological parameters to the $B \to K\pi$ amplitudes comes from the annihilation term b_3, i.e. from ρ_A . This term behaves effectively as the charming-penguin parameter, enhancing the Cabibbo-favored amplitude.

Notice that a vanishing ρ_A (and ρ_H), which turns out to be compatible with the data, does not mean that the phenomenological contribution is negligible. In fact, the parameters are defined so that the phenomenological terms are functions of $X_{A(H)} = (1 + \rho_{A(H)}) \log(m_B/\mu_h)$, where the scale μ_h is assumed to be 0.5 GeV [9].

4 Non-leptonic B decays and the extraction of γ

The presence of complex phenomenological parameters in the amplitudes makes the extraction of γ very problematic. We checked using the $|V_{ub}/V_{cb}|$-constrained fit that almost any value of γ is allowed, given the uncertainty on $\tilde{P}_1$. This seems a general problem which make us doubt recent claims proposing non-leptonic B decays as an effective tool for the CKM matrix determination. Even more, we think that the combination of the contraint from $B \to K\pi$ decays on γ with the others can even be misleading. The reason is very simple: γ is looked for through the effect of interefence terms in the branching ratios. The presence of a competing amplitude with a new phase, i.e. the one containing the phenomenological parameter, makes the extraction of γ much more complicated. Although weak and strong phases can be disentangled in principle, in practice we checked that not only the task is very difficult now, but the situation improves slowly as data become more accurate, even when the CP asymmetries will be measured.

Concerning various analyses based on the *improved* QCD factorization claiming to find a "large" value of $\gamma \sim 90^o$, we just notice that, as far as we know, they all assume the bound $|\rho_A| < 1$, suggested in ref. [9] as a theoretical prejudice and supported by the observation that even $|\rho_A| = 0$ produces a good fit to $\mathcal{B}(B \to K\pi)$. A better fit, however, can be obtained letting $|\rho_A|$ take values up to about 3. As shown in ref. [15], by doing so, the contribution of the constraint from non-leptonic B decays to a global fit of γ becomes totally negligible. In other words, for $|\rho_A| \sim 3$, the annihilation amplitude containing ρ_A becomes competitive with the others, improving the fit to the $\mathcal{B}$s on the one hand and weakening the predictivity on γ on the other.

References

[1] M. Ciuchini, E. Franco, G. Martinelli and L. Silvestrini, Nucl. Phys. B **501**, 271 (1997) [arXiv:hep-ph/9703353].

[2] M. Ciuchini, R. Contino, E. Franco, G. Martinelli and L. Silvestrini, Nucl. Phys. B **512**, 3 (1998) [Erratum-ibid. B **531**, 656 (1998)] [arXiv:hep-ph/9708222].

[3] P. Colangelo, G. Nardulli, N. Paver and Riazuddin, Z. Phys. C **45**, 575 (1990).

[4] A. J. Buras and L. Silvestrini, Nucl. Phys. B **569**, 3 (2000) [arXiv:hep-ph/9812392].

[5] M. Beneke, G. Buchalla, M. Neubert and C. T. Sachrajda, Phys. Rev. Lett. **83**, 1914 (1999) [arXiv:hep-ph/9905312].

[6] M. Beneke, G. Buchalla, M. Neubert and C. T. Sachrajda, Nucl. Phys. B **591**, 313 (2000) [arXiv:hep-ph/0006124].

[7] H.-N. Li, these proceedings and references therein.

[8] M. Ciuchini, E. Franco, G. Martinelli, M. Pierini and L. Silvestrini, Phys. Lett. B **515**, 33 (2001) [arXiv:hep-ph/0104126].

[9] M. Beneke, G. Buchalla, M. Neubert and C. T. Sachrajda, Nucl. Phys. B **606**, 245 (2001) [arXiv:hep-ph/0104110].

[10] M. Beneke, these proceedings.

[11] M. Neubert and B. D. Pecjak, JHEP **0202**, 028 (2002) [arXiv:hep-ph/0202128].

[12] C. Isola, M. Ladisa, G. Nardulli, T. N. Pham and P. Santorelli, Phys. Rev. D **65**, 094005 (2002) [arXiv:hep-ph/0110411].

[13] R. Patterson, these proceedings.

[14] M. Ciuchini *et al.*, JHEP **0107**, 013 (2001) [arXiv:hep-ph/0012308].

[15] M. Ciuchini, Nucl. Phys. Proc. Suppl. **109**, 307 (2002) [arXiv:hep-ph/0112133].

May 16, session 3.

Session Chair: G. Bonneaud

Recent Results in Theories of Hadronic B Decays

PQCD approach to exclusive B decays

H-n. Li

The Soft-Collinear Effective Field Theory

I. Stewart

Experimental results from the Tevatron and LEP

Status of D0 for B Physics

R. Van Kooten

New Results on B_s^0 Mixing from LEP

S. R. Armstrong

PQCD approach to exclusive B decays

Hsiang-nan Li
Institute of Physics
Academia Sinica
Taipei, Taiwan 115, Republic of China

1 Introduction

The conventional approach to two-body nonleptonic B meson decays is based on FA [1], in which, however, there exist several serious theoretical drawbacks. For example, FA breaks the scale independence of decay amplitudes. It has been shown that the problem of the scale dependence in FA can be transformed into the one of infrared divergences in the generalized FA [2, 3]. In the PQCD approach [4, 5, 6, 7] the infrared divergences in the corrections to the four-fermion vertices are treated in the presence of the spectator quark [8]. Therefore, the leading-twist B meson (light meson) wave function ϕ_B (ϕ_h) can be defined, which absorbs the two-particle reducible infrared divergences on the B meson (light meson) side. In this treatment the external quarks remain on-shell, and the problem of the scale dependence is resolved without breaking gauge invariance. Following the above reasoning, the $B \to hh$ decay amplitudes are written as the convolution,

$$A = \phi_B \otimes H^{(6)} \otimes \phi_{h1} \otimes \phi_{h2} \otimes S \ , \tag{1}$$

where the six-quark amplitude $H^{(6)}$ corresponds to the diagrams with a hard gluon emitted from the spectator quark [4, 5, 9], and S denotes the Sudakov factor.

In PQCD strong phases mainly arise from the annihilation amplitudes, which are almost imaginary [10, 11, 12, 13]. The detailed reason is referred to [14]. The strong phases are large, since they appear at the same order as the factorizable amplitudes. Because of the large imaginary annihilation amplitudes, significant CP asymmetries are expected in the PQCD analyses of two-body nonleptonic B meson decays, such as $B \to K\pi$, $\pi\pi$ [15] and $B \to \rho K$, ωK [16]. The latter modes are especially sensititve to the annihilation contributions. It has been pointed out [17] that contribution from intrinsic charms, one of the higher Fock states of the B meson bound state, reduces the magnitude but does not flip the sign of the $B \to K\pi$ CP asymmetries in the decays. The PQCD predictions with this subleading contribution included is then more consistent with data [18]. It implies that PQCD has caught the correct leading picture of exclusive B meson decays.

2 Sudakov Effects

In PQCD calculations small parton transverse momenta k_T are included [19, 20], which smear the end-point singularities from small momentum fractions [21]. The resummation of the resultant double logarithms $\ln^2(Pb)$, P denotes the dominant light-cone component of a meson momentum, and b is the variable conjugate to k_T, leads to a Sudakov form factor $\exp[-s(P,b)]$. This factor suppresses the long-distance contributions from the large b region with $b \sim 1/\overline{\Lambda}$, where $\overline{\Lambda} \equiv M_B - m_b$, M_B being the B meson mass, represents a soft scale. The suppression renders k_T^2 flowing into the hard amplitudes of order $k_T^2 \sim O(\overline{\Lambda} M_B)$. The off-shellness of internal particles then remain of $O(\overline{\Lambda} M_B)$ even in the end-point region, and the singularities are removed. Since the end-point singularities do not exist [20, 22], the arbitrary cutoffs introduced in QCDF [23, 24] are not necessary. Therefore, factorizable, nonfactorizable and annihilation amplitudes can be estimated in a more consistent way in PQCD than in QCDF.

It is easy to understand the increase of k_T^2 from $O(\overline{\Lambda}^2)$, carried by the valence quarks which just come out of the initial meson wave functions, to $O(\overline{\Lambda} M_B)$, carried by the quarks which are involved in the hard weak decays. Consider the simple deeply inelastic scattering of a hadron. The transverse momentum k_T carried by a parton, which just come out of the hadron distribution function, is initially small. After infinite many gluon radiations, k_T becomes of $O(Q)$, when the parton is scattered by the highly virtual photon, where Q is the large momentum transfer from the photon. The evolution of the hadron distribution function from the low scale to Q is described by the Dokshitzer-Gribov-Lipatov-Altarelli-Parisi (DGLAP) equation [25]. The mechanism of the DGLAP evolution in DIS is similar to that of the Sudakov evolution in exclusive B meson decays. The difference is only that the former is the consequence of the single-logarithm resummation, while the latter is the consequence of the double-logarithm resummation.

3 Penguin Enhancement

The leading factorizable contributions involve four-quark hard amplitudes in QCDF, but six-quark hard amplitudes in PQCD. This distinction also implies different characteristic scales in the two approaches: the former is characterized by m_b, while the latter is characterized by the virtuality of internal particles of order $\sqrt{\overline{\Lambda} M_B} \sim 1.5$ GeV [10, 11, 13]. It has been known that to accommodate the $B \to K\pi$ and $\pi\pi$ data, penguin contributions must be large enough. In QCDF one relies on chiral enhancement by increasng the mass m_0 to a large value $m_0 \sim$ 3-4 GeV [26]. Because of the renormalization-group evolution effect of the Wilson coefficients associated with the QCD penguin operators, the lower hard scale leads to dynamical penguin

enhancement in PQCD. Whether dynamical enhancement or chiral enhancement is responsible for the large $B \to K\pi$ branching ratios can be tested by measuring the $B \to \phi K$ modes [14, 27]. In these modes penguin contributions dominate, such that their branching ratios are insensitive to the variation of the unitarity angle ϕ_3. Because the ϕ meson is a vector meson, the mass m_0 is replaced by the physical mass $M_\phi \sim 1$ GeV, and chiral enhancement does not exist. If the branching ratios of the $B \to \phi K$ decays are around 4×10^{-6} [28, 29], chiral enhancement may be essential for the penguin-dominated decay modes. If the branching ratios are around 10×10^{-6} as predicted in PQCD [14, 30], dynamical enhancement may be essential.

4 $B \to D^0\pi^0$ and $B \to \pi^+\pi^0$

It can be shown that the relative importance of the different topologies of diagrams for the $B \to D\pi$ decays is given by

$$\text{emission} : \text{nonfactorizable} = 1 : \frac{M_D}{M_B} , \tag{2}$$

which approaches $1 : \overline{\Lambda}/M_B$ as the D meson mass M_D reduces to the pion mass of $O(\overline{\Lambda})$. Since the factorizable and nonfactorizable diagrams contribute to the parameters a_1 and a_2 in PQCD, respectively, the ratio $|a_2|/a_1 \sim 0.3$ is obtained. Moreover, the imaginary nonfactorizable amplitudes determine the relative phase of the factorizable and nonfactorizable contributions, which is about 60^o. It has been found that the PQCD predictions for the $B \to D\pi$ branching ratios [31],

$$B(D^0\pi^-) \sim 4.8 \times 10^{-3} , \quad B(D^+\pi^-) \sim 3.0 \times 10^{-3} , \quad B(D^0\pi^0) \sim 0.2 \times 10^{-3} , \tag{3}$$

are consistent with the experimental data, including the recently observed one for the $\overline{B}_d \to D^{(*)0}\pi^0$ decay [32, 33].

Therefore, it is difficult to explain the large $B \to \pi^+\pi^0$ braching ratio around 7×10^{-6} observed by BELLE recently [18]. This large branching ratio implies large a_2 for the $B \to \pi\pi$ decays, which is in conflict with the PQCD power counting rules. Final-state-interaction is unlikely to resolve this controversy either, since the upper bound on the $B \to K^+K^-$ branching ratio has strongly constrained its effect [34]. Fortunately, the BABAR result for the $B \to \pi^+\pi^0$ braching ratio announced at this conference has a central value around 4×10^{-6}, which is consistent with the PQCD prediction.

5 Conclusion

I have briefly reviewed the PQCD approach to two-body nonleptonic B meson decays. The PQCD predictions for the branching ratios and the CP asymmetries of varous

modes with one single parameter, the shape parameter associated with the B meson wave function, are in agreement with the experimental data [35]. The $B \to K\eta'$ data are an exception, which may indicate a significant gluon content of the η' meson [36]. In the future we shall work out the next-to-leading-order and next-to-leading-power corrections to the decay amplitudes.

I thank members in the PQCD working group for useful discussions. The work was supported in part by the National Science Council of R.O.C. under the Grant No. NSC-90-2112-M-001-077, by the National Center for Theoretical Science of R.O.C., and by Grant-in Aid for Special Project Research (Physics of CP Violation) and by Grant-in Aid for Scientific Exchange from Ministry of Education, Science and Culture of Japan.

References

[1] M. Bauer, B. Stech, and M. Wirbel, Z. Phys. C **29**, 637 (1985); Z. Phys. C **34**, 103 (1987).

[2] A. Ali and C. Greub, Phys. Rev. D **57**, 2996 (1998).

[3] H.Y. Cheng and B. Tseng, Phys. Rev. D **58**, 094005 (1998).

[4] C.H. Chang and H-n. Li, Phys. Rev. D **55**, 5577 (1997).

[5] T.W. Yeh and H-n. Li, Phys. Rev. D **56**, 1615 (1997).

[6] M. Dahm, R. Jakob, and P. Kroll, Z. Phys. C **68**, 595 (1995).

[7] B. Melic, Phys. Rev. D **59**, 074005 (1999).

[8] H.Y. Cheng, H-n. Li, and K.C. Yang, Phys. Rev. D **60**, 094005 (1999).

[9] C.Y. Wu, T.W. Yeh, and H-n. Li, Phys. Rev. D **53**, 4982 (1996); Phys. Rev. D **55**, 237 (1997).

[10] Y.Y. Keum, H-n. Li and A.I. Sanda, Phys. Lett. B **504**, 6 (2001); Phys. Rev. D **63**, 054008 (2001).

[11] C. D. Lü, K. Ukai, and M. Z. Yang, Phys. Rev. D **63**, 074009 (2001).

[12] C.D. Lü and M.Z. Yang, hep-ph/0011238.

[13] Y.Y. Keum and H-n. Li, Phys. Rev. D **63**, 074006 (2001).

[14] C.H. Chen, Y.Y. Keum, and H-n. Li, Phys. Rev. D **64**, 112002 (2001).

[15] K. Ukai and A.I. Sanda, hep-ph/0109001.

[16] C.H. Chen, Phys. Lett. B **525**, 56 (2002).

[17] S. Brodsky and S. Gardner, Phys. Rev. D **65**, 054016 (2992).

[18] see the BABAR and BELLE talks presented at this conference.

[19] H-n. Li and G. Sterman, Nucl. Phys. **B381**, 129 (1992).

[20] H-n. Li and H.L. Yu, Phys. Rev. Lett. **74**, 4388 (1995); Phys. Lett. B **353**, 301 (1995); Phys. Rev. D **53**, 2480 (1996).

[21] A. Szczepaniak, E.M. Henley, and S. Brodsky, Phys. Lett. B **243**, 287 (1990).

[22] H-n. Li, hep-ph/0102013.

[23] M. Beneke, G. Buchalla, M. Neubert, and C.T. Sachrajda, Phys. Rev. Lett. **83**, 1914 (1999); Nucl. Phys. **B591**, 313 (2000).

[24] M. Beneke, G. Buchalla, M. Neubert, and C.T. Sachrajda, Nucl. Phys. **B606**, 245 (2001).

[25] V.N. Gribov and L.N. Lipatov, Sov. J. Nucl. Phys. **15**, 428 (1972); G. Altarelli and G. Parisi, Nucl. Phys. **B126**, 298 (1977); Yu.L. Dokshitzer, Sov. Phys. JETP **46**, 641 (1977).

[26] N.G. Deshpande, X.G. He, W.S. Hou and, S. Pakvasa, Phys. Rev. Lett. **82**, 2240 (1999); W.S. Hou, J.G. Smith, and F. Würthwein, hep-ex/9910014.

[27] H-n. Li, hep-ph/0103305, talk presented at the 4th International Workshop on B Physics and CP Violation (BCP4), Ise-shima, Japan, Feb. 2001.

[28] X.G. He, J.P. Ma, and C.Y. Wu, Phys. Rev. D **63**, 094004 (2001).

[29] H.Y. Cheng and K.C. Yang, Phys. Rev. D **64**, 074004 (2001).

[30] S. Mishima, Phys. Lett. B **521**, 252 (2002).

[31] T. Kurimoto, C.D. Lu, and H-n. Li, in preparation.

[32] Belle Coll., K. Abe *et al.*, hep-ex/0109021.

[33] CLEO Coll., T.E. Coan, hep-ex/0110055.

[34] C.H. Chen and H-n. Li, Phys. Rev. D **63**, 014003 (2001), and references therein.

[35] Y.Y. Keum, H-n. Li, and A.I. Sanda, hep-ph/0201103.

[36] E. Kou and A.I. Sanda, hep-ph/0106159.

The Soft-Collinear Effective Field Theory

Iain W. Stewart
INT, Department of Physics
University of Washington
Box 351550
Seattle, WA 98195

1 Introduction

Understanding the dependence of results on non-perturbative contributions is important for extracting interesting results out of both high and low energy experminents. In general, to understand hadronic uncertainties we need a separation of short $p \sim Q$ and long $p \sim \Lambda_{\rm QCD}$ distance fluctuations. For processes in QCD with momentum transfers $Q \gg \Lambda_{\rm QCD}$, the short distance part is calculable in terms of Wilson coefficients or hard scattering functions. The long distance contributions can be arranged into universal non-perturbative matrix elements which can be extracted from data or calculated on the lattice. This process of separating short and long distance fluctuations is sometimes referred to as factorization.

In B physics a proper understanding of hadronic uncertainties is crucial since the size of typical expansion parameters $\Lambda_{\rm QCD}/m_b$, $\Lambda_{\rm QCD}/m_c$, or $\sqrt{\Lambda_{\rm QCD}/m_b}$ leaves room for power corrections to play a non-negligible role. For many processes Heavy Quark Effective Theory (HQET) provides the conceptual framework for quantifying the factorization between the scales $m_{b,c}$ and $\Lambda_{\rm QCD}$. A well known example is the extraction of the CKM matrix element $|V_{cb}|$ from knowledge about the form factors in $B \to D^* \ell\nu$ decays. At zero recoil the leading result is fixed by Heavy Quark Symmetry [2], and the first power corrections vanish [3]. More recently important progress has been made at reducing the dominant model dependence by computing the matrix elements of $1/m_Q^2$ operators on the Lattice [4]. For inclusive $B \to X_c \ell\nu$ and $B \to X_u \ell\nu$ decays the non-perturbative HQET matrix elements $\overline{\Lambda}$ and λ_1 are actively being extracted from experimental data [5].

Since the B is so heavy, many of its decays produce energetic light hadrons. For these decays the energy of the hadron E_H in the B rest frame is an additional perturbative scale, and HQET alone does not separate the perturbative and non-perturbative information. Examples of such processes include the decays $B \to D\pi$, $B \to \pi\pi$, $B \to K\pi$, the large recoil region in $B \to \pi\ell\nu$, $B \to \rho\ell\nu$, $B \to K^*\gamma$, and $B \to K\ell^+\ell^-$, and the endpoint spectra of the inclusive decays $B \to X_u\ell\nu$ and

Type	Momenta $(+,-,\perp)$	Field Scaling	Operators
collinear	$p^\mu \sim (\lambda^2, 1, \lambda)$	$\xi_{n,p} \sim \lambda$	$\overline{\mathcal{P}}$, $W_n \sim \lambda^0$
		$(A^+_{n,p},\ A^-_{n,p},\ A^\perp_{n,p}) \sim (\lambda^2,1,\lambda)$	$\mathcal{P}^\mu_\perp \sim \lambda$
soft	$p^\mu \sim (\lambda, \lambda, \lambda)$	$q_{s,p} \sim \lambda^{3/2}$	$S_n \sim \lambda^0$
		$A^\mu_{s,p} \sim \lambda$	$\mathcal{P}^\mu \sim \lambda$
usoft	$k^\mu \sim (\lambda^2, \lambda^2, \lambda^2)$	$q_{us} \sim \lambda^3$	$Y_n \sim \lambda^0$
		$A^\mu_{us} \sim \lambda^2$	

Table 1: Power counting for SCET momenta and fields as well as momentum label operators ($\overline{\mathcal{P}}, \mathcal{P}^\mu_\perp, \mathcal{P}^\mu$) and collinear and soft Wilson lines induced by integrating out offshell fluctuations (W, S_n) and the usoft Wilson line Y_n induced by a collinear field redefinition as described in the text.

$B \to X_s\gamma$. The nature of factorization in these decays shares features in common with many exclusive and inclusive hard scattering processes. Examples are $\gamma^*\gamma \to \pi^0$ at large q^2 and the $x \sim 1$ endpoint region of deep inelastic scattering.

In this talk I discuss an effective field theory that has been developed for processes with energetic hadrons, which is referred to as the Soft-Collinear Effective Theory (SCET) [6, 7, 8, 9]. SCET can be used for both hard scattering processes [10] and B-physics. This theory makes symmetries relevant in the large energy limit explicit at the level of the Lagrangian and operators (such as the reduction of spin structures, helicity constraints, and collinear gauge invariance). Furthermore, SCET has a transparent power counting in $\lambda = \Lambda_{\rm QCD}/Q$ (or $\lambda = \sqrt{\Lambda_{\rm QCD}/Q}$) so that power corrections can be investigated in a systematic way [11, 12, 13]. This includes processes not amenable to an operator product expansion such as exclusive decays. The renormalization group improvement of operators in the effective theory sums single infrared logs, as well as double Sudakov logarithms when they appear. Finally, SCET allows proofs of factorization theorems to be simplified and carried out in a gauge invariant way.

2 Formalism

The factorization of scales in the effective theory is carried out by describing long distance fluctuations with $p^2 \lesssim Q^2\lambda^2$ using effective theory fields, and those with $p^2 \gg Q^2\lambda^2$ by computable short distance Wilson coefficients. Typical processes require collinear fields and in addition either soft or usoft fields. Examples are $B \to X_s\gamma$ which needs collinear and usoft fields, and $B \to D\pi$ which needs collinear and soft fields. This field content is summarized in Table 1 together with the scaling of the

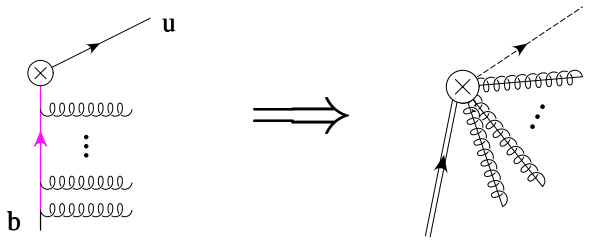

Figure 1: Tree level matching for the leading order heavy-to-light current

momenta and fields with the expansion parameter λ [6, 7]. The momenta scales Q, $Q\lambda$, and $Q\lambda^2$ are separated by making phase redefinitions to pull out the larger momenta, $\phi_n(x) = \sum_p e^{-ip\cdot x}\phi_{n,p}(x)$. Derivatives on the new fields then always pick out the small scale, $\partial^\mu\phi_{n,p}(x) \sim (Q\lambda^2)\phi_{n,p}(x)$, while the large momenta are picked out by introducing label operators, for example $\overline{\mathcal{P}}\,\xi_{n,p} = (\overline{n}\cdot p)\,\xi_{n,p}$. Since $\overline{\mathcal{P}} \sim \lambda^0$ in the power counting the hard coefficients $C(\overline{\mathcal{P}})$ are arbitrary functions of this operator [8], which can be determined by matching. More generally we have functions $C(\omega_i)\prod_i \delta(\omega_i - \overline{\mathcal{P}})$ where the delta functions are inserted inside collinear operators in the most general locations allowed by gauge and reparameterization invariance.

Furthermore, there are gluon fields which are order λ^0 in the power counting, namely $\overline{n}\cdot A_{n,q} \sim 1$. Integrating out offshell fluctuations builds up Wilson lines in these fields, such as in the example [7] of matching the full theory heavy-to-light current $\overline{u}\Gamma b$ onto the SCET current, $J_0 = C(\overline{\mathcal{P}})\,\overline{\xi}_{n,p}W\Gamma h_v$. In fact the $\overline{n}\cdot A_{n,q}$ field can be traded for the Wilson line

$$W \;=\; \Big[\sum_{\text{perms}} \exp\Big(-\frac{g}{\overline{\mathcal{P}}}\,\overline{n}\cdot A_{n,q}(x)\Big)\Big]\,, \tag{1}$$

since the covariant derivative $i\overline{n}\cdot D_c = \overline{\mathcal{P}} + g\overline{n}\cdot A_{n,q} = W\,\overline{\mathcal{P}}\,W^\dagger$. Soft Wilson lines $S_n[n\cdot A_s]$ are also built up by integrating out offshell fluctuations [9]. Beyond tree level the structure of operators containing factors of W or S_n is protected by collinear and soft gauge transformations [8, 9].

In general we have three types of gluon fields, collinear, soft, and usoft. These are the fields associated with gauge transformations $U(x)$ which have support over collinear, soft, and usoft momenta respectively [9]. The usoft fields A^μ_{us} are dynamical quantum fields which due to their slow variation appear as background fields to the soft and collinear quarks and gluons. For a gauge transformation with support over collinear momenta it is convenient to factor out the large momentum components, $U(x) = \sum_R e^{-iR\cdot x}\,\mathcal{U}_R(x)$. The collinear gluon field then transforms as

$$A^\mu_{n,p} \to \mathcal{U}_Q A^\mu_{n,R}\mathcal{U}^\dagger_{Q+R-p} + \frac{1}{g}\,\mathcal{U}_Q[i\mathcal{D}^\mu\mathcal{U}^\dagger_{Q-p}]\,, \tag{2}$$

where $i\mathcal{D}^\mu = n^\mu \overline{\mathcal{P}}/2 + \mathcal{P}_\perp^\mu + \overline{n}^\mu in\cdot D/2$. On the other hand an usoft gauge transformation has $i\partial^\mu U(x) \sim (Q\lambda^2)U(x)$. For the most general collinear gauge transformation with dependence on all x^μ it is not possible to completely separate usoft and collinear components, so for this case the ultrasoft gluon field also transforms. In fact $\mathcal{U}_R(x)$ itself is an usoft gauge transformation since it no longer has a large phase. A simple mnemonic is that gauge transformations that do not impart large momentum to the original field are usoft. Beyond leading order these more general transformations must be considered to correctly constrain operators as pointed out in Ref. [11]. For example, we have

$$A_{us}^\mu \to \mathcal{U}_R A_{us}^\mu \mathcal{U}_R^\dagger + \mathcal{U}_R \frac{i}{g}\partial_\mu \mathcal{U}_R^\dagger \,. \tag{3}$$

The transformation does not induce large momentum in the ultrasoft field because the large momenta in $\mathcal{U}_R$ and $\mathcal{U}_R^\dagger$ cancel. Gauge invariance constrains the form of the Lagrangian at leading and subleading orders. For the explicit form of the leading order gluon and quark actions $\mathcal{L}_c^{(0)}$ we refer the reader to Ref. [9], for higher order terms in the collinear quark action to Refs. [11, 16], and for the mixed collinear-usoft quark action to Ref. [13].

Besides the constraints from gauge invariance on collinear operators there are addition constraints from the way in which Lorentz invariance is realized in the effective theory. The collinear fields are defined by introducing two auxillary light-like vectors, n and $\overline{n}$, such that $n\cdot\overline{n} = 2$. Naively the presence of these vectors breaks Lorentz invariance. However, in practice Lorentz invariance is restored order by order in the power counting by a reparameterization invariance (RPI) [15]. For the collinear theory the study of RPI was initiated in Ref. [11] and generalized to the three most general classes of allowed transformations in Ref. [16]. For Lagrangians and operators with collinear fields, RPI gives non-trivial constraints between the Wilson coefficients of operators at different orders in the power expansion. In general there is no way of deducing these constraints using only the full theory.

Finally, it is worth discussing why the proof of factorization theorems is simplified by using the effective theory. The factorization between hard and collinear fluctuations or soft and collinear fluctuations is simplified by the fact that it takes place at the level of matching onto the effective theory. The resulting structures are constrained by the symmetries of the low energy theory as already discussed. The factorization between collinear and usoft interactions is simplified by the fact that many cancellations occur in a universal way at the level of the effective Lagrangian. For instance, at lowest order the actions for usoft and collinear particles can be factorized by a simple field redefinition on the collinear fields, $\xi_{n,p} = Y_n \xi_{n,p}^{(0)}$ and $A_{n,p} = Y_n A_{n,p}^{(0)} Y_n^\dagger$, where $Y_n = P\exp[ig\int_{-\infty}^x ds\, n\cdot A_{us}(sn)]$. This transformation moves all leading order usoft interactions from the collinear Lagrangian $\mathcal{L}_c^{(0)}$ into the external operators and currents, where cancellations due to the unitarity of the usoft Wilson line, $Y_n^\dagger Y_n = 1$,

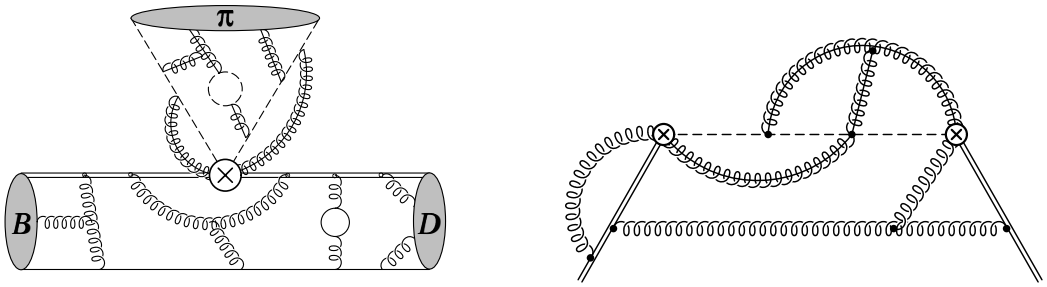

Figure 2: Pictures of how the factorization of interactions occurs in $B \to D\pi$ and $B \to X_s\gamma$.

are more readily seen [9].

3 Results

I briefly discuss two B-physics applications of SCET, the exclusive decay $B \to D\pi$ and the inclusive process $B \to X_s\gamma$.

For the decay $B \to D\pi$ the energy of the outgoing pion in the rest frame of the B is $E_\pi = 2.310\,\mathrm{GeV}$. Since this energy is large it is useful to consider this decay as being in the situation where $Q \gg \Lambda_{\rm QCD}$ with $Q = m_b$, m_c, or E_π. In this limit, SCET has been used to prove the following factorization theorem [14]

$$\langle D^{(*)}\pi|H_w|B\rangle = N F^{B\to D^{(*)}}(0) \int_0^1 d\xi\; T(\xi,Q,\mu)\; \phi_\pi(\xi,\mu) + \ldots\,, \tag{4}$$

where the ellipses denote terms that vanish faster than the leading term as $Q \to \infty$. The relevant terms in the electroweak Hamiltonian are $H_W = C_1 O_1 + C_8 O_8$, where $O_1 = \overline{d}_L \gamma^\mu u_L \overline{c}_L \gamma_\mu b_L$ and $O_8 = \overline{d}_L T^A \gamma^\mu u_L \overline{c}_L T^A \gamma_\mu b_L$. Eq. (4) was proposed in Ref. [17], proven to two-loops in Ref. [18], and proven to all orders in α_s in Ref. [14]. The idea behind the proof is shown in Fig. 2. After integrating out offshell fluctuations the leading order interactions involve soft gluons exchanged between quarks in the B and D which build up the $B \to D$ form factor $F^{B\to D}$, and collinear gluons exchanged between quarks in the pion building up the light-cone pion wavefunction $\phi_\pi(x)$. It should be remarked that the effective theory analysis is carried out at an operator level so it does not explicitly rely on perturbation theory.

For the proccess $B \to X_s\gamma$ in the region of photon energies $E_\gamma \gtrsim m_B/2 - \Lambda_{\rm QCD} \simeq 2.2\,\mathrm{GeV}$ the particles in X_s are collimated in a collinear jet with offshellness $p_X^2 \simeq m_B \Lambda_{\rm QCD}$. In this process the B meson is dominated by usoft dynamics and the

leading power prediction from factorization is [19]

$$\frac{1}{\Gamma_0}\frac{d\Gamma}{dE_\gamma} = H(m_b,\mu)\int_{2E_\gamma-m_b}^{\overline{\Lambda}} dk^+\, S(k^+,\mu)\, J(k^+ + m_b - 2E_\gamma,\mu)\,. \tag{5}$$

The SCET has been used to give a simple direct proof of this result [9]. After the collinear field redefinitions, the usoft interactions rearrange themselves to leave only diagrams such as the one shown in Fig. 2. In Eq. (5) H encodes calculable m_b scale contributions, J encodes $\sqrt{m_b\Lambda_{\rm QCD}}$ scale contributions, and S is the non-perturbative shape function. This factorization formula is required to describe the CLEO data on the photon energy spectrum [20].

To summarize, the soft-collinear effective theory allows factorization proofs to be simplified and formulated at the level of an effective Lagrangian and operators. Essentially the same steps are applied for many exclusive and inclusive processes. Finally, SCET provides us with a new framework for investigating power corrections, and can be used to classify subleading non-perturbative matrix elements.

This work was supported in part by the Department of Energy under the grant DE-FG03-00-ER-41132. I would like to thank Christian Bauer and Dan Pirjol for enjoyable collaboration on the results presented here.

References

[1] A. V. Manohar and M. B. Wise, Cambridge Monogr. Part. Phys. Nucl. Phys. Cosmol. **10**, 1 (2000).

[2] N. Isgur and M.B. Wise, Phys. Lett. B **232**, 113 (1989); Phys. Lett. B **232**, 113 (1989).

[3] M. E. Luke, Phys. Lett. B **252**, 447 (1990).

[4] A. S. Kronfeld, this proceedings (with P. B. Mackenzie, J. N. Simone, S. Hashimoto and S. M. Ryan), arXiv:hep-ph/0207122.

[5] K. Ecklund, this proceedings.

[6] C. W. Bauer, S. Fleming and M. Luke, Phys. Rev. D **63**, 014006 (2001).

[7] C. W. Bauer, S. Fleming, D. Pirjol, I. W. Stewart, Phys. Rev. D **63**, 114020 (2001).

[8] C. W. Bauer and I. W. Stewart, Phys. Lett. B **516**, 134 (2001).

[9] C. W. Bauer, D. Pirjol and I. W. Stewart, Phys. Rev. D **65**, 054022 (2002).

[10] C. W. Bauer, S. Fleming, D. Pirjol, I. Z. Rothstein and I. W. Stewart, arXiv:hep-ph/0202088.

[11] J. Chay and C. Kim, arXiv:hep-ph/0201197 and arXiv:hep-ph/0205117.

[12] C. W. Bauer, D. Pirjol, and I. W. Stewart, arXiv:hep-ph/0205289.

[13] M. Beneke, A. P. Chapovsky, M. Diehl, and T. Feldmann, arXiv:hep-ph/0206152.

[14] C. W. Bauer, D. Pirjol and I. W. Stewart, Phys. Rev. Lett. **87**, 201806 (2001).

[15] M. E. Luke and A. V. Manohar, Phys. Lett. B **286**, 348 (1992).

[16] A. V. Manohar, T. Mehen, D. Pirjol, I. W. Stewart, Phys. Lett. B **539**, 59 (2002).

[17] D. Politzer and M. Wise, Phys. Lett. **B257**, 399 (1991).

[18] M. Beneke, G. Buchalla, M. Neubert and C. T. Sachrajda, Nucl. Phys. B **591**, 313 (2000).

[19] G. P. Korchemsky and G. Sterman, Phys. Lett. B **340**, 96 (1994).

[20] E.Thorndike, this proceedings (for CLEO, hep-ex/0206067).

Status of D0 for B Physics

R. Van Kooten for the D0 Collaboration
Physics Department
Indiana University
Bloomington, IN 47405
rickv@fnal.gov

1 Introduction

In light of the voluminous data being collected at the B factories, it is worthwhile examining why it is interesting to study B physics at the Tevatron at Fermilab (Batavia, Illinois). Both D0 and CDF enjoy a large rate of production with $\sigma(p\overline{p} \to b\overline{b}) \approx 150\ \mu$b at a collision energy of 2 TeV compared to $\sigma(e^+e^- \to b\overline{b}) \approx 7$ nb at the Z^0 peak, and $\sigma(e^+e^- \to B\overline{B}) \approx 1$ nb at the $\Upsilon(4S)$ peak. Also, in contrast to the B factories running at the $\Upsilon(4S)$ peak where only B_d^0 and $B^\pm$ are produced, all b hadron species including B_s, B_c, and Λ_b are produced. Measurements of B_s mixing are important in the understanding of the CKM triangle, and a great deal can be learned from the properties and behavior of hadrons containing heavier quarks besides the b.

2 Run 2 B Physics

Run 1 for D0 ended in 1996 and work began on the Main Injector and upgrading the detector as described in the next section. Run 2 is defined by the running of the Tevatron with the Main Injector at an increased collision energy of 2 TeV (from 1.8 TeV) and increased luminosity. Run 2a is planned to have an integrated luminosity of 2 fb^{-1} and Run 2b of 15–20 fb^{-1}.

Some of the more important topics of the planned D0 Run 2 B physics program are summarized in Table 1. Question marks following the decays $B \to \pi^+\pi^-$ and $B_s \to K^+K^-$ imply that although effort will be made to isolate these samples, it is unclear whether D0's triggering capability will allow this collection with reasonable bandwidth.

3 Upgraded D0 Detector

The described program of B physics could only be undertaken if the Run 1 D0 detector were upgraded. The Run 2 detector upgrade retained the excellent Run 1 liquid

QCD tests	cross sections, correlations,
charmonium polarization	
CP violation and CKM angles	$\sin 2\beta$ through $B \to J/\psi K_S$;
	α, γ through $B \to \pi^+\pi^-$?, $B_s \to K^+K^-$?
Non-SM CP Violation	$B_s \to J/\psi\phi$
B_s mixing	$B_s \to D_s n\pi$, $B_s \to D_s \ell\mu$
Spectroscopy and Lifetimes	B_d^0, B^+, B_s^0, B_c, Λ_b, double heavy baryons
Rare decays	$B \to \ell^+\ell^- X_s$, $B \to \ell^+\ell^-$

Table 1: Summary of important topics in planned B physics program.

argon/uranium calorimeter, while increasing the speed of its readout. The muon toroids were retained, and the muon system was upgraded for better muon identification and triggering, particularly suited for tagging b's decaying semileptonically. Most importantly for B physics, a new tracker operating in a solenoidal magnetic field was added. Further details of the detector can be found elsewhere [1].

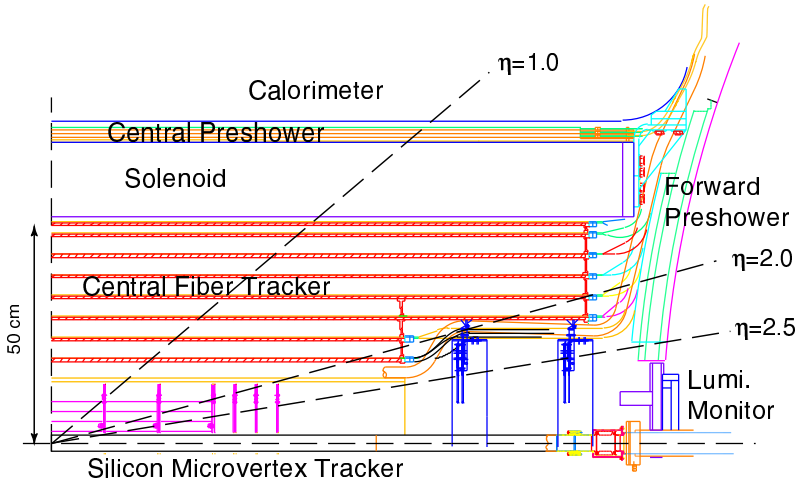

Figure 1: D0 Upgrade detector tracking system.

Figure 1 illustrates the new tracker. Working outwards in radius, the silicon microvertex detector (SMT) consists of six barrels (four layers) of single and double-sided silicon strip sensors interspersed with double-sided disks providing 800k channels with a single hit space resolution of 10 μm, leading to good impact parameter resolution. The central fiber tracker (CFT) provides the necessary momentum resolution, and is made up of eight concentric barrels of scintillating optical fiber doublets (half at stereo angles of $\pm 3^\circ$) mounted on carbon fiber tubes. Single hit r-ϕ resolutions are

80–100 μm. Clear optical fibers carry the light to 77k channels of visible light photon detectors and also provide a fast pick-off for a track trigger. Following a 2 T superconducting solenoid, a central (and forward at larger η's) preshower detector of triangular scintillator strips with embedded wavelength-shifting fibers improves non-isolated electron identification to aid in semileptonic b tagging.

Although the rate for b production is high, the hadronic environment still results in a challenging signal to background, with a total hadronic background of $\sigma_{\rm had}^{\rm tot} \approx 75$ mb to be compared to $\sigma_{b\bar{b}} \approx 0.1$ mb. To address this, we have a pipelined Level-3 trigger that will have the capability to trigger on tracks with significant impact parameter at Level 2 and on tracks in given momenta ranges at Level 1. In addition, there will often be one or more overlapping minimum bias events on the event of interest, with an expected average of 2.0 at Run 2a's projected peak luminosity.

The projected performance of the D0 upgrade detector is a momentum resolution of $\delta p_T/p_T^2 = 0.002$ combining the SMT and CFT measurements and tracking out to $|\eta| < 3$ using the forward silicon disks. The fitted primary vertex should have a resolution of 15–30 μm in r-ϕ and secondary vertices found with resolutions of 40 μm (r-ϕ) and 80 μm (r-z). The upgrade detector has excellent lepton coverage for both triggers and identification: muons in the range $p_T > 2.0$ GeV, $|\eta| < 2.0$ and electrons over $p_T > 2.0$ GeV, $|\eta| < 2.5$. The impact parameter resolution is expected to asymptotically approach 15 μm for high-momentum tracks. Comparisons of detector performance to these expected benchmarks will be shown in the next section.

4 Current Data and Performance

The D0 upgrade detector physically rolled in to place Jan. 2001 and the first Run 2 collisions occurred in April 2001. Until Nov. 2001, activities were dominated by commissioning the silicon detector, establishing timing, and commissioning the DAQ and online systems. Given the importance of tracking in B physics, critical path items were late Analog Front End (AFE) boards that were essential for reading out the central fiber tracker and preshower detectors. In Summer 2001, only a very restrictive slice in ϕ was instrumented for CFT axial readout. During a shutdown in Nov. 2001, a large fraction of CFT axial AFE boards were installed and commissioned over the winter. Due to this missing readout, many commissioning tracking studies were performed with silicon-only tracking. The silicon SMT detector itself is operating very well with 95% of the barrel sensors, 96% of the small-z F-disks, and 87% of the larger-z H-disks operational.

Only by the end of winter 2002 were the CFT axial channels fully instrumented and CFT stereo fully instrumented by the end of April 2002, i.e., it is only until very recently that D0 has had its full tracking system available. Until May 2002, the Tevatron delivered approximately 35 pb^{-1} and the D0 detector recorded about

10 pb^{-1} of this in physics runs.

Paramount to being able to carry out the B physics program is good impact parameter resolution and the ability to form precise primary and secondary vertices. Using current data, comparisons between expectations and current performance are made. For high multiplicity primary vertices (e.g., $N_{\rm track} \geq 14$), a primary vertex resolution of 46 μm has been measured in the transverse x-y plane. Other measurements indicate this resolution contains a convolution over a transverse beam size of approximately 30 μm. The impact parameter resolution measured with respect to this primary vertex is currently found to be 62 μm for global tracks (SMT and CFT point measurements) with transverse momentum $p_T > 0.5$ GeV as shown in Fig. 2(a). This asymptotically approaches a current value of 20 μm for high-p_T tracks and is compared to Monte Carlo expectations in Fig. 2(b). It is clear that progress on alignment of the tracking chambers has resulted in resolutions already approaching expected values.

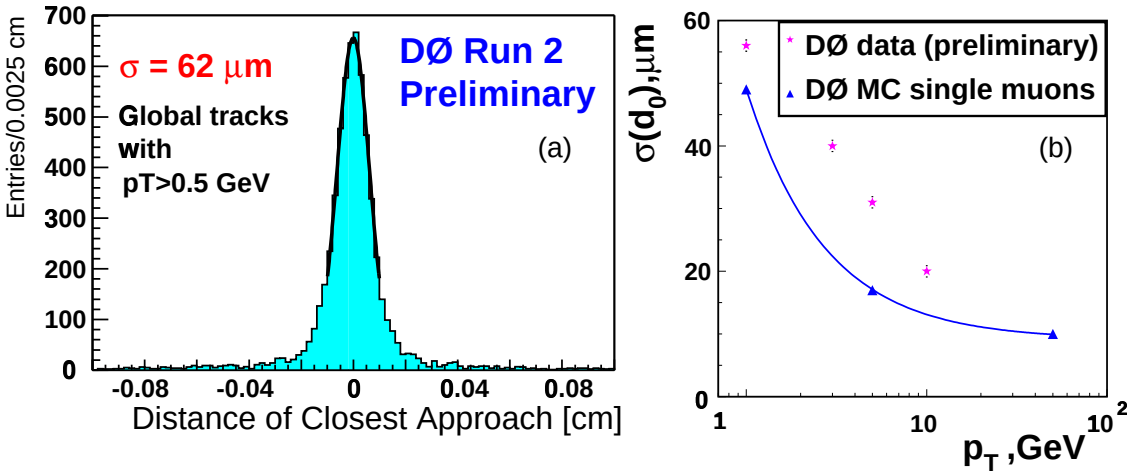

Figure 2: (a) Impact parameter resolution for D0 global tracks for $p_T > 0.5$ GeV and (b) behavior as a function of track p_T compared to Monte Carlo expectations.

5 Evidence for b production

One of the first systems to be reliably commissioned was the muon system and a benchmark analysis is the check of the muon plus jet rate due to $b \to \mu$. Muons reconstructed in only the muon system without a central track match (due to commissioning delays of the CFT) were associated with jets if close in angle: $\delta R = \sqrt{\delta\phi^2 + \delta\eta^2} < 0.7$. The measured differential cross section is shown in Fig. 3(a) for the indicated kinematic region. The shape is consistent with MC predictions as well as Run 1 D0

results [2]. Since the conference, the absolute rate has been measured as well and confirmed to be consistent with expectations.

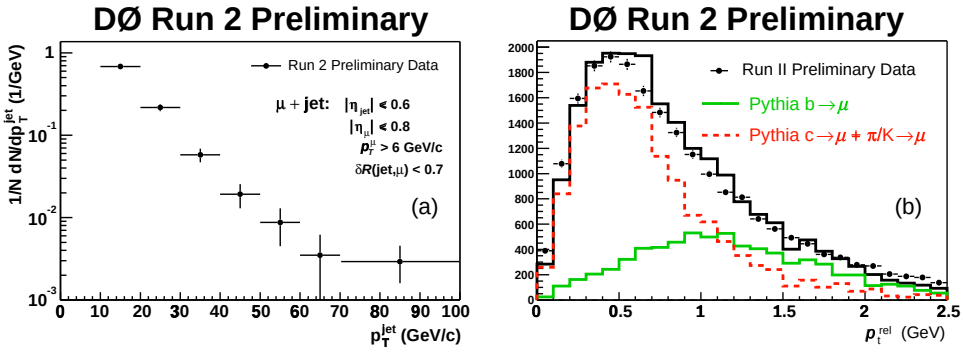

Figure 3: (a) Differential cross section for the rate of muons associated with jets (see text) in the range $|\eta_{\rm jet}| < 0.6$, $|\eta_\mu| < 0.8$, and $p_T^\mu > 6$ GeV; (b) fit to the transverse momentum of the muon with respect to the muon plus jet axis, i.e., $p_t^{\rm rel}$, to extract the b rate.

The muons in this sample will be due to $b \to \mu$, $b \to c \to \mu$, $c \to \mu$, and $\pi/K \to \mu$ decays in flight. The decay muon from the heavier b quark will tend to get a larger transverse momentum kick relative to the jet axis, $p_t^{\rm rel}$. Fig. 3(b) shows typical fits in this parameter to extract the b content. Entries at large values of $p_t^{\rm rel}$ are due to b hadrons, and also provide a method for identifying b jets. Current work using muons with a central track match shows substantial improvement in separation of $b \to \mu$ from backgrounds in the same parameter.

Using this muon plus jet sample and demanding $p_t^{\rm rel} > 1.5$ GeV to enhance the b content, tracks can be examined for evidence of b lifetime information. A signed impact parameter significance is formed where the sign is determined if the track in question crosses the jet axis upstream (positive) or downstream of the found primary vertex. Figure 4(a) shows the signed impact parameter significance (i.e., the distance of closest approach (dca) divided by its error) for an unbiased di-jet sample for $|{\rm dca}| <$ 1.0 mm to reduce contributions due to K_S^0 and Λ. The negative side of the distribution should be indicative of the resolution, and its mirror image is also superimposed on to the positive side of the distribution. The small excess is due to residual K_S^0 and Λ decays as well as small amounts of b jets in the sample. Figure 4 shows the same for the b-enhanced sample that shows a similar resolution as the di-jet sample, but a clear excess of tracks with significant impact parameters due to b content.

Using the di-jet sample, probability density functions can be formed for the observed resolution and Fig. 5(a) shows the resulting probability that tracks came from the interaction point (IP) or primary vertex. The spike on the positive side near zero shows that there is an excess of tracks with small probability of coming from the IP,

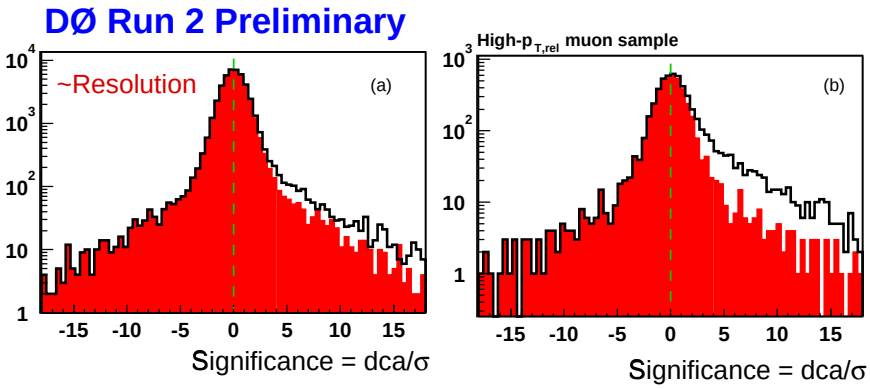

Figure 4: (a) Signed impact parameter significance (distance of closest approach (dca) divided by its error) for tracks in an unbiased di-jet sample with track $p_T > 1.5$ GeV, more than 10 total hits (SMT+CFT) and $|\mathrm{dca}| < 1.0$ mm. The negative side of the distribution is also reflected to the positive side. (b) The same distribution in the muon plus jet sample with $p_t^{\mathrm{rel}} > 1.5$ GeV to enhance the b-jet content.

i.e., tracks from secondary vertices carrying lifetime information. Taking the product of these track probabilities over the tracks in a jet, the probability that the jet is due to a light quark is shown in Fig. 5(b). This is the first time that lifetime information has been measured in the D0 detector.

The next step in utilizing lifetime information is the formation of secondary vertices. The important "golden" channel of $B^0 \to J/\psi K_S^0$ to measure the $\sin 2\beta$ parameter of CP violation serves as a useful benchmark to evaluate detector performance. The first physics objects reconstructed using both CFT axial and stereo tracks are two-prong secondary vertices from K_S^0 decays. The invariant mass as shown in Fig. 6(a) is found with a resolution of 5.1 MeV, close to MC expectations of 5.0 MeV demonstrating that the momentum resolution of the trackers is approaching nominal values.

Figure 6(b) shows the reconstruction of $J/\psi \to \mu^+\mu^-$ (and Υ's) where the muons have a CFT track match. The resultant mass resolution of 118 MeV improves to approximately 70 MeV if only tracks with both SMT and CFT hits are used. This can be compared to a resolution of 50–60 MeV expected from MC simulations. After the conference, decay lengths of reconstructed J/ψ secondary vertices due to $B \to J/\psi X$ as shown in Fig. 7 have been used to find a lifetime consistent with the PDG [3] value.

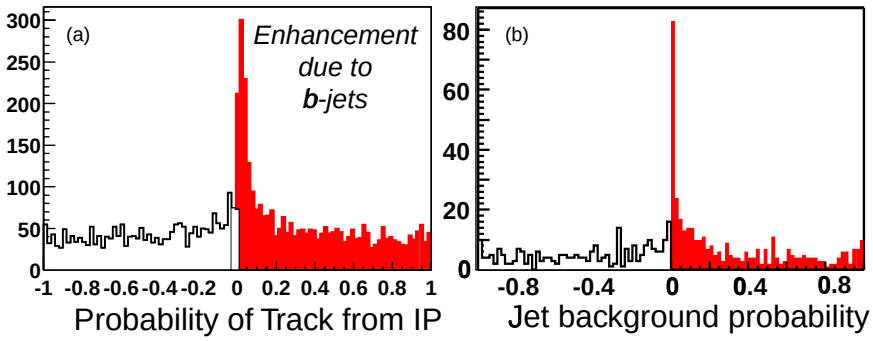

Figure 5: (a) From track significance values in the $p_t^{\rm rel} > 1.5$ GeV muon plus jet sample, probability that a track is from the interaction point or primary vertex; (b) normalized product of these track probabilities for the tracks in the jet. The peak is due to enhancement of b-jet content.

6 Some expectations for Run 2a

Continuing with expectations on the precision with which $\sin 2\beta$ could be measured using $B^0 \to J/\psi K_S^0$ events, the strengths of the D0 detector for such a B physics measurement are summarized in Table 2. One would measure the decay length of the B^0 decaying into $J/\psi K_S^0$, and tag the b quark flavor at production using a same-side tag of pion charge (from the primary) or an opposite-side tag by examining the lepton and/or jet charge. Defining tagging efficiency as $\epsilon = N_{\rm tag}/N_{\rm tot}$, and the dilution factor D as the asymmetry between "right" (R) and "wrong" (W) tags, $D = (N_R - N_W)/(N_R + N_W)$, the overall flavor tag quality can be quantified by ϵD^2. Although the D0 upgrade detector does not have kaon identification for opposite-side tagging, this is balanced by excellent muon and electron coverage for lepton tagging, and good forward tracking for determining jet charge. We also expect to be able to trigger on $J/\psi \to e^+e^-$ assisted by information from the preshower subdetectors.

Using these projections, and the expectation of 30–40k reconstructed events from the 2 fb^{-1} of Run 2a, an error of $\delta \sin 2\beta \approx 0.04$ is predicted [4].

Another high priority B physics analysis is the measurement of B_s^0 mixing. Current limits exclude $x_s = \Delta m_s/\Gamma_s > 21$ at 95% C.L. [3], while a global fit to a number of CKM triangle measurements in the framework of the Standard Model predicts [5] $x_s = 25.2^{+2.2}_{-1.0}$, although new physics can easily result in a much larger prediction. This very important measurement should therefore be in reach of the Tevatron experiments.

D0 has made Monte Carlo studies of both the semileptonic and hadronic decays of B_s^0 to extract this mixing. In the hadronic mode, which has the advantage of no missing neutrino, decays of $B_s^0 \to D_s^-\pi^+(\pi^+\pi^-)$; $D_s^- \to \phi\pi^-$, and $\phi \to K^+K^-$ can

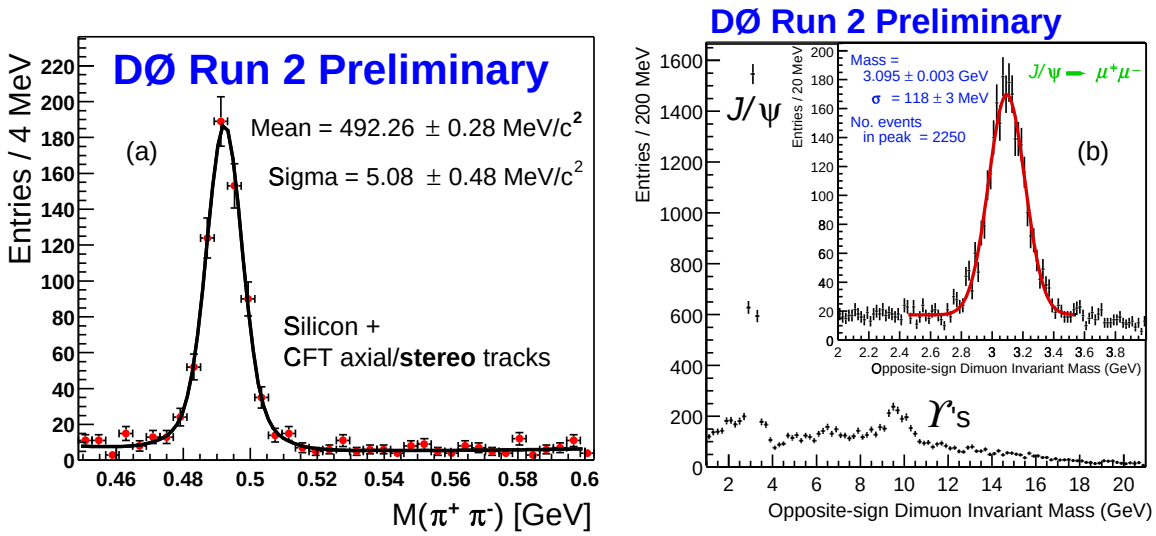

Figure 6: (a) Reconstructed $K^0_S \to \pi^+\pi^-$ decays for tracks with both CFT axial and stereo tracks; (b) reconstruction of $J/\psi \to \mu^+\mu^-$ decays for muons with a CFT central track match.

be reconstructed. Triggers will be from leptons on the opposite side, and this lepton charge will tag the initial flavor. The final flavor will be tagged by the charge of the D_s. Approximately 2000 events are expected in 2 fb^{-1}, and with a signal-to-background ration of 0.5, and a pessimistic proper time resolution of 0.098 ps, the resulting projected reach on measuring x_s for this channel is shown in Fig. 8.

Tag	D0 Strength	Flavor Tag Quality, ϵD^2
Same side tag	–	2.0
Soft lepton tag	μ and e coverage and identification	3.1
Jet charge tag	forward tracking	4.7
Opposite-side kaon tag	*no K identification*	–
Combined		9.8

Table 2: Summary of predicted performance and strengths of flavor tagging in the CP violation channel $B^0 \to J/\psi K^0_S$.

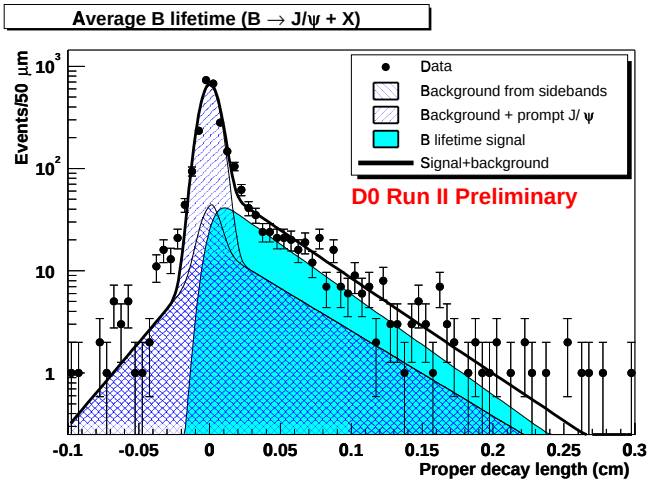

Figure 7: Proper decay length distribution for reconstructed J/ψ secondary vertices. The background is determined from J/ψ mass sidebands and prompt J/ψ Monte Carlo.

7 Future

The D0 upgrade detector with its tracking upgrades is much better suited for B physics than the Run 1 detector. The detector is still being commissioned, but we have observed lifetime information from b hadrons for the first time in the D0 detector, and are approaching data quality to soon allow preliminary B physics results.

Detector commissioning will continue with debugging, calibration, and alignment of the subdetectors and refinement of reconstruction algorithms to select physics objects. The full tracking system has just recently been available and secondary vertexing is rapidly improving as well as the prospects for tagging electrons (for b quark identification and $J/\psi \rightarrow e^+e^-$) using a road method and the preshower subdetectors.

The next large jump in performance will come from increasing the scope of the trigger system. The Level 2 trigger is coming online, a Level 1 central track trigger is expected at the end of summer 2002, and a Level 2 silicon track trigger able to fire on tracks with large impact parameter significance should be available fall 2002.

Of course, what is also needed is integrated luminosity and the Tevatron's performance has fallen short of expectations. Task forces at Fermilab have been addressing this low luminosity, and integrated luminosities of 300 pb^{-1} by the end of 2002 have been promised by laboratory management. The D0 collaboration eagerly looks forward to this data and the B physics that it holds for the future.

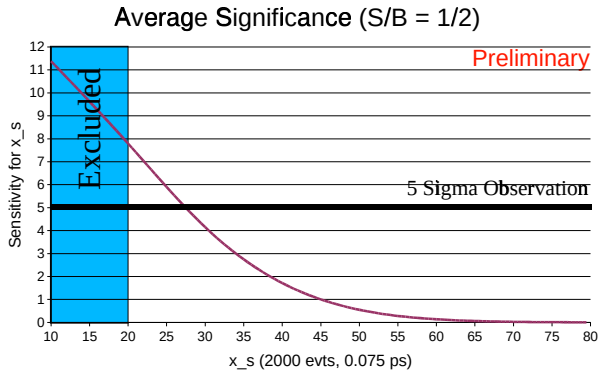

Figure 8: Projected reach on measuring x_s in Run 2a in the hadronic channel described in the text assuming a signal-to-background ratio of 0.5 and a proper decay time resolution of 0.098 ps.

References

[1] V. Buscher, "Status of the D0 Detector Upgrade for Run II," Int. J. Mod. Phys. A **16S1C**, 1068 (2001);
J. Ellison [D0 Collaboration], "The D0 detector upgrade and physics program," arXiv:hep-ex/0101048.

[2] B. Abbott *et al.* [D0 Collaboration], Phys. Rev. Lett. **84**, 5478 (2000) [arXiv:hep-ex/9907029].

[3] Particle Data Group, K. Hagiwara *et al.*, Phys. Rev. **D 66** (2002) 010001.

[4] K. Anikeev *et al.*, "B physics at the Tevatron: Run II and beyond," arXiv:hep-ph/0201071.

[5] M. Ciuchini, "Status of the CKM matrix," Nucl. Phys. Proc. Suppl. **109**, 307 (2002) [arXiv:hep-ph/0112133].

New Results on $\mathrm{B_s^0}$ Mixing from LEP

Stephen R. Armstrong
CERN EP Division
CH-1211 Geneva 23, SWITZERLAND

1 Introduction

A prime goal of contemporary heavy flavour physics is the observation of $\mathrm{B_s^0}$-$\overline{\mathrm{B}}_\mathrm{s}^0$ oscillations and determination of the mass difference Δm_s to which the oscillation frequency is proportional. With the already well-measured quantity Δm_d from studies of $\mathrm{B_d^0}$-$\overline{\mathrm{B}}_\mathrm{d}^0$ oscillations [1], this would permit the extraction of the ratio of the CKM V_ts and V_td matrix elements

$$\frac{\Delta m_\mathrm{s}}{\Delta m_\mathrm{d}} = \frac{m_{\mathrm{B_s}}}{m_{\mathrm{B_d}}}\frac{|V_\mathrm{ts}|^2}{|V_\mathrm{td}|^2}\xi^2, \quad \xi^2 = \frac{F_{\mathrm{B_s}}^2 B_{\mathrm{B_s}}}{F_{\mathrm{B_d}}^2 B_{\mathrm{B_d}}}. \tag{1}$$

The theoretical uncertainties of roughly 10% are embedded in the ξ^2 parameter, the ratio of the decay constants and bag parameters of the $\mathrm{B_s^0}$ and $\mathrm{B_d^0}$ mesons. The phenomenological implication of $\mathrm{B_s^0}$-$\overline{\mathrm{B}}_\mathrm{s}^0$ oscillations is a proper time-dependent asymmetry in the probability to observe a *mixed* decay (*i.e.*, $\mathrm{B_s^0}\to\overline{\mathrm{B}}_\mathrm{s}^0\to X$) compared to an *unmixed* decay (*i.e.*, $\mathrm{B_s^0}\to\mathrm{B_s^0}\to X'$). These probabilities are given as

$$\mathcal{P}_\mathrm{mixed}(t) = \Gamma_\mathrm{s}\tfrac{\mathrm{e}^{-\Gamma_\mathrm{s}t}}{2}[1-\cos(\Delta m_\mathrm{s}t)], \quad \mathcal{P}_\mathrm{unmixed}(t) = \Gamma_\mathrm{s}\tfrac{\mathrm{e}^{-\Gamma_\mathrm{s}t}}{2}[1+\cos(\Delta m_\mathrm{s}t)], \tag{2}$$

assuming CP conservation and small lifetime differences. The challenge to experiments in measuring a value for Δm_s is to determine if the $\mathrm{B_s^0}$ meson decay is a mixed or unmixed one, and to measure the proper time associated to it.

The LEP experiments ALEPH [2], DELPHI [3, 4], and OPAL [5] have investigated $\mathrm{B_s^0}$-$\overline{\mathrm{B}}_\mathrm{s}^0$ oscillations as have SLD [6] and CDF [7]. This paper focuses on new (*i.e.*, released in early 2002) results from ALEPH [2] which motivate new LEP results on $\mathrm{B_s^0}$-$\overline{\mathrm{B}}_\mathrm{s}^0$ oscillations and briefly reviews the results from DELPHI and OPAL.

2 Experimental Strategy

At LEP, $\mathrm{B_s^0}$ mesons are produced from hadronic decays of the Z boson ($\mathrm{e^+e^-}\to\mathrm{Z}\to\mathrm{b\overline{b}}$). The boosted b hadrons result in a characteristic displaced vertex topology relative to the interaction point, forming the basis of most heavy flavour physics analyses.

The experimental strategy common to all analyses studying B_s^0-$\overline{B}_s^0$ oscillations can be grouped into four categories discussed below. Figure 1 illustrates components of this strategy.

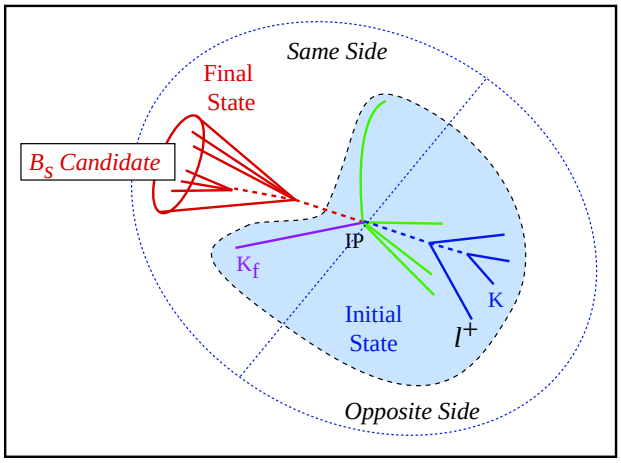

Figure 1: A diagram illustrating components of the experimental strategy. The event is divided into two hemispheres with respect to the thrust axis; the hemisphere containing the B_s^0 candidate is referred to as the *Same Side* while the other is the *Opposite Side*.

- **B_s^0 Selection and Event Purity Determination**
  Candidate B_s^0 events are selected from LEP data collected between 1991 and 1995 (roughly 4 million hadronic Z decays per experiment).[1] Table 1 summarizes different selections used by the LEP experiments. Figures 2 and 3 show invariant mass distributions obtained from the ALEPH fully exclusive and semi-exclusive analyses. A selection-dependent event-by-event purity improves the statistical power of the event sample [2]. A probability for each candidate to originate from signal and background components is used in the oscillation fit described below.

- **Tagging the Initial and Final States**
  A determination of the anti-particle/particle state of the B_s^0 candidate at its production (initial) and decay (final) is the key component of the analyses. The Final State tagging depends upon the selection. For fully exclusive decays, no ambiguity exists as all decay products are known. For the inclusive analyses with semileptonic B_s^0 decays, the charge of the lepton is used accounting for the non-zero mistag associated with cascade decays $b \to c \to \ell$. Initial State tagging is more complicated: information from both the Same and Opposite Sides may

[1] In one case, the ALEPH fully exclusive B_s^0 selection, Z peak calibration data from LEP2 are included boosting the sample by about 400 000 hadronic events.

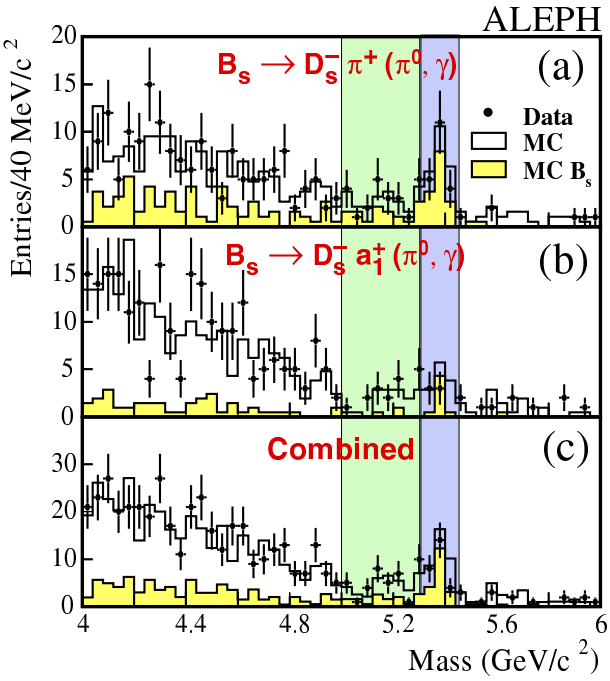

Figure 2: Invariant mass distributions for the reconstructed B_s^0 candidates in the ALEPH fully-exclusive selection [2]. Data (dots with error bars) and the simulation (histograms) are shown: a) the $D_s^- \pi^+ (\pi^0, \gamma)$ channel (a total of 44 events); b) the $D_s^- a_1^+ (\pi^0, \gamma)$ channel (a total of 36 events); and c) the sum of the two. The lightly and darkly shaded vertical bands show the satellite regions and the main peak area defining the mass selection windows.

be used as the flavour of the b hadron in the Opposite Side is anti-correlated with that of the B_s^0 at production. In each case, a variety of discriminants are used. The Opposite Side tag may rely upon jet charges, primary and secondary vertex charges, and lepton and kaon particle identification techniques. The Same Side information must necessarily exclude B_s^0 decay products, attempting to build discriminants based upon fragmentation tracks; identified kaons from fragmentation (produced in conjunction with the B_s^0) provide powerful tagging information. Again, a variety of kinematic and particle-identification-based discriminants are used. The Same and Opposite Side tags are then combined to yield an overall Initial State tag. The new ALEPH analyses [2] use series of neural networks (NN) to combine information, the final NN output is shown in Figure 4.

- **Measurement of Proper Time of the B_s^0 Decay**
  Proper time t is given as $t = lm/p$ where m is the B_s^0 mass; the B_s^0 momentum p and the measured decay length l must be measured. For the fully exclusive mode, the B_s^0 momentum is determined with excellent precision from knowledge

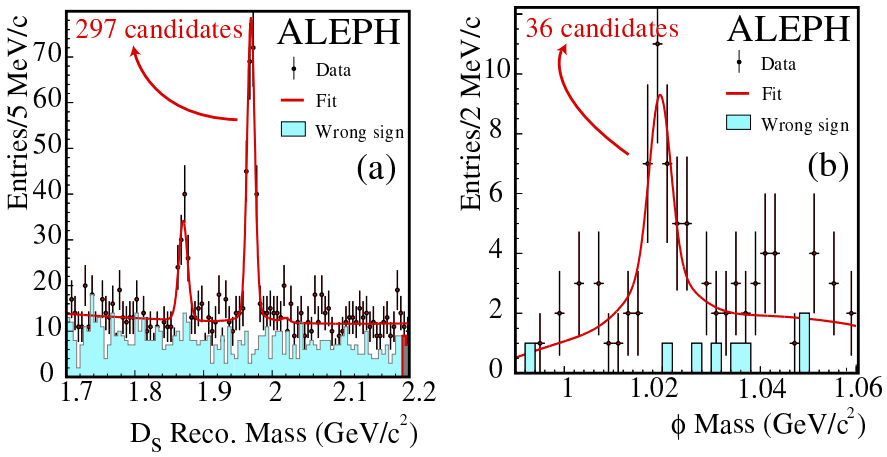

Figure 3: Invariant mass distributions for the ALEPH semi-exclusive selection [2] showing a) the selected D_s^- candidates with $D_s^-\ell^+$ combinations for hadronic D_s^- decays, and b) the selected ϕ candidates for semileptonic D_s^- decays in data (dots with error bars).

of the momenta of all of the decay products. In more inclusive selections with semileptonic B_s^0 decays, a correction is done to account for missing neutrino momentum based upon event energy-momentum conservation; uncertainties associated with this correction procedure dominate the momentum resolution. The decay length is determined by the distance between the primary vertex and the B_s^0 decay vertex. At LEP, the primary vertex may be determined on an event-by-event basis. The secondary vertex determination is again selection-dependent, and the best precision (*e.g.*, 180 μm for the ALEPH fully exclusive selection [2]) is obtained from the fully exclusive modes. More inclusive measurements suffer from a less precise knowledge of the B_s^0 flight direction (*e.g.*, missing neutrinos from semileptonic B decay) onto which the primary-secondary vertex distance is projected.

- **Determination of Δm_s**
  A signal likelihood function can be constructed from the probability density function for mixed and unmixed events given in Equation 2. A procedure referred to as the Amplitude Method [10] replaces Δm_s in the probabilities by a hypothesized oscillation frequency ω and an *amplitude* $\mathcal{A}$ in front of the oscillation term. This permits combination of analyses including the systematic uncertainties. The likelihood is maximized with respect to the amplitude for each ω. An amplitude consistent with zero is expected for values of ω far below the true value of Δm_s; an amplitude consistent with unity is expected for values of ω very close to the true value of Δm_s. A range of ω may be excluded at 95% C.L. if $\mathcal{A} + 1.645\sigma_{\mathcal{A}} < 1$.

Selection	Decay Modes	Sample (events)	Purity %	LEP Experiment	Δm_s Limit obs. (exp.) ps^{-1}
Fully Exclusive	$B_s^0 \to D_s^- (\pi^+ \text{ or } a_1^+)$ $B_s^0 \to \overline{D}^0 K^- (\pi^+ \text{ or } a_1^+)$	50 – 80	50 – 80	ALEPH [2]	2.5 (0.4)
				DELPHI [4]	†4.0 (3.2)†
Semi-Exclusive	$B_s^0 \to D_s^{(*)-} \ell^+ \nu_\ell$ † $B_s^0 \to D_s^{(*)-} h^+$ †	10^2 – 10^3	40 – 60	ALEPH [2]	7.2 (7.5)
				DELPHI [3, 4]	7.4 (8.1)
				OPAL [5]	1.0 (4.1)
Semi-Inclusive	$B_s^0 \to \ell^+ \nu_\ell + X$	10^4 – 10^5	10 – 20	ALEPH [2]	11.4 (14.0)
				DELPHI [8]	2.0 (7.8)
				OPAL [9]	5.2 (7.0)
Fully Inclusive	$B_s^0 \to X$	5×10^5	10	DELPHI [8]	1.2 (4.9)

Table 1: A summary of the LEP experiments' B_s^0-$\overline{B}_s^0$ oscillation selections, their characteristics, and the resulting 95% C.L. lower limit on Δm_s. DELPHI combine their Fully Exclusive and Semi-Exclusive $D_s^- h^+$ results providing only a combined exclusive result, denoted by the †.

3 Results

Results of all LEP studies of B_s^0-$\overline{B}_s^0$ oscillations are summarized in Table 1. Results in terms of amplitude versus hypothesized Δm_s are shown in Figure 5 for the semi-exclusive analyses of DELPHI [3] and OPAL [5]. The corresponding plots for each of the new ALEPH analyses [2] are shown in Figure 6.

The combination of LEP results with those of CDF and SLD is shown in Figure 7 [11]. For this world combination, an observed 95% C.L. lower limit on Δm_s of $14.9\,ps^{-1}$ is obtained with an expectation of $19.3\,ps^{-1}$. There is an apparent difference between the expected and observed limits which suggests that a signal may lie in this region. Furthermore, there is an enticing deviation away from consistency with a zero amplitude hypothesis between 16 and $18\,ps^{-1}$ which may hint at a signal; however the statistical significance of this deviation is below 2σ.

4 Conclusions

To date, no experiment has been able to resolve oscillations. It is presumed that the oscillation frequency lies beyond the current experimental sensitivity to discover it at the level of 5σ; however, there may be a hint of signal in the Δm_s region between 16 and 18 ps^{-1}. Further data from Run II of the Tevatron and results of future CDF and D0 studies may soon be available with the hope of discovering evidence for B_s^0-$\overline{B}_s^0$ oscillations.

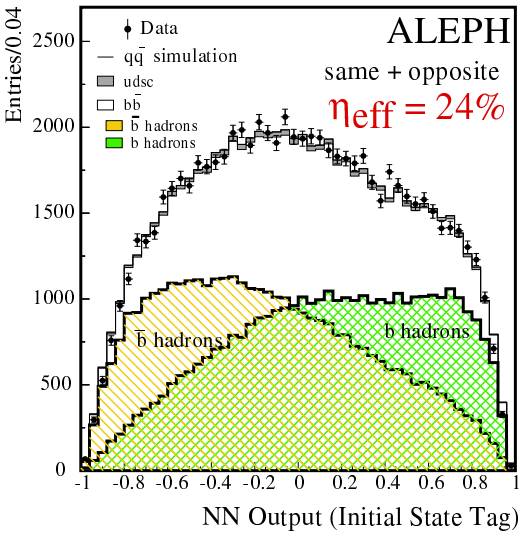

Figure 4: The ALEPH neural network-based Initial State tagging variable shown here for the semi-inclusive analysis in selected data (dots with error bars) and simulation (histograms) [2].

Acknowledgements

This presentation summarizes the work of the ALEPH, DELPHI, and OPAL collaborations as well as the LEP B Oscillations Working Group. As a member of the ALEPH collaboration, I wish to thank my colleagues in the CERN accelerator divisions for the successful operation of LEP. I am grateful to Dr. Duccio Abbaneo for his help in preparing this presentation as well as members of the ALEPH Heavy Flavour Group and the LEP B Oscillations Working Group. Dr. Markus Elsing also provided valuable input and suggestions.

References

[1] The Particle Data Group, Eur. Phys. J. **C15** (2000) 1.

[2] ALEPH Collaboration, CERN-EP/2002-016 (Submitted to Eur. Phys. J. C).

[3] DELPHI Collaboration, Eur. Phys. J. **C16** (2000) 555.

[4] DELPHI Collaboration, Eur. Phys. J. **C18** (2000) 229.

[5] OPAL Collaboration, Eur. Phys. J. **C19** (2001) 241.

[6] SLD Collaboration, SLAC-PUB-8568 (August 2000), contributed to the XXXth International Conference on High Energy Physics (ICHEP 2000), Osaka, Japan; SLD Collaboration, SLAC-PUB-8598 (August 2000), contributed to the XXXth International Conference on High Energy Physics (ICHEP 2000), Osaka, Japan.

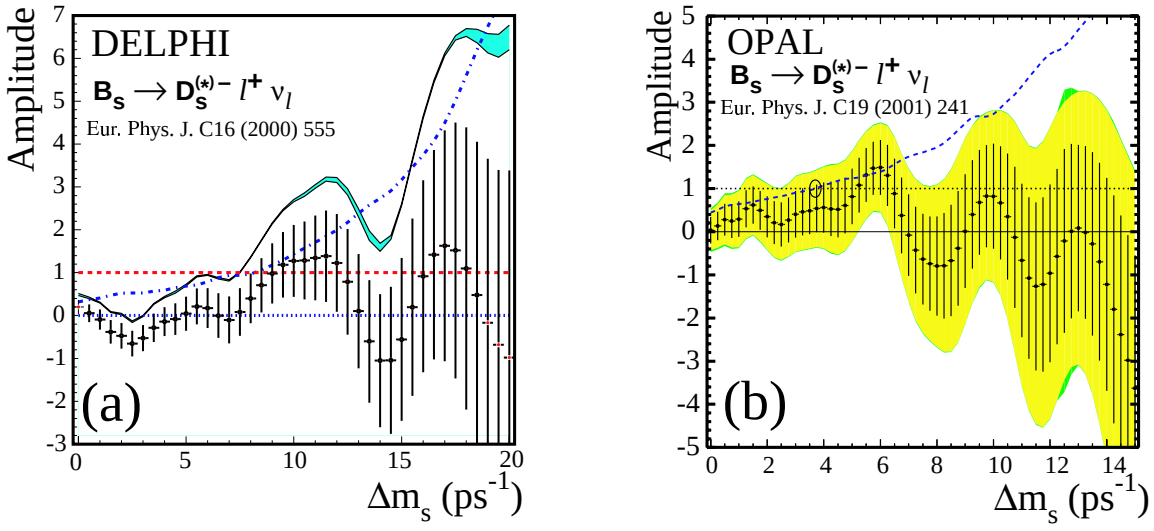

Figure 5: Plots showing Amplitude versus hypothesized Δm_s for a) the DELPHI semi-exclusive analysis [3], and b) the OPAL semi-exclusive analysis [5]. In the case of the a) DELPHI analysis, an observed (expected) 95% C.L. lower limit of 7.4 ps^{-1} (8.1 ps^{-1}) is obtained; b) OPAL analysis yields 1.0 ps^{-1} (4.1 ps^{-1}).

[7] CDF Collaboration, Phys. Rev. Lett. **82** (1999) 3576.

[8] DELPHI Collaboration, DELPHI 2000-104 CONF 380 (July 2000), contributed to the XXXth International Conference on High Energy Physics (ICHEP 2000), Osaka, Japan.

[9] OPAL Collaboration, Eur. Phys. J. **C11** (1999) 587.

[10] H.-G. Moser and A. Roussarie, Nucl. Instrm. Meth. **A384** (1997) 491;
D. Abbaneo and G. Boix, J. High Enrg. Phys. **JHEP08** (1999) 4.

[11] The LEP B Oscillation Working Group, `http:///lepbosc.web.cern.ch/LEPBOSC/`.

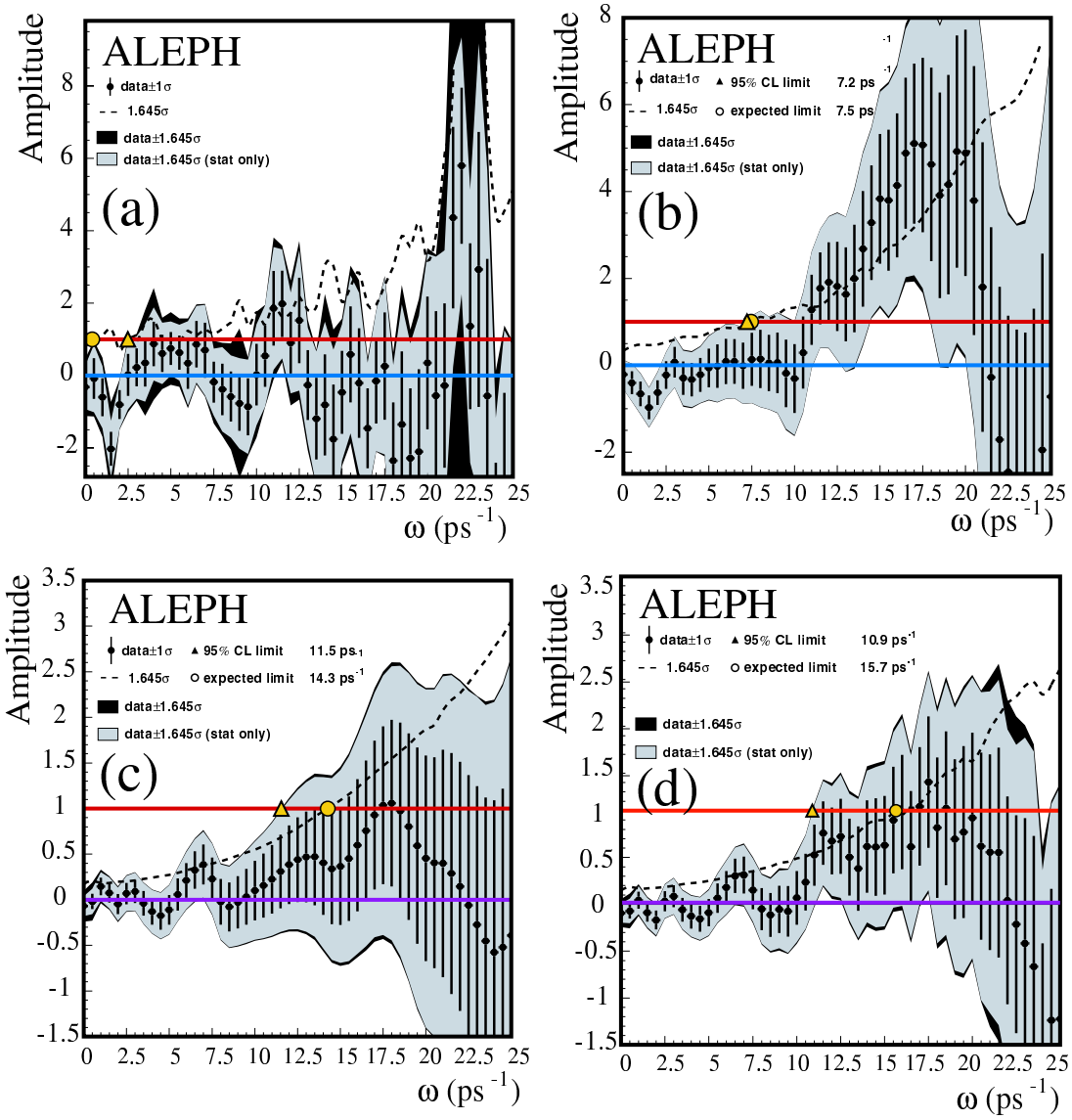

Figure 6: The new ALEPH results [2] shown here in terms of Amplitude versus hypothesized Δm_s (ω) for a) the fully exclusive analysis, b) the semi-exclusive $D_s\ell$ analysis, c) the semi-inclusive lepton analysis, and d) the combination of the three. In each case an observed (expected) 95% C.L. lower limit is set on Δm_s: a) $2.4\,\mathrm{ps}^{-1}$ ($0.3\,\mathrm{ps}^{-1}$), b) $7.2\,\mathrm{ps}^{-1}$ ($7.4\,\mathrm{ps}^{-1}$), c) $11.4\,\mathrm{ps}^{-1}$ ($14.0\,\mathrm{ps}^{-1}$), and d) $10.9\,\mathrm{ps}^{-1}$ ($15.7\,\mathrm{ps}^{-1}$).

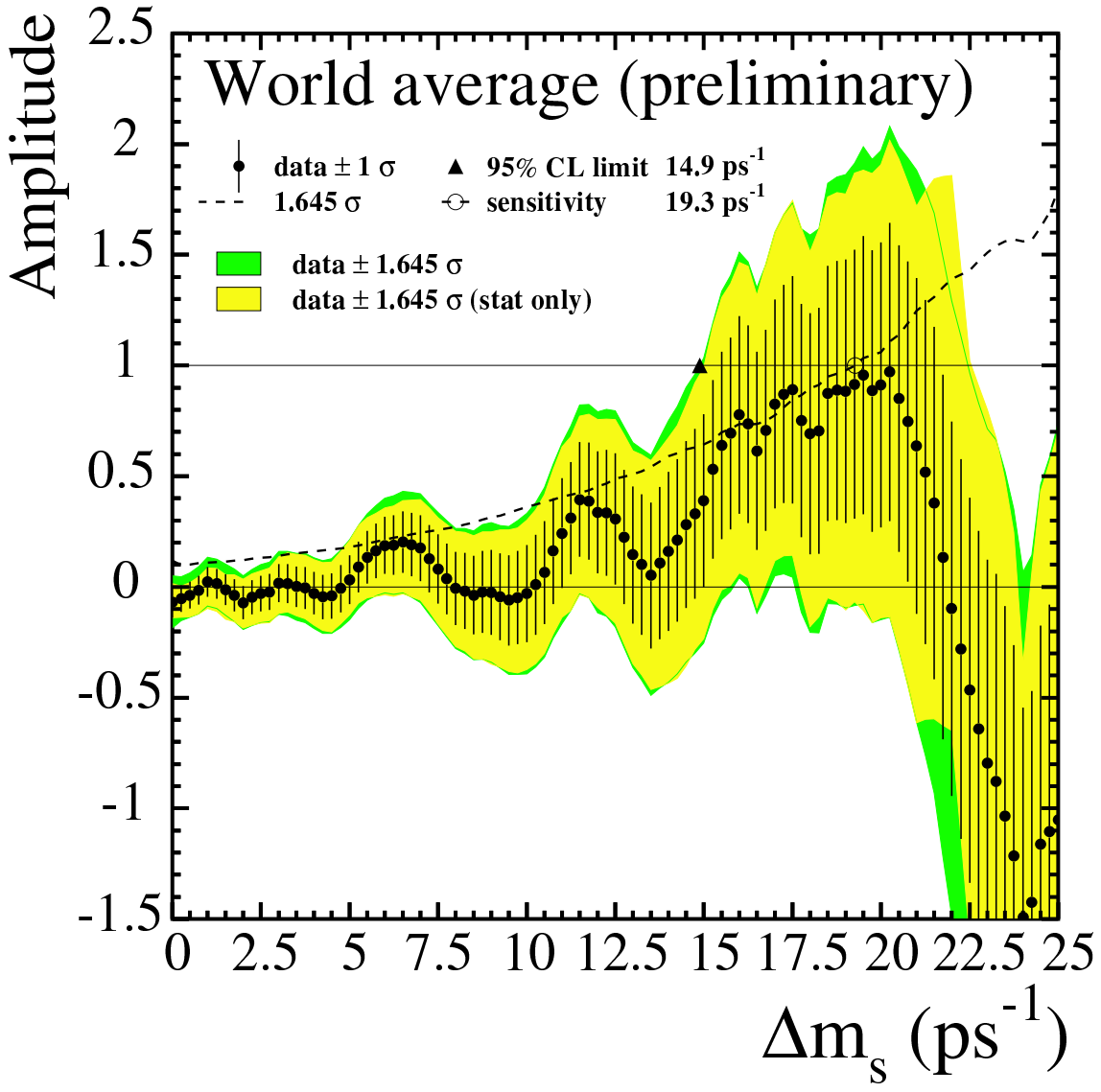

Figure 7: The combined B_s^0 oscillation results from ALEPH, CDF, DELPHI, OPAL, and SLD shown as amplitude versus hypothesized Δm_s [11]. The dots with error bars show the fitted aplitude values and uncertainties. An observed (expected) 95% C.L. lower limit on Δm_s of $14.9\,\mathrm{ps}^{-1}$ ($19.3\,\mathrm{ps}^{-1}$) is obtained.

May 17, session 1.

Session Chair: V. Luth

Cosmology

CP violation and cosmology

A. Kusenko

New Ideas about CP in B Decays and CKM Determination

Measuring α using $B \to K^{(*)}\overline{K}^{(*)}$ Decays

D. London

CP violation and cosmology

Alexander Kusenko
Department of Physics and Astronomy
University of California, Los Angeles, CA 90095-1547
and
RIKEN BNL Research Center
Brookhaven National Laboratory, Upton, NY 11973

1 Introduction

CP violation may have played a crucial role in the formation of matter in the universe. It must have, if the inflationary cosmology is right, thus ruling out the (very unpalatable) possibility that the baryon asymmetry was an initial condition of the Big Bang. If inflation took place, as most of us believe based on the growing observational evidence, it made the universe devoid of matter and set the stage for reheating. The baryon asymmetry then must have been produced at some later point through CP-violating processes.

2 CP violation and electroweak baryogenesis

That CP, as well as C and B must be broken for baryogenesis to work, was first noted by Sakharov [1]. In 1967 the only reason for considering the baryon number violation was theorists' ambitions. Neither experiment, nor favored theoretical models supported this hypothesis. In addition to breaking the symmetries, one needs an out-of-equilibrium state of the universe to generate the asymmetry.

The advent of the Standard Model and 't Hooft's discovery of a baryon number violating instanton provided a requisite source of B violation. The Standard Model also incorporates C, P, and CP breaking. Although the baryon number violation is highly suppressed in the Standard Model at zero temperature, Kuzmin, Rubakov, and Shaposhnikov [2] realized that at high temperatures the baryon number violating processes could go unsuppressed. In addition, the universe might be out of thermal equilibrium at the time of the electroweak phase transition. Hence, Kuzmin, Rubakov, and Shaposhnikov [2] put forth a very plausible and appealing possibility that the baryon asymmetry might arise from the Standard Model physics, at the time of the electroweak phase transition [3].

Unfortunately, in the minimal Standard Model, this scenario does not work. First, the phase transition is too weak, unless the Higgs mass is $M_{_H} < 45$ GeV, which is ruled out by experiment. Second, the CP violation from the CKM matrix makes a vanishing contribution to baryon asymmetry because it is suppressed by a product of Yukawa couplings [5].

Baryogenesis in the supersymmetric extensions of the Standard Model is less problematic because the additional scalar states can provide both the new sources of CP violation [6, 7, 8, 9] and a way to make the phase transition more strongly first-order [11, 12, 13]. The phase transition is stronger if one of the stops is very light [12]. The new sources of CP violation may come, for example, from the chargino mass matrix:

$$\overline{\psi}_R M_\chi \psi_L = (\overline{\widetilde{w}^+},\ \overline{\widetilde{h}_2^+})_R \begin{pmatrix} m_2 & gH_2(x) \\ gH_1(x) & \mu \end{pmatrix} \begin{pmatrix} \widetilde{w}^+ \\ \widetilde{h}_1^+ \end{pmatrix}_L + \text{h.c.} \qquad (1)$$

As long as m_2 and μ are complex, spatially varying phases in the bubble wall provide a source of (spontaneous) CP violation [10, 7]. The remaining window for electroweak baryogenesis in the MSSM is very narrow [4]; several parameters must be adjusted to maximize the resulting baryon asymmetry (in particular, one must assume that the wall is very thin, take $\tan\beta < 3$, and choose the "optimal" bubble wall velocity $v_w \approx 0.02$), as shown in Fig. 1.

CP violation from the chargino sector (1) may enhance the B_s mixing as compared to the Standard Model value [14], especially if the stop is light (Fig. 2). In practice, however, this effect is observable only if the CKM matrix elements are known to a very high precision. In particular, one would need to reduce theoretical uncertainties in V_{ub} to 5-10% and in $\sin 2\beta$ to a few percent.

3 CP violation and leptogenesis

If a lepton asymmetry of the universe formed after inflation but before the electroweak phase transition, the sphalerons, which violate B and L but preserve $(B-L)$, would convert (roughly, a half of) the lepton asymmetry into a baryon asymmetry. This observation gave rise to an extremely appealing scenario of leptogenesis [15]. The relevant CP violation may reside in the neutrino mass matrix, which, in general, has a number of complex phases [16, 17].

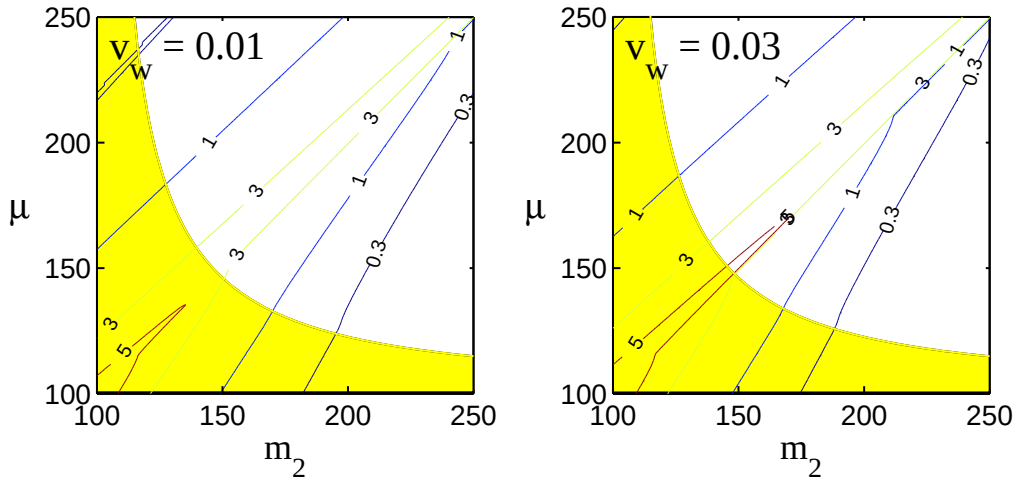

Figure 1: Contours of constant baryon asymmetry in units 10^{-10} with $\sin\delta_\mu = 1$ for (a) $v_w = 0.01$ and (b) $v_w = 0.03$. Mass units are GeV/c^2. Shaded regions are excluded by the LEP2 limit on the chargino mass, $m_{\chi^\pm} > 104$ GeV/c^2. To maximize the baryon asymmetry, one assumes that $\tan\beta \lesssim 3$ and that the bubble wall is very narrow, $\ell_w \simeq 6/T$. From J.M. Cline et al. [4].

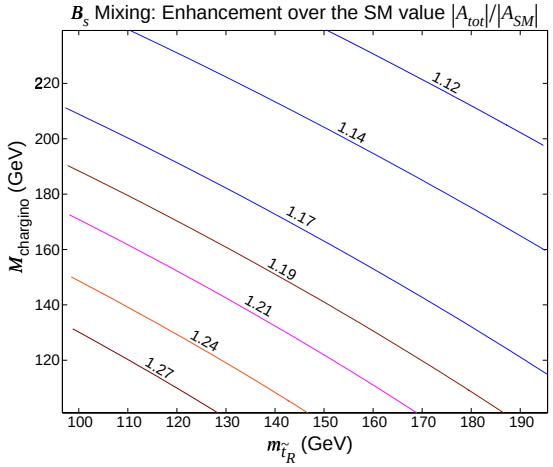

Figure 2: Enhancement of B_s in the MSSM, for parameters consistent with electroweak baryogenesis [14].

4 Transient CP violation, baryogenesis, and dark matter

In addition to CP violation hard-wired into the lagrangian, some manifestations of CP non-conservation may occur for a short period of time in the early universe, during which time the baryon asymmetry might have formed. A well-know example is the Affleck-Dine scenario for baryogenesis [18, 19], in which CP violating seeds may be effectively amplified by the motion of the scalar condensate. Similarly, electroweak baryogenesis at preheating [20, 21, 22, 23] can take advantage of CP-violating motions of time-dependent condensates during preheating [23]. CP violation of this kind is poorly constrained by experiment because it becomes small after thermalization.

4.1 Affleck-Dine baryogenesis and dark-matter-genesis

In models with low-energy supersymmetry inflation can lead to formation of the Affleck-Dine condensate [18, 19] with a large VEV. A high-scale physics undoubtedly violates B and CP through higher-dimension operators. Hence, the motion of the scalar condensate after inflation is not B and CP symmetric. Thus, the universe acquires a baryon asymmetry. The Affleck-Dine scenario [18] is simple, appealing, and flexible in that the final baryon asymmetry can easily be made consistent with the data.

In addition, the Affleck-Dine baryogenesis can produce dark matter as well. In general, the Affleck-Dine condensate does not remain homogeneous and can break up [24] into SUSY Q-balls [25]. This affords a number of interesting possibilities for generating baryons and dark matter simultaneously [24, 26, 27].

Since baryons and dark matter arise form the same physical process,

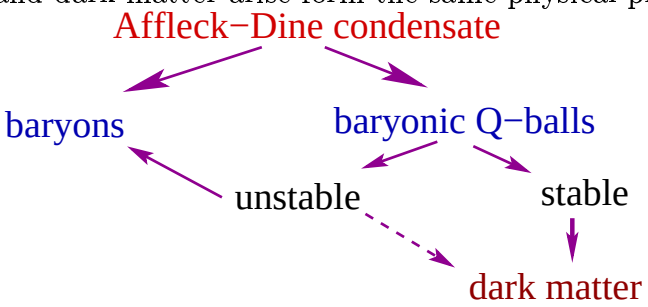

the ratio of $\Omega_{\rm dark}$ to Ω_B may have a natural explanation in some models [28].

4.2 Electroweak baryogenesis at preheating

Several viable scenarios for electroweak baryogenesis at preheating were presented in Ref. [23]. For example, a modified spontaneous baryogenesis a la Cohen, Kaplan, and Nelson [7] becomes very efficient at preheating. Their original scenario used

the variation of the Higgs field inside a wall of a bubble formed in a first-order phase transition. A similar effect can occur at preheating uniformly in space, on the horizon scales [23]. One can obtain the desired baryon asymmetry in a Standard Model supplemented by an additional Higgs doublet and an inflaton sector [23]. The difference with the scenario proposed by Cohen, Kaplan and Nelson [7] is that in our case CP violation occurs homogeneously in space, not only inside a bubble wall. In addition, the final prediction for the baryon asymmetry in the CKN scenario was very far from the equilibrium value because the sphaleron rate was slow on the time scales associated with the growth of bubbles. In the case of preheating, the Higgs parameters change slowly in time while the baryon number non-conservation is rapid. This allows a slow adiabatic adjustment of the baryon number to that which minimizes the free energy.

Several additional sources of CP violation might affect the physics of preheating and facilitate baryogenesis [23].

5 Strong CP violation and the axion cosmology

The QCD vacuum is a superposition $|\theta\rangle = \sum_n \exp\{-in\theta\}|n\rangle$ of topologically distinct vacuum states $|n\rangle$. As a result, the QCD Lagrangian can be written as

$$\mathcal{L}_{QCD} = \mathcal{L}_{\rm pert} + \overline{\theta}\frac{g^2}{32\pi^2}F\tilde{F}, \tag{2}$$

where

$$\overline{\theta} = \theta + \arg\det M \tag{3}$$

Experimentally, the value of $\overline{\theta}$ must vanish to a high precision, $\overline{\theta} \ll 10^{-10}$. However, if all the quarks have non-zero masses, there is no (simple) reason why the phase in the Yukawa matrix should cancel the QCD vacuum phase, unless $\overline{\theta}$ relaxes to zero dynamically, by a VEV of a scalar field. This elegant solution to the strong CP problem was proposed by Peccei and Quinn [29]. The breaking of a global U(1) symmetry gives rise to a light scalar field, the axion [30].

Several models can accommodate an axion consistent with the existing experimental bounds [31]. A light, weakly interacting axion makes a good candidate for dark matter. The present experimental limits are shown in (Fig. 3).

6 Conclusions

There is every reason to believe that matter-antimatter asymmetry is a consequence of CP non-conservation in particle physics. On the other hand, CP violation from

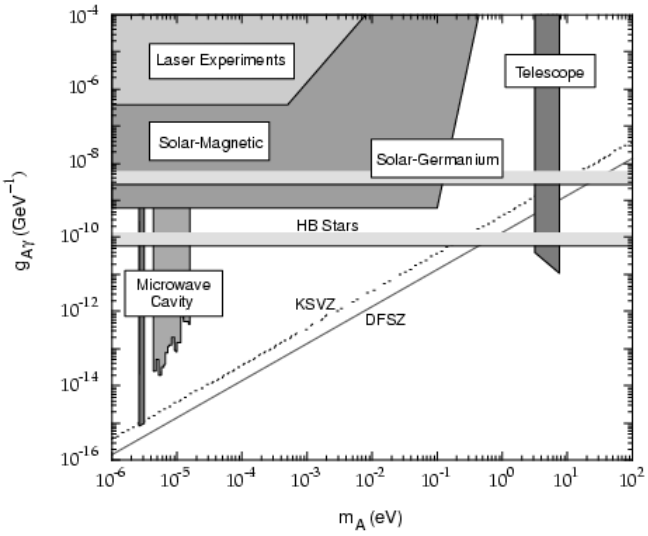

Figure 3: Exclusion regions for the axion mass vs. coupling, from Particle Data Book [32].

the quark mixing is not sufficient for baryogenesis. This implies the existence of new, yet undiscovered, sources of CP violation in nature.

7 Acknowledgments

The author thanks J. Cline and H. Murayama for helpful discussions. This work was supported in part by the DOE grant DE-FG03-91ER40662.

References

[1] A. D. Sakharov, Sm Zh. Eksp. Teor. Fiz. **5** (1967) 32 .

[2] V. A. Kuzmin, V. A. Rubakov and M. E. Shaposhnikov, Phys. Lett. B **155**, 36 (1985).

[3] For review, see, *e.g.*, V. A. Rubakov and M. E. Shaposhnikov, Usp. Fiz. Nauk **166**, 493 (1996) [Phys. Usp. **39**, 461 (1996)] ; A. G. Cohen, D. B. Kaplan and A. E. Nelson, Ann. Rev. Nucl. Part. Sci. **43**, 27 (1993)

[4] J. M. Cline, M. Joyce and K. Kainulainen, Phys. Lett. B **417**, 79 (1998); *ibid.*, B **448**, 321 (1999); JHEP **0007**, 018 (2000).

[5] S. M. Barr, G. Segre and H. A. Weldon, Phys. Rev. D **20**, 2494 (1979).

[6] M. Dine, P. Huet, R. J. Singleton and L. Susskind, Phys. Lett. B **257**, 351 (1991); M. Dine, P. Huet and R. J. Singleton, Nucl. Phys. B **375**, 625 (1992).

[7] A. G. Cohen, D. B. Kaplan and A. E. Nelson, Phys. Lett. B **263**, 86 (1991).

[8] A. G. Cohen and A. E. Nelson, Phys. Lett. B **297**, 111 (1992).

[9] J. M. Cline, K. Kainulainen and A. P. Vischer, Phys. Rev. D **54**, 2451 (1996).

[10] T. D. Lee, Phys. Rev. D **8**, 1226 (1973); Phys. Reports **9**, 143 (1974); S. Weinberg, Phys. Rev. Lett. **37**, 657 (1976).

[11] J. R. Espinosa, Nucl. Phys. B **475**, 273 (1996) ; D. Bodeker, P. John, M. Laine and M. G. Schmidt, Nucl. Phys. B **497**, 387 (1997).

[12] M. Carena, M. Quiros and C. E. Wagner, Phys. Lett. B **380**, 81 (1996); Nucl. Phys. B **524**, 3 (1998).

[13] J. M. Cline and G. D. Moore, Phys. Rev. Lett. **81**, 3315 (1998).

[14] H. Murayama and A. Pierce, hep-ph/0201261.

[15] M. Fukugita and T. Yanagida, Phys. Lett. B **174**, 45 (1986).

[16] L. Wolfenstein, Phys. Rev. D **18** (1978) 958; V. D. Barger, K. Whisnant and R. J. Phillips, Phys. Rev. Lett. **45**, 2084 (1980). A. Kusenko and R. Shrock, Phys. Lett. B **323**, 18 (1994); hep-ph/9403315; W. Buchmuller and D. Wyler, Phys. Lett. B **521**, 291 (2001); H. Fritzsch and Z. z. Xing, Phys. Lett. B **517**, 363 (2001); M. Frigerio and A. Y. Smirnov, arXiv:hep-ph/0202247; D. Chang, A. Masiero and H. Murayama, arXiv:hep-ph/0205111; G. Altarelli and F. Feruglio, arXiv:hep-ph/0206077.

[17] B. Kayser, these Proceedings.

[18] I. Affleck and M. Dine, Nucl. Phys. B **249**, 361 (1985).

[19] M. Dine, L. Randall and S. Thomas, Nucl. Phys. **B458** (1996) 291; R. Allahverdi, B. A. Campbell and J. R. Ellis, Nucl. Phys. B **579**, 355 (2000) Nucl. Phys. B **619**, 729 (2001).

[20] L. M. Krauss and M. Trodden, Phys. Rev. Lett.**83**, 1502 (1999).

[21] J. García-Bellido, D. Grigoriev, A. Kusenko, and M. Shaposhnikov, Phys. Rev. D **60**, 123504 (1999).

[22] J. M. Cornwall and A. Kusenko, Phys. Rev. D **61**, 103510 (2000) J. Garcia-Bellido and D. Y. Grigoriev, JHEP **0001**, 017 (2000).

[23] J. M. Cornwall, D. Grigoriev and A. Kusenko, Phys. Rev. D **64**, 123518 (2001)

[24] A. Kusenko and M. E. Shaposhnikov, Phys. Lett. B **418**, 46 (1998); K. Enqvist and J. McDonald, Phys. Lett. B **425**, 309 (1998)

[25] A. Kusenko, Phys. Lett. B **405**, 108 (1997); Phys. Lett. B **404**, 285 (1997); A. Kusenko, V. Kuzmin, M. E. Shaposhnikov and P. G. Tinyakov, Phys. Rev. Lett. **80**, 3185 (1998).

[26] K. Enqvist, J. McDonald: Phys. Lett. B **425**, 309 (1998); Phys. Rev. Lett. **81**, 3071 (1998); Phys. Lett. B **440**, 59 (1998); Phys. Rev. Lett. **83**, 2510 (1999)

[27] S. Kasuya and M. Kawasaki, Phys. Rev. D **61**, 041301 (2000); Phys. Rev. D **62**, 023512 (2000); Phys. Rev. D **64**, 123515 (2001). S. Kasuya, Phys. Lett. B **515**, 121 (2001).

[28] K. Enqvist and J. McDonald, Nucl. Phys. B **538**, 321 (1999); M. Laine and M. E. Shaposhnikov, Nucl. Phys. B **532**, 376 (1998); M. Fujii and T. Yanagida, arXiv:hep-ph/0206066.

[29] R. D. Peccei and H. R. Quinn, Phys. Rev. Lett. **38**, 1440 (1977); Phys. Rev. D **16**, 1791 (1977).

[30] S. Weinberg, Phys. Rev. Lett. **40**, 223 (1978); F. Wilczek, Phys. Rev. Lett. **40**, 279 (1978).

[31] For review, see, *e.g.*, R. D. Peccei, Phys. Scripta **T36**, 218 (1991); J. E. Kim, arXiv:astro-ph/0002193; K. van Bibber and D. Kinion, Nucl. Phys. Proc. Suppl. **91** (2001) 376.

[32] D.E. Groom et al., Europ. Phys. J., C15 (2000) 1.

Measuring α using $B \to K^{(*)}\overline{K}^{(*)}$ Decays[1]

Alakabha Datta and David London
Laboratoire René J.-A. Lévesque
Université de Montréal
C.P. 6128, succ. centre-ville
Montréal, QC, CANADA H3C 3J7

The *raison d'être* for measuring CP violation in the B system is to test the standard model (SM) [1]. As always, the hope is that we will find evidence for the presence of new physics.

There are many signals of new physics, but only a handful are of the "smoking-gun" variety, i.e. they are free of hadronic uncertainties, and hence independent of theoretical input. All of these rely on the measurement of CP-violating rate asymmetries in B decays. They include

- $B^0_d(t) \to \Psi K_S$ vs. $B^0_d(t) \to \phi K_S$. Both of these decay modes probe the CP phase β within the SM.
- $B^\pm \to DK^\pm$ vs. $B^0_s(t) \to D^\pm_s K^\mp$. Similarly, both of these modes can be used to measure γ.
- $B^0_s(t) \to \Psi\phi$. The CP asymmetry for this decay is expected to vanish within the SM (to a good approximation).

In all cases, any deviation from the SM predictions indicates the presence of new physics.

However, these signals have something in common: they are all sensitive to new physics in the $b \to s$ flavour-changing neutral current (FCNC). In the first case, the new physics enters in the $b \to s$ penguin amplitude, while in the last two cases, it affects B^0_s–$\overline{B}^0_s$ mixing.

This then begs the question: are there clean probes of new physics in the $b \to d$ FCNC? However, the answer to this is *no*.

To see this, consider the $b \to d$ penguin amplitude, which can be written as

$$A = P_u\, V^*_{ub} V_{ud} + P_c\, V^*_{cb} V_{cd} + P_t\, V^*_{tb} V_{td}\ , \tag{1}$$

where the P_i $(i = u, c, t)$ represent the contributions from the internal i-quark. Due to the unitarity of the Cabibbo-Kobayashi-Maskawa (CKM) matrix, any one CKM combination can be eliminated in terms of the other two. (Note that, unlike the $b \to s$ penguin amplitude, here all three combinations of CKM matrix elements are of the same order.) There are thus three ways of writing this amplitude:

[1] Talk given by David London

1. $A = (P_u - P_c)V_{ub}^* V_{ud} + (P_t - P_c)V_{tb}^* V_{td}$,
2. $A = (P_c - P_u)V_{cb}^* V_{cd} + (P_t - P_u)V_{tb}^* V_{td}$,
3. $A = (P_u - P_t)V_{ub}^* V_{ud} + (P_c - P_t)V_{cb}^* V_{cd}$.

In the first case, the relative weak phase between the two contributions is α, while in the second and third cases, it is β and γ, respectively. Therefore, there is an ambiguity — called the *CKM ambiguity* — in the definition of the relative weak phase in the $b \to d$ penguin amplitude. Because of this, it is impossible to cleanly extract weak-phase information from $b \to d$ penguins. Thus, in order to test for new physics in the $b \to d$ FCNC, we need a theoretical assumption which will break the CKM ambiguity [2]. This fact will be important in what follows.

Consider the pure $b \to d$ penguin decay $B_d^0 \to K^0 \overline{K}^0$. Its amplitude can be written

$$A = P_u\, V_{ub}^* V_{ud} + P_c\, V_{cb}^* V_{cd} + P_t\, V_{tb}^* V_{td} = \mathcal{P}_{uc}\, e^{i\gamma}\, e^{i\delta_{uc}} + \mathcal{P}_{tc}\, e^{-i\beta}\, e^{i\delta_{tc}} \ . \tag{2}$$

Note that the magnitudes of the CKM combinations $V_{ub}^* V_{ud}$ and $V_{tb}^* V_{td}$ have been absorbed into $\mathcal{P}_{uc}$ and $\mathcal{P}_{tc}$. In this parametrization, there are 4 theoretical parameters: $\mathcal{P}_{uc}$, $\mathcal{P}_{tc}$, $\Delta \equiv \delta_{uc} - \delta_{tc}$, and the CP phase α.

Recall that the time-dependent decay rate for a B_d^0 to decay to a final state f can be written as

$$\Gamma(B_d^0(t) \to f) \sim X + Y \cos \Delta m t - Z_I \sin \Delta m t \ , \tag{3}$$

where

$$X \equiv \frac{|A|^2 + |\overline{A}|^2}{2} \ , \quad Y \equiv \frac{|A|^2 - |\overline{A}|^2}{2} \ , \quad Z_I \equiv \mathrm{Im}\left(e^{-2i\beta} A^* \overline{A}\right) \ . \tag{4}$$

What is important here is that there are only 3 experimental observables. However, as noted above, there are 4 theoretical unknown quantities describing the decay $B_d^0 \to K^0 \overline{K}^0$. Thus, as expected, one cannot extract any of these theoretical parameters. However, it is always possible to express three of the unknowns in terms of the fourth. In particular, a little algebra allows us to write

$$\mathcal{P}_{tc}^2 = \frac{Z_R \cos 2\alpha + Z_I \sin 2\alpha - X}{\cos 2\alpha - 1} \ , \tag{5}$$

where $Z_R \equiv \mathrm{Re}\left(e^{-2i\beta} A^* \overline{A}\right)$. (Note that Z_R is not independent: $Z_R^2 = X^2 - Y^2 - Z_I^2$.)

A similar analysis can be applied to the decay $B_d^0 \to K^* \overline{K}^*$, where K^* represents any excited kaon, such as $K^*(892)$, $K_1(1270)$, etc. In this case we can write

$$\mathcal{P}_{tc}'^{\,2} = \frac{Z_R' \cos 2\alpha + Z_I' \sin 2\alpha - X'}{\cos 2\alpha - 1} \ , \tag{6}$$

where the primed observables correspond to the decay $B_d^0 \to K^* \overline{K}^*$. By combining Eqs. (5) and (6), we obtain

$$\frac{\mathcal{P}_{tc}^2}{{\mathcal{P}'_{tc}}^2} = \frac{Z_I \sin 2\alpha + Z_R \cos 2\alpha - X}{Z'_I \sin 2\alpha + Z'_R \cos 2\alpha - X'} \ . \tag{7}$$

Note that the CKM information in $\mathcal{P}_{tc}$ and $\mathcal{P}'_{tc}$ (the magnitudes of $V_{ub}^* V_{ud}$ and $V_{tb}^* V_{td}$) cancels in the ratio. The key point here is the following: *if we knew the value of* $\mathcal{P}_{tc}^2/{\mathcal{P}'_{tc}}^2$, *we could extract* α.

We now turn to the analogous processes in the B_s^0 system. Consider $B_s^0 \to K^0 \overline{K}^0$, which is a pure $b \to s$ penguin decay. Its amplitude can be written

$$A^{(s)} = P_u^{(s)} V_{ub}^* V_{us} + P_c^{(s)} V_{cb}^* V_{cs} + P_t^{(s)} V_{tb}^* V_{ts} = \mathcal{P}_{uc}^{(s)} e^{i\gamma} e^{i\delta_{uc}^{(s)}} + \mathcal{P}_{tc}^{(s)} e^{i\delta_{tc}^{(s)}} \ . \tag{8}$$

The difference between $b \to s$ penguins and $b \to d$ penguins is that, here, $V_{ub}^* V_{us}$ is $O(\lambda^4)$ while $V_{tb}^* V_{ts}$ is $O(\lambda^2)$. Thus, $\mathcal{P}_{uc}^{(s)}$ is negligible compared to $\mathcal{P}_{tc}^{(s)}$, so that the measurement of $B(B_s^0 \to K^0 \overline{K}^0)$ gives $|\mathcal{P}_{tc}^{(s)}|$. Similarly, the measurement of $B(B_s^0 \to K^* \overline{K}^*)$ gives $|\mathcal{P}_{tc}^{\prime(s)}|$.

We now make the claim that

$$\frac{{\mathcal{P}_{tc}^{(s)}}^2}{{\mathcal{P}_{tc}^{\prime(s)}}^2} = \frac{\mathcal{P}_{tc}^2}{{\mathcal{P}'_{tc}}^2} \ . \tag{9}$$

Note that the CKM matrix elements cancel in the ratios, so that this is a relation among hadronic parameters. This theoretical assumption breaks the CKM ambiguity. Thus, by combining this relation with that in Eq. (7), one can extract the CP phase α from the pure penguin decays $B_{d,s}^0 \to K^{(*)} \overline{K}^{(*)}$ [3]. A similar method applies to non-CP-conjugate decays of the form $K^0 \overline{K}^*$, $K^* \overline{K}^0$.

Of course, the precision with which α can be obtained depends on the theoretical uncertainty in the above relation. As we will argue below, the theoretical error is small, at most 5% (and may well be even smaller).

Before discussing the theoretical error, we briefly examine some of the experimental considerations in putting this method to use. The branching ratios for decays dominated by $b \to d$ penguins are expected to be $O(10^{-6})$. Combined with the fact that B_s^0 decays are involved, this suggests that this method is most appropriate for hadron colliders. In addition, since the $K^{(*)}$ and $\overline{K}^{(*)}$ mesons can be detected via their decays to charged π's and K's, no π^0 detection is needed – all that is necessary is good K/π separation. This is very important for most hadron colliders. (Of course, if π^0's can actually be detected, this will improve the prospects for using the method.) Finally, it should be possible to trigger on a final-state K^* at hadron colliders, so that final states such as $K^* \overline{K}^0$, $K^0 \overline{K}^*$ and $K^* \overline{K}^*$ will probably be favoured.

The method does have a potential weakness: α is extracted with a 16-fold discrete ambiguity. However, this is not as serious as it appears at first glance. First, the ambiguity can be reduced to 4-fold by considering two different $K^{(*)}\overline{K}^{(*)}$ final states. Examples of these include $K^0\overline{K}^0$ and $K^*\overline{K}^*$, $K^0\overline{K}^*$ and $K^*\overline{K}^0$, or two different helicity states of $K^*\overline{K}^*$. Second, we expect P_u and P_c in $b \to d$ penguins to be at most 50% of P_t. This implies that $\mathcal{P}_{uc}/\mathcal{P}_{tc} < 0.5$ for all decays. By adding this theoretical constraint, the discrete ambiguity can be reduced to 2-fold: α, $\alpha + \pi$.

There are two other methods on the market for cleanly measuring α: (i) the isospin analysis of $B \to \pi\pi$ decays [4], and (ii) the Dalitz-plot analysis of $B \to \rho\pi$ decays [5]. Both of these methods have their problems. The isospin analysis requires the measurement of $B^0_d \to \pi^0\pi^0$, whose branching ratio may be quite small. And in the Dalitz-plot analysis, one must understand the continuum background to $B \to \rho\pi$ decays with considerable accuracy, and have a correct description of $\rho \to \pi\pi$ decays. Both of these issues may be difficult to resolve. In light of this, the $B \to K^{(*)}\overline{K}^{(*)}$ method could potentially give us the first reasonably clean measurement of α. However, regardless of which is first, a discrepancy in the values of α obtained from these different methods would point clearly to new physics in the $b \to d$ penguin.

We now turn to a brief examination of the theoretical uncertainty in Eq. (9). We claim the equality of the double ratio of matrix elements:

$$\frac{r_t}{r_t^*} \equiv \frac{\left\langle K^0\overline{K}^0 \right| H_d \left| B^0_d \right\rangle / \left\langle K^0\overline{K}^0 \right| H_s \left| B^0_s \right\rangle}{\left\langle K^*\overline{K}^* \right| H_d \left| B^0_d \right\rangle / \left\langle K^*\overline{K}^* \right| H_s \left| B^0_s \right\rangle} = 1 \ . \tag{10}$$

The two decays in r_t are related by U-spin (i.e. flavour $SU(3)$ symmetry), and similarly for r_t^*. We can therefore write

$$r_t = \frac{\left\langle K^0\overline{K}^0 \right| H_d \left| B^0_d \right\rangle}{\left\langle K^0\overline{K}^0 \right| H_s \left| B^0_s \right\rangle} = 1 + C_{SU(3)} \ , \quad r_t^* = \frac{\left\langle K^*\overline{K}^* \right| H_d \left| B^0_d \right\rangle}{\left\langle K^*\overline{K}^* \right| H_s \left| B^0_s \right\rangle} = 1 + C^*_{SU(3)} \ , \tag{11}$$

where $C_{SU(3)}$ and $C^*_{SU(3)}$ are both expected to be $\sim 25\%$ (i.e. the typical size of $SU(3)$-breaking effects). Thus,

$$\frac{r_t}{r_t^*} = 1 + (C_{SU(3)} - C^*_{SU(3)}) \ . \tag{12}$$

Now, apart from $SU(3)$, there is no symmetry limit in which $(C_{SU(3)} - C^*_{SU(3)}) \to 0$, so that one might guess that the $SU(3)$ corrections to r_t/r_t^* are also $\sim 25\%$. However, as we argue below, we expect significant cancellations between $C_{SU(3)}$ and $C^*_{SU(3)}$.

At the quark level, the $SU(3)$ breaking vanishes in the limit $m_b \to \infty$, so that the hamiltonians describing the decays $B^0_d \to K^0\overline{K}^0$ and $B^0_s \to K^0\overline{K}^0$ are equal to $O(\Delta M_B/M_B) \simeq 2\%$. Writing

$$\begin{aligned} r_t &= \left\langle K^0\overline{K}^0 \right| H_d \left| B^0_d \right\rangle / \left\langle K^0\overline{K}^0 \right| H_s \left| B^0_s \right\rangle \\ &= \left\langle K^0\overline{K}^0 \right| H_d \left| B^0_d \right\rangle / \left\langle K^0\overline{K}^0 \right| U^\dagger H_d U \left| B^0_s \right\rangle \ , \end{aligned} \tag{13}$$

we see that there are two main sources of $SU(3)$-breaking corrections: (i) "final-state" corrections, $U\left|K^0\overline{K}^0\right\rangle \neq \left|K^0\overline{K}^0\right\rangle$, and (ii) "initial-state" corrections, $U\,|B_s^0\rangle \neq |B_d^0\rangle$.

The key observation here is that the sources of $SU(3)$ breaking in r_t^* are very similar to those in r_t: $U\left|K^*\overline{K}^*\right\rangle \neq \left|K^*\overline{K}^*\right\rangle$ and $U\,|B_s^0\rangle \neq |B_d^0\rangle$. It is therefore not unreasonable to expect sizeable cancellations between $C_{SU(3)}$ and $C^*_{SU(3)}$ in Eq. (12), and indeed this is what is found in model calculations. Such calculations suggest that both the final-state and initial-state corrections are at the level of 1–2%. Furthermore, this can be tested experimentally. For the final-state corrections, one needs to measure the kaon light-cone distribution at the scale of m_b, while information about the size of initial-state corrections can be obtained from measurements of the $D, D_s \to K, K^*$ form factors. For all the details concerning the size of the theoretical uncertainty, as well as the experimental tests, we refer the reader to Ref. [3].

To summarize, we have presented a new method for obtaining the CP phase α via measurements of $B^0_{d,s} \to K^{(*)}\overline{K}^{(*)}$ decays. This method is particularly appropriate for hadron colliders since some of the branching ratios are small $[O(10^{-6})]$, and since B_s^0 decays are involved. Furthermore, the final-state particles can be detected via their decays to charged particles only; no π^0 detection is needed. By comparing the value of α extracted from this method with that obtained in $B \to \pi\pi$ or $B \to \rho\pi$ decays, one can detect the presence of new physics in the $b \to d$ penguin amplitude. The method does require theoretical input. However, model calculations suggest that the theoretical uncertainty is at most 5%, and might well be even smaller. Furthermore, these estimates can be tested experimentally. The method is therefore quite clean.

D.L. is thanks the organizers of FPCP2002 for a wonderful conference. This work was financially supported by NSERC of Canada.

References

[1] For a review of CP violation in the B system, see, for example, *The BaBar Physics Book*, eds. P.F. Harrison and H.R. Quinn, SLAC Report 504, October 1998.

[2] D. London, N. Sinha and R. Sinha, *Phys. Rev.* **D60**: 074020 (1999).

[3] A. Datta and D. London, *Phys. Lett.* **533B**, 65 (2002).

[4] M. Gronau and D. London, *Phys. Rev. Lett.* **65**, 3381 (1990).

[5] A.E. Snyder and H.R. Quinn, *Phys. Rev.* **D48**, 2139 (93); H.R. Quinn and J.P. Silva, *Phys. Rev.* **D62**: 054002 (2000).

May 17, session 2.

Session Chair: K. Schubert

Recent Hot Results from B factories

Hot topics from BaBar

V. Shelkov

New BaBar Results on Rare Leptonic B Decays

V. Halyo

Three-body charmless $B \to Khh$ decays at Belle

A. Garmash

$B^- \to \omega K^-/\pi^-$ and Time-dependent CPV in $B^0 \to \eta' K_S$ at Belle

K. F. Chen

Hot topics from BABAR

Vasia Shelkov
BaBar Collaboration
Lawrence Berkeley National Laboratory
Berkeley, USA

1 Introduction

We present preliminary results of searches for B mesons decaying into the charmless final states, using around 50 fb^{-1} of data collected at the $\Upsilon(4S)$ resonance with the *BABAR* detector at the SLAC PEP-II asymmetric B Factory. We describe measurements with the BaBar data of the branching fractions for B decays to charmless quasi-two-body final states containing η' mesons. We find $\mathcal{B}(B^+ \to \eta' K^+) = (67 \pm 5 \pm 5) \times 10^{-6}$, $\mathcal{B}(B^0 \to \eta' K^0) = (46 \pm 6 \pm 4) \times 10^{-6}$, and $\mathcal{B}(B^0 \to \eta' K^{*0}) = (4.0^{+3.5}_{-2.4} \pm 1.0) \times 10^{-6}$ ($< (13.3) \times 10^{-6}$). We also measure the branching fractions $\mathcal{B}(B^\pm \to K^\pm \pi^\mp \pi^\pm) = (59.2 \pm 4.7 \pm 4.9) \times 10^{-6}$ and $\mathcal{B}(B^\pm \to K^\pm K^\mp K^\pm) = (34.7 \pm 2.0 \pm 1.8) \times 10^{-6}$, and provide the 90% confidence upper limits $\mathcal{B}(B^\pm \to \pi^\pm \pi^\mp \pi^\pm) < 15 \times 10^{-6}$ and $\mathcal{B}(B^\pm \to K^\pm K^\mp \pi^\pm) < 7 \times 10^{-6}$.

2 Charmless B meson decays to $\eta' K$ or $\eta' K^{*0}$

In this note, we report results of searches for B decays to three charmless quasi-two-body final states involving η' mesons. We include the decay modes $B^+ \to \eta' K^+$, $B^0 \to \eta' K^0$ and $B^0 \to \eta' K^{*0}$. These data contain an on-peak integrated luminosity of 56.4(52.0) fb^{-1} for the $B \to \eta' K (B^0 \to \eta' K^{*0})$ analyses. In addition there is 6.4 fb^{-1} of off-peak exposure. The full on-peak sample corresponds to $(61.6 \pm 0.7) \times 10^6$ $B\overline{B}$ pairs. A B meson candidate is characterized kinematically by the difference in energy $\Delta E = (E_0 E_B - \boldsymbol{p_0} \cdot \boldsymbol{p_B} - \frac{1}{2}s)/\sqrt{s}$, and beam energy constrained mass $m_{EC} = \sqrt{{E^*_B}^2 - {p^*_B}^2}$. Backgrounds arise primarily from combinatorics among light quark pair events from the continuum under the $\Upsilon(4S)$. Decays from genuine B mesons predominantly produce charmed, hence heavier daughters that are kinematically distinct from the charmless modes we seek. We extract the signal yields with a maximum likelihood fit to sets of weakly correlated observables. Each of the PDFs typically involves several parameters that are determined with various samples of data and Monte Carlo and are fixed for the ML fit. The input variables used in the fits are ΔE, M_{ES}, the invariant mass of the resonance R candidate (m_R), the Fisher

discriminant ($\mathcal{F}$), and, where relevant, the the helicity angle of the ρ ($\mathcal{H}$). The PDF determination for the likelihood fit is accomplished with use of signal Monte Carlo for the signal decays, and sideband data for the continuum background. Peaking distributions (signal masses, ΔE, $\mathcal{F}$) are parameterized

Table 1: Final ML fit results.

Quantity	$\eta'_{\eta\pi\pi}K^+$	$\eta'_{\rho\gamma}K^+$	$\eta'_{\eta\pi\pi}K^0$	$\eta'_{\rho\gamma}K^0$	$\eta'_{\eta\pi\pi}K^{*0}$	
					Run 1	Run 2
Events to fit						
On-resonance	2199	34492	665	7400	656	1074
Off-resonance	254	3847	59	790	92	138
Signal yield						
On-res data	152^{+14}_{-13}	293^{+23}_{-22}	29^{+7}_{-6}	106^{+14}_{-13}	$0.0^{+1.3}_{-0.0}$	$5.2^{+3.9}_{-2.8}$
Off-res data	$-1.6^{+1.8}_{-0.9}$	$-1.3^{+4.0}_{-2.9}$	$0.0^{+0.7}_{-0.0}$	$0.0^{+2.8}_{-0.0}$	$0.0^{+0.5}_{-0.0}$	$0.0^{+0.6}_{-0.0}$
Combinations/event	1.18	1.08	1.18	1.07	1.15	1.10
$B\overline{B}$ BG subtraction	0	13 ± 6	0	4.1 ± 2.1	0.7 ± 1.4	0.9 ± 1.1
MC ϵ (%)	23.1	24.0	23.5	24.5	16.9	16.9
ML-fit ϵ/bias (%)	99.0	94.4	100.0	97.0	105.9	105.3
Trk/Neut/PID corr. (%)	96.1	96.2	102.1	102.2	96.8	96.8
$\prod \mathcal{B}_i$ (%)	17.4	29.5	6.0	10.1	11.5	11.5
Corr. $\epsilon \times \prod \mathcal{B}_i$ (%)	3.82	6.42	1.43	2.46	1.99	1.98
Stat. sign. (σ)	26	20	10	15	0	1.9
$\mathcal{B}(\times 10^{-6})$	65 ± 6	71 ± 6	32 ± 7	67 ± 9	$0^{+2.2}_{-0.0}$	$7.9^{+5.8}_{-4.2}$
UL (stat. only)	–	–	–	–	8.7	17
UL (incl. syst.)	–	–	–	–	12	24

Table 1 shows the results for off-peak and on-peak data. The statistical error on the number of events is taken as the change in the central value when the quantity $\chi^2 \equiv -2\ln\mathcal{L}$ changes by one unit. The statistical significance is taken as the square root of the difference between the value of χ^2 for zero signal and the value at its minimum. We illustrate the best fit likelihood function by projection of the yields and PDFs in m_{ES} and ΔE, with cuts to emphasize the signal-like events. It can be found in Figure 1. We are left with about a three standard deviation discrepancy between our measurements of $B^0 \to \eta' K^0$ in the two η' decay modes. We include in the following section the cross checks we have performed to rule out unaccounted systematics that could affect either result. Finding no evidence of inconsistency within either mesurement, we present the weighted average for this as well as the charged mode as our final measurements of the neutral and charged

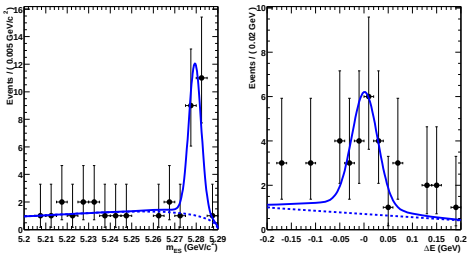

Figure 1: Projection of the on-resonance data and PDF projected onto (left) m_{ES} and (right) ΔE, for $B^0 \to \eta'(\eta' \to \eta\pi^+\pi^-)K^0$.

$B \to \eta' K$ branching fractions. For modes where the central value is not significant, we include systematics in the 90% CL upper limit. This approach amounts to folding systematics in quadrature into the likelihood function before integrating to obtain the 90% CL. We have found significant event yields in five of the decay chains studied here, as reported in Table 1. Where we have multiple chains for a given mode we combine the results, representing the uncorrelated errors by distributions in $\chi^2 = -2\log\frac{\mathcal{L}}{\mathcal{L}_{\max}}$ which are added. Where the significance is less than four standard deviations, we quote also (Bayesian) 90% C.L. upper limits, defined by the solution B to the condition $\int_0^B \mathcal{L}(b)db / \int_0^\infty \mathcal{L}(b)db = 0.9$. The final results are: $\mathcal{B}(B^+ \to \eta' K^+) = (67 \pm 5 \pm 5) \times 10^{-6}$, $\mathcal{B}(B^0 \to \eta' K^0) = (46 \pm 6 \pm 4) \times 10^{-6}$, $\mathcal{B}(B^0 \to \eta' K^{*0}) = (4.0^{+3.5}_{-2.4} \pm 1.0) \times 10^{-6}$ ($< (13.3) \times 10^{-6}$). They are generally in agreement with those previously reported, with smaller errors (more restrictive limit). In particular we confirm the rather larger than predicted [2] rate for $B \to \eta' K$ obtained by the CLEO Collaboration [3]. Conjectured sources of η' enhancement include flavor singlet [4], charm enhanced [8], and constructively interfering internal penguin diagrams [2, 5].

3 Measurements of the branching fractions of charmless three-body charged B decays

We present updated preliminary results on the branching fractions of charged charmless three-body $B^\pm \to h^\pm h^\mp h^\pm$ decays, where $h = \pi$ or K, with no assumptions about intermediate resonances and with open charm contributions subtracted. Charge conjugate initial and final states are assumed throughout this document, unless stated otherwise. The data sample consists of 56.2 million $B\overline{B}$ pairs, corresponding to an integrated luminosity of 51.5 fb^{-1} collected at the $\Upsilon(4S)$ resonance (on-resonance) during the 2000-2001 run. Charged particles are identified by the Cherenkov angle θ_c

and the number of photons measured with the DIRC. The typical separation between pions and kaons varies from $> 8\ \sigma$ at 2.0GeV/$c$to 2.5σ at 4.0GeV/c, where σ is the average resolution on θ_c. The kaon selection efficiency is approximately 80%, which is the product of the particle identification algorithm efficiency with geometrical acceptance, for a pion mis-identification probability of 2%. The total branching fraction for each $B^{\pm} \to h^{\pm}h^{\mp}h^{\pm}$ mode is measured over the whole Dalitz plot - all resonant and non-resonant contributions are included. A set of selection criteria is applied to reconstruct each mode separately. Each Dalitz plot is divided into many equal area cells to enable us to find the selection efficiency as a function of position in the Dalitz plot. We also take into account continuum backgrounds and cross-feed between each signal mode from K and π mis-identification. We use dE/dx information from the SVT and DCH, and the Cherenkov angle and number of photons measured by the DIRC for tracks with momenta above 700 MeV/c, to identify charged pions and kaons. Since we are only interested in charmless decays, we need to veto candidates that contain charm mesons. We remove B candidates when the invariant mass of the combination of any two of its daughter tracks (of opposite charge) is within 3 σ of the mass of D^0, J/ψ or $\psi(2S)$ mesons. Here, σ is 10.0 MeV/$c^2$for D^0 and 15.0 MeV/$c^2$for J/ψ and $\psi(2S)$. All possible kaon and pion combinations are tested for the D^0 veto, while only the K^+K^- and $\pi^+\pi^-$ hypotheses are tested for the J/ψ and $\psi(2S)$ vetoes, since the background from these decays is from leptonic decays, in which the leptons have been mis-identified as pions or kaons. The electron veto helps to reduce the combinatorial background from J/ψ and $\psi(2S)$ decays that would otherwise pass the 3 σ invariant mass veto. We reduce tlight quark and charm continuum backgrounds by imposing requirements on two topological event shape variables computed in the $\Upsilon(4S)$ rest frame: the cosine of the angle θ_T and Fisher discriminant [6]. The residual background level is estimated from the observed number of events in a sideband region, located near to the signal region in the m_{ES}- ΔE plane, and then extrapolating into the signal region by using a multiplicative factor, R. We define R to be the ratio of the number of background candidates in the signal region to the number in the sideband region. As mentioned previously, the branching fractions for each signal mode are measured over the whole Dalitz plot, and each Dalitz plot is divided up into many cells so that the bin-by-bin variation of the selection efficiency can be found for each plot. The signal region is defined to be $|m_{ES} - m_B| < 8.0$ MeV/c^2 and $|\Delta E - \langle \Delta E \rangle| < 60.0$ MeV, where $\langle \Delta E \rangle$ is the mean value of ΔE for on-resonance data for the calibration sample $B^- \to D^0\pi^-$, $D^0 \to K^-\pi^+$, and m_B is the nominal mass of the charged B meson [7]. The GSB region is defined to be $5.21 < m_{ES} < 5.25$ GeV/c^2 and $|\Delta E - \langle \Delta E \rangle| < 100.0$ MeV. The Dalitz plot for each signal mode is divided into cells with equal area 1.0 GeV^4, and large samples of Monte Carlo signal events are used to obtain the signal and cross-feed selection efficiencies across each Dalitz plot. Table 2 shows the signal and cross-feed selection efficiencies for the modes, averaged over the Dalitz plots. The uncertainties on the signal efficiencies and cross-feed prob-

Table 2: Efficiencies and cross-contamination probabilities between the signal modes derived from Monte Carlo samples. For example, the probability that an event $K^{\pm}\pi^{\mp}\pi^{\pm}$ will be reconstructed as $\pi^{\pm}\pi^{\mp}\pi^{\pm}$ is $(1.7 \pm 0.1) \times 10^{-2}$.

Selected as	Input Decay Mode			
	$\pi^{\pm}\pi^{\mp}\pi^{\pm}$	$K^{\pm}\pi^{\mp}\pi^{\pm}$	$K^{\pm}K^{\mp}\pi^{\pm}$	$K^{\pm}K^{\mp}K^{\pm}$
$\pi^{\pm}\pi^{\mp}\pi^{\pm}$	$(15.3 \pm 0.2) \times 10^{-2}$	$(1.7 \pm 0.1) \times 10^{-2}$	$(1.4 \pm 0.9) \times 10^{-4}$	$(1.1 \pm 3.2) \times 10^{-5}$
$K^{\pm}\pi^{\mp}\pi^{\pm}$	$(3.6 \pm 0.4) \times 10^{-3}$	$(15.1 \pm 0.2) \times 10^{-2}$	$(3.2 \pm 0.2) \times 10^{-2}$	$(4.0 \pm 1.7) \times 10^{-4}$
$K^{\pm}K^{\mp}\pi^{\pm}$	$(0.0 \pm 0.2) \times 10^{-3}$	$(2.9 \pm 0.4) \times 10^{-3}$	$(17.7 \pm 0.3) \times 10^{-2}$	$(5.5 \pm 0.2) \times 10^{-2}$
$K^{\pm}K^{\mp}K^{\pm}$	$(0.0 \pm 0.2) \times 10^{-3}$	$(0.0 \pm 0.2) \times 10^{-3}$	$(1.7 \pm 0.2) \times 10^{-3}$	$(21.6 \pm 0.3) \times 10^{-2}$

abilities are the combination of statistical errors on the number of events selected in the Monte Carlo samples relative to the total number generated, as well as systematic uncertainties arising from the difference between Monte Carlo simulation and on-resonance data. The fractional uncertainties for the Dalitz plot variation for the cross-feed probabilities ($\Delta\epsilon_i''/\epsilon_i''$) are approximately 30%. Finally, there is a systematic uncertainty on the overall normalisation, $N_{B\overline{B}}$, which is obtained from a dedicated study to find the number of B mesons produced in the data sample. This is found to have a systematic uncertainty of 1.5%. Figures 2 to 5 show the ΔE and m_{ES} distributions for the signal region for each of the modes. Each plot shows the expected levels continuum and $B\overline{B}$ background (solid and dashed lines, respectively). Figures 6 to 9 show the unbinned Dalitz plots for the signal modes in the GSB and signal regions, where no efficiency corrections have been applied. Only the upper half of the symmetrical Dalitz plot is shown for the $B^{\pm} \to \pi^{\pm}\pi^{\mp}\pi^{\pm}$ and $B^{\pm} \to K^{\pm}K^{\mp}K^{\pm}$ channels, where the x and y axes show the minimum and maximum values of the Dalitz plot variables, respectively. There are clear signals for the modes $B^{\pm} \to K^{\pm}\pi^{\mp}\pi^{\pm}$ and $B^{\pm} \to K^{\pm}K^{\mp}K^{\pm}$. No signal is observed for $B^{\pm} \to K^{\pm}K^{\mp}\pi^{\pm}$, and the result for $B^{\pm} \to \pi^{\pm}\pi^{\mp}\pi^{\pm}$ is interpreted as an upper limit on the branching fraction, although there is a positive excess of signal events with 2.2 σ significance. Since there are a large number of events in the selected samples, we can assume that the number of signal and background events observed in the signal region are Gaussian distributed. The 90% C.L. upper limits are computed using the standard prescription for a one-sided confidence interval from a Gaussian distributed measurement.

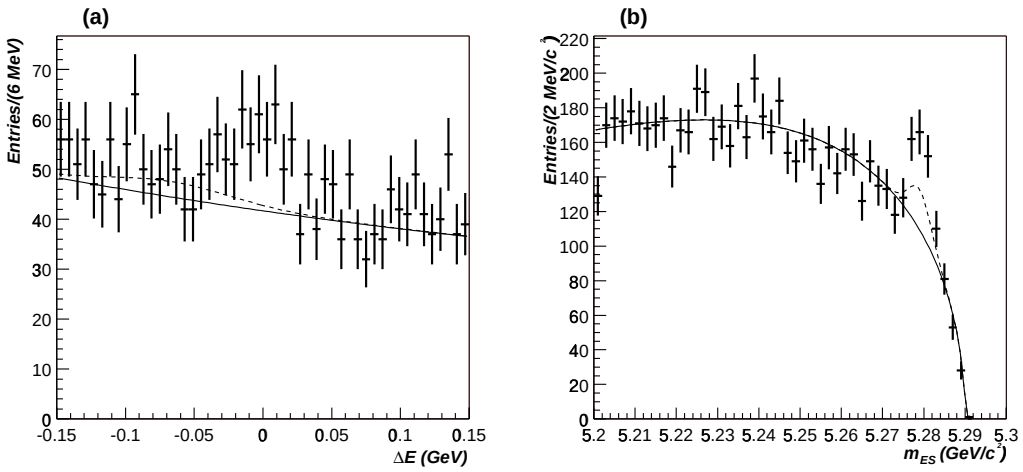

Figure 2: On-resonance signal region ΔE (a) and m_{ES} (b) distributions for $B^{\pm} \to \pi^{\pm}\pi^{\mp}\pi^{\pm}$. The solid lines show the expected level of continuum background, using appropriately normalised background shapes from the sideband regions in on-resonance data. The dotted lines show the expected level of $B\overline{B}$ background, which is obtained from the sum of Gaussian distributions from Monte Carlo estimated cross-feed and $D^0\pi$ events, each normalised to the number of events observed in on-resonance data that passed the selection criteria for $B^{\pm} \to \pi^{\pm}\pi^{\mp}\pi^{\pm}$.

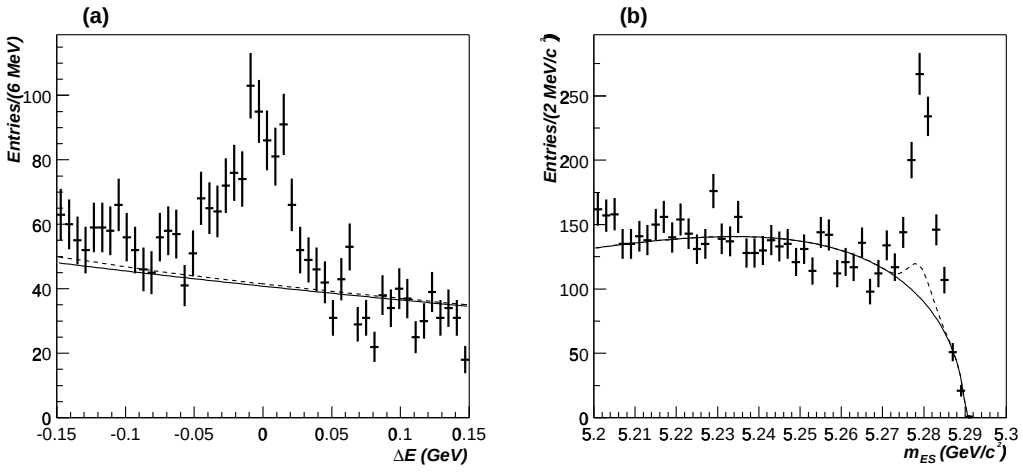

Figure 3: On-resonance signal region ΔE (a) and m_{ES} (b) distributions for $B^{\pm} \to K^{\pm}\pi^{\mp}\pi^{\pm}$.

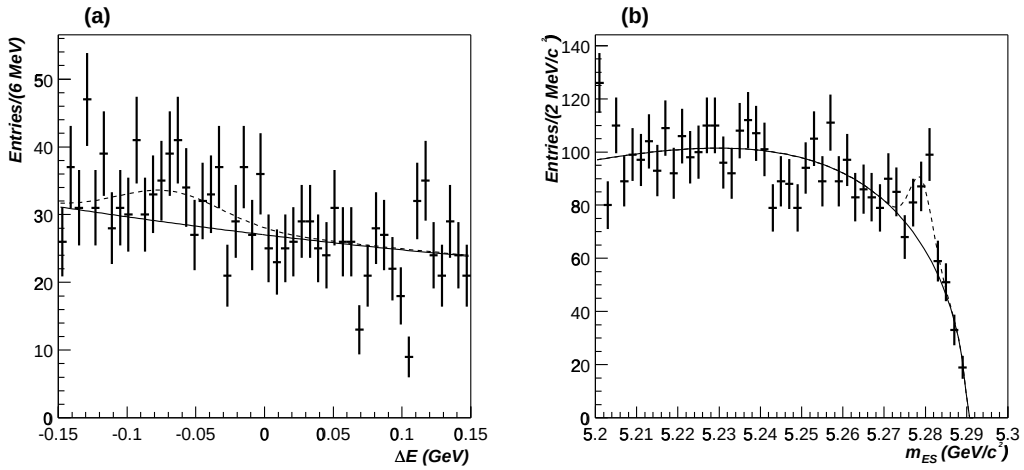

Figure 4: On-resonance signal region ΔE (a) and m_{ES} (b) distributions for $B^{\pm} \to K^{\pm}K^{\mp}\pi^{\pm}$.

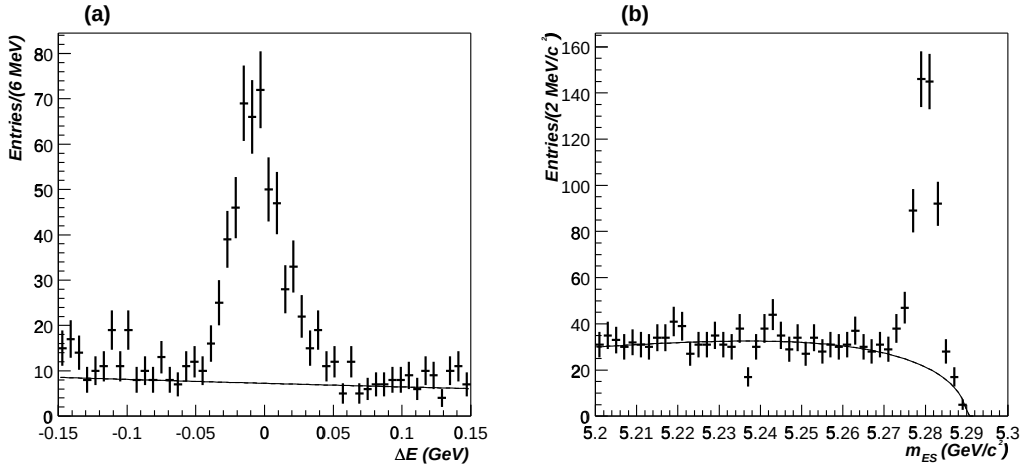

Figure 5: On-resonance signal region ΔE (a) and m_{ES} (b) distributions for $B^{\pm} \to K^{\pm}K^{\mp}K^{\pm}$.

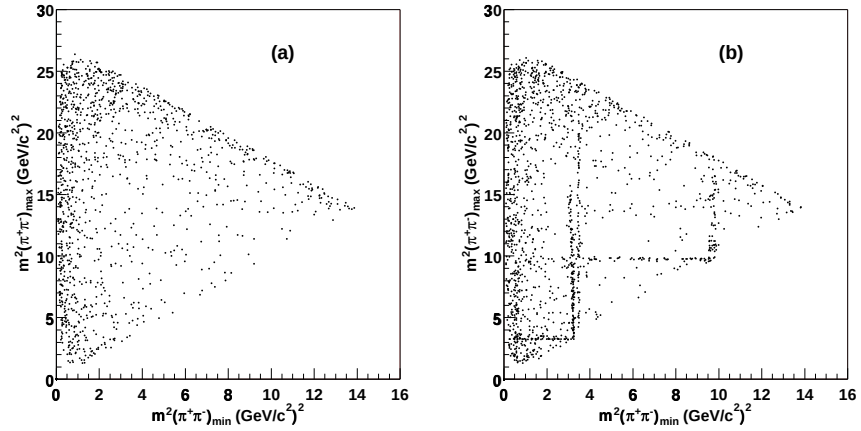

Figure 6: Unbinned Dalitz plots for on-resonance data for $B^{\pm} \to \pi^{\pm}\pi^{\mp}\pi^{\pm}$ for GSB region (a) and signal region (b). No efficiency corrections have been applied, and the open charm contributions are included in the plots.

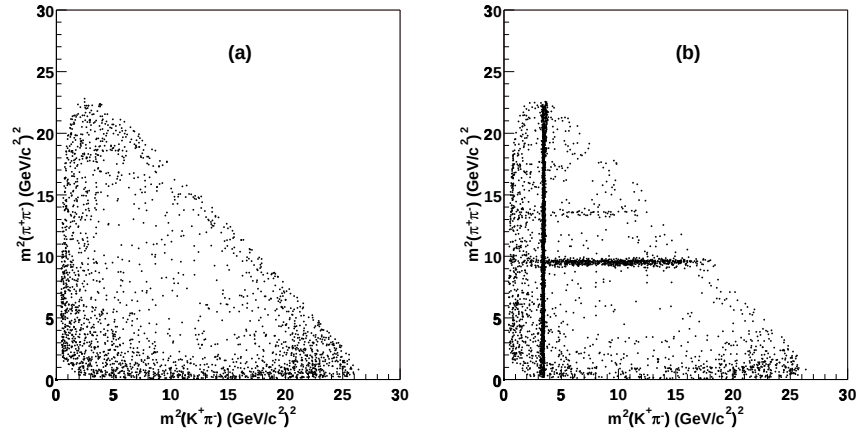

Figure 7: Unbinned Dalitz plots for on-resonance data for $B^{\pm} \to K^{\pm}\pi^{\mp}\pi^{\pm}$ for GSB region (a) and signal region (b).

The preliminary results are: $Br(\pi^{\pm}\pi^{\mp}\pi^{\pm}) < 15 \times 10^{-6}$, $Br(K^{\pm}\pi^{\mp}\pi^{\pm}) = (59.2 \pm 4.7 \pm 4.9) \times 10^{-6}$, $Br(K^{\pm}K^{\mp}\pi^{\pm}) < 7 \times 10^{-6}$, and $Br(K^{\pm}K^{\mp}K^{\pm}) = (34.7 \pm 2.0 \pm 1.8) \times 10^{-6}$.

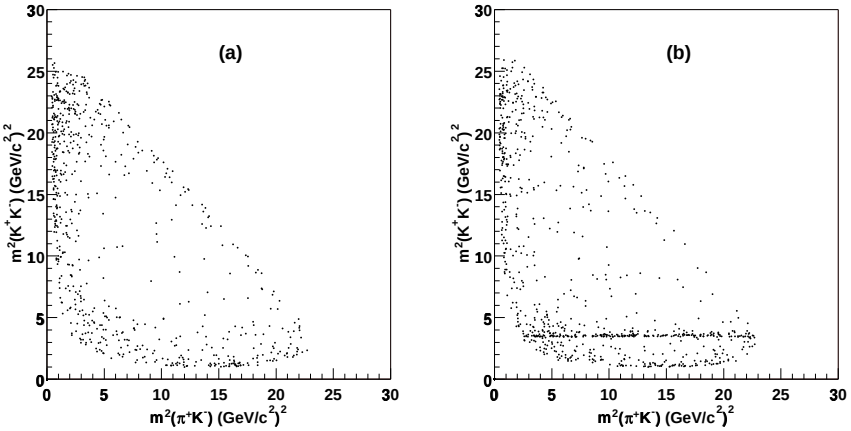

Figure 8: Unbinned Dalitz plots for on-resonance data for $B^{\pm} \to K^{\pm}K^{\mp}\pi^{\pm}$ for GSB region (a) and signal region (b).

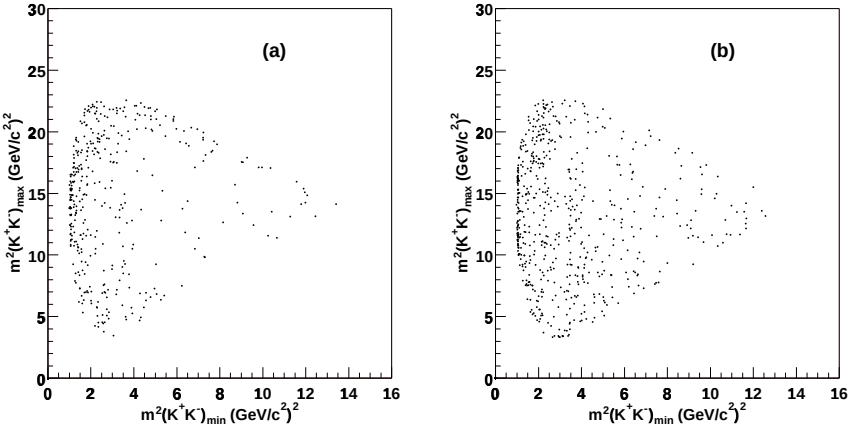

Figure 9: Unbinned Dalitz plots for on-resonance data for $B^{\pm} \to K^{\pm}K^{\mp}K^{\pm}$ for GSB region (a) and signal region (b).

References

[1] Charmless hadronic B decays at BABAR, Marcella Bona (for the BABAR Collaboration) submitted to EPS HEP 2001, hep-ex/0111017

[2] A. Ali, G. Kramer, and C. D. Lü, Phys. Rev. D **58**, 094009 (1998); Y. H. Chen

et al., Phys. Rev. D **60**, 094014 (1999).

[3] CLEO Collaboration (S. J. Richichi *et al.*) Phys. Rev. Lett. **85**, 520 (2000); CLEO CONF 99-12 (1999).

[4] M. Gronau and J. L. Rosner, Phys. Rev. D **53**, 2516 (1996); A. S. Dighe, M. Gronau, and J. L. Rosner, Phys. Rev. Lett. **79**, 4333 (1997); M. R. Ahmady, E. Kou, and A. Sugamoto, Phys. Rev. D **58**, 014015 (1998); D. Du, C. S. Kim, and Y. Yang, Phys. Lett. **B426**, 133 (1998).

[5] H. J. Lipkin, Phys. Lett. B **254**, 247 (1991).

[6] CLEO Collaboration, D. M. Asner *et al.,* "Search for Exclusive Charmless Hadronic B Decays", Phys. Rev. D **53**, 1039 (1996), hep-ex/9508004.

[7] Particle Data Group, D. E. Groom *et al.,* Eur. Phys. Jour. C **15**, 1 (2000).

[8] I. Halperin and A. Zhitnitsky, Phys. Rev. D **56**, 7247 (1997); E. V. Shuryak and A. Zhitnitsky, *ibid.* **57**, 2001 (1998).

New BaBar Results on Rare Leptonic B Decays

Valerie Halyo
Stanford Linear Accelerator Center
2575 Sand Hill Rd.
Menlo Park, CA, 94025
U.S.A

1 Abstract

New preliminary BaBar results for rare leptonic decays $B^-\to K^-\nu\overline{\nu}$ and $B^0\to\ell^+\ell^-$ are reported. Using data collected at the $\Upsilon(4S)$ with the BaBar detector, no evidence for a signal was found yielding the corresponding upper limits at the 90% confidence level: $\mathcal{B}(B^-\to K^-\nu\overline{\nu}) < 9.4 \times 10^{-5}$ for 50.7fb^{-1} , $\mathcal{B}(B^0\to e^+e^-) < 3.3\times 10^{-7}$, $\mathcal{B}(B^0\to\mu^+\mu^-) < 2.0\times 10^{-7}$ and $\mathcal{B}(B^0\to e^\pm\mu^\mp) < 2.1\times 10^{-7}$ using 54.4fb^{-1} .

2 $B^-\to K^-\nu\overline{\nu}$

The exclusive decay $B^-\to K^-\nu\overline{\nu}$ is characterized by the absence of the long distance contributions and by the fact that the effective Hamiltonian is represented in the Standard Model (SM) by only one operator. In the SM the decay proceeds via the W box and Z penguin diagrams as can be seen in fig 1. This mode probes the quark mixing parameter $|V_{ts}|$. The SM prediction is $\mathcal{B}(B^-\to K^-\nu\overline{\nu}) = 3.8^{+1.2}_{-0.6}\times 10^{-6}$ [4][5] and the previous best limit obtained by CLEO is $\mathcal{B}(B^-\to K^-\nu\overline{\nu}) < 2.4\times 10^{-4}$ [1]. Enhancement beyond the SM can arise from various types of models [2]. The highly constrained models where the existing bounds on other Flavor Changing Neutral Current processes imply that the rate for $B^-\to K^-\nu\overline{\nu}$ can not exceed the SM prediction by more than a factor of a few. In this category we have for example the Multi Higgs Doublet Models and the Left Right symmetric models. Enhancement by one or two orders of magnitude can arise from models with an extra vector-like down quark or models with leptophobic $Z^{'}$ bosons [3]. Last are the unconstrained models where the couplings responsible of enhancing $B^-\to K^-\nu\overline{\nu}$ are to a large extent independent of current existing experiment bounds. An example which belongs to this category is supersymmetric models without R-parity.

The presence of two neutrinos in the final state precludes the use of any kinematic constraints on the signal B meson. The strategy adopted for the BaBar analysis was to look for a charged kaon with momentum $p^* > 1.5\,\mathrm{GeV}$ in the $\Upsilon(4S)$ frame recoiling

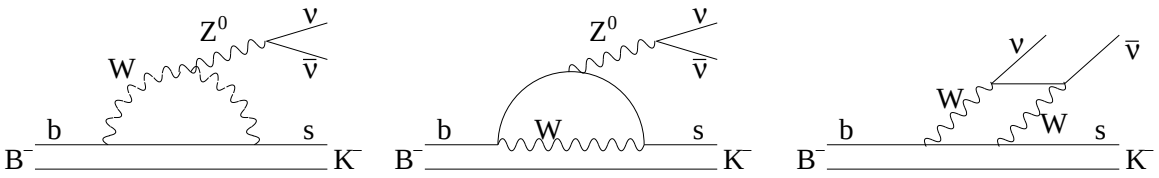

Figure 1: Standard Model Feynman diagrams for $B^- \to K^- \nu\overline{\nu}$.

against a semileptonic decay $B^+ \to \overline{D}^0 \ell^+ \nu(X)$ where X represent either a null or a photon or a π^0 from higher mass charm states. The exclusively reconstructed B meson is referred in the following as the tag B. The BaBar standard practice of blind analysis was followed to prevent biases. The low multiplicity of the signal decay reduces the combinatorieal background in the tag B reconstruction allowing the semileptonic decay $B^+ \to \overline{D}^0 \ell^+ \nu(X)$ to be cleanly reconstructed. The $\overline{D}^0$ is reconstructed in the $K^+\pi^-$, $K^+\pi^-\pi^-\pi^+$ and $K^+\pi^-\pi^0$ modes. This method results in roughly 0.5% of tag reconstruction efficiency. The data used in the analysis consist of 50.7fb^{-1} collected at the $\Upsilon(4S)$ resonance corresponding to 56.3×10^6 $B\overline{B}$ events and 6.4fb^{-1} collected just below $B\overline{B}$ threshold. The kinematics for the $B^- \to K^- \nu\overline{\nu}$ decays in the simulation is based on the form factor model in [4].

Hadronic events were selected once an electron or muon with a momentum above 1.3 GeV in the $\Upsilon(4S)$ rest frame was identified. Than $\overline{D}^0$ candidates were reconstructed in one of the $K^+\pi^-$, $K^+\pi^-\pi^-\pi^+$ and $K^+\pi^-\pi^0$ decay modes. The kinematic requirement on the angle between the B and the reconstructed $D\ell$, calculated in the $\Upsilon(4S)$ frame was used to suppress background and restrict the kinematics of the $\overline{D}^0\ell^+$ to be consistent with coming from a semileptonic B decay. The requirment $-2.5 < \cos\theta_{B\ D\ell} < 1.1$ was imposed, using

$$\cos\theta_{B\,D\ell} = \frac{2\,E_B E_{D\ell} - m_B^2 - m_{D\ell}^2}{2\,|\vec{p}_B||\vec{p}_{D\ell}|} \quad . \tag{1}$$

where E_B and $|\vec{p}_B|$ are respectively the energy and magnitude of the momentum of the B meson in the $\Upsilon(4S)$ frame.

A special double tag sample was used to extract a correction to the efficiency calculated from signal Monte Carlo (MC). The sample was reconstructed by first finding a suitable $\overline{D}^0\ell^+$ candidate where the $\overline{D}^0$ decays to $K^+\pi^-$, and then looking for a second $D\ell$ candidate in any of the accepted $\overline{D}^0$ modes. The observed rate of double tags per fb^{-1} in the data is 0.85 ± 0.11 times the rate in the simulation leading to a correction to the the signal efficiency by a factor 0.92 ± 0.06 where the uncertainty is taken as a systematic error. The uncertainty in the efficiency of several of the selection criteria were also studied using the double-tagged sample. The total relative uncertainty on the selection efficiency was found to be $\delta\epsilon/\epsilon = 8.7$ % where

the tagging efficiency and ($E_{\rm left}$) the remaing neutral energy after the tag B and its daughter were removed contribute the most.

The distribution of events in the search plane defined by the variables[1] $E_{\rm left}$ and $(m_D - m_D^{\rm fit})/\sigma_D^{\rm fit}$ is shown in fig 2. We observe 2 events in the signal box, defined by the requirements $E_{\rm left} < 0.5\,{\rm GeV}$ and $(m_D - m_D^{\rm fit}) < 3\sigma_D^{\rm fit}$. The expected background from the MC is 2.2 events. The background at present appears to be mostly $c\bar{c}$ events.

The Poisson upper limit calculated at 90% C.L. without background subtraction is

$$\mathcal{B}(B^- \to K^- \nu\overline{\nu}) < 9.4 \cdot 10^{-5} \tag{2}$$

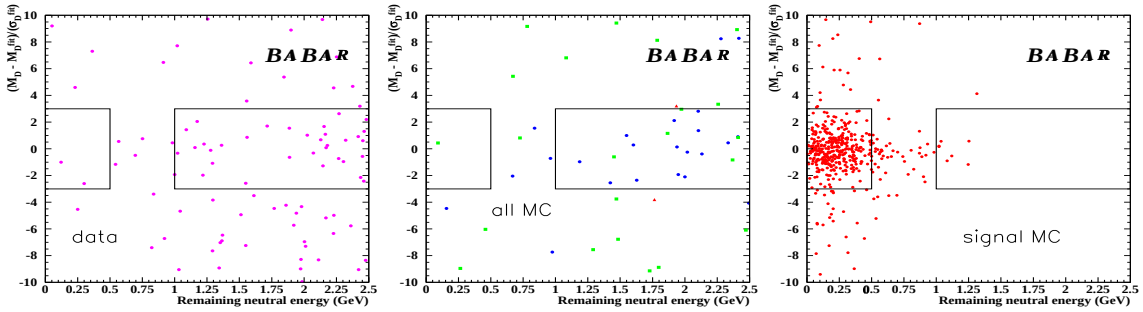

Figure 2: The distribution of events in the $((m_D - m_D^{\rm fit})/\sigma_D^{\rm fit}\ E_{\rm left})$ plane for on-peak data, generic $B\overline{B}$ and continuum MC and signal MC. In the generic MC plot the blue circles show the contribution from $B\overline{B}$ events, the green squares show the contribution from $c\bar{c}$ and the red triangles show the contribution from $u\overline{u}/d\overline{d}/s\overline{s}$. The generic MC contributions needs to be scaled by a factor of 1.09, 2.21 and 3.56 for the $B\overline{B}$, $c\bar{c}$ and $u\overline{u}/d\overline{d}/s\overline{s}$ contributions respectively to correspond to the on-peak data luminosity.

3 $B^0 \to l^+ l^-$

$B^0 \to l^+ l^-$ proceeds in the SM through the three dominant W box and Z penguin diagrams shown in fig. 3. Even though these diagrams are similar to the one that lead to $B^- \to K^- \nu\overline{\nu}$ these decays are further helicity suppressed by factors of m_l^2. Both $B^0 \to l^+ l^-$ and $B^- \to K^- \nu\overline{\nu}$ FCNC transitions provide an essential opportunity to test the SM and offer a complementary strategy in the search for new physics by probing the indirect effects of new particles and interactions. The SM theoretical branching ratio predictions are 1.9×10^{-15} for $B^0 \to e^+ e^-$, 8.0×10^{-11} for $B^0 \to \mu^+ \mu^-$ and null for $B^0 \to e^\pm \mu^\mp$ although recent neutrino mixing experiment results suggest that the branching ratio would be less than 10^{-15}. To date these decays have not

[1] The quantities $m_D^{\rm fit}$ and $\sigma_D^{\rm fit}$ are the mean and sigma from Gaussian fits to the D^0 invariant mass spectrum. Separate values are calculated for each D^0 decay mode in data and simulation. $E_{\rm left}$ is the remaing neutral energy after the tag B and its daughter were removed

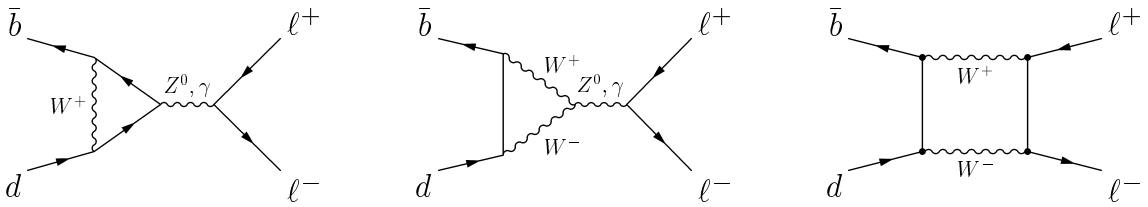

Figure 3: Standard Model Feynman diagrams for $B^0 \to \ell^+\ell^-$.

been observed and the current best limits from CLEO and Belle are summarized in table 2 [6]-[7]. Since these processes are highly suppressed in the SM they are potentially sensitive probes of physics beyond the SM. Models such as MHDM with Natural Flavor Conservation and large $tan\beta$ can give up to an order of magnitude enhancement [8]. The enhancment in models with an extra vector-like down quark can be to up to two orders [9]. Large enhancement may also arise from Minimal Supersymmetric Models with large $tan\beta$ [10] or Supersymmetric models without R-parity.

The decay $B^0 \to l^+l^-$ offers a very clean experimental signature in the BaBar detector. The two high momentum leptons can be measured precisely and identified with high purity in the detector. Relatively low backgrounds arise from the continuum consisting mostly of non-resonant $e^+e^- \to q\overline{q}$ production where $q = u, d, s, c$. The main contribution in the case of $B^0 \to e^+e^-$ is from pairs of real electrons in $c\overline{c}$ production; the contribution of misidentified hadron-electron pairs is negligible. Two-photon events contribute a significant background. Misidentification of muons is significantly more important in the case of $B^0 \to \mu^+\mu^-$, as evidenced by an increased background expectation from uds events. For the $B^0 \to \mu^+\mu^-$ channel, the background from two-photon processes is negligible.

The main measurement criteria are used to suppress different background events. The multiplicity cut $N_{mult} = N_{Trk} + N_\gamma/2 \geq 6, E_\gamma > 80$MeV suppresses radiative Bhabha events while maintaining a higher efficiency than a simple stringent multiplicity cut. The tracks are restricted to the central region of the detector using a polar angle cut which is efficient in removing QED background due to its strong dependence on the polar angle. As mentioned above, the main background process comes from continuum events which exhibit a two jet structure and produce high momentum approximately back to back tracks satisfying the requirements imposed on our candidate events. Two different shape variables suppress this kind of background: $|\cos\theta_T| < 0.84$ where θ_T is the angle between the thrust axes of the B-candidate and the rest of the event and the event thrust magnitude $|T| < 0.9$. The lepton pair is selected by simultaneous requirements on the energy difference ΔE and the energy-substituted mass m_{ES} defined in the following. The invariant energy difference of the B-meson candidate and the energy-substituted mass m_{ES} are calculated as

$$\Delta E = \frac{p_B \cdot p_i - s/2}{\sqrt{s}} \qquad m_{ES} = \sqrt{(s/2 + \mathbf{p}_B \cdot \mathbf{p}_i)^2/E_i^2 - \mathbf{p}_B^2} \tag{3}$$

where $\sqrt{s}$ is the CMS energy, p_B and p_i denote the four-momenta of the B-meson candidate and the initial state.

The signal box is defined in the (m_{ES} ΔE) plane and was obtained for each of the $B^0 \to l^+ l^-$ mode separately using an upper limit optimization. The size of the signal and Grand Sideband (GSB) was chosen to be roughly $[+2, -2]\sigma$ of the expected resolution in ΔE and $[+2, -2]\sigma$ for m_{ES}. In the cases of $B^0 \to e^+ e^-$ and $B^0 \to e^\pm \mu^\mp$, the signal box size in ΔE were relaxed to roughly $[+2, -3]\sigma$ and $[+2, -2.5]\sigma$ to account for increased amounts of final state radiation and bremsstrahlung.

The resulting efficiencies for the three $B^0 \to l^+ l^-$ are given in table 1. The number of events observed in the GSB appears in figure 4. In order to estimate the number of background events in the signal box an unbinned maximum likelihood fit was done using an Argus fit for the m_{ES} distribution and an exponential fit for ΔE distribution. The results are given in table 1. There are three sources of systematic uncertainties: The normalization, the signal efficiency and the background estimate. The systematic uncertainties for the different variables were estimated using a control sample of $B \to J/\Psi K_s^0$ with $J/\Psi \to \ell^+ \ell^-$. Since there is no control sample for $B^0 \to e^\pm \mu^\mp$ the error for $B^0 \to e^+ e^-$ was assigned to $B^0 \to e^\pm \mu^\mp$ and the total systematic errors amount to 8.6%, 5.2% and 8.6% for $B^0 \to e^+ e^-$,$B^0 \to \mu^+ \mu^-$ and $B^0 \to e^\pm \mu^\mp$ respectively where the main contribution is from m_{ES} and ΔE.

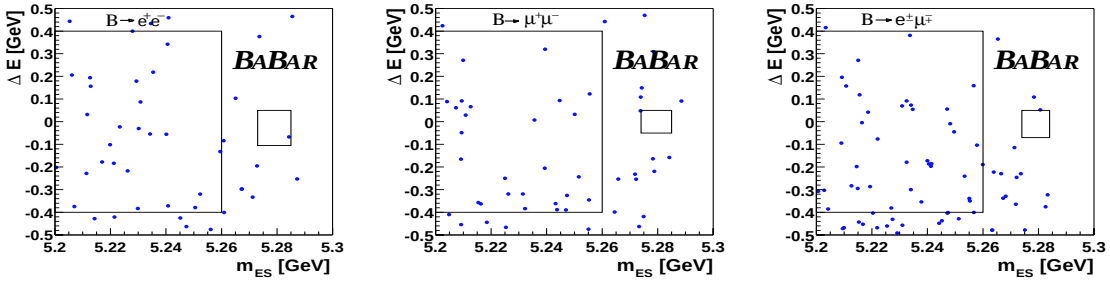

Figure 4: Unblinded ($m_{ES}, \Delta E$) distributions with 25, 26 and 37 events in the GSB for $B^0 \to e^+ e^-$,$B^0 \to \mu^+ \mu^-$ and $B^0 \to e^\pm \mu^\mp$ respectively.

After unblinding, we observed 1 event in the signal box for $B^0 \to e^+ e^-$ and none for the rest of the channels are summarized in table 1. The unblinded ($m_{ES}, \Delta E$) distributions for the three channels are shown in figs [4]. The observation are compatible with the expected background. We do not perform background subtraction for the determination of the branching fraction (upper limit).

The upper limits on the branching ratios for $B^0 \to l^+ l^-$ obtained at the 90% confidence level are summarized in table 1.

Channel	N_{exp}	N_{obs}	N_{BG}	ε[%]	UL (90% CL)
$B^0 \to e^+e^-$	1×10^{-8}	1	0.60 ± 0.24	$19.3 \pm 0.40_{stat} \pm 1.60_{syst}$	3.3×10^{-7}
$B^0 \to \mu^+\mu^-$	4×10^{-3}	0	0.49 ± 0.19	$18.8 \pm 0.28_{stat} \pm 2.00_{syst}$	2.0×10^{-7}
$B^0 \to e^\pm\mu^\mp$	—	0	0.51 ± 0.17	$18.3 \pm 0.38_{stat} \pm 1.50_{syst}$	2.1×10^{-7}

Table 1: Summary of analysis. N_{exp} is the number of expected signal events assuming a branching fraction of 10^{-15}. N_{obs} is the number of observed events in the signal box. N_{BG} is the expected number of background events in the signal box.

4 Results

A summary of the BaBar preliminary results for the rare leptonic B decays are given in table 2 in comparison with CLEO and Belle results.

Mode	CLEO	Belle	Babar
$\mathcal{B}(B^- \to K^-\nu\overline{\nu})$	2.4×10^{-4}	-	9.4×10^{-5}
$\mathcal{B}(B^0 \to e^+e^-)$	8.3×10^{-7}	6.3×10^{-7}	3.3×10^{-7}
$\mathcal{B}(B^0 \to \mu^+\mu^-)$	6.1×10^{-7}	2.8×10^{-7}	2.0×10^{-7}
$\mathcal{B}(B^0 \to e^\pm\mu^\mp)$	15.0×10^{-7}	9.4×10^{-7}	2.1×10^{-7}
Luminosity	$9.1\,\text{fb}^{-1}$	$21.3\,\text{fb}^{-1}$	$54.4\,\text{fb}^{-1}$

Table 2: Summary of BaBar, CLEO and Belle results for rare leptonic B decay.

References

[1] T. E. Browder *et al.* [CLEO Collaboration], Phys. Rev. Lett. **86**, 2950 (2001).

[2] Y. Grossman, Z. Ligeti and E. Nardi, Nucl. Phys. **B465**, 369-398 (1996); hep-ph/9510378.

[3] K. Leroux and D. London, Phys. Lett. **B526**, 97-103, (2002); hep-ph/0111246.

[4] G. Buchalla, G. Hiller and G. Isidori, Phys. Rev. D **63**, 014015 (2001); hep-ph/0006136.

[5] P. Colangelo *et al.* Phys. Lett. **B395**, 339-344, (1997); hep-ph/9610297.

[6] CLEO Collaboration, T. Bergfeld *et al.*, Phys. Rev. D **62**, 0991102(R) (2000)

[7] BELLE Collaboration, K. Abe *et al.*, BELLE-CONF-0127 (2001)

[8] H. E. Logan, U. Nierste. Nucl.Phys. **B586**, 39-55 (2000); hep-ph/0004139.

[9] M. Gronau and D. London, Phys. Rev. D **55**, 2845 (1997); hep-ph/9608430.

[10] K.S. Babu, Christopher Kolda. Phys. Rev. Lett. **84**, 228-231 (2000); hep-ph/9909476. C. Bobeth, T. Ewerth, F. Kruger and J. Urban, Phys. Rev. D **64** 074014 (2001); hep-ph/0204225.

Three-body charmless $B \to Khh$ decays at Belle

Alexei Garmash (representing the Belle Collaboration)
High Energy Accelerator Research Organization (KEK)
1-1 Oho, Tsukuba, JAPAN

Study of three-body B decays can significantly broaden the understanding of B meson decay mechanisms and provide additional possibilities for CP violation searches. The decays of B mesons to charmless three-body Khh final states can be described by a $b \to u$ tree-level spectator diagram and a $b \to s(d)g$ one-loop penguin diagram. (Although $b \to u$ W-exchange, annihilation, or vertical W loop diagrams can also contribute to these final states, they are expected to be smaller and we neglect them for simplicity.) Three-body decays of B mesons to final states with odd numbers of kaons (s-quarks) are expected to proceed dominantly via the $b \to sg$ penguin transition since the $b \to u$ contribution in these cases has an additional CKM suppression. In contrast, decays with two kaons in final state proceed via $b \to u$ tree transition (with possible contribution from $b \to dg$ penguin), and have no contribution from $b \to sg$ penguin. From this simple consideration we can naively expect that the $K\pi\pi$ and KKK final states have the largest signal among other three-body Khh final states. The observation of $K^{+(0)}\pi^+\pi^-$ and $K^{+(0)}K^+K^-$ final states has been reported recently by the Belle Collaboration [1, 2]. Here, we report the results of a study of B mesons decays to three-body $K\pi\pi$, $KK\pi$, and KKK final states, where no prior assumptions are made about intermediate hadronic resonances. The inclusion of charge conjugate states is implicit throughout this report.

The data sample used for this analysis was collected with the Belle detector [3] operating at the KEKB asymmetric energy e^+e^- collider. It consists of 43 fb^{-1} taken at the $\Upsilon(4S)$ resonance, corresponding to 45.3×10^6 produced $B\overline{B}$ pairs.

Charged tracks are selected with a set of track quality requirements based on the average hit residual and on the distances of closest approach to the interaction point. We also require that the transverse track momenta be greater than 0.1 GeV/c to reduce the low momentum combinatoric background. Charged kaons and pions are identified basing on dE/dx measurements by the central drift chamber, information from threshold Čerenkov counters and time-of-flight scintillation counters. Tracks that identified as protons or electrons are rejected. Neutral kaons are reconstructed via their decay chain $K^0(\overline{K}^0) \to K_S \to \pi^+\pi^-$. The invariant mass of the two pions is required to satisfy $|M(\pi^+\pi^-) - M_{K^0}| < 10$ MeV/c^2 and the displacement of the $\pi^+\pi^-$ vertex from the interaction point in the transverse (r-ϕ) plane is required to be greater than 0.1 cm and less than 20 cm. The K_S flight direction and combined pion pair momentum direction in the r-ϕ plane must agree within 0.2 radians. Photons are

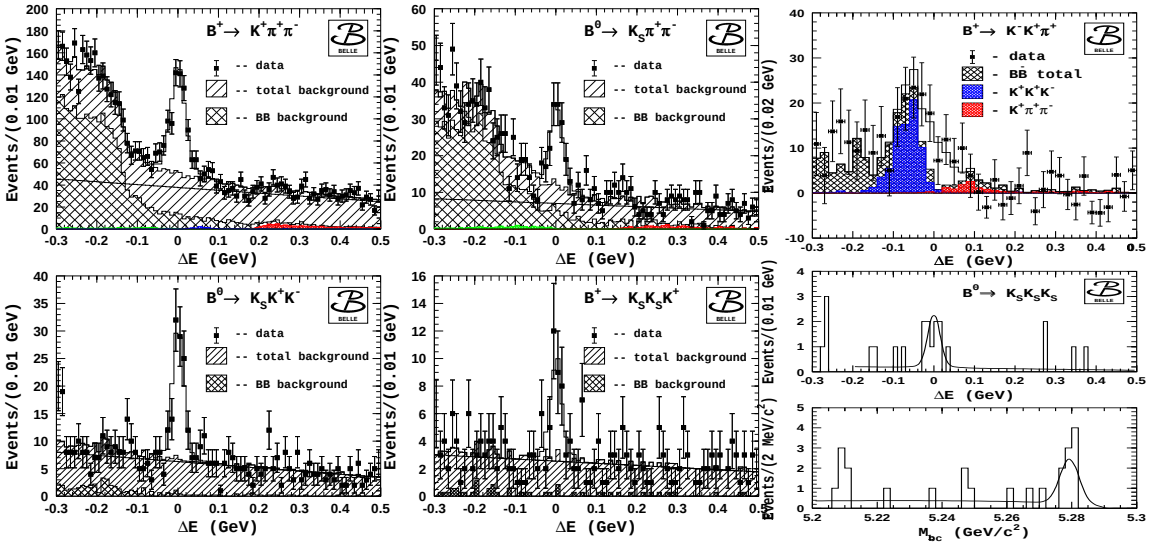

Figure 1: The ΔE distributions for three-body final states.

identified as isolated clusters in the electromagnetic calorimeter with energy greater than 50 MeV. Pairs of photons with an invariant mass within 15 MeV of the π^0 nominal mass are considered as π^0 candidates. The reconstructed π^0 momentum is required to be more than 0.2 GeV/c.

We reconstruct B mesons in three-body $K\pi\pi$, $KK\pi$, and KKK final states with charged or neutral (not more than one) pions and charged or neutral kaons. The candidate events are identified by their center of mass (CM) energy difference, $\Delta E = (\sum_i E_i) - E_{\rm b}$, and the beam constrained mass, $M_{\rm bc} = \sqrt{E_{\rm b}^2 - (\sum_i \vec{p}_i)^2}$, where $E_{\rm b} = \sqrt{s}/2$ is the beam energy in the CM frame, and $\vec{p}_i$ and E_i are the CM three-momenta and energies of the candidate B meson decay products. We select events with $M_{\rm bc} > 5.20$ GeV/c^2 and $-0.30 < \Delta E < 0.50$ GeV, and define a *signal* region of $|M_{\rm bc} - M_B| < 9$ MeV/c^2 and $|\Delta E| < 0.04$ GeV and two ΔE *sideband* regions defined as -0.08 GeV $< \Delta E < -0.05$ GeV and 0.05 GeV $< \Delta E < 0.15$ GeV.

To suppress the large combinatorial background which is dominated by two-jet-like $e^+e^- \to q\overline{q}$ continuum events, variables that characterize the event topology are used. The procedure is described in detail in Ref. [1]. The potentially dangerous sources of background from other B decays were studied with a large sample of $B\overline{B}$ Monte Carlo (MC) events. As a result of this study we found that $B \to Dh$, where h stands for a charged pion or kaon, produce the dominant background to the most of the three-body final states. To suppress this background we introduce D veto cut: we reject candidates if any two-particle invariant mass is consistent with a $D \to K\pi$ hypothesis, independently of the PID information. In the analysis of $K^{+(0)}\pi^+\pi^-$ final states we also apply a charmonium veto: candidates, with a two-pion invariant mass

Mode	Eff., %	Yield, events	$\mathcal{B}, 10^{-6}$ ($43\,\mathrm{fb}^{-1}$)	$\mathcal{B}, 10^{-6}$ ($29\,\mathrm{fb}^{-1}$), Ref.[1]
$K^+\pi^-\pi^+$	21.1	463 ± 32	59.3 ± 4.1	$55.6 \pm 5.8 \pm 7.7$
$K^0\pi^-\pi^+$	5.23	94.7 ± 14.4	41.7 ± 7.2	$53.2 \pm 11.3 \pm 9.7$
$K^+\pi^-\pi^0$	11.6	$173^{+30.5}_{-29.6}$	–	$47.1 \pm 8.2 \pm 6.3$
$K^+K^+K^-$	22.2	289 ± 20	35.8 ± 2.5	$35.3 \pm 3.7 \pm 4.3$
$K^0K^+K^-$	7.10	88.8 ± 11.8	32.3 ± 4.8	$34.8 \pm 6.7 \pm 6.5$
$K_SK_SK^+$	5.76	27.5 ± 6.7	13.1 ± 3.2	–
$K_SK_SK_S$	3.86	$8.2^{+3.5}_{-2.9}$	$5.5^{+2.3}_{-1.9}$	–
$K^+K^-\pi^+$	13.8	49 ± 15	$9.1 \pm 2.8 (< 14)$	< 12
$K^+K^+\pi^-$	14.2	-4.7 ± 9	< 2.0	< 3.2
$K^-\pi^+\pi^+$	17.0	14 ± 12	< 5.4	< 7.0
$K^0K^\pm\pi^\mp$	4.53	1 ± 11	< 9.2	< 13.4
$K_SK_S\pi^+$	5.31	-6.4 ± 8.1	< 3.3	–

Table 1: Summary table of three-body results.

consistent with $J/\psi(\psi(2S))\to\mu^+\mu^-$ are rejected.

The ΔE distributions for some of the three-body final states are shown in Fig. 1, where the points with errors represent the experimental data, and histograms show the expected background distributions. To extract the signal yield in the $K\pi\pi$ and KKK final states, we fit the ΔE distributions to the sum of signal and background components. The signal shape is parameterized by a double Gaussian function with the same mean. There are two sources of background: $q\overline{q}$ continuum background that is approximated by the linear function and $B\overline{B}$ background which is final state dependent. The shape of the $B\overline{B}$ background for each particular three-body final state was determined using a large set ($\sim$3.5 times the data set) of MC events. The $q\overline{q}$ and $B\overline{B}$ component are also shown in Fig. 1. The $B\overline{B}$ is found to be substantial in $K\pi\pi$ final states, while it gives very small contribution in three-kaon final states. For other final states, a different technique is used for signal yield extraction. We subdivide the ΔE region into 20 MeV bins and determine the signal yield in each bin from the fit to the corresponding $M_{\rm bc}$ spectrum. The signal yield from the $M_{\rm bc}$ fit is then plotted as a function of ΔE. The results for the $K^+K^-\pi^+$ final state is shown in Fig. 1 as points with errors, where the $B\overline{B}$ contribution is also shown. The more detailed description can be found in Ref. [1].

The results of the fit are summarized in Table 1. Statistically significant signals are observed in $K^{+(0)}\pi^+\pi^-$, $K^+\pi^-\pi^0$ and all three-kaon final states. The resulting branching fractions for the three-body final states are presented in Table 1, where the results of Ref. [1] are also included for comparison.

To examine possible intermediate quasi-two-body states, we analyze two-particle mass spectra. The $K^+\pi^-$ and $\pi^+\pi^-$ invariant mass spectra for the $B^+\to K^+\pi^+\pi^-$

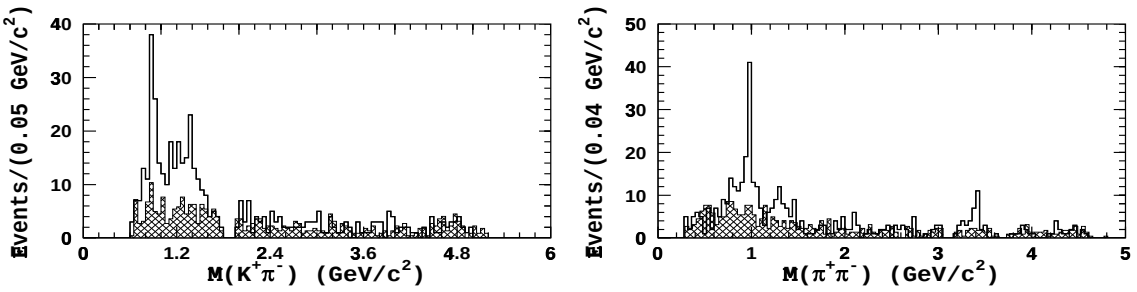

Figure 2: The $K^+\pi^-$ and $\pi^+\pi^-$ invariant mass spectra for the $K^+\pi^+\pi^-$ final state.

signal are shown in Fig. 2. To suppress the feed-across between the $\pi^+\pi^-$ and $K^+\pi^-$ states, we require the $K^+\pi^-$ ($\pi^+\pi^-$) invariant mass to be larger than 2.0 (1.5) GeV/c^2 when making the $\pi^+\pi^-$ ($K^+\pi^-$) projection. The hatched histograms shown in Fig. 2 are the corresponding two-particle invariant mass spectra for the background events in the ΔE sidebands with proper normalization. The Dalitz plot analysis procedure is described in Ref. [1] in detail.

In conclusion, the results of the branching ratio measurement for the B decays to three-body $K\pi\pi$, $KK\pi$, and KKK final states are presented, where the $K_SK_SK^+$ and $K_SK_SK_S$ final states are observed for the first time. We also report 3σ evidence for the signal in $K^+K^-\pi^-$ final state. The analysis of quasi-two-body final states reveals large signals of $B^+\to f_0(980)K^+$, $B^+\to K^*(892)^0\pi^+$ in $K^+\pi^+\pi^-$ final state and $B^+\to\phi K^+$ in $K^+K^+K^-$ final state. The measured branching fraction product for the $f_0(980)K^+$ final state is $\mathcal{B}(B^+\to f_0(980)K^+)\times\mathcal{B}(f_0(980)\to\pi^+\pi^-) = (9.6^{+2.5+1.5+3.4}_{-2.3-1.5-0.8})\times10^{-6}$. This is the first observation of a B meson decay to a charmless scalar-pseudoscalar final state. We find that effects of interference between different quasi-two-body intermediate states can have significant influence on the observed two-particle mass spectra and a full amplitude analysis of three-body B meson decays is required for a more complete understanding. This will be possible with increased statistics.

We wish to thank the KEKB accelerator group for the excellent operation of the KEKB accelerator.

References

[1] A. Garmash *et al.* (Belle Collaboration), Phys. Rev. D **65**, 092005 (2002).

[2] T.J. Gershon *et al.* (Belle Collaboration), hep-ex/0205033;
H.C. Huang *et al.* (Belle Collaboration), hep-ex/0205062.

[3] A. Abashian *et al.* (Belle Collaboration), Nucl. Instr. Meth. A **479**, 117 (2002).

$B^-\to\omega K^-/\pi^-$ and Time-dependent CPV in $B^0\to\eta' K_S$ at Belle

Kai-Feng Chen
Department of Physics
National Taiwan University
Taipei 106, Taiwan, R.O.C.

1 Introduction

Charmless hadronic B decays are interesting for testing our understanding of heavy quark physics and search for CP violation. We report the measurements of charmless $B^-\to\omega\pi^-$ and $B^-\to\omega K^-$ decays. The $B^-\to\omega K^-$ mode was first reported by CLEO collaboration in 1998 [1], but superseded by nonobseravtion with a larger data set [2]. This result is supported by BaBar in 2001 [3]. The $B^-\to\omega\pi^-$ channel has also been reported by CLEO and BaBar collaborations. However, we find a significant signal in the $B^-\to\omega K^-$ mode. The data used in this analysis were based on an integrated luminosity of 29.4 fb^{-1} data sample on the $\Upsilon(4S)$ resonance taking by the Belle detector at the KEK B-factory.

Kobayashi and Maskawa (KM) showed CP violation could be accommodated in the Standard Model [4] (SM) in 1973. In the model, the CP violation arises from a complex phase in the weak interaction quark mixing matrix [5]. Belle and BaBar collaborations have measured the CP-violating parameter sin2ϕ_1 from $B^0\to c\bar{c}K^0$ decays. The $B^0\to\eta' K_S$ decay is also sensitive to the parameter sin2ϕ_1 and provides important tests of the KM model. Within the framework of SM, the charmless decay $B^0\to\eta' K_S$ are dominated by $b\to s$ penguin diagrams and a small color-suppressed $b\to u$ tree contribution. However, since the branching fractions of $B\to\eta' K$ decays are larger than current theoretical prediction, there might be an additional new phase beyond SM.

The time-dependent CP asymmetry is given by

$$\begin{aligned} A_{CP}(\Delta t) &= \frac{\Gamma(\overline{B^0}\to\eta' K_S)-\Gamma(B^0\to\eta' K_S)}{\Gamma(\overline{B^0}\to\eta' K_S)+\Gamma(B^0\to\eta' K_S)} \\ &= A_{\eta' K_S}\cos(\Delta m\Delta t)+S_{\eta' K_S}\sin(\Delta m\Delta t), \end{aligned}$$

where the CP-violating parameters $A_{\eta' K_S}$ and $S_{\eta' K_S}$ are expressed as

$$A_{\eta' K_S} = \frac{|\lambda|^2 - 1}{|\lambda|^2 + 1}, \quad S_{\eta' K_S} = \frac{2\mathrm{Im}\lambda}{|\lambda|^2 + 1}, \tag{1}$$

where λ is a complex parameter that depends on both $B^0 - \overline{B^0}$ mixing and on the decay amplitude for $B^0(\overline{B^0}) \to \eta' K_S$. $|\lambda|$ is close to 1 in the SM with a good approximation. The measurement of CP-violating parameters in the decay $B \to \eta' K$ is based on a 41.8 fb^{-1} data sample.

The KEKB asymmetric e^+e^- (3.5 GeV e^+ and 8 GeV e^-) collider operates on the $\Upsilon(4S)$ resonance. The $\Upsilon(4S)$ is produced with a Lorentz boost of $\beta\gamma = 0.425$ along the beam direction (z).

The Belle detector [6] is a general-purpose detector operating under 1.5 T magnetic field. It consists of a three layer silicon vertex detector (SVD), a central drift chamber (CDC) with 50 layers. Charged hadrons are distinguished by combining the information from an array of aerogel threshold Cerenkov counters (ACC), a time-of-flight scintillation counters (TOF), and the dE/dx measurements from CDC. Photons are detected in an array of 8736 CsI(Tl) crystals (ECL) located inside the magnet.The flux-return outside of the coil is instrumented for detection of muon and K_L (KLM).

2 Observation of $B^\pm \to \omega K^\pm$ Decay

Charged tracks are required to be inconsistent with electrons or muons, and are identified as kaons or pions according to a K/π likelihood ratio (KID), $\mathcal{L}_K/(\mathcal{L}_K + \mathcal{L}_\pi)$, where the $\mathcal{L}_{K(\pi)}$ is given by

$$\mathcal{L}_{K(\pi)} = \mathcal{L}^{\mathrm{ACC}}_{K(\pi)} \times \mathcal{L}^{\mathrm{TOF}}_{K(\pi)} \times \mathcal{L}^{dE/dx}_{K(\pi)}, \tag{2}$$

where $\mathcal{L}^{\mathrm{ACC}}_{K(\pi)}$, $\mathcal{L}^{\mathrm{TOF}}_{K(\pi)}$, and $\mathcal{L}^{dE/dx}_{K(\pi)}$ are the likelihood for ACC, TOF, and dE/dx from CDC measurement respectively. Neutral pions are reconstructed from pairs of photons, each consisting of energy greater than 50 MeV, with the $m_{\gamma\gamma}$ within a $\pm 3\sigma$ (σ = 5.4 MeV/c^2) mass window around the π^0 mass. A mass constrained fit is applied on the π^0 candidates. ω meson candidates are obtained by combining $\pi^+\pi^-\pi^0$ with invariant mass within ± 30 MeV/c^2 of the nominal ω mass. The momentum of candidate π^0's under ω is required to be greater than 350 MeV/c. This cut gives 84% efficiency, but removes 60% combinatorial background.

A charged kaon or a pion track is selected to combine with an ω candidate to form a $B^\pm$ candidate. B mesons are identified by two kinematic variables, the beam-constrained mass $M_{bc} = \sqrt{(E^{\mathrm{CM}}_{\mathrm{beam}})^2 - (p^{\mathrm{CM}}_B)^2}$ and the energy difference $\Delta E = E^{\mathrm{CM}}_B - E^{\mathrm{CM}}_{\mathrm{beam}}$, where the $E^{\mathrm{CM}}_{\mathrm{beam}} = \sqrt{s}/2 = 5.29$ GeV is the CM beam energy. The resolutions are 3 MeV/c^2 for M_{bc} and 23 MeV for ΔE from Monte Carlo simulations.

Continuum $e^+e^- \to q\overline{q}$ process is the dominant background in this analysis. The $q\overline{q}$ consists of light quark (u, d, s, or c) pairs. The continuum events which are jet-like

have to be suppressed compared to the spherical $B\overline{B}$ events. A Fisher discriminant [7] is defined containing modified Fox-Wolfram moments [8]. We use a likelihood ratio method combining the Fisher discriminant, B-meson direction, and the helicity angle which is defined as the angle between the B flight direction and the vector perpendicular to the ω decay plane in the ω rest frame. The probability density functions (PDFs) are determined by Monte Carlo simulation. A signal (background) likelihood $\mathcal{L}_s$ ($\mathcal{L}_b$) is calculated by the PDFs for each event. The likelihood ratio is formed by $LR = \mathcal{L}_s/(\mathcal{L}_s + \mathcal{L}_b)$, and a cut $LR > 0.85$ is made to reject 95% continuum background but keeping 50% signal events.

Background from charmed and charmless B decays such as $B \to \omega K^*$, $B \to \omega\rho$, and non-resonant $B^- \to K^-\pi^+\pi^-\pi^0$ are studied by Monte Carlo simulation up to 20 times larger than current data amount. These backgrounds are negligible in the M_{bc}-ΔE signal region ($M_{bc} > 5.27$ GeV/c^2 and $|\Delta E| < 0.1$ GeV).

The signal yields are extracted by an unbinned maximum likelihood fit on M_{bc} and ΔE together. The signal PDF for M_{bc} is a Gaussian, and for ΔE [9], parameters are determined by MC simulation and calibrated by the $B^- \to D^0\pi^-$ decay, where D^0 decays to $K^-\pi^+\pi^0$. Background PDFs are threshold functions [10] determined from MC simulation. The yields are summarized in Table 1. The M_{bc} and ΔE projections of candidate events are shown in Figure 1.

The systematic uncertainties associated with the fit are determined by varying the parameters in the fitting functions by $\pm 1\sigma$ of their nominal values. The systematic error of ω detection efficiency is determined from detailed studies of charged particle tracking, π^0 detection, and particle identification. A 5% systematic error is assigned to the continuum suppression cut from $B^- \to D^{*0}\pi^-$ data and MC study. The combined uncertainty of the efficiency is 10.1%.

We make the consistency check of our analysis without KID requirement. Figure 2 shows the ΔE distribution and scatter plot of KID versus ΔE. The ωK^- signals are peaking at -51 MeV, where the $\omega\pi^-$ signals are placed at zero. The ΔE distributions confirm the ωK^- signals are larger than $\omega\pi^-$. We also examine the ω properties to confirm the ωK^- signal candidates. The ω invariant mass spectrum and the cosine of the helicity angle of the B candidate events are also shown in Figure 2.

We also measure the asymmetry in $B^\pm \to \omega K^\pm$ decays to search for direct CP violation. The asymmetry is defined as

$$A_{CP} = \frac{N(\omega K^-) - N(\omega K^+)}{N(\omega K^-) + N(\omega K^+)}. \tag{3}$$

The asymmetry is measured to be $-0.21 \pm 0.28 \pm 0.03$. The 90% confidence level interval is given by $-0.70 < A_{CP} < 0.28$.

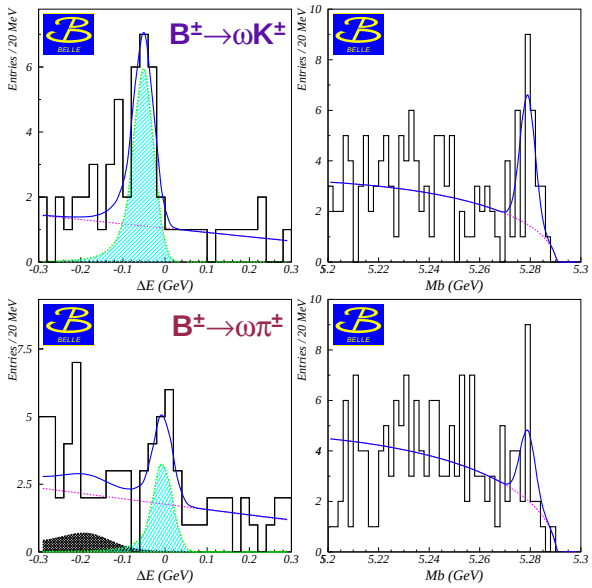

Figure 1: The M_{bc} and ΔE projection plots of $B^-\to\omega K^-$ and $B^-\to\omega\pi^-$ modes.

3 Search of Time-dependent CP Asymmetry in $B\to\eta' K$ Decay

The $B\to\eta' K$ event selection is described in the previous published branching ratio measurement [11]. The CP fit analysis is done nearly the same as the $B\to\pi^+\pi^-$ case.

The $K_S\to\pi^+\pi^-$ candidates are reconstructed with a pair of charged tracks with pion mass assumption. A ± 16 MeV/c^2 to the nominal K_S mass window cut is applied. Two decay channels are used for η' reconstruction: $\eta'\to\eta\pi^+\pi^-$ with the η decays to two photons and $\eta'\to\rho^0\gamma$. Candidate photons from η (η') are required to have a energy greater than 50 MeV (100 MeV). The B meson candidates are formed by combining η' and a K_S ($K^\pm$). The kinematic variables, ΔE and M_{bc} are used to identify B signal candidates.

The dominant background to $B\to\eta' K$ modes are $e^+e^-\to q\overline{q}$ continuum events, just like the $B\to\omega h$ modes. A loose cut of $|\cos\theta_T| < 0.9$ [11] is used rejecting 50% of the

	Signal Yield	Σ	$\epsilon(\%)$	BF $(\times 10^{-6})$	UL $(\times 10^{-6})$
ωK^-	$19.7^{+5.8+0.7}_{-4.7-0.5}$	6.4σ	6.3	$9.9^{+2.7}_{-2.4}\pm 1.0$	-
$\omega\pi^-$	$10.6^{+4.3+0.4}_{-4.5-0.6}$	3.3σ	7.7	$4.3^{+2.0}_{-1.8}\pm 0.5$	< 8.2

Table 1: The results of $B^-\to\omega K^-$ and $B^-\to\omega\pi^-$ decays.

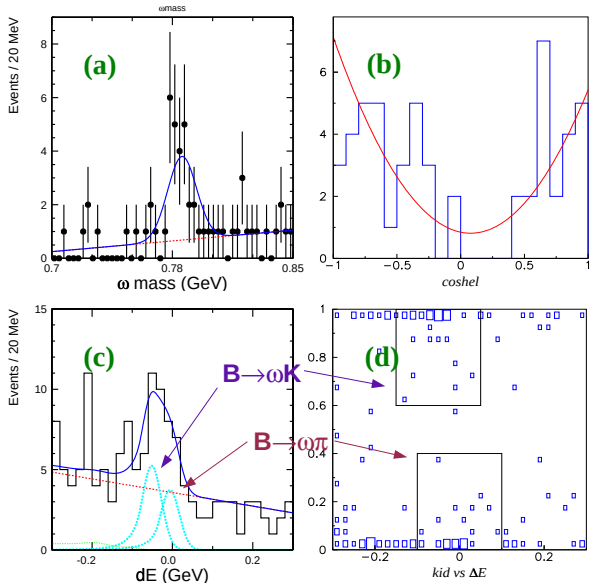

Figure 2: (a) The $\pi^+\pi^-\pi^0$ invariant mass spectrum. (b) The cosine of the helicity angle of $B\to\omega h$ modes. (c) The ΔE distribution without KID information. (d) The Belle KID versus ΔE spectrum.

background but retaining 90% of signal events.

The $\eta'\to\eta\pi^+\pi^-$ mode is clean enough after the $\cos\theta_T$ selection, but the $\eta'\to\rho^0\gamma$ is not as clean. We introduce a likelihood ratio method which is very close to the $B\to\omega h$ analysis. The only difference is the helicity angle of $\eta'\to\rho^0\gamma$ mode is defined with ρ^0 in η' rest frame. Finally, a $LR > 0.5$ is applied to reject 81% of the background and keep 80% of the signal. Other generic $B\overline{B}$ backgrounds mainly come from the decay of B to charm. They contribute 8.1% for the $\eta'(\to\rho^0\gamma)K_S$ mode but negligible in the $\eta'\to\eta\pi^+\pi^-$ modes. The projection plots for ΔE and M_{bc} of $\eta' K^\pm$ and $\eta' K_S$ decays are shown in Figure 3.

Leptons, charged pions, Λ's and kaons are not associated with the reconstructed $B^0\to\eta' K_S$ decay are used to identify the flavor of the accompanying B meson. The algorithm is the same as the $\sin 2\phi_1$ measurement. The vertex positions for $\eta' K_S$ and $B_{\rm tag}$ decays are reconstructed using tracks with at least two SVD hits in z axis and tracks from K_S candidates are removed.

The proper-time interval resolution for the signal, $R_{\rm sig}(\Delta t)$, is obtained by convolving a sum of two Gaussians. A main component due to the SVD vertex resolution and charmed meson lifetimes, with a tail component caused by poorly reconstructed tracks. The mean and width of the Gaussians are calculated event-by-event from the vertex fit error and the χ^2 values. The background resolutions, $R_{q\overline{q}}(\Delta t)$ and $R_{B\overline{B}}(\Delta t)$, have the same form but the parameters are determined from sideband

events and generic B Monte Carlo. We obtain the lifetimes of charged and neutral B mesons with the same procedure, and the results agree with the world average values.

The CP violation parameters, $A_{\eta' K_S}$ and $S_{\eta' K_S}$, are determined by performing an unbinned maximum-likelihood fit to the measured Δt distributions. The expected PDF for signal,

$$P_{\rm sig}(\Delta t) = \frac{e^{-|\Delta t|/\tau_{B^0}}}{4\tau_{B^0}}\{1 + q \cdot (1 - 2w_l) \cdot A_{CP}(\Delta t)\}, \tag{4}$$

is used in the fit. The τ_{B^0} and Δm_d are fixed to their world average values [12]. The PDF used for the background distribution is

$$P_{\rm bkg}(\Delta t) = \{f_\tau \cdot \frac{e^{-|\Delta t|/\tau_{\rm bkg}}}{2\tau_{\rm bkg}} + (1 - f_\tau) \cdot \delta(\Delta t)\}/2, \tag{5}$$

where f_τ is the background fraction with an effective lifetime $\tau_{\rm bkg}$. Parameters for continuum background are determined from sideband data. The PDF shape for $B\overline{B}$ background is from Monate Carlo simulation.

The likelihood value for each event are defined as:

$$P_i = \int f^l_{\rm sig} P_{\rm sig}(\Delta t') R_{\rm sig}(\Delta t_i - \Delta t') + f^l_{q\overline{q}} P_{q\overline{q}}(\Delta t') R_{q\overline{q}}(\Delta t_i - \Delta t')$$

$$+ f^l_{B\overline{B}} P_{B\overline{B}}(\Delta t') R_{B\overline{B}}(\Delta t_i - \Delta t') d\Delta t', \tag{6}$$

where the f^l_k(subscript k = sig, $q\overline{q}$, or $B\overline{B}$, and $l = 6$) are the weighted probability functions determined on an event-by-event basis as a function of ΔE and M_{bc}.

In the fit, $A_{\eta' K_S}$ and $S_{\eta' K_S}$ are free parameters that are determined by maximizing the likelihood function $\mathcal{L} = \Pi P_i$ over all $B^0 \to \eta' K_S$ candidates. The CP asymmetry parameters obtained from a total 73 $\eta' K_S$ signal events after subtracting the background are

$$\begin{aligned} S_{\eta' K_S} &= 0.28 \pm 0.55\ ({\rm stat})^{+0.07}_{-0.08}\ ({\rm syst}), \\ A_{\eta' K_S} &= 0.13 \pm 0.32\ ({\rm stat})^{+0.09}_{-0.06}\ ({\rm syst}). \end{aligned}$$

Figure 4 shows the Δt distributions for B^0 ($\overline{B^0}$) tagged events, and raw asymmetry of the $\eta' K_S$ sample.

We determine the systematic error due to fitting parameters (physics parameters, wrong tag fractions, signal and background PDFs) by repeating the fit after varying the parameters by $\pm 1\sigma$ determined from the data or MC.

A number of checks are also performed. The $\eta' K^\pm$ sample is analyzed in the same way as $\eta' K_S$. A fit to 230 candidate events give $S = 0.11 \pm 0.29$ and $A = -0.27 \pm 0.17$ consistent with no asymmetry. The other check by floating the $B^\pm$ (B^0) lifetime

in the $B^{\pm}$ (B^0) sample is performed. The $B^{\pm}$ (B^0) lifetime determined with $\eta' K^{\pm}$ ($\eta' K_S$) samples is $1.54^{+0.14}_{-0.13}$ ($1.58^{+0.31}_{-0.26}$) ps, consistent with world average value [12].

In summary, we measure the time-dependent CP asymmetry parameters in $B^0(\overline{B^0}) \to \eta' K_S$ decay based on 41.8 fb^{-1} data sample collected with the Belle detector. The results, $S_{\eta' K_S} = 0.28 \pm 0.55\ (\mathrm{stat})^{+0.07}_{-0.08}\ (\mathrm{syst})$ and $A_{\eta' K_S} = 0.13 \pm 0.32\ (\mathrm{stat})^{+0.09}_{-0.06}\ (\mathrm{syst})$, are the first measurements of CP asymmetry parameters related to ϕ_1 with a charmless B^0 decay. With more data, the uncertainty in $S_{\eta' K_S}$ can be reduced and impose tighter constraints on the phases from physics beyond the Standard Model.

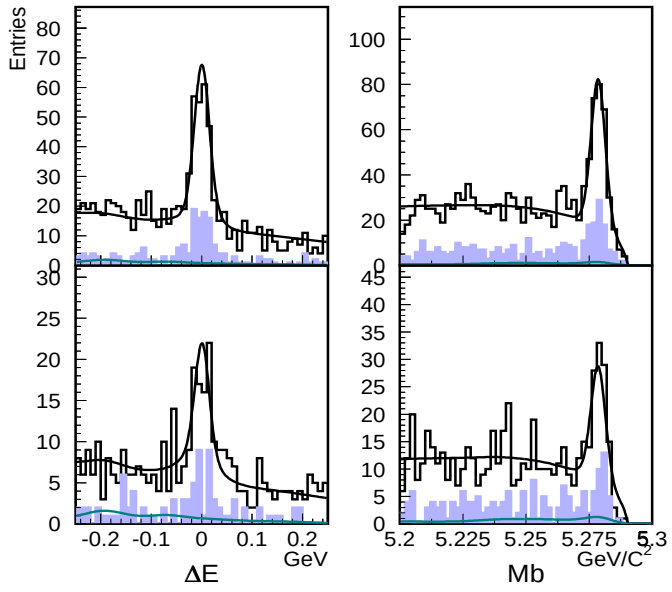

Figure 3: The M_{bc} and ΔE projection plots of $B^{\pm} \to \eta' K^{\pm}$ and $B^0 \to \eta' K_S$ modes.

References

[1] CLEO Collaboration, T. Bergfeld *et al.*, Phys. Rev. Lett. **81**, 272 (1998).

[2] CLEO Collaboration, C.P. Jessop *et al.*, Phys. Rev. Lett. **85**, 2881 (2000).

[3] BaBar Collaboration, B. Aubert *et al.*, Phys. Rev. Lett. **87**, 221802 (2001).

[4] D. London and A. Soni, Phys. Lett. **B 407** (1997) 61.

[5] M. Kobayashi and T. Maskawa, Prog. Theor. Phys. **49** (1973) 652.

[6] Belle Collaboration, A. Abashian *et al.*, Nucl. Inst. Meth. **A 479** (2002) 117.

[7] R. A. Fisher, Annals of Eugenics, **7**, 179 (1936).

[8] Belle Collaboration, K. Abe *et al.*, Phys. Rev. Lett. **87**, 101801 (2001).

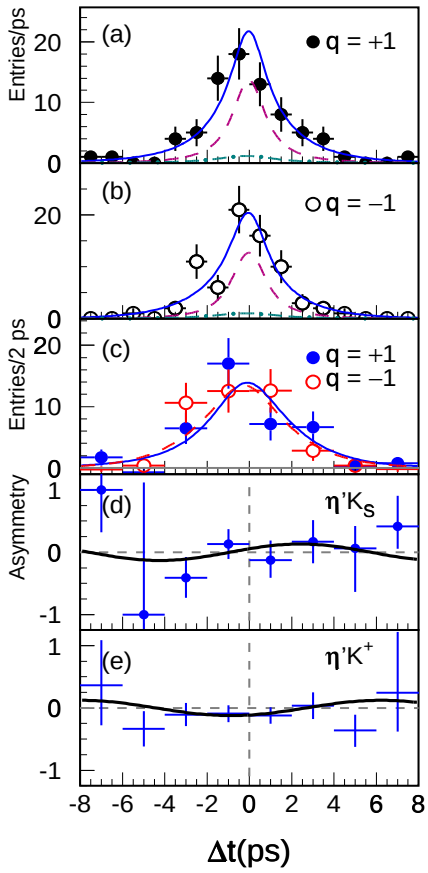

Figure 4: (a) The Δt distribution for B^0 tagged events. (b) The Δt distribution for $\overline{B^0}$ tagged events. (c) B^0 and $\overline{B^0}$ tagged events overlaid after background subtraction. (d) The asymmetries versus Δt plot. The solid curve is obtained from CP fit. (e) The asymmetries versus Δt plot for $\eta' K^{\pm}$.

[9] J. E. Gaiser *et al.*, Phys. Lett. **D 34** , 711 (1986).

[10] H. Albrecht *et al.*, Phys. Lett. **B 241** , 278 (1990).

[11] Belle Collaboration, K. Abe *et al.*, Phys. Lett. **B 517** (2001) 309.

[12] Particle Data Group, D. E. Groom *et al.*, Eur. Phys. J. **C 15** (2000) 1.

May 17, session 3.

Session Chair: H. Jawahery

Charm Physics I

Charm Lifetimes, $D^0 - \overline{D}^0$ Mixing and Double $c\bar{c}$ Continuum Production

Pavel Pakhlov
Institute of Theoretical and Experimental Physics
117259 Moscow, RUSSIA

1 Charm Lifetimes

The study of charm hadron lifetimes, which span one order of magnitude, is essential for understanding of strong interactions. Improved precision of the charm lifetimes measurements stimulates the development of theoretical models which are now able to explain quantatively the observed lifetime hierarchy.

The FOCUS Collaboration presents the most accurate measurement of the lifetime of D^0 and D^+ mesons using the samples of $\sim$140,000 $D^0 \to K^-\pi^+$, $\sim$68,000 $D^0 \to K^-\pi^+\pi^+\pi^-$, and $\sim$110,000 $D^+ \to K^-\pi^+\pi^+$ candidates. A lifetime fit is performed to the proper time distribution in the signal region. The proper time is extracted from the distance between the primary and secondary vertices. The vertexing algorithm is found to provide very uniform proper time acceptance. The measured lifetimes are $409.6 \pm 1.1 \pm 1.5$ fs for D^0 and $1039.4 \pm 4.3 \pm 7.0$ fs for D^+, where the first error is statistical and the second is systematic. The details of this analysis can be found in Ref. [1]. These results are in good agreement with the measurements of other experiments [2, 3] but surpass them in accuracy by a factor of $2-3$.

2 $D^0 - \overline{D}^0$ Mixing

In presence of $D^0 \leftrightarrow \overline{D}^0$ transitions the flavour eigenstates are different from the mass eigenstates, characterized by a mass splitting (Δm) and a width difference ($\Delta\Gamma$). Two different mechanisms which are responsible for $D^0 - \overline{D}^0$ mixing (quark box diagrams and long-distance hadronic interations) are suppressed by GIM mechanism and $SU(3)_{\rm FL}$ symmetry. The $D^0 - \overline{D^0}$ mixing parameters defined as $x = \Delta m/\Gamma$ and $y = \Delta\Gamma/2\Gamma$ are predicted to be smaller than 10^{-3} in the SM. However x can be significantly enhanced by non-SM processes while final state interactions and $SU(3)_{\rm FL}$-breaking can encance y to a level achievable by the current experimental sensitivity.

The FOCUS measurement [4] of y_{CP} (which is, in the CP-conserving limit, equal to y) of $(3.42 \pm 1.39 \pm 0.74)\%$ has aroused additional interest in $D^0 - \overline{D}^0$ mixing. More recent experimental measurements by the CLEO and Belle Collaborations [5, 3]

have not confirmed, though they have not completely refuted, the large FOCUS y_{CP} value. Recently the BaBar Collaboration has performed a new measurement of the parameter y_{CP} based on a data sample of $57.8\,\mathrm{fb}^{-1}$ collected with the BaBar detector, at the PEP-II asymmetric e^+e^- collider. D^0 candidates, reconstructed in $K\pi$, KK and $\pi\pi$ decay modes, are required to be produced in $D^{*+} \to D^0\pi^+$ decay. This provides samples of unsurpassed purity. Finally $158,000$ $D^0 \to K\pi$, $16,500$ $D^0 \to KK$, and $8,350$ $D^0 \to \pi\pi$ candidates with signal purities of about 99.5%, 97.1% and 92.4% respectively are selected within the D^0 signal region. The D^0 proper time is derived, in the plane transverse to the beam direction, from the flight length defined as the distance between the D^0 and D^{*+} vertices projected on the D^0 transverse momentum. An unbinned maximum likelihood fit is used to extract the lifetime for the three D^0 samples. The results of the fits are shown in Figure 1 superimposed on the proper time distributions for the three decay modes.

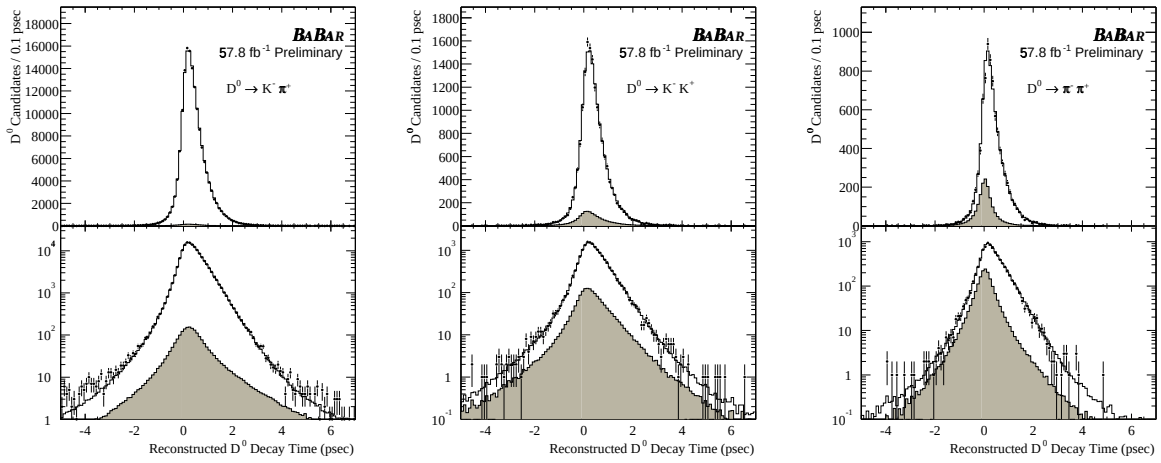

Figure 1: The open histogram represents the result of the unbinned maximum likelihood fit; the shaded one is the portion assigned to the background by the fit.

The measured values of y_{CP} for the KK and $\pi\pi$ modes are equal to $(1.5\pm1.3^{+0.6}_{-0.7})\%$ and $(1.0\pm1.7^{+1.2}_{-1.4})\%$ respectively. Their average of $y_{CP} = (1.4\pm1.0^{+0.6}_{-0.7})\%$ is consistent with zero but suggests a positive value not incompatible with the FOCUS result.

3 Double $c\bar{c}$ Continuum Production

Prompt charmonium production in e^+e^- annihilation provides an opportunity to study both perturbative and non-perturbative effects in QCD. The NRQCD [6, 7, 8, 9] model predicts that prompt J/ψ production at $\sqrt{s} \approx 10.6\,\mathrm{GeV}$ is dominated by $e^+e^- \to J/\psi\, gg$, with additional contributions from $J/\psi\, g$, $J/\psi\, c\bar{c}$ and other processes. Both BaBar and Belle Collaborations [10] presented cross-section measurements for

prompt J/ψ and $\psi(2S)$ production, and studies of their kinematic properties, which were compared to predictions of the models. However, these results do not constrain the contributions from particular mechanisms.

The Belle Collaboration presents the results of a search for $J/\psi\, c\bar{c}$ production, *i.e.* double $c\bar{c}$ production, where the additional $c\bar{c}$ pair fragments into either charmonium or charmed hadrons. The analysis is based on $46.2\,\mathrm{fb}^{-1}$ of data, collected at the $\Upsilon(4S)$ and nearby continuum with the Belle detector at the KEKB asymmetric energy storage rings. The details of event selection and J/ψ reconstruction can be found in Ref. [11].

Distributions of the mass of the system recoiling against the J/ψ candidate—the "recoil mass"—are shown in Fig. 2*a*, for both J/ψ signal and sideband regions. The recoil mass is defined as $M_{\mathrm{recoil}} = \sqrt{(E_{CMS} - E_{J/\psi})^2 - p^2_{J/\psi}}$. A clear threshold near $2\,m_c$ can be seen for the J/ψ signal region. The region $2\,m_c < M_{\mathrm{recoil}} < 2\,m_D$ is studied

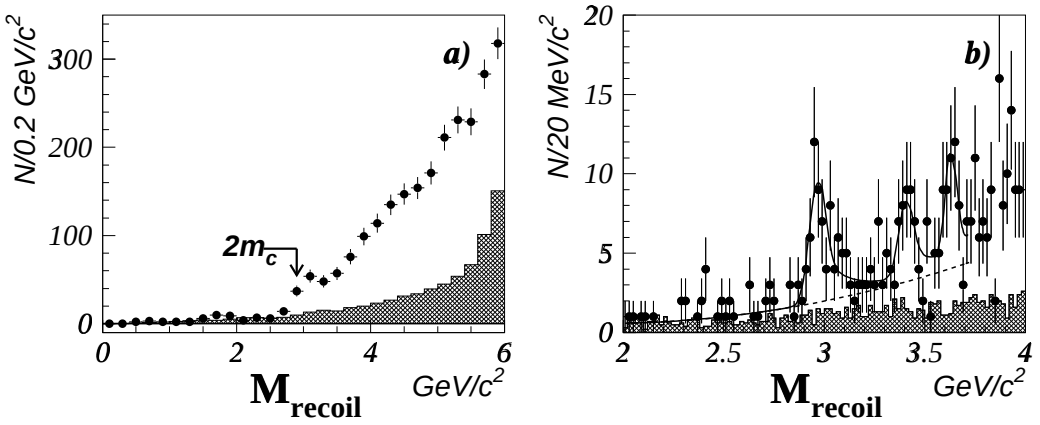

Figure 2: a) The recoil mass distribution for the J/ψ signal region (points) and scaled sidebands (hatched histogram). b) The recoil mass distribution after refitting the J/ψ candidate with a mass constraint for the J/ψ signal region (points) and scaled sidebands (hatched histogram). The curve represents the fit.

in more detail in order to search for production of J/ψ together with an additional charmonium state. A mass constrained fit is applied to the J/ψ candidates before determining $p_{J/\psi}$ to improve the M_{recoil} resolution. The resulting recoil mass spectrum in the data is presented in Fig. 2*b*: a clear peak is observed around $3\,\mathrm{GeV}/c^2$ which can be interpreted as $e^+e^- \to J/\psi\,\eta_c$. Additional peaks at recoil masses consistent with the χ_{c0} and $\eta_c(2S)$ mass are also seen. The fit procedure is described in detail in Ref. [11] and the fit results are presented in Table 1. To determine the $e^+e^- \to J/\psi\,\eta_c\,(\gamma)$ cross-section the signal yield is corrected for the reconstruction efficiency obtained from the Monte Carlo. Because of the selection requirement that the total charged multiplicity in the event be greater than 4, the recoil system must contain

at least three charged tracks: this removes η_c decays into 0 or 2 charged tracks plus neutrals. As η_c branching fractions are poorly known, the result is expressed in terms of the product $\sigma(e^+e^- \to J/\psi\,\eta_c\,(\gamma)) \times \mathcal{B}(\eta_c \to \geq 4\,\text{charged})$, and found to be $(0.033\,^{+0.007}_{-0.006} \pm 0.009)$ pb.

To study the $J/\psi\,c\bar{c}$ mechanism in the region $M_{\text{recoil}} \geq 2\,m_D$, a search is performed for fully reconstructed D^{*+} and D^0 decays in events with a J/ψ meson. Real $J/\psi D$ combinations from $B\overline{B}$ decays are totally discarded by the event selection using the kinematical properties of $B\overline{B}$ events. For selected $J/\psi D^{*+}$ candidates the scatter plot of the dilepton mass versus the $D^0\pi^+$ mass, and the $D^0\pi^+$ mass projection, are shown in Figs. 3*a,b*. The signal yield, found from a simultaneous fit to the $D^0\pi^+$ mass distributions for J/ψ signal and sideband windows, is equal to $N_{J/\psi\,D^{*+}} = 10.1^{+3.6}_{-3.0}$, with significance $\sigma_{J/\psi\,D^{*+}} = 5.3$. A plot of dilepton versus $K^-\pi^+(K^-K^+)$ masses,

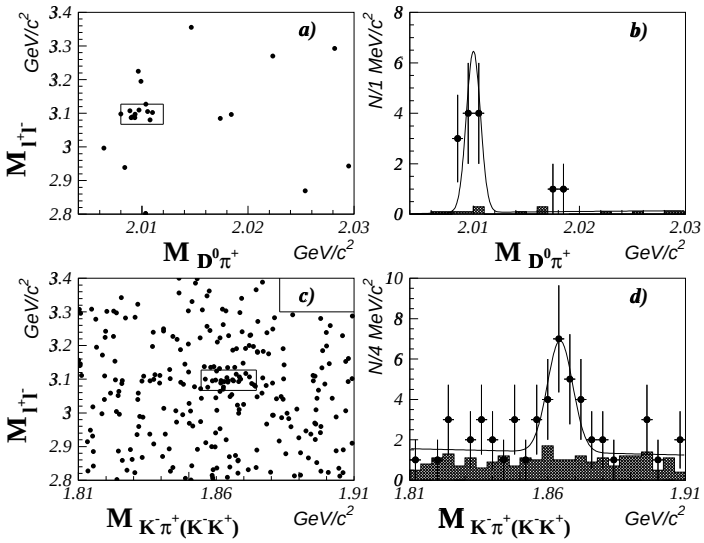

Figure 3: Results of a search for associated production of J/ψ and charm mesons: a) the scatter plot $M(l^+l^-)$ vs $M(D^0\pi^+)$; b) projection onto the $M(D^0\pi^+)$ axis; c) the scatter plot $M(l^+l^-)$ vs $M(K^-\pi^+(K^+K^-))$; d) projection onto the $M(K^-\pi^+(K^+K^-))$ axis. Points with error bars show the J/ψ signal region and the hatched histograms show the scaled sidebands. The curves represent the fit.

	N	$M\,[\text{GeV}/c^2]$	σ
$J/\psi\,\eta_c$	67^{+13}_{-12}	2.962 ± 0.013	6.7
$J/\psi\,\chi_{c0}$	39^{+14}_{-13}	3.403 ± 0.014	3.3
$J/\psi\,\eta_c(2S)$	42^{+15}_{-13}	3.622 ± 0.012	3.4

Table 1: The results of the fit to the recoil mass distribution.

and the projection onto the $K^-\pi^+(K^-K^+)$ mass axis, are shown in Figs. 3*c,d*. A simultaneous fit to the $K^-\pi^+$ (K^-K^+) mass distribution in the J/ψ signal window and the sideband finds $N_{J/\psi\,D^0} = 14.9^{+5.4}_{-4.8}$, with significance $\sigma_{J/\psi\,D^0} = 3.7$. Correcting for the efficiencies found by the Monte Carlo simulation, the cross-sections of $e^+e^- \to J/\psi\,D^{*+}\,X$ and $e^+e^- \to J/\psi\,D^0\,X$ are found to be $(0.53\,^{+0.19}_{-0.15} \pm 0.14)$ pb and $(0.87\,^{+0.32}_{-0.28} \pm 0.20)$ pb respectively. From these values the $e^+e^- \to J/\psi\,c\bar{c}$ cross-section can be derived in model-dependent way, using the model predictions for $c\bar{c}$ fragmentation rates into D^{*+} and D^0. Using the Lund model and averaging over two results the $e^+e^- \to J/\psi\,c\bar{c}$ cross-section is calculated to be $(0.87\,^{+0.21}_{-0.19} \pm 0.17)$ pb. This $J/\psi\,c\bar{c}$ cross-section is an order of magnitude larger than predicted in Refs. [7, 9, 12], and contradicts the NRQCD expectation that the $J/\psi\,c\bar{c}$ fraction is small [7, 9].

References

[1] J.M. Link *et al.* (FOCUS Collab.), Phys. Lett. **B537**, 192 (2002).

[2] P.L. Frabetti *et al.* (E687 Collab.), Phys. Lett. **B323**, 459 (1994); G. Bonvicini *et al.* (CLEO Collab.), Phys. Rev. Lett. **82**, 4586 (1999); E.M. Aitala *et al.* (E791 Collab.), Phys. Rev. Lett. **83**, 32 (1999).

[3] K. Abe *et al.* (Belle Collab.), Phys. Rev. Lett. **88**, 162001 (2002).

[4] J. M. Link *et al.* (FOCUS Collab.), Phys. Lett. **B485**, 62 (2000).

[5] S. E. Csorna *et al.* (CLEO Collab.), Phys. Rev. **D65**, 092001 (2002)

[6] E. Braaten and S. Fleming, Phys. Rev. Lett. **74**, 3327 (1995); P. Cho and M. Wise, Phys. Lett. **B346**, 129 (1995); M. Cacciari, M. Greco, M. L. Mangano, and A. Petrelli, *ibid.* **B356**, 553 (1995).

[7] P. Cho and A. K. Leibovich, Phys. Rev. D **53**, 150 (1996); **53**, 6203 (1996). S. Baek, P. Ko, J. Lee, and H. S. Song, J. Kor. Phys. Soc. **33**, 97 (1998).

[8] E. Braaten and Yu-Qi Chen, Phys. Rev. Lett. **76**, 730 (1996).

[9] F. Yuan, C.-F. Qiao, and K.-T. Chao, Phys. Rev. D **56**, 321 (1997).

[10] B. Aubert *et al.* (BaBar Collab.), Phys. Rev. Lett. **87** 162002 (2001); K. Abe *et al.* (Belle Collab.), Phys. Rev. Lett. **88**, 052001 (2002).

[11] K. Abe *et al.* (Belle Collab.), hep-ex/0205104, Submitted to Phys. Rev. Lett.

[12] V. V. Kiselev, A. K. Likhoded, and M. V. Shevlyagin, Phys. Lett. **B332**, 411 (1994).

Light Scalar Mesons in Charm Meson Decays

Ignacio Bediaga
Representing the Fermilab E791 Collaboration
Centro Brasileiro de Pesquisas Físicas,
Rua Xavier Sigaud 150, 22290, Rio de Janeiro, Brazil
bediaga@cbpf.br

Abstract

We present recent results on scalar light mesons based on Dalitz plot analyses of charm decays from Fermilab experiment E791. Low mass scalar mesons are found to have large contributions to the decays studied, $D^+ \to K^-\pi^+\pi^+$ and $D^+, D_s^+ \to \pi^-\pi^+\pi^+$. These results demonstrate the importance of charm decays as a new environment for the study of light meson physics.

1 Introduction

Here we present an overview of the results we obtained analysing the decays $D_s^+ \to \pi^-\pi^+\pi^+$ [1], $D^+ \to \pi^-\pi^+\pi^+$ [2] and $D^+ \to K^-\pi^+\pi^+$ [3], using data collected in 1991/92 by Fermilab experiment E791 from $500 GeV/c \pi - - nucleon$ interactions. For details see [ref791].

To obtain these results, we had to introduce a new approach in Dalitz plot analysis in order to extract the mass and width of the scalar resonances by allowing them as floating parameters in the fit. We begin this paper presenting the general method, applied in the $D^+ \to K^-\pi^+\pi^+$ Dalitz-plot analysis, then we discuss the $D_s^+ \to \pi^-\pi^+\pi^+$ and $D^+ \to \pi^-\pi^+\pi^+$ studies using the same procedure.

2 The $D^+ \to K^-\pi^+\pi^+$ Dalitz-plot Analysis

From the original 2×10^{10} events collected by E791, and after reconstruction and selection criteria, we obtained the $k^-\pi^+\pi^+$ sample shown in Figure 1(a). The cross-hatched region contains the events selected for the Dalitz-plot analysis. There are 15090 events in this sample, of which 6% are background.

Figure 1(b) shows the Dalitz-plot for these events. The plot presents a rich structure, where we can observe the clear bands from $\overline{K}^*(890)\pi^+$, and an accumulation of events at the upper edge of the diagonal, due to heavier resonances. To study the resonant substructure, we perform an unbinned maximun-likelihood fit to the data, with

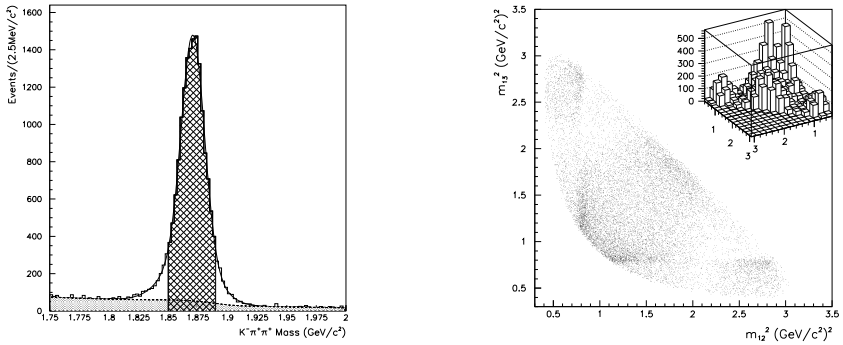

Figure 1: (a) The $K^-\pi^+\pi^+$ invariant mass spectrum. The filled area is background; (b) Dalitz plot corresponding to the events in the dashed area of (a).

probability distribution functions (PDF's) for both signal and background sources. In particular, for each candidate event, the signal PDF is written as the square of the total physical amplitude $\mathcal{A}$ and it is weighted for the acceptance across the Dalitz plot (obtained by Monte Carlo (MC)) and by the level of signal to background for each event, as given by the line shape of Figure 1(a). The background PDF's (levels and shapes) are fixed for the Dalitz-plot fit, according to MC and data studies.

We begin describing our first approach to fit the data, which represents the conventional Dalitz-plot analysis including the known $K\pi$ resonant amplitudes ($\mathcal{A}_n,\ n \geq 1$), plus a constant non-resonant contribution. The resonance amplitudes used to describe the signal, Breit-Wigner parametrizations with Blatt-Weisskopf damping factors are described in reference [3].

Using this model with well-known resonances, we find contributions from the following channels: the non-resonant, responsible for more than 90% of the decay rate, followed by $\overline{K}_0^*(1430)\pi^+$, $\overline{K}^*(892)\pi^+$, $\overline{K}^*(1680)\pi^+$ and $\overline{K}_2^*(1430)\pi^+$. The decay fractions and relative phases are available in reference [3].

To evaluate the fit quality, we compute a χ^2 from binned, two-dimensional distributions of data and decay model events. The χ^2 comes from the differences in the binned numbers of events between the data and the model (from a fast MC simulation). We obtain $\chi^2/\nu = 2.7$ (ν being the number of degrees of freedom), with a corresponding confidence level (CL) of 10^{-11}. We thus conclude that a model with the known $K\pi$ resonances, plus a non-resonant amplitude, is not able to describe the $D^+ \to K^-\pi^+\pi^+$ Dalitz plot satisfactorily. Thus, we are led to try an extra scalar resonance in our fit model. This second fit model, is constructed by the inclusion of an extra scalar state with unconstrained mass and width. For consistency, the mass and width of the other scalar state, the $K_0^*(1430)$, are also free parameters of the fit. We adopt a better description for these scalar states by introducing gaussian-type form-factors [5] to take into account the finite size of the decaying mesons.

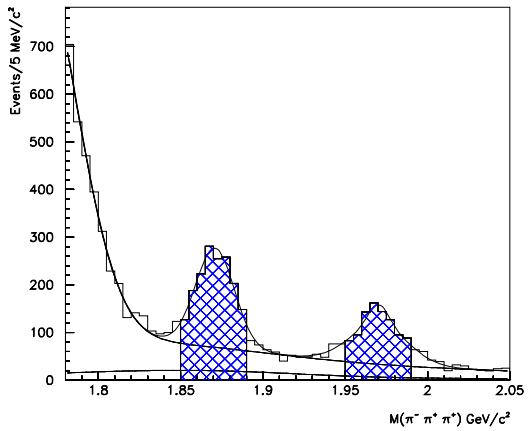

Figure 2: The $\pi^-\pi^+\pi^+$ invariant mass spectrum. The dashed line represent the total background. Events used for the Dalitz analyses are in the hatched areas.

Using this model, we obtain the values of $797 \pm 19 \pm 42$ MeV/c^2 for the mass and $410 \pm 43 \pm 85$ MeV/c^2 for the width of the new scalar state (first error statistical, second error systematic), referred to here as the κ. The values of mass and width obtained for the $K_0^*(1430)$ are respectively $1459 \pm 7 \pm 6$ MeV/c^2 and $175 \pm 12 \pm 12$ MeV/c^2, appearing heavier and narrower than presented by the PDG [6]. The decay fractions and relative phases with systematic errors, are given in reference [3]. The $\kappa\pi^+$ state is now the dominant channel with decay fraction about 50%.

3 The $D_s^+ \to \pi^-\pi^+\pi^+$ Results

In Figure 2 we show the $\pi^-\pi^+\pi^+$ invariant mass distribution for the sample collected by E791 after reconstruction and selection criteria [1, 2]. Besides combinatorial background, reflections from the decays $D^+ \to K^-\pi^+\pi^+$, $D^0 \to K^-\pi^+$ (plus one extra π^+ track) and $D_s^+ \to \eta'\pi^+$, $\eta' \to \rho^0(770)\gamma$ are all taken into account. The hatched regions in Figure 2 show the samples used for the Dalitz-plot analyses. There are 1686 and 937 candidate events for D^+ and D_s^+ respectively, with a signal to background ratio of about 2:1. The Dalitz plots for these events are shown in Figure 3, the axes corresponding to the two $\pi^-\pi^+$ invariant-masses squared.

For the $D_s^+ \to \pi^-\pi^+\pi^+$ events in Figure 3(a), the signal amplitude includes all channels with well known dipion resonances [6]: $\rho^0(770)\pi^+$, $f_0(980)\pi^+$, $f_2(1270)\pi^+$, $f_0(1370)\pi^+$, $\rho^0(1450)\pi^+$ and the non-resonant, assumed constant across the Dalitz plot.

The measured $f_0(980)$ standard Breit-Wigner parameters are $m_0 = 975 \pm 3$

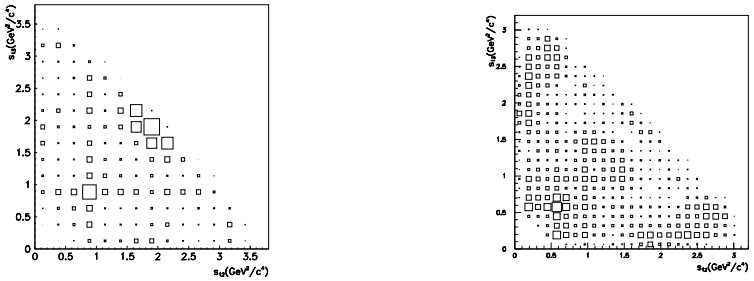

Figure 3: (a) The $D_s^+ \to \pi^-\pi^+\pi^+$ Dalitz plot and (b) the $D^+ \to \pi^-\pi^+\pi^+$ Dalitz plot. Since there are two identical pions, the plots are symmetrized.

MeV/c^2 and $\Gamma_0 = 44 \pm 2 \pm 2$ MeV/c^2. The confidence level of the fit for $D_s^+ \to \pi^-\pi^+\pi^+$ is 35%.The decay fractions and relative phases, with systematic errors, are given in reference [1]. The $f_0(980)\pi^+$ state is the dominant channel with decay fraction about 50%.

In Figure 4 we show the $\pi^-\pi^+$ mass-squared projections for data (points) and model (solid lines, from fast-MC).

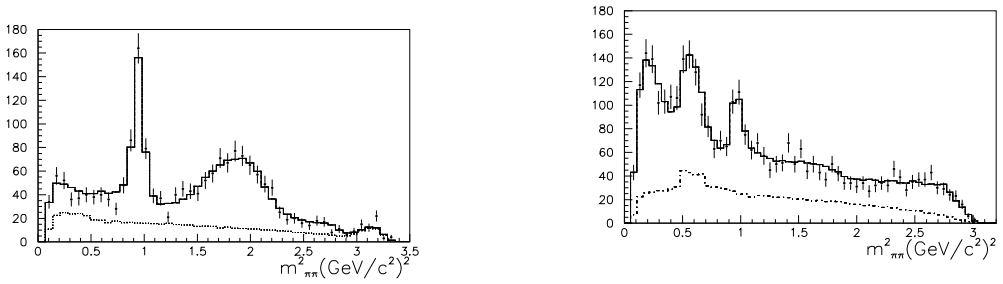

Figure 4: (a) s_{12} and s_{13} ($m^2_{\pi\pi}$) projections for $D_s^+ \to \pi^-\pi^+\pi^+$ data (dots) and our best fit (solid). (b) s_{12} and s_{13} projections for $D^+ \to \pi^-\pi^+\pi^+$ data (dots) and our best fit (solid) for models with $\sigma(500)\pi^+$ amplitude. In both figures the dashed distribution corresponds to the expected background level.

4 The $D^+ \to \pi^-\pi^+\pi^+$ Results

In a first approach, we try to fit the $D^+ \to \pi^-\pi^+\pi^+$ Dalitz plot of Figure 3(b) with the same amplitudes used for the $D_s^+ \to \pi^-\pi^+\pi^+$ analysis. Using this model, the non-resonant, the $\rho^0(1450)\pi^+$, and the $\rho^0(770)\pi^+$ amplitudes are found to dominate [2]. However, this model does not describe the data satisfactorily, especially at low

$\pi^-\pi^+$ mass squared [2]. The χ^2/ν obtained from the binned Dalitz plot for this model is 1.6, with a CL less than 10^{-5}.

To investigate the possibility that another $\pi^-\pi^+$ resonance contributes to the $D^+ \to \pi^-\pi^+\pi^+$ decay, we add an extra scalar resonance amplitude to the signal PDF, with mass and width as floating parameters in the fit.

We find that this model improves our fit substantially. The mass and the width of the extra scalar state are found to be $478^{+24}_{-23} \pm 17$ MeV/c^2 and $324^{+42}_{-40} \pm 21$ MeV/c^2, respectively. Refering to this state as the $\sigma(500)$, we observe that the $\sigma(500)\pi^+$ channel produces the largest decay fraction [2]; the non-resonant amplitude, which is dominant in the model without $\sigma(500)\pi^+$, drops substantially. The model with the sigma describes the data very well, as can be seen by the $\pi\pi$ mass squared projection in Fig. 4(b). The χ^2/ν is now 0.9, with a corresponding confidence level of 91%.

5 Conclusion

From the data of the Fermilab E791 experiment, we studied the Dalitz plots of the decays $D^+ \to K^-\pi^+\pi^+$, $D_s^+ \to \pi^-\pi^+\pi^+$, and $D^+ \to \pi^-\pi^+\pi^+$. In these three final states, the scalar intermediate resonances were found to give the largest contributions to the decay rates. We obtained strong evidence for the existence of the $\sigma(500)$ and κ scalar mesons, measuring their masses and widths. We also obtained new measurements for masses and widths of the other scalars studied, $f_0(980)$, $f_0(1430)$ and $K_0^*(1430)$.

The results presented here show the potential of D meson decays for the study of light meson spectroscopy, in particular in the scalar sector [7].

References

[1] E791 Collaboration, E.M. Aitala *et al.*, Phys. Rev. Lett. **86**, 765 (2001).

[2] E791 Collaboration, E.M. Aitala *et al.*, Phys. Rev. Lett. **86**, 770 (2001).

[3] E.M. Aitala *et al.* hep-ex/0204018, submitted to Phys. Rev. Lett.

[4] J.A. Appel, Ann. Rev. Nucl. Part. Sci. **42**, 367 (1992); D. Summers *et al.*, hep-ex/0009015; S. Amato *et al.*, Nucl. Instr. Meth. A **324**, 535 (1993); E.M. Aitala *et al.*, Eur. Phys. J. direct C **4**, 1 (1999); S. Bracker *et al.*, hep-ex/9511009.

[5] N.A. Törnqvist, Z. Phys. C **68**, 647 (1995).

[6] Particle Data Group, D.E. Groom *et al.*, Eur. Phys. Jour. C **15**, 1 (2000).

[7] F.E. Close and N. Törnqvist, hep-ph/0204205.

A Review of Charmed Baryon Experimental Data

John Yelton
Physics Department
U. of Florida
Gainesville, FL 32611-8440

1 Introduction

This is a review of the experimental results on charmed baryons, with the accent on those reported most recently.

2 Motivation

The charmed baryon sector is the richest quark spectroscopy available for study. Compared with mesons there are *more* states as there are more possibilities for orbital excitations. More importantly, the extra mass associated with these excitations is less (because it is inversely proportional to a measure of the center-of-mass), leading to less phase space for decays and *narrower* states. The charm quark is sufficiently massive for the states to be described as a combination of a heavy quark and a light di-quark - this picture does not work well for strange baryons. The charmed baryon sector is much easier to study experimentally than the B baryon sector. It also offers a good laboratory for studying weak decays as there are four weakly decaying singly charmed baryons.

3 Techniques

There are two main techniques that have been used in recent years for charmed baryons studies. Fixed target experiments, such as FOCUS, SELEX and E-791 at Fermilab, have a long pathlength for charm decays which can be used as a tag, and also can yield accurate lifetime measurements. Spectroscopy has tended to be easier at e^+e^- machines operating at around 10 GeV (notably CLEO, now joined by BELLE). In the e^+e^- continuum, around 40% of events are charm. Running at the Λ_c^+ threshold has not been done for a long time but there is hope that CLEO_c will do this in the future.

4 The Greek Alphabet of Charmed Baryons

We always consider a charmed baryon as the combination of a (heavy) charm quark and a light di-quark, which has its own well-defined quantum numbers J^P_{LIGHT}. This combines with the charm quark to give the overall J^P of the state. If the two light quarks are u and/or d then the particle is either a Λ_c or a Σ_c. The former are anti-symmetric under interchange of the two light quarks and are iso-scalars, the latter are symmetric under interchange and are iso-triplets. When one of the two light quarks is a strange quark the baryons are called Ξ_c states, and if both light quarks are strange it is an Ω_c.

5 The Λ_c^+ Ground State

More than thirty decay modes of the Λ_c^+ have been measured. A recent contribution comes from BELLE[1] who have measured a series of comparatively rare decays that are either Cabibbo-suppressed (such as the first observation of ΛK^+) or unambiguously due to W-exchange diagrams. There have also been two recent measurements of the Λ_c^+ lifetime, from SELEX[2] ($\tau(\Lambda_c^+) = 198.1 \pm 7.0 \pm 5.6$ fs) and FOCUS ($\tau(\Lambda_c^+) = 204.6 \pm 3.4 \pm 2.4$ fs [3]). The PDG 2001[4] number of of 188 ± 7 seems to be edging up. This is of course a short lifetime by charm standards, presumably because W-exchange is an allowed method for Λ_c^+ decays, as has been shown directly.

6 Recent Σ_c and Σ_c^* Results

The doubly charged and neutral Σ_c states are relatively easy to observe as they decay with a charged pion to the Λ_c^+ ground state. The masses of all three Σ_c states have been well measured. Two recent measurements from CLEO[5] and FOCUS[6] measure the natural widths, with all results being around 2 MeV. The singly charged states decay via a π^0 decay which is usually harder to detect experimentally. There are fewer measurements of the Σ_c^* states because their large natural widths cause complications. The singly charged state was only recently reported by CLEO[7]. Looking at all the results, we can note that a) there is little isospin splitting, but the singly charged state may be a little lighter than the others in line with predictions[8], b) the width of the $\frac{3}{2}$ states is around seven times that of the $\frac{1}{2}$ states - this is in line with predictions that this ratio depends only on a few simple numerical factors plus phase-space[9], and c) a very naive quark model which predicts that the mass splitting between the spin-weighted average of the Σ^*-Σ system and the ground state should be independent of the heavy quark mass, and the splitting between the $\frac{3}{2}$ and $\frac{1}{2}$ states is inversely proportional to heavy quark mass. The strange and charmed $\Sigma - \Lambda$ system obeys this scaling law very well. I expect it to do so in the B-system also.

7 Higher States

Allowing orbital angular momentum into the picture produces a large number of predicted states. Some of these can be expected to be narrow and some very wide. With the $L = 1$ between the heavy quark and the light di-quark, there should be 2 Λ_{c1} states (well known and well measured) and no fewer than 5 iso-triplets of Σ_c states. Most people use a numerical subscript to denote the spin of the light diquark. Alternatively, having $L = 1$ between the two light quarks produced 5 Λ_c states and 2 iso-triplets of Σ_c's. All these particles (except maybe some above pD threshold), will cascade down via (multi-)pion decays to the ground-state Λ_c. CLEO have found two bumps in $\Lambda_c^+\pi^+\pi^-$[10]. One is wide, and they like the identification as the first two Σ_{c1} states. The second is more interesting as it is fairly narrow, and they identify it as the first of the second generation of orbitally excited Λ_c particles. This particular state has no allowed single pion decay available. These observations have yet to pique the theorists interest. Figure 1 shows a guess of the spectroscopy of the $\Lambda_c - \Sigma_c$ states, based upon a very simple potential model. The states that CLEO guesses correspond to their bumps are denoted by bold lines.

8 The Ξ_c Spectrum

The *csu* and *csd* quark combinations are referred to as Ξ_c^+ and Ξ_c^0 respectively. Their spectroscopy follows the lines of the $\Lambda_c - \Sigma_c$ pattern, except that it comprises only iso-doublets, rather than iso-singlet and iso-triplets. The first 10 states (analagous to the those up to and including the $\Lambda_{c1}(2630)$) have been reported. Nine of these first observations were by CLEO[11] and many of them have yet to be confirmed. The Ξ_c^+ groundstate has been known since the eighties (although first sightings[12] were controversial), and its lifetime has been measured several times with a PDG (2001)[4] average of 330^{+60}_{-40} fs. Since then have been two more measurements of this lifetime. The CLEO II.V detector selects a clean sample of Ξ_c^+ decays, but its pathlength resolution is comparable to the individual pathlengths. It finds $503 \pm 47 \pm 18$ fs[13]. FOCUS has more events[14], worse signal-to-noise, but much better lifetime resolution. It obtains $439 \pm 22 \pm 9$ fs. It seems that the Ξ_c^+ lifetime is creeping up.

9 The Ω_c

The $\Omega_c(css)$ combination was reported many times over the last two decades, but we can safely say now that most have been shown to be incorrect on mass and/or cross-section grounds. The E-687 peak in $\Sigma^+K^-K^-\pi^+$ is the one that still looks impressive[15]. In 2001 CLEO[16] found a good looking peak using the sum of 5 "expected" decay modes (not including $\Sigma^+K^-K^-\pi^+$). Now BELLE[17] has (prelimi-

nary) results shoding an extremely clean peak in $\Omega^-\pi^+$. Their mass ($2693.7 \pm 1.3^{+1.1}_{-1.0}$ MeV) agrees well with the CLEO number ($2694.6 \pm 2.6 \pm 1.9$ MeV). There is no doubt that the Ω_c has been discovered.

A recent analysis by CLEO finds semi-leptonic decays of the Ω_c. They reconstruct 760 ± 32 Ω^- baryons (it is clearly tough to produce an sss state in e^+e^- annihilations). They then look for correlations with correctly charged electrons. After subtraction of backgrounds, they find an excess of 11.4 ± 3.8 events that are attributable to $\Omega_c \to \Omega^- e^+ \nu$ events. The ratio of the simplese hadronic decay mode $\Omega^-\pi^+$ to this semi-leptonic mode is $0.41 \pm 0.19 \pm 0.04$. This is similar to analagous ratios in Ξ_c^0 and Λ_c^+ decays.

10 Doubly charmed baryons

Theorists have always enjoyed predicting the masses of the doubly charmed baryons Ξ_{cc}^{++} (ccu) and $\Xi_c c^+$ (ccd). SELEX have shown[18] peak (of only 3 σ significance and definitely preliminary) in the decay mode $\Lambda_c^+ K^-\pi^+\pi^+$. The mass is 3.79 GeV. I do not understand what processes must be involved to produce enough of them so that an individual decay mode of one of the states will make around 1% of the Λ_c^+ candidates in their sample.

11 Conclusion

There have been 22 charmed baryon states reported in the literature, though many of them need to be confirmed. They display a spectroscopy that is complex, yet orderly and comprehensible. There remains more work to be done on spectroscopy, and work is still active in understanding decay mechanisms. In the future, BELLE and BaBar are the experiments best placed for new discoveries, and CLEO_c operating at Λ_c^+ threshold could also make complementary contributions.

References

[1] K.Abe *et al.,* Phys. Lett **B524** 247 (2002).

[2] A. Kushnirenko *et al.,* PRL **86** 5243 (2001).

[3] J. M. Link *et al.,* PRL **88**, 161801 (2002).

[4] D. E. Groom *et al.,* Eur. Phys. J. **C15** (2000), 1. with 2001 update (URL:http://pdg.lbl.gov/).

[5] M. Artuso *et al.,* Phys. Rev. **D65** 071101, (2002).

[6] J. M. Link *et al.,* Phys. Lett. **B525**, 205 (2002).

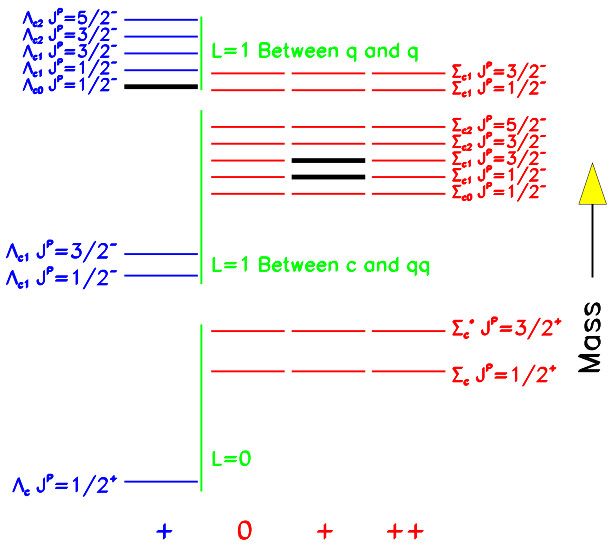

Figure 1: The author's view of the expected mass spectrum of singly-charmed baryons.

[7] R. Ammar *et al.*, PRL **86** 1167 (2001).

[8] J. Franklin, Phys. Rev. **D 59**, 117502 (1999).

[9] J.Rosner, Phys. Rev. **D 52**, 6461 (1995).

[10] M. Artuso *et al.*, PRL **86** 4479 (2001).

[11] S.E.Csorna *et al.*, PRL **86**, 2232 (2001), J. Alexander *et al.*, PRK **83** 3390 (1999), C. P. Jessop *et al.*, PRK **82** 492 (1999), L. Gibbons *et al.*, PRL **77**, 810 (1996), P. Avery *et al.*, PRK **75**, 4364 (1995),

[12] S. Biagi *et al.* Phys. Lett. **122B** 455 (1983).

[13] A.H.Mahmood *et al.*, Phys. Rev. **D65** 031102 (2002).

[14] J. M. Lin *et al.*, Phys. Lett. **B523** (2001).

[15] P. L. Frabetti *et al.*, Phys. Lett. **B338** 106 (1994).

[16] D.Cronin-Hennessy *et al.*, PRL **86** 3730 (2001).

[17] Private communication, P. Pakhlov (ITEP) on behalf of BELLE.

[18] For latest SELEX results, see their homepage http:///fn781a.fnal.gov/

Rare Decays Recent Results from FOCUS (+Theory)

Will E. Johns (for the FOCUS collaboration)
Department of Physics and Astronomy
Vanderbilt University
Nashville, TN USA

1 Introduction

The search for rare decays of charm particles is reaching a point where long range effects should be observable in the next few years. In order to perform the analysis of such small data sets, several techniques have become *de facto* standards in the last decade. In this talk, we will show new rare charm decay results from the FOCUS experiment. The analysis has been performed utilizing a bootstrap technique which we will describe below.

2 Technique

The FOCUS analysis technique has emphasized a careful approach to the treatment of backgrounds in a limited statistics analysis. The usual approach is to select cuts to optimize signal efficiency relative to background sidebands. This "blind" technique, where the signal region is masked off, can still lead to a downward fluctuation of the sidebands relative to the masked off "signal" region and a more conservative limit on average.

Further, authors frequently use the technique outlined in reference [1] to calculate the confidence levels used in the calculation of their limits. The approach in [1] does not explicitly include fluctuations in the background. Indeed, the PDG [3] suggests presenting a measure of the experimental sensitivity in addition to the reported limit whenever experiments quote a result since none of the methods suggested [3], including [2], properly deal with fluctuations in the background and bias in selecting the data.

For our analysis, we chose a method [4] which includes the background fluctuations directly into the calculation of the likelihood. The probability of finding a signal rate μ and a background rate b given x events in a signal region and y events in background sidebands is described by:

$$P_{\mu,b}(x,y) = \frac{(\mu+b)^x e^{-(\mu+b)}}{x!} \; \frac{(\tau b)^x e^{-(\tau b)}}{y!}.$$

Where τ is the ratio of the number of background events in the sideband regions to the signal region. The τ is determined via Monte Carlo. Rolke and Lopez [4] have shown that this method for determining an upper limit provides better coverage than [1].

Methods presented by Rolke and Lopez have also been shown to reduce bias in the selection of optimal cuts [5]. Briefly, one uses the computed sensitivity on an ensemble of bootstrapped (sample with replacement) events from the data. The cuts chosen by each selected set in this manner are applied to a second, independent, bootstrapped sample. A sensitivity as well as an upper limit are computed from the second sample. The sensitivity and branching ratio quoted are the median values of the ensemble of results from the second bootstrap.

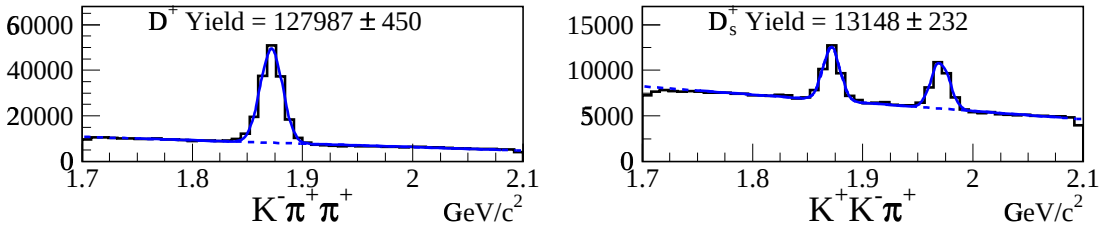

Figure 1: Modes used to normalize the rare decay modes. The yields are shown for the loosest cut grid combination.

The data for the analyses presented in this talk were collected using the Wide-band photoproduction experiment FOCUS during the 1996–1997 fixed–target run at Fermilab. The FOCUS detector is a large aperture, fixed–target spectrometer with excellent vertexing and particle identification used to measure the interactions of high energy photons on a segmented BeO target. The FOCUS beamline [6] and detector [7, 8] have been described elsewhere.

To provide a clean sample of D^+'s and D_s^+'s, we look for D's through the 3-body decay chain $D^+(D_s^+) \to h^\mp \mu^\pm \mu^+$ where the h represents a pion or a kaon. We use a cut grid based on kinematic variables and particle ID algorithm results that have been shown to be effective for other charm decays. The grid includes cuts on the significance of separation between the interaction and decay vertices (L/σ), the confidence level of the vertex fit of the decay vertex, the confidence level that a particle is identified as a muon, the momentum of muon candidates, and Čerenkov likelihoods based on different particle hypotheses used to separate pions and kaons [8]. The normalizing

modes used to compute the branching ratios for D^+ and D_s^+ are shown in Figure 1 for the loosest cuts in the grid.

3 Results and Systematic Checks

The dominant systematic effects in this analysis have been estimated to occur from the absolute branching ratios [9] used to calibrate the normalization modes. The systematic errors, which averaged about 7.6% for the D^+ modes and 27.6% for the D_s^+ modes, were added to the result using the technique outlined in [2]. As a check on the dual bootstrap, another technique was used that selected a unique cut *set* based on the results of the cut grid. The cuts used to determine the best sensitivities in the first bootstrap are examined for all modes and a best set is determined based on the most likely cut combination. This cut set is then applied to all modes *once* in the spirit of a more traditional "blind" analysis.

The results of the analysis are presented in Table 1 below. There is good agreement between the dual bootstrap, the sensitivity and the single cut systematic check. Note that the only mode where the result and the sensitivity show a marked difference is in $D^+ \to K^- \mu^+ \mu^+$ which might indicate more contamination from $D^+ \to K^- \pi^+ \pi^+$ than anticipated.

Decay Mode	Result	Sensitivity	Single Cut
$D^+ \to K^+ \mu^+ \mu^-$	9.2×10^{-6}	7.5×10^{-6}	11.8×10^{-6}
$D^+ \to K^- \mu^+ \mu^+$	13.1×10^{-6}	4.8×10^{-6}	12×10^{-6}
$D^+ \to \pi^+ \mu^+ \mu^-$	8.8×10^{-6}	7.6×10^{-6}	7.5×10^{-6}
$D^+ \to \pi^- \mu^+ \mu^+$	4.8×10^{-6}	5.6×10^{-6}	5.2×10^{-6}
$D_s^+ \to K^+ \mu^+ \mu^-$	3.6×10^{-5}	3.3×10^{-5}	3.8×10^{-5}
$D_s^+ \to K^- \mu^+ \mu^+$	1.3×10^{-5}	2.1×10^{-5}	2.0×10^{-5}
$D_s^+ \to \pi^+ \mu^+ \mu^-$	2.6×10^{-5}	3.1×10^{-5}	1.8×10^{-5}
$D_s^+ \to \pi^- \mu^+ \mu^+$	2.9×10^{-5}	2.3×10^{-5}	2.2×10^{-5}

Table 1: FOCUS results with incorporated systematic errors for the modes shown. Each number represents a 90% upper limit for the brancing ratio of the decay mode listed.

4 Comparisons to Experiment and Theory

In Figure 2 below, we show the FOCUS branching ratio limits for the dual bootstrap technique described in the text. Our results are a substantial improvement over

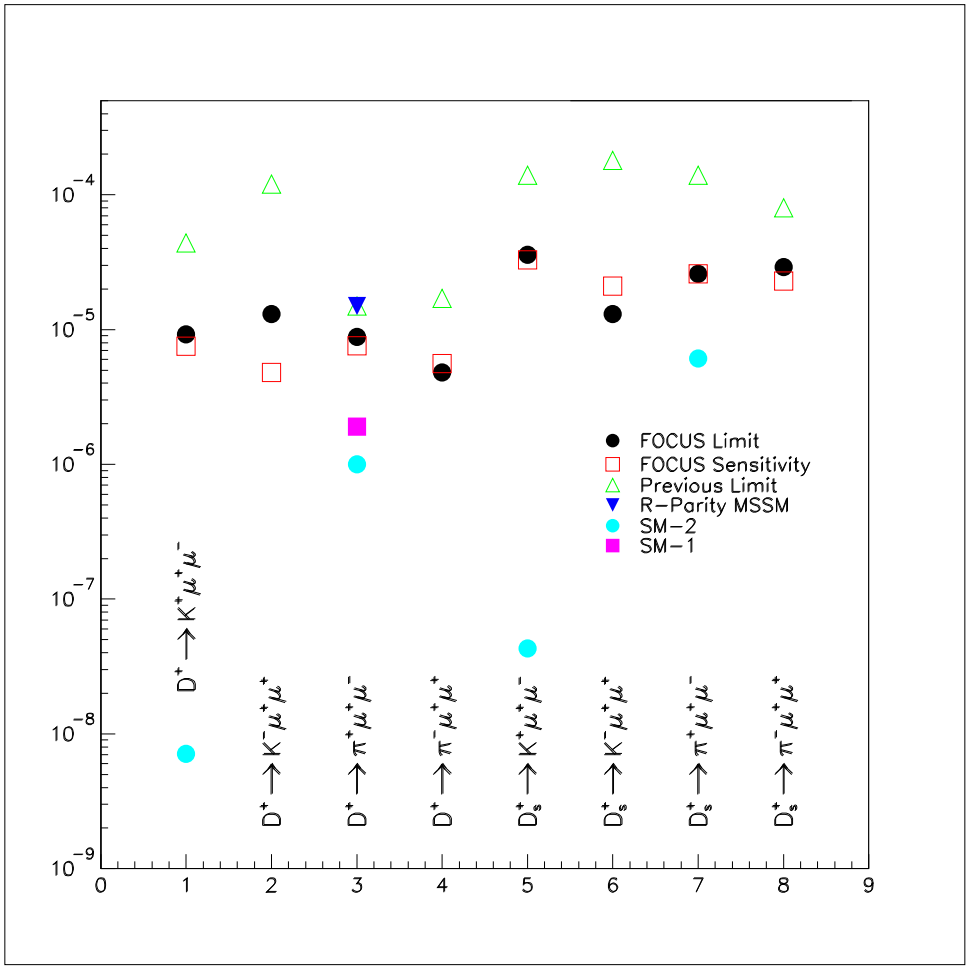

Figure 2: FOCUS results compared to other experiments and theory. The previous limits, except for the E687 $D^+ \to K^-\mu^+\mu^+$ [12] are from Fermilab experiment E791 [10]. The theory estimates come from [13] (R-Parity MSSM and SM-1) and [14] (SM-2). Note that the SM estimates from [13] use a formalism close to [15], and at present there is some discrepancy in the invariant M_{ll} mass behavior for the SM estimates in [13] and [14]. The results for four-body decays measured by E791 [11] are not shown.

previous results [12, 10] and FOCUS sets a new limit for the MSSM R-Parity violating prediction [13] for the branching ratio $D^+ \to \pi^+\mu^+\mu^-$ of 8.8×10^{-6} @ 90% C.L..

I am grateful to Daniel Engh for supplying all the FOCUS results presented in this note. I am also grateful to Gustavo Burdman and Paul Singer for their patience during several very useful conversations.

References

[1] G. J. Feldman and R. D. Cousins, Phys. Rev. D **57**, 3873 (1998) [arXiv:physics/9711021].

[2] R. D. Cousins and V. L. Highland, Nucl. Instrum. Meth. A **320**, 331 (1992).

[3] F. James and R. Cousins, Eur. Phys. J. C **15**, 195 (2000).

[4] W. A. Rolke and A. M. Lopez, Nucl. Instrum. Meth. A **458**, 745 (2001) [arXiv:hep-ph/0005187].

[5] W. A. Rolke and A. M. Lopez, arXiv:hep-ph/0206139.

[6] P. L. Frabetti *et al.*, Nucl. Instrum. Meth. A **329**, 62 (1993).

[7] P. L. Frabetti *et al.* [E-687 Collaboration], Nucl. Instrum. Meth. A **320**, 519 (1992).

[8] J. M. Link *et al.* [FOCUS Collaboration], Nucl. Instrum. Meth. A **484**, 270 (2002) [arXiv:hep-ex/0108011].

[9] D. E. Groom *et al.* [Particle Data Group Collaboration], Eur. Phys. J. C **15**, 1 (2000).

[10] E. M. Aitala *et al.* [E791 Collaboration], Phys. Lett. B **462**, 401 (1999) [arXiv:hep-ex/9906045].

[11] E. M. Aitala *et al.* [E791 Collaboration], Phys. Rev. Lett. **86**, 3969 (2001) [arXiv:hep-ex/0011077].

[12] P. L. Frabetti *et al.* [The E687 Collaboration], Phys. Lett. B **398**, 239 (1997).

[13] G. Burdman, E. Golowich, J. Hewett and S. Pakvasa, arXiv:hep-ph/0112235.

[14] S. Fajfer, S. Prelovsek and P. Singer, Phys. Rev. D **64**, 114009 (2001) [arXiv:hep-ph/0106333].

[15] P. Singer and D. X. Zhang, Phys. Rev. D **55**, 1127 (1997) [arXiv:hep-ph/9612495].

May 17, session 4.

Session Chair: M. Artuso

Future Experiments in Heavy Flavor Physics

CLEO-c and CESR-c: Allowing Quark Flavor Physics to Reach its Full Potential

I. Shipsey

B-physics and CP violation with LHCb

G. Carboni

The BTeV experiment at the Tevatron collider

J. C. Wang

The Super B Factory

D. G. Hitlin

CLEO-c and CESR-c: Allowing Quark Flavor Physics to Reach its Full Potential.

Ian Shipsey
Deprtment of Physics
Purdue University
West Lafayette, IN 47907, U.S.A.

Abstract

We report on the physics potential of a proposed conversion of the CESR machine and the CLEO detector to a charm and QCD factory: "CLEO-c and CESR-c" that will make crucial contributions to quark flavor physics this decade, and may offer our best hope for mastering non-perturbative QCD, which is essential if we are to understand strongly coupled sectors in the new physics that lies beyond the Standard Model.

1 Executive Summary

The goals of quark flavor physics are: to test the consistency of the Standard Model (SM) description of quark mixing and CP violation, to search for evidence of new physics, and to sort between new physics scenarios initially uncovered at the LHC. This will require a range of measurements in the quark flavor changing sector of the SM at the per cent level. These measurements will come from a variety of experiments including BABAR and Belle and their upgrades, full exploitation of the facilities at Fermilab (CDF/D0/BTeV) and at the LHC (CMS/ATLAS/LHC-b), and experiments in rare kaon decays.

However, the window to new physics that quark flavor physics can provide, has a curtain drawn across it. The curtain represents hadronic uncertainty. The study of weak interaction phenomena, and the extraction of quark mixing matrix parameters remain limited by our capacity to deal with non-perturbative strong interaction dynamics. Techniques such as lattice QCD (LQCD) directly address strongly coupled theories and have the potential to eventually determine our progress in many areas of particle physics. Recent advances in LQCD have produced a wide variety of calculations of non-perturbative quantities with accuracies in the 10-20% level for systems involving one or two heavy quark such as B and D mesons, and Ψ and Υ quarkonia. The techniques needed to reduce uncertainties to 1-2% precision exist, but the path to higher precision is hampered by the absence of accurate charm data against which to test and calibrate the new theoretical techniques.

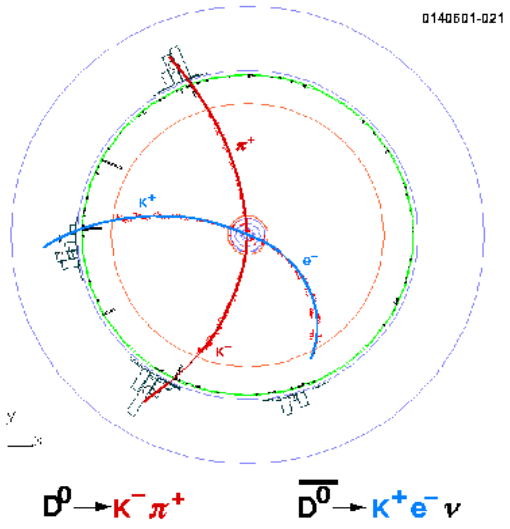

Figure 1: A doubly tagged event at the $\psi(3770)$.

To meet this challenge the CLEO collaboration has proposed to operate CLEO and CESR as a charm and QCD factory at charm threshold where the experimental conditions are optimal. In a three year focused program CLEO-c will obtain charm data samples one to two orders of magnitide larger than any previous experiment operating in this energy range, and with a detector that is significantly more powerful than any previous detector to operate at charm threshold. CLEO-c has the potential to provide a unique and crucial validation of LQCD with accuracies of 1-2%.

If LQCD is validated, CLEO-c data will lead to a dramatic improvement in our knowledge of the quark couplings in the charm sector. In addition CLEO-c validation of lattice calculations, combined with B factory, Tevatron, and LHC data will allow a significant improvement in our knowledge of quark couplings in the beauty sector. The impact CLEO-c will have on our knowledge of the CKM matrix makes the experiment an essential step in the quest to understand the origin of CP violation and quark mixing. CLEO-c allows quark flavor physics to reach its full potential, by enabling the heavy flavor community to draw back the curtain of hadronic uncertainty, and thereby see clearly through the window to the new physics that lies beyond the SM. Of equal importance, CLEO-c allows us to significantly advance our understanding and control over strongly-coupled, non-perturbatyive quantum field theories in general. An understanding of strongly coupled theories will be a crucial element in helping to interpret new phenomena at the high energy frontier.

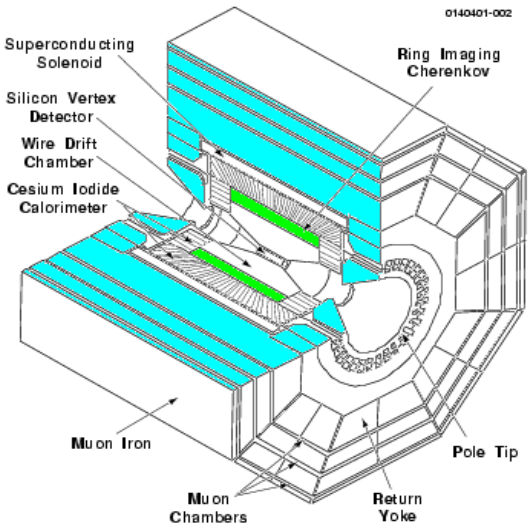

Figure 2: The CLEO III detector.

2 Introduction

For many years, the CLEO experiment at the Cornell Electron Storage Ring, CESR, operating on the $\Upsilon(4S)$ resonance, has provided most of the world's information about the B_d and B_u mesons. At the same time, CLEO, using the copious continuum pair production at the $\Upsilon(4S)$ resonance has been a leader in the study of charm and τ physics. Now that the asymmetric B factories have achieved high luminosity, CLEO is uniquely positioned to advance the knowledge of quark flavor physics by carrying out several measurements near charm threshold, at center of mass energies in the 3.5-5.0 GeV region. These measurements address crucial topics which benefit from the high luminosity and experimental constraints which exist near threshold but have not been carried out at existing charm factories because the luminosity has been too low, or have been carried out previously with meager statistics. They include:

1. Charm Decay constants f_D, f_{D_s}
2. Charm Absolute Branching Fractions
3. Semileptonic decay form factors
4. Direct determination of V_{cd} & V_{cs}
5. QCD studies including:
   Charmonium and bottomonium spectroscopy
   Glueball and exotic searches

Table 1: Summary of CLEO-c charm decay measurements.

Topic	Reaction	Energy (MeV)	L (fb^{-1})	current sensitivity	CLEO-c sensitivity
Decay constant					
f_D	$D^+ \to \mu^+\nu$	3770	3	UL	2.3%
f_{D_s}	$D_s^+ \to \mu^+\nu$	4140	3	14%	1.9%
f_{D_s}	$D_s^+ \to \mu^+\nu$	4140	3	33%	1.6%
Absolute Branching Fractions					
$Br(D^0 \to K\pi)$		3770	3	2.4%	0.6%
$Br(D^+ \to K\pi\pi)$		3770	3	7.2%	0.7%
$Br(D_s^+ \to \phi\pi)$		4140	3	25%	1.9%
$Br(\Lambda_c \to pK\pi)$		4600	1	26%	4%

Measurement of R between 3 and 5 GeV, via scans
Measurement of R between 1 and 3 GeV, via ISR

6. Search for new physics via charm mixing, CP violation and rare decays

7. τ decay physics

The CLEO detector can carry out this program with only minimal modifications. The CLEO-c project is described at length in [1] - [11]. A very modest upgrade to the storage ring is required to achieve the required luminosity. Below, we summarize the advantages of running at charm threshold, the minor modifications required to optimize the detector, examples of key analyses, a description of the proposed run plan, and a summary of the physics impact of the program.

2.1 Advantages of running at charm threshold

The B factories, running at the $\Upsilon(4S)$ will have produced 500 million charm pairs by 2005. However, there are significant advantages of running at charm threshold:

1. Charm events produced at threshold are extremely clean.

2. Double tag events, which are key to making absolute branching fraction measurements, are pristine.

3. Signal/Background is optimum at threshold.

4. Neutrino reconstruction is clean.

5. Quantum coherence aids D mixing and CP violation studies.

These advantages are dramatically illustrated in Figure 1, which shows a picture of a simulated and fully reconstructed $\psi(3770) \to D\overline{D}$ event.

2.2 The CLEO-III Detector : Performance, Modifications and issues

The CLEO III detector, shown in Figure 2, consists of a new silicon tracker, a new drift chamber, and a Ring Imaging Cherenkov Counter (RICH), together with the CLEO II/II.V magnet, electromagnetic calorimeter and muon chambers. The upgraded detector was installed and commissioned during the Fall of 1999 and Spring of 2000. Subsequently operation has been very reliable (see below for a caveat) and a very high quality data set has been obtained. To give an idea of the power of the CLEO III detector in Figure 3 (left plot) the beam constrained mass for the Cabibbo allowed decay $B \to D\pi$ and the Cabibbo suppressed decay $B \to DK$ with and without RICH information is shown.

The latter decay was extremely difficult to observe in CLEO II/II.V which did not have a RICH detector. In the right plot of Figure 3 the penguin dominated decay $B \to K\pi$ is shown. This, and other rare B decay modes are observed in CLEO III with branching ratios consistent with those found in CLEO II/II.V, and are also in agreement with recent Belle and BABAR results. Figure 3 is a demonstration that CLEO III performs very well indeed.

Unfortunately, there is one detector subsystem that is not performing well. The CLEO III silicon has experienced an unexpected and unexplained loss of efficiency. The silicon detector will be replaced with a wire vertex chamber for CLEO-c. We note that if one was to design a charm factory detector from scratch the tracking would be entirely gas based to ensure that the detector material was kept to a minimum. CLEO-c simulations indicate that a simple six layer stereo tracker inserted into the CLEO III drift chamber, as a silicon detector replacement, would provide a system with superior momentum resolution compared to the current CLEO III tracking system.

Due to machine issues we plan to lower the solenoid field strength to 1.0 T from 1.5 T. All other parts of the detector do not require modification. The dE/dx and Ring Imaging Cerenkov counters are expected to work well over the CLEO-c momentum range. The electromagnetic calorimeter works well and has fewer photons to deal with at 3-5 GeV than at 10 GeV. Triggers will work as before. Minor upgrades may be required of the Data Acquisition system to handle peak data transfer rates. The conclusion is that, with the addition of the replacement wire chamber, CLEO is expected to work well in the 3-5 GeV energy range at the expected rates.

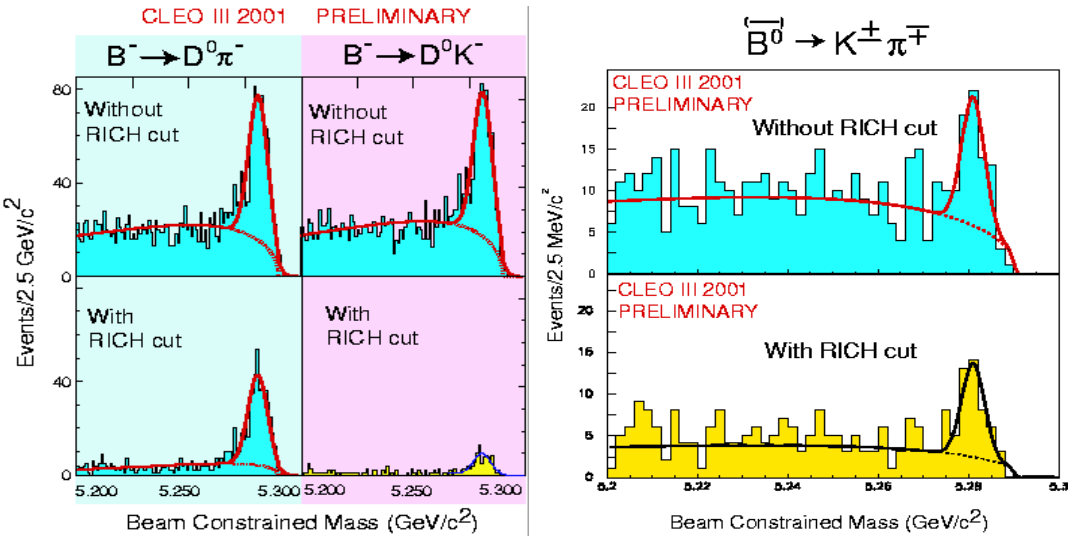

Figure 3: (Left) Beam constrained mass for the Cabibbo allowed decay $B \to D\pi$ and the Cabibbo suppressed decay $B \to DK$ with and without RICH information. The latter decay was extremely difficult to observe in CLEO II/II.V which did not have a RICH detector. (Right) The penguin dominated decay $B \to K\pi$. Both of these modes are observed in CLEO III with branching ratios consistent with those found in CLEO II/II.V.

2.3 Machine Conversion

Electron positron colliders are designed to operate optimally within a relatively narrow energy range. As the energy is reduced below design, there is a significant reduction in synchrotron radiation, which is the primary means of cooling the beam. In consequence, the luminosity drops, roughly as the beam energy to the fourth power. Without modification to the machine, CESR performance in the 3-5 GeV energy range would be modest, well below $10^{31}\mathrm{cm}^{-2}\mathrm{s}^{-1}$. CESR conversion to CESR-c requires 18 m of wiggler magnets, to increase transverse cooling, at a cost of $\sim$ \$4M. With the wigglers installed, CESR-c is expected to achieve a luminosity in the range $2 - 4 \times 10^{32}\mathrm{cm}^{-2}\mathrm{s}^{-1}$ where the lower (higher) luminosity corresponds to $\sqrt{s} = 3.1(4.1)\mathrm{GeV}$.

2.4 Examples of analyses with CLEO-c

The main targets for the CKM physics program at CLEO-c are absolute branching ratio measurements of hadronic, leptonic and semileptonic decays. The first of these provides an absolute scale for all charm and hence all beauty decays. The second

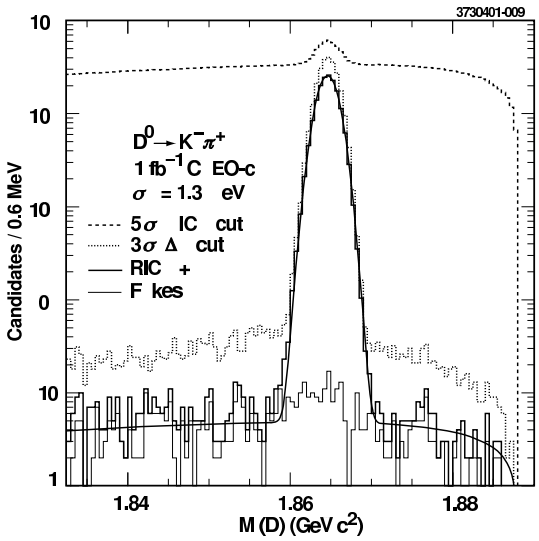

Figure 4: $K\pi$ invariant mass in $\psi(3770)\to D\overline{D}$ events showing a strikingly clean signal for $D\to K\pi$. The y axis is a logarithmic scale. The signal to background ratio is $\sim$ 5000/1.

measures decay constants and the third measures form factors and, in combination with theory, allows the determination of V_{cd} and V_{cs}.

Absolute branching ratios

The key idea is to reconstruct a D meson in any hadronic mode. This, then, constitutes the tag. Figure 4 shows tags in the mode $D\to K\pi$. Note the y axis is a log scale. Tag modes are very clean. The signal to background ratio is $\sim$ 5000/1 for the example shown. Since $\psi(3770)\to D\overline{D}$, reconstruction of a second D meson in a tagged event to a final state X, corrected by the efficiency which is very well known, and divided by the number of D tags, also very well known, is a measure of the absolute branching ratio $Br(D\to X)$. Figure 5 shows the $K^-\pi^+\pi^+$ signal from doubly tagged events. It is approximately background free. The simplicity of $\psi(3770)\to D\overline{D}$ events combined with the absence of background allows the determination of absolute branching ratios with extremely small systematic errors. This is a key advantage of running at threshold.

Leptonic decay $D_s\to\mu\nu$

This is a crucial measurement because it provides information which can be used to extract the weak decay constant, f_{D_s}. The constraints provided by running at threshold are critical to extracting the signal.

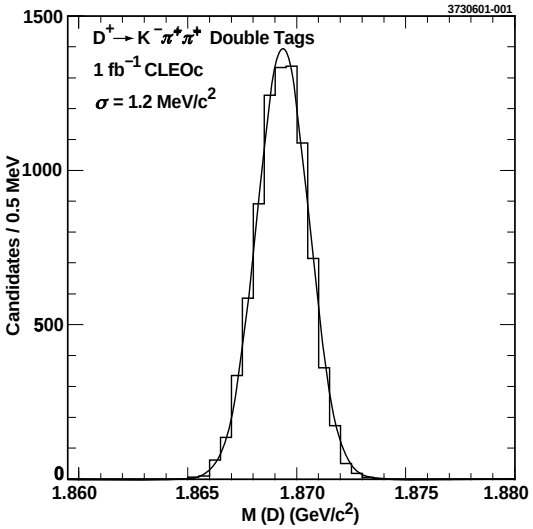

Figure 5: $K\pi\pi$ invariant mass in $\psi(3770)\to D\overline{D}$ events where the other D in the event has already been reconstructed. A clean signal for $D\to K\pi\pi$ is observed and the absolute branching ratio $Br(D\to K\pi\pi)$ is measured by counting events in the peak.

The analysis procedure is as follows:

1. Fully reconstruct one D_s, this is the tag.
2. Require one additional charged track and no additional photons.
3. Compute the missing mass squared (m_ν^2) which peaks at zero for a decay where only a neutrino is unobserved.

The missing mass resolution, which is of order $\sim m_{\pi^0}$, is sufficient to reject the backgrounds to this process as shown in Fig. 6. There is no need to identify muons, which helps reduce the systematic error. One can inspect the single prong to make sure it is not an electron. This provides a check of the background level since the leptonic decay to an electron is severely helicity-suppressed and no signal is expected in this mode.

Semileptonic decay $D\to\pi e^+\nu$

The analysis procedure is as follows:

1. Fully reconstruct one D, this constitutes the tag.
2. Identify one electron and one hadronic track.

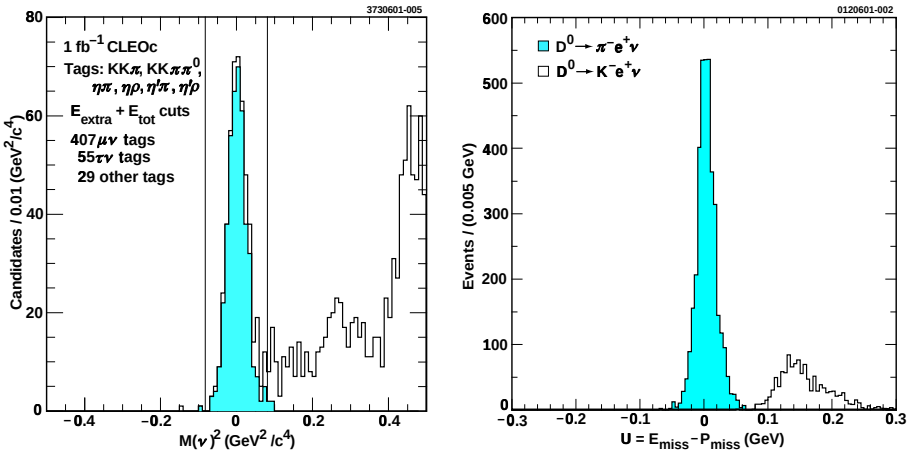

Figure 6: (Left) Missing mass squared for $D_s\overline{D_s}$ tagged pairs produced at $\sqrt{s} = 4100$ MeV. Events due to the decay $D_s \to \mu\nu$ are shaded. (Right) The difference between the missing energy and missing momentum in $\psi(3770) \to D\overline{D}$ tagged events for the Cabibbo suppressed decay $D \to \pi\ell\nu$ (shaded). The unshaded histogram arises from the ten times more copiously produced Cabibbo allowed transition $D \to K\ell\nu$ where the K is outside the fiducial volume of the RICH.

3. Calculate the variable, $U = E_{miss} - P_{miss}$, which peaks at zero when only a neutrino has escaped detection, which is the case for semileptonic decays.

Using the above procedure results in the right plot of Figure 6. With CLEO-c for the first time it will become possible to make precise branching ratio and absolute form factor measurements of every charm meson semileptonic pseudoscalar to pseudoscalar and pseudoscalar to vector transition. This will be a lattice validation data set without equal. Figure 7 shows the current precision with which the absolute semileptonic branching ratios of charm particles are known, and the precision attainable with CLEO-c.

2.5 Run Plan

CLEO-c must run at various center of mass energies to achieve its physics goals. The "run plan" currently used to calculate the physics reach is given below. This plan assumes CESR-c achieves design luminosity. Item 1 is prior to machine conversion, while the remaining items are post machine conversion.

1. 2002 : Υ's – 1-2 fb^{-1} each at $\Upsilon(1S), \Upsilon(2S), \Upsilon(3S)$
   Spectroscopy, electromagnetic transition matrix elements, the leptonic width. Γ_{ee}, and searches for the yet to be discovered h_b, η_b with 10-20 times the existing world's data sample. As of July 2002, most of this data has been collected.

Table 2: Summary of direct CKM reach with CLEO-c

Topic	Reaction	Energy (MeV)	L (fb^{-1})	current sensitivity	CLEO-c sensitivity
V_{cs}	$D^0 \to K\ell^+\nu$	3770	3	16%	1.6%
V_{cd}	$D^0 \to \pi\ell^+\nu$	3770	3	7%	1.7%

2. 2003 : $\psi(3770)$ – 3 fb^{-1}
   30 million events, 6 million tagged D decays (310 times MARK III)

3. 2004 : 4100 MeV – 3 fb^{-1}
   1.5 million D_sD_s events, 0.3 million tagged D_s decays (480 times MARK III, 130 times BES)

4. 2005 : J/ψ – 1 fb^{-1}
   1 billion J/ψ decays (170 times MARK III, 20 times BES II)

2.6 Physics Reach of CLEO-c

Tables 1, 2 , and 3, and Figures 7 and 8 summarize the CLEO-c measurements of charm weak decays, and compare the precision obtainable with CLEO-c to the expected precision at BABAR which expects to have recorded about 500 million charm pairs by 2005. While BABAR data allows improvement in the precision with which these quantities can be measured, CLEO-c clearly achieves far greater precision for many measurements. The reason for this is the ability to measure absolute branching ratios by tagging, and the absence of background at threshold. For charm quantities where CLEO-c is not dominant, it will remain comparable in sensitivity, and complementary in technique, to the B factories. Also shown in Table 3 is a summary of the data set size for CLEO-c and BES II at the J/ψ and ψ', and the precision with which R, the ratio of the e^+e^- annihilation cross section into hadrons to mu pairs, can be measured. The CLEO-c data sets are over an order of magnitude larger, the precision with which R is measured is a factor of three higher, in addition the CLEO detector is vastly superior to the BES II detector.

Taken together the CLEO-c datasets at the J/ψ and ψ' will be qualitatively and quantitatively superior to any previous dataset in the charmonium sector thereby providing discovery potential for glueballs and exotics without equal.

2.7 CLEO-c Physics Impact

CLEO-c will provide crucial validation of Lattice QCD, which will be able to calculate with accuracies of 1-2%. The CLEO-c decay constant and semileptonic data will

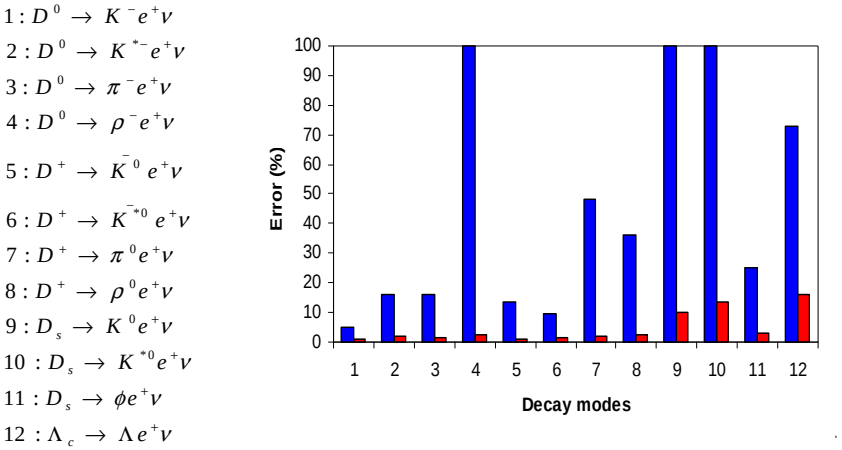

Figure 7: Absolute branching ratio current precision from the PDG (left entry) and precision attainable at CLEO-c (right entry) for twelve semileptonic charm decays.

Table 3: Comparision of CLEO-c reach to BABAR and BES

Quantity	CLEO-c	BaBar	Quantity	CLEO-c	BES-II
f_D	2.3%	10-20%	$\#J/\psi$	10^9	5×10^7
f_{D_s}	1.7%	5-10%	ψ'	10^8	3.9×10^6
$Br(D^0 \to K\pi)$	0.7%	2-3%	4.14 GeV	$1fb^{-1}$	$23pb^{-1}$
$Br(D^+ \to K\pi\pi)$	1.9%	3-5%	3-5 R Scan	2%	6.6%
$Br(D_s^+ \to \phi\pi)$	1.3%	5-10%			

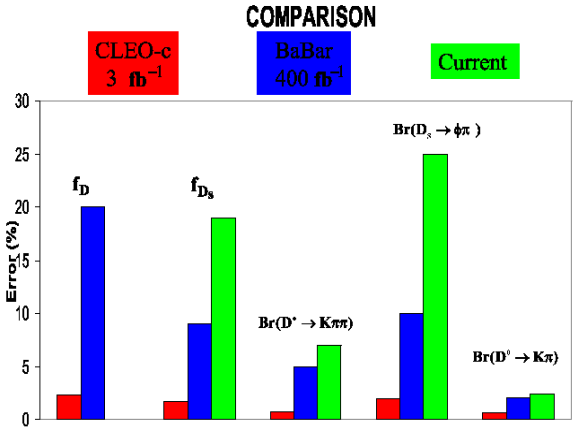

Figure 8: Comparison of CLEO-c (left) BABAR (center) and PDG2001 (right) for the charm meson decay constants and three important charm meson hadronic decay branching ratios.

provide a "golden", and timely test while CLEO-c QCD and charmonium data provide additional benchmarks. CLEO-c will provide dramatically improved knowledge of absolute charm branching fractions which are now contributing significant errors to measurements involving b's in a timely fashion. CLEO-c will significantly improve knowledge of CKM matrix elements which are now not very well known. V_{cd} and V_{cs} will be determined directly by CLEO-c data and LQCD, or other theoretical techniques. V_{cb}, V_{ub}, V_{td} and V_{ts} will be determined with enormously improved precision using B factory and Tevatron data, once the CLEO-c program of lattice validation is complete. Table 4 provides a summary of the situation. CLEO-c data alone will also allow new tests of the unitarity of the CKM matrix. The unitarity of the second row of the CKM matrix will be probed at the 3% level. CLEO-c data will also test unitarity by measuring the ratio of the long sides of the squashed cu triangle to 1.3%.

Finally the potential to observe new forms of matter; glueballs, hybrids, etc. in J/ψ decays and new physics through sensitivity to charm mixing, CP violation, and rare decays provides a discovery component to the program.

I would like to thank my CLEO colleagues for providing the opportunity to represent the collaboration at this conference. It is a privilege to be part of the CLEO collaboration. I thank Ikaros Bigi, Gustavo Burdman, Andreas Kronfeld, Peter Lepage, Zoltan Ligeti and Matthias Neubert for valuable discussions. Finally, I thank Nigel Lockyer and his support team for the superb organization of this conference.

Table 4: Current knowledge of CKM matrix elements (row one). Knowledge of CKM matrix elements after CLEO-c (row two). The improvement in the precision with which V_{cd} and V_{cs} are known is attainable with CLEO-c data combined with Lattice QCD. The improvement in precision with which V_{cb}, V_{ub}, V_{td}, and V_{ts} are known is obtained from CLEO-c validated Lattice QCD calculations and B factory and Tevatron data.

V_{cd}	V_{cs}	V_{cb}	V_{ub}	V_{td}	V_{ts}
7%	16%	5%	25%	36%	39%
1.7%	1.6%	3%	5%	5%	5%

References

[1] "CLEO-c and CESR-c : A New Frontier of Weak and Strong Interactions", CLNS 01/1742.

[2] "Report of Snowmass 2001 Working Group E2: Electron-positron Colliders for the phi to the Z", I. Shipsey on behalf of the E2 convenors, G. Burdman, J. Butler, I. Shipsey, and H. Yamamoto. Talk at the final plenary session of Snowmass, 2001. A written version of this talk is available as Z.Zhao hep-ex/0201047, to be published in *Proceedings of the 2001 DPF Snowmass Summer Study on the Future of Particle Physics.* 'All E2 working group talks (refs. 2-11) may be found at http://www.physics.purdue.edu/Snowmass2001_E2/

[3] "Another look at Charm: the CLEO-c physics program", M. Artuso, talk to the E2 Working Group.

[4] "CLEO-c and CESR-c : A New Frontier of Weak and Strong Interactions", I. Shipsey, talk to a joint E2/P2/P5 Working Group session.

[5] "Projected Non-perturbative QCD Studies with CLEO-c", S. Dytman, talk to the E4 Working Group.

[6] "CLEO-c and R measurements", L. Gibbons, talk to the E2 Working Group.

[7] "An Introduction to CLEO-c ", L. Gibbons, talk to the E2 Working Group.

[8] "CLEO-C reach in D meson Decays : Measuring absolute D meson branching fractions, D decay constants,and CKM matrix elements", D. Cassel, talk to the E2 Working Group.

[9] "Beyond the Standard Model: the clue from charm", M. Artuso, talk to the E2 Working Group.

[10] "A case for running CLEO-C at the ψ' ($\sqrt{s}$ = 3686 MeV)", S. Pordes, talk to the E2 Working Group.

[11] "Experimental Aspects of Tau Physics at CLEO-c", Y. Maravin, talk to the E2 Working Group.

B-physics and CP violation with LHCb

Giovanni Carboni
Università degli Studi di Roma "Tor Vergata" and INFN, Roma, Italy
Present address: CERN, Geneva, Switzerland

on behalf of the LHCb Collaboration

1 Physics motivation

The LHC machine will have a unique potential for the study of CP violation in the B system [1]. At $\sqrt{s} = 14$ TeV the B production cross-section is estimated to be around 0.5 mb, yielding about 10^{12} $b\bar{b}$ pairs per year at the modest luminosity of $2\ 10^{32}$ cm^{-2}s^{-1}.

LHCb is the only dedicated experiment designed to exploit this potential with an optimized detector, incorporating particle identification and vertex detector at trigger level [2]. LHCb can work for years at constant luminosity, independently from the other intersections, thus collecting clean events of constant quality.

Most of the Technical Design Reports (TDRs) for the various detector sub-systems have been approved [3], and construction of magnet and calorimeters has already started. The experiment is expected to begin operation at the LHC startup.

2 The Detector

A schematic drawing of the LHCb detector is shown in Fig. 1. It is a single-arm open spectrometer using a large dipole magnet for momentum measurement. This choice exploits the fact the B production is largest in the forward direction.

Immediately surrounding the interaction point there is the silicon Vertex Locator (VELO)[3]. The VELO is built in two halves, placed in "Roman Pots" on both sides of the beam, that can be moved close to it during data taking, or retracted during machine injection. Both halves accomodate 25 measuring stations, each made of two half-disks of 300 μm single-side Si sensors (120k channels), allowing the measurement of the r and ϕ coordinates, with stereo angle. To minimize the thickness of the wall separating the detectors from the machine vacuum, the detectors are operated under secondary vacuum. The VELO can measure decay lengths with accuracies from 220 to 375 μm, giving a sensitivity of 54 ps^{-1} for Δm_s.

The tracking system comprises a large aperture warm dipole magnet [3] ($\int Bdl \approx 4$ Tm) and nine tracking stations. To cope with the increasing particle density at small

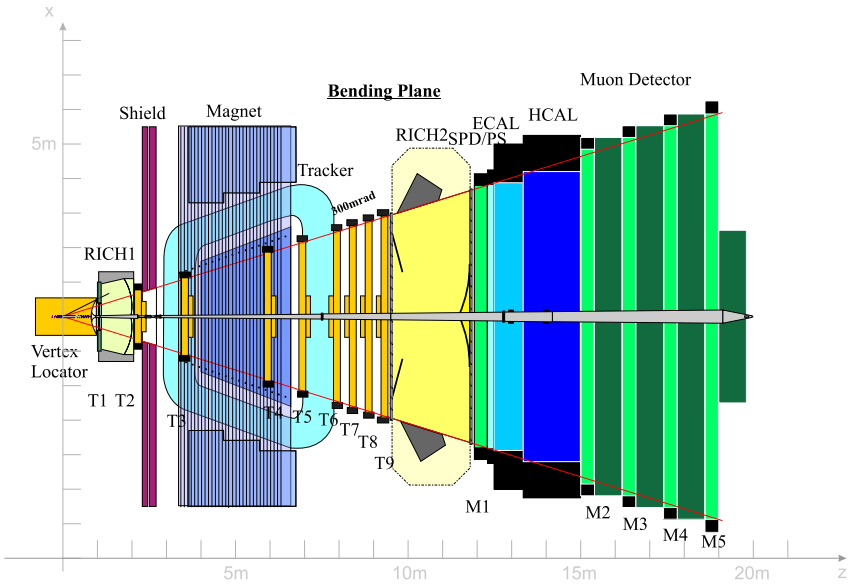

Figure 1: Schematic view of the LHCb detector.

angles, the tracker is divided into inner and outer subsystems. The outer part is built with 5 mm straw tubes, where the inner part uses Silicon strip detectors. The average momentum resolution is 0.3 % up to 200 GeV/c, yielding a mass resolution between 4 and 22 MeV/c^2. Prototypes of the straw tubes (3 m long) have been built and are under test in HERA-B [3].

Particle identification is provided by two RICH detectors [3], covering the momentum range from 1 to 100 GeV/c. In RICH1 (upstream the magnet), two radiators share the same photodetectors: silica Aerogel is effective in the region of momenta from $p \approx 1$ GeV/c to $p \approx 20$ GeV/c and C_4F_{10} gas covers up to $p \approx 65$ GeV/c. The forward (downstream) RICH2 uses CF_4 gas allowing $K - \pi$ separation up to 100 GeV/c.

The readout (400 kchannels) is based on hybrid photodiodes (HPDs). A 1024-pixel silicon sensor is enclosed in the tube envelope, with the binary readout chip bonded to it. This Pixel Chip, developed in collaboration with Alice, and fabricated in 0.25 μm technology, has a readout speed of 40 MHz.

The calorimeter system provides trigger and identification capabilities for electrons, photons and hadrons [3]. It comprises three main components: *i)* the Pb-scintillator Preshower detector (PS), *ii)* the Pb-scintillator "Shashlyk" electromagnetic calorimeter (ECAL) and *iii)* the Fe-scintillator tile calorimeter *à la* ATLAS for hadrons (HCAL). In all of these detectors WLS fibers are used to collect the light from the scintillator plates. Multi-anode photomultipliers are used in the Preshower readout.

The Muon Detector [3] comprises five stations (M1-M5), with M1 placed upstream the Preshower. Muons tracks are first identified in the M2-M4 stations, then the tracks are extrapolated to M1, to provide a measurement of p_T for the trigger. The system totals more than 1300 chambers of varying dimensions. About 2/3 of the chambers are MWPC type, with wire and/or cathode pad readout. Small wire-wire and wire-cathode spacing (1.5 mm and 2.5 mm respectively) ensure high efficiency within the 25 ns crossing. The remaining 1/3 chambers are RPCs, covering the regions with lower particle rates.

3 LHCb-light

Much work is being done to optimize the LHCb experiment by reducing the material budget in the tracking part of the detector from the 0.6 X_0 and 0.2 λ of the initial design. This will improve electron and photon detection and tracking efficiency. In the "LHCb-light" detector an Al-Be beam pipe will be used, and the number of VELO stations will be reduced from 25 to 21, with thinner Silicon sensors. For RICH1 a lighter, composite mirror, will be used. A more drastic change is the reduction in the number of tracking stations, by eliminating those inside the magnet. In the new design, three stations (ST1-ST3) are placed downstream the magnet. The technology of these stations will be like in the original design (straw tubes externally, Silicon strip detectors internally.) One more station (TT1) will be located between RICH1 and the magnet. This will consist of two measuring planes placed at short distance (about 30 cm.) The fringe field of the magnet is enough to allow momentum measurement at the trigger level (see below.) An adequate magnetic shielding for the photon detectors will be incorporated in the RICH1 design. The preferred technology for TT1 is Silicon. A new tracking strategy is being developed, and the results are promising.

The TDR for the light detector is in preparation.

4 The trigger

The ratio of the B cross-section to the total inelastic cross-section at LHC energies is expected to be $\simeq 5\ 10^{-3}$, implying in nominal working conditions a rate of 50 kHz of B events. This value is so large that even a perfect trigger picking up only B events would be insufficiently selective. Therefore the trigger system must be designed to enrich the sample with the desired decay modes.

The LHCb trigger is based on 4 levels [4]. Level 0 (L0) uses information from the calorimeters and muon detector to build a high-p_T trigger which is fully pipelined at 40 MHz with a fixed latency of 4 μs. The output rate of L0 trigger is ≈ 1 MHz.

Level 1 (L1) uses track and vertex topology distinct triggers implemented in a small CPU farm. Its maximum latency is 1.7 ms, and it reduces the rate to ≈ 40

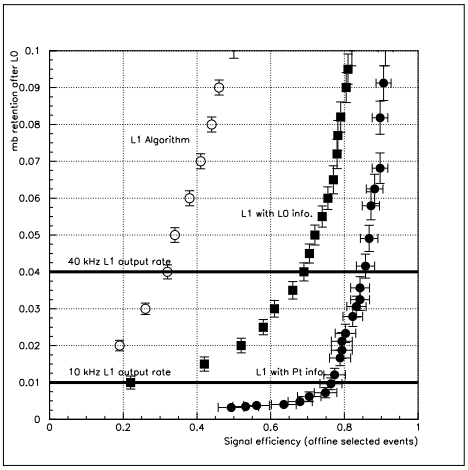

Figure 2: Minimum bias retention after L0 vs. efficiency for $B^0 \to \pi^+\pi^-$, normalized to events that would have been selected offline. Left: L1 algorithm [2]; center: with L0 information added, right: with p_T measurement (see text). L1 output rates (10 and 40 kHz) are shown.

kHz. The zero-suppressed data are sent to the DAQ farm after a positive L1 decision. Levels 2 and 3 perform further software selections finally rejecting uninteresting $b\bar{b}$ events, to achieve a final output rate of 200 Hz.

A recent development of L1 trigger uses the association of L0 candidates (in calorimeter and muon detectors) with L1 VELO tracks with large impact parameter. The $E_T(p_T)$ information from L0 improves significantly the performance of the L1 trigger. At 40 kHz output rate the efficiencies for $B^0 \to \pi^+\pi^-$ and $B^0 \to J/\psi\,(\mu^+\mu^-)K^0_S$ are about 70 % and 90% respectively (see Fig. 2.)

The fringing field of the magnet (about 1/10 of its peak value) makes possible to measure momentum with relative accuracy of 20% in a tracking station upstream the magnet. The improvement obtained in this way is also shown in Fig. 2. Station TT1 (see Section 3) will be optimized in order to use this information at L1. Preliminary results show that the efficiency for $B^0 \to \pi^+\pi^-$ is about 85% at 40 kHz output rate.

5 Physics performance

The primary goal of LHCb is to overconstrain the CKM matrix by measuring the angles and the sides of the unitarity triangle in several channels. LHCb is also naturally equipped to perform many cross-checks and control measurements to monitor and correct a variety of systematic effects. Table 1 summarizes the performance of LHCb for the measurements of the most important CKM parameters.

Table 1: LHCb physics performance summary for one year data taking at $L = 2\ 10^{32}\ \mathrm{cm}^{-2}\mathrm{s}^{-1}$

Observable	Channel	Events (*: tagged)	Physics Performance
β	$B_d \to J/\psi\, K^0_S$	$> 40\mathrm{k}^*$	$\sigma(\beta) = 0.6^o$
α	$B_d \to \pi^+\pi^-$	$4.9\mathrm{k}^*$	Theory dependent
	$B_d \to \rho\pi$	$1.3\mathrm{k}^*$	$\sigma(\alpha) = 5^o - 10^o$
γ	$B_d \to D^*\pi$	$530\mathrm{k}^*$	$\sigma(\gamma) \approx 10^o$
	$B_s \to D_s K$	$2.4\mathrm{k}^*$	$\sigma(\gamma) \approx 10^o$
$\delta\gamma$	$B_s \to J/\psi\, \phi$	370k	$\sigma(\delta\gamma) \simeq 2^o$
$\lvert V_{td}/V_{ts}\rvert$	$B \to \mu^+\mu^- X$	17k	11% rel. error
Δm_s	$B_s \to D_s\pi$	34 k	$\sigma(\Delta m_s) = 0.01\mathrm{ps}^{-1}$

6 Conclusion

LHCb can exploit at their best the physics possibilities offered by the LHC machine in the field of B physics. The detector is optimized for precision and statistics and can operate on LHC for many years, in stable and optimal luminosity conditions. LHCb has an efficient and robust trigger that gives access to a very large spectrum of decay channels. Particle identification, indispensable to study some channels, is effective over all the momentum spectrum and gives the experiment enhanced flexibility.

References

[1] Proceedings of the 1999 CERN Workshop on Standard Model Physics (and more) at the LHC. G. Altarelli and M. Mangano editors, CERN-2000-004, 2000.

[2] LHCb Technical Proposal, CERN/LHCC 98-4, 1998.

[3] The approved Technical Design Reports for Magnet, Calorimeters, Muon System, Outer Tracker, RICH and Online System can be found on *http://lhcb.web.cern.ch/lhcb/TDR/TDR.htm*.

[4] F. Teubert, Proc. 3rd International symposium on LHC physics and detectors, Chia, 2001 (to be published in EPJdirect) and references therein.

The BTeV experiment at the Tevatron collider

Jianchun Wang representing the BTeV Collaboration
Department of Physics
Syracuse University
Syracuse, NY 13244

1 Physics Motivation

The BTeV experiment is designed to study beauty and charm physics at the Fermilab Tevatron collider. Our goals are to make an exhaustive search for physics beyond the Standard Model (SM) and make precise measurements of the SM parameters. The important measurements to make involve CP violation, mixing, and rare decays of hadrons containing b or c quarks.

The CP violation in the SM originates from quark mixing with complex terms in the CKM matrix. The unitarity of the CKM matrix allows us to construct 6 triangles. The most commonly used triangle arises from the orthogonality of the d and b columns: $V_{ud}^* V_{ub} + V_{cd}^* V_{cb} + V_{td}^* V_{tb} = 0$, which defines the the CKM phases α, β and γ with the constraint that $\alpha + \beta + \gamma = \pi$. Other independent angles are χ and χ' where:

$$\chi = arg\left(-\frac{V_{cs}^* V_{cb}}{V_{ts}^* V_{tb}}\right), \quad \chi' = arg\left(-\frac{V_{ud}^* V_{us}}{V_{cd}^* V_{cs}}\right).$$

While α, β and γ maybe relatively large, the angle χ is small, and χ' is even smaller. One goal of the BTeV experiment is to measure the CKM phases: α, β, γ and χ.

We usually measure a trigonometric function of the angles. For example, the decay $B^\circ \to J/\psi K_s$ measures $\sin(2\beta)$. There is a 4-fold ambiguity generated by conversion from $\sin(2\beta)$ to β. The ambiguity can be reduced by finding $\cos(2\beta)$.

Inconsistencies in determinations of CKM parameters using different physics processes may also reveal new physics. One good candidate is the decay mode $B^\circ \to \phi K_s$. The CP asymmetry in the SM for this mode is the same as for $B^\circ \to J/\psi K_s$. In models containing new physics both the mixing amplitude and the decay amplitude can be modified by new phases. However, the $J/\psi K_s$ decay being tree level does not usually pick up any new phase, while the loop level ϕK_s decay is likely to have a new phase. Then the CP asymmetry in $B^o \to J/\psi K_s$ becomes proportional to $\sin(2\beta + \theta_D)$, while in $B^o \to \phi K_s$ we have $\sin(2\beta + \theta_D + \theta_A)$. Thus a measurement of the difference in CP asymmetries between these two modes would definitively demonstrate new physics and measure the decay phase θ_A of the new physics [1].

The angle χ can be extracted by measuring the time dependent CP violation asymmetry using CP eigenstates in B_s decay modes. Silva and Wolfenstein [2, 3] show that the χ measurement is a critical check to the SM by seeing if

$$\sin\chi = \left|\frac{V_{us}}{V_{ud}}\right|^2 \frac{\sin\beta \ \sin\gamma}{\sin(\beta+\gamma)} \quad .$$

The BTeV can measure χ in the decay modes $B_s \to J/\psi\eta^{(\prime)}$, where $\eta \to \gamma\gamma$ and $\eta' \to \rho^\circ\gamma$, or $\pi^+\pi^-\eta$. Since χ is very small (≈ 0.03), we need several years data collection to have a reasonable precise measurement.

2 The One-arm Spectrometer

The BTeV detector is an one-arm spectrometer covers the angular region between 10-300 mrad with respect to the beam as shown in Fig. 1. It fully exploits two advantages of the "forward" direction: the correlation in the direction of the $b\bar{b}$ pair produced, and the boost that allows an easier identification of detached vertices. This provides efficient flavor tagging and sensitivity to a great variety of heavy flavor decays.

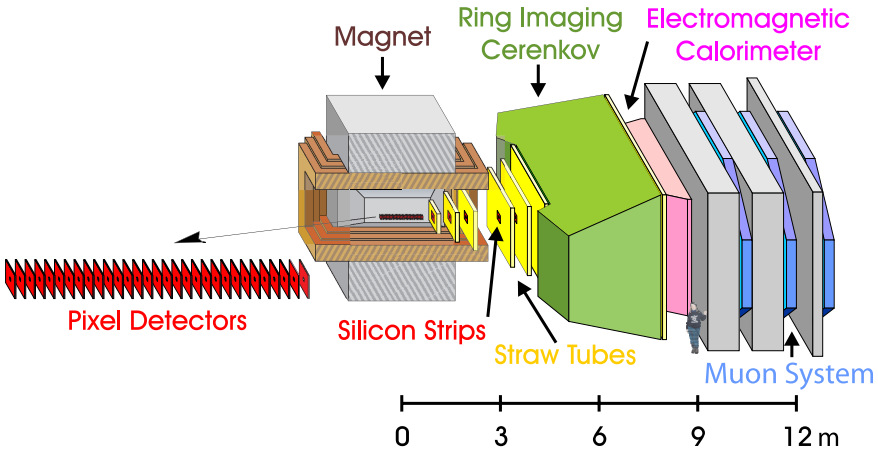

Figure 1: Layout of the BTeV spectrometer.

The spectrometer consists of: a planar precision vertex detector made from silicon pixels, a forward tracking system comprised of silicon strips near the beam and straw tube chambers at larger radius, a Ring-Imaging Cherenkov Detector (RICH), an $PbWO_4$ electromagnetic calorimeter, a muon system, and a deadtimeless trigger and DAQ system. Here we will give a brief description on some key sub-detectors. More information can be found elsewhere [4].

The pixel vertex detector locates inside an 1.6 Tesla dipole magnetic field [5]. It provides accurate vertex information for offline analysis, and delivers very clean,

precision space points to the vertex trigger. The pixel vertex detector consists of 30 stations of doublets along the beam direction, with pixel size $50 \times 400 \mu m^2$. The pixel geometry is chosen to provide excellent signal-to-noise, spatial resolution, high speed and low occupancy. A beam test of prototype pixel detectors had been carried on in 1999-2000 at Fermilab. The resolution is excellent, better than the 9 μm requirement [6]. A simulation package describes the detector performance quite well [7].

The BTeV RICH detector is designed to separate $\pi/K/p$ in a momentum range of 3 to 70 GeV [8]. It is essential to CP violation studies, providing separation of specific final states, such as $K^+\pi^-$ from $\pi^+\pi^-$, and flavor tagging. The RICH detector is also a fine supplement to the electromagnetic calorimeter and the muon detector in lepton identification. It increases significantly the reconstruction efficiency in interesting modes like $B^\circ \to J/\psi K_s$. We use freon (C_4F_{10}) gaseous radiator to generate Cherenkov light in the optical frequency range. The light is focused by mirrors onto Hybrid Photo-Diode (HPD) tubes at upstream. To separate kaons from protons below the threshold of gaseous radiator, an liquid radiator (C_5F_{10}) is used and the light is focused onto the side of the vessel and detected by PMT array.

BTeV uses radiation hard lead tungsten scintillation crystals ($PbWO_4$) to detect photons and electrons [9]. The crystals are 220 mm long (25 X_0) and have very small transverse cross-section ($\approx 28 \times 28 mm^2$), providing excellent segmentation. The light is collected by PMT. Sample crystals were tested in a beam at Protvino, Russia. The energy and position resolutions were demonstrated to be excellent.

With a nominal luminosity of $2 \times 10^{32} cm^{-2} s^{-1}$, the Tevatron delivers 2×10^{11} b-hadron per year. It is an ideal place for study of b-physics. It is also a severe challenge to the data acquisition (DAQ) system: Only a small portion of inelastic events are from heavy quarks, and the interaction rate is very high at the bunching spacing of 132 ns.

The BTeV trigger system mainly relies on the sophisticated detached vertex trigger, using lifetime to distinguish "B" events from others [10]. It uses hits provided by the pixel vertex detector. The parallel pipelines are implemented at Level 1, thus it is deadtimeless. At Level 2 and Level 3, there is much more time to have refined reconstruction. With the robust system, the total event rate is reduced from 7.6 MHz to 2 - 4 kHz. The trigger efficiency for a typical beauty decays is greater than 50%.

3 Physics Reach

We used GEANT-based Monte Carlo simulation to calculate the physics reach. A full pattern recognition was done at trigger level. Although there are fewer resources at this level than in offline analysis, the algorithm was demonstrated to have high efficiency and very few false tracks. For "offline" analysis, pattern recognition is not included since it has very little impact due to the excellent segmentation of the

Decay modes	# of Events	S/B	Parameter	Error or (Value)
$B^\circ \to \pi^+\pi^-$	14,600	3	Asymmetry	0.030
$B_s \to D_s^+ K^-$	7,500	7	γ	8°
$B^\circ \to J/\psi K_s$	168,000	10	$\sin(2\beta)$	0.017
$B_s \to D_s^+ \pi^-$	59,000	3	x_s	(75)
$B^- \to \overline{D}^\circ (K^+\pi^-) K^-$	170	1		
$B^- \to D^\circ (K^+K^-) K^-$	1,000	> 10	γ	13°
$B^- \to K_s \pi^-$	4,600	1		$< 4^\circ +$
$B^\circ \to K^+\pi^-$	62,100	20	γ	theory errors
$B^\circ \to \rho^+\pi^-$	5,400	4.1		
$B^\circ \to \rho^\circ \pi^\circ$	780	0.3	α	$\sim 4^\circ$
$B_s \to J/\psi\eta$	2,800	15		
$B_s \to J/\psi\eta'$	9,800	30	$\sin(2\chi)$	0.024

Table 1: BTeV physics reach in CKM parameters for 10^7s data

Decay modes	**BTeV** (10^7 **s**)			B**-factories (500 fb**$^{-1}$**)**		
	Yield	Tagged	S/B	Yield	Tagged	S/B
$B_s \to J/\psi\eta^{(\prime)}$	12,650	1,645	> 15	0		
$B^- \to \phi K^-$	6,325	6,325	> 10	700	700	4
$B^o \to \phi K_s$	1,150	115	5.2	250	75	4
$B^o \to K^{*o}\mu^+\mu^-$	2,530	2,530	11	$\sim$50	$\sim$50	3
$B_s \to \mu^+\mu^-$	6	0.7	> 15	0		
$B^o \to \mu^+\mu^-$	1	0.1	> 10	0		
$D^{*+} \to \pi^+ D^o$, $D^o \to K^-\pi^+$	$\sim 10^8$	$\sim 10^8$	large	8×10^5	8×10^5	large

Table 2: Reconstructed events in new physics modes for BTeV and e^+e^- B-factories

pixel detector. The charged tracks are fitted with Kalman filter. Realistic shower reconstruction, particle identification programs are also used. The results on CKM parameters for 10^7s running at nominal luminosity are shown in Table 1. The accuracies in all cases are quite promising.

The BTeV data samples will be large enough to test new physics. In Table 2 we list some of the event samples relevant to new physics studies with one "snow mass" year data collection. Also shown in comparison are samples from e^+e^- B factories that has 500 fb^{-1} accumulated data, approximately the expected amount when BTeV starts. The BTeV will easily surpass the e^+e^- B factories and also have accesses to the important CP violation measurements that need to be made in B_s modes.

The LHCb experiment will be the main competitor to the BTeV experiment. Compare to LHCb, BTeV has more robust trigger system that use detached vertex trigger at the first level. In the "golden" mode $B_s \to D_s K^-$ for γ measurement, although

LHCb has initial advantages in b cross-section, the yield and signal to background ratio are compatible between the two experiments. The BTeV possesses much better electromagnetic calorimeter. And thus it is superior in α measurement that relies on $B^\circ \to \rho^+\pi^-, \rho^\circ\pi^\circ$ decay modes.

4 Conclusions

Many R&D activities are going on. Test beam runs at Fermilab with the Pixel and Muon systems and at Protvino with the EM calorimeter have been very successful and will continue. System tests on RICH, straws and silicon will be carried out soon. Progress has been made on the trigger and DAQ. We have received IT funding from the NSF to develop fault-tolerant, fault-adaptive software to control the trigger system in real time. This is named "The Real Time Embedded Systems" (RTES) project.

I quote the PAC recommendation here as conclusion: "... BTeV has designed and prototyped an ambitious trigger that will use B decay displaced vertices as its primary criterion. This capability, together with BTeV's excellent electromagnetic calorimetry and particle ID and enormous yields, will allow this experiment to study a broad array of B and B_s decays. BTeV has a broader physics reach than LHCb and should provide definitive measurements of CKM parameters and the most sensitive tests for new physics in the flavor sector."

References

[1] Y. Nir, arXiv:hep-ph/9911321.

[2] J. P. Silva and L. Wolfenstein, Phys. Rev. D **55**, 5331 (1997).

[3] R. Aleksan, B. Kayser and D. London, Phys. Rev. Lett. **73**, 18 (1994).

[4] J. C. Wang, Int. J. Mod. Phys. A **16S1C**, 1062 (2001).

[5] S. Kwan [BTeV Collaboration], Nucl. Instrum. Meth. A **408**, 235 (1998).

[6] J. A. Appel *et al.*, Nucl. Instrum. Meth. A **485**, 411 (2002).

[7] M. Artuso and J. C. Wang, Nucl. Instrum. Meth. A **465**, 115 (2000).

[8] T. Skwarnicki [BTeV Collaboration], Nucl. Instrum. Meth. A **408**, 204 (1998).

[9] S. R. Menary [BTeV Collaboration], Nucl. Instrum. Meth. A **446**, 253 (2000).

[10] P. Lebrun, Int. J. Mod. Phys. A **16S1C**, 1153 (2001).

The Super B Factory

David G. Hitlin
Department of Physics
California Institute of Technology
Pasadena, CA 91125 USA

1 Introduction

This contribution addresses the future of the study of quark physics in e^+e^- annihilation, at the $\Upsilon(4S)$and $\Upsilon(5S)$, over the next decade and beyond. A more detailed treatment can be found in Ref. [1].

The search for new physics in the quark sector involves direct searches for new particles (*e.g.* squarks), precise tests of standard model predictions for rare decay branching fractions and decay distributions to search for new amplitudes in loop processes, and overconstrained tests of the CKM matrix. A very high luminosity asymmetric B Factory can make unique contributions to these studies, as well as providing capabilities complementary to those of experiments at hadronic machines.

2 Physics Motivation and Capability

Precision tests of CKM unitarity require the percent level precision on the measurement of sin2β obtainable at a 10^{36} asymmetric B Factory as well as the several percent precision obtainable on sin2α and sin2γ with very large samples of rare hadronic B decays. In particular, measurements of the separate branching ratios of $B(B^0 \to \pi^0\pi^0)$ and $B(\overline{B}^0 \to \pi^0\pi^0)$ decays, possible only at an e^+e^- B Factory, are vital to obtain a precise value of α with minimal theoretical assumptions [2],[3]. Taken together with concomitant improvements in our understanding of the magnitudes of CKM matrix elements, which require new techniques involving tagging and exclusive reconstruction of B semileptonic decays, as well as anticipated improvements in lattice gauge calculations, this program is capable of tests of CKM unitarity of exquisite precision. Measurements of the third angle γ are difficult, but can be done to excellent precision at a 10^{36} machine, both by the comparison of $b\to c\bar{u}s$ and $b\to u\bar{c}s$ decays using $B\to DK$ transitions at the $\Upsilon(4S)$[4], and measurements of $B_s\to D^{(*)\pm}K^{(*)\mp}$ decays at the $\Upsilon(5S)$ [5].

Table 1 summarizes the precision obtainable on the angles of the unitarity triangle at an experiment with 500 fb^{-1} and 10 ab^{-1}, corresponding to 1 year of running at

CKM Angle	*BABAR* (0.5 ab^{-1})	Super*BABAR* (10 ab^{-1})	BTeV†	LHCb	Atlas/CMS
sin2β ($B^0 \to J/\psi K^0_S$)	0.037	0.008	0.025	0.014	0.021/0.025
sin2β ($B \to \phi K_s$)	0.25	0.056			
sin2α ($B^0 \to \pi^+\pi^-$)	0.14	0.032	0.024	0.056	0.10/0.17
$\alpha_{\rm Eff.} - \alpha$ ($B^0 \to \pi^0\pi^0$)	$< 18°$	$< 7°$	-	-	-
sin$(2\beta + \gamma)$ ($B^0 \to D^*\pi$)	0.15	0.03			
γ ($B \to DK$)	-	$< 2.5°$	$< 10.0°$	$< 19.°$	
γ ($B_s \to D_s K$)	-	$< 15°$	$< 7.0°$	$< 13.°$	

‡Two armed version of BTeV

Table 1: Summary of the estimated precision of CKM angle measurements for both *BABAR* and Super*BABAR*, compared to planned experiments at hadronic colliders.

10^{36} luminosity, with that obtainable with planned and proposed experiments at hadronic colliders. The determination of γ using the $\Upsilon(5S)$ requires a separate data set of 1 ab^{-1}. In general, multiple complementary measurements of the CKM angles are possible. The 10^{36} collider has the capability to measure all three *CP*-violating angles of the unitarity triangle to the level warrented by the precision of theoretical calculations.

Table 2 compares the sensitivity of experiments with 500 fb^{-1}, the target total sample for *BABAR*, and with 10 ab^{-1}, corresponding to 1 year of running at 10^{36} luminosity, with that obtainable with planned and proposed experiments at hadronic colliders. The 10^{36} collider compares quite favorably with hadronic experiments, in rare inclusive and exclusive modes, and particularly in radiative modes. Note also that only an e^+e^- experiment can produce a sample of tagged decays.

3 SuperPEP-II

The next generation asymmetric B Factory requires a significant increase in luminosity, approaching 10^{36}cm^{-2}s^{-1}, well beyond the already record-setting performance of PEP-II and KEKB. It appears that such a luminosity is feasible; initial parameters of SuperPEP-II, a very high luminosity asymmetric B Factory are being developed, incorporating several new ideas from the successful operation of the present generation accelerators. In this regime, the luminosity lifetime is primarily determined by the collisions themselves, and is typically a few minutes, requiring continuous injection. This has a positive consequence: the ratio of average to peak luminosity in SuperPEP-II can be increased by 30% due to continuous injection, thereby directly improving the ability to integrate luminosity. In fact, with continuous injection, the standard "Snowmass Year" factor should be increased by 30%. With continuous injection, the operation of this accelerator will be qualitatively different from present colliders.

The next generation asymmetric B Factory will operate mainly at the $\Upsilon(4S)$with

		Hadron Collider Experiments			e^+e^- B Factories	
Decay Mode	Branching Fractions	**CDF D0** (2 fb^{-1})	**BTeV† LHCb** (10^7 s)	**ATLAS CMS** (1 Year)	***BABAR* BELLE** (0.5 ab^{-1})	**10^{36}** (10 ab^{-1})
$B \to X_s\gamma$	$(3.3 \pm 0.3) \times 10^{-4}$				11K	220K
					1.7K (B Tagged)	34K (B Tagged)
$B \to K^*\gamma$	5×10^{-5}	170	25K		6K	120K
$B \to \rho(\omega)\gamma$	2×10^{-6}				300	6K
$B \to X_s\mu^+\mu^-$	$(6.0 \pm 1.5) \times 10^{-6}$		3.6K		300	6K
$B \to X_s e^+e^-$					350	7K
$B \to K^*\mu^+\mu^-$	$(2 \pm 1) \times 10^{-6}$	60-150	2.2K/4.5K	665/4.2K	120	2.4K
$B \to K^* e^+e^-$					150	3K
$B \to X_s\nu\overline{\nu}$	$(4.1 \pm 0.9) \times 10^{-5}$				8	160
$B \to K^*\nu\overline{\nu}$	5×10^{-6}				1.5	30
$B_d^0 \to \tau^+\tau^-$	10^{-7}					
$B_s^0 \to \mu^+\mu^-$	10^{-9}	5/1.5-6	5/11	9/7		
$B_d^0 \to \mu^+\mu^-$	8×10^{-11}	0/0	1/2	0.7/20		
$B \to \tau\nu$	5×10^{-5}				17	350
$B \to \mu\nu$	1.6×10^{-7}				8	150
$B^0 \to \gamma\gamma$	10^{-8}				0.4	8
†Two armed version of BTeV						

Table 2: Reconstructed rare B decays in hadronic and e^+e^- experiments

a center-of-mass energy of 10.58 GeV, with an energy asymmetry a bit smaller than currently used; a period of operation at the $\Upsilon(5S)$ may also be desirable. For the present study the PEP-II tunnel geometry was used, with beam energies of 7.47 and 3.73 GeV, as a reduced energy asymmetry considerably reduces RF costs and power consumption. To increase the luminosity about two orders of magnitude the beam currents must be raised an order of magnitude and the beam cross sectional area reduced an order of magnitude while keeping the beam-beam tune shifts under control. The parameters shown in Table 3 are self-consistent but further optimization is certainly possible [6].

The observed beam-beam tune shifts in PEP-II now approach 0.07. The expected tune shifts in this new accelerator could be larger. It has been observed in PEP-II that by adjusting the tunes the luminosity can be increased significantly 10% at the expense of the beam lifetime. (This beam lifetime will be called the beam-beam lifetime.) Higher luminosity for the same current means higher tune shifts. The new accelerator can take advantage of continuous injection to push the tune shifts to significantly higher values and consequently the beam-beam lifetimes to significantly lower values. The beam-beam lifetime in present colliders is about 100 minutes. The design assumption is that the tune shifts can be increased from 0.07 to at least 0.10 by reducing the beam-beam lifetime from 100 minutes to $\sim$5 minutes.

The interaction region will likely have a geometry that combines the best features of the PEP-II and KEK-B designs [7]. The cone angle separating the accelerator and

	SuperHER	SuperLER
Beam energy (GeV)	7.47	3.73
Beam current (A)	11	22
Number of bunches	7000	
Bunch length	1.7	
Beam lifetime τ_b (min)	5	3
$\beta^*(x/y)$ (mm)	15	1.5
Emittance (x/y) (nm)	44	0.44
Beam size at IP (x/y) (μm)	81	0.8
Beam-beam tune shifts	0.10	
RF frequency (MHz)	956	
Luminosity ($cm^{-2}s^{-1}$)	10^{36}	

Table 3: Parameter list for a 10^{36} collider in the PEP-II tunnel at SLAC.

detector components can be about 300 mrad, as at present. The LER quadrupoles for this accelerator can be moved significantly closer to the IP than in PEP-II using superconducting Q1 and Q2 magnets with stronger gradients, such as those used in the HERA upgrade [8]. The HER quadrupoles can also be moved closer because the LER quadrupoles have been moved. A crossing angle of about 1.5 mrad is used to help separate the beams at the first parasitic beam-beam crossing. The beams are horizontally separated by about 12 σ_x at the first parasitic crossing.

The HER vacuum system must dissipate over 16 kW/m of synchrotron radiation power. The chambers will likely be made with an antechamber with a continuous built-in photon stop. The design of bellows (expansion) modules would be very difficult for these high currents and short bunch lengths. Instead, the plan is to use a concept investigated for the PEP-II rings but not implemented. The vacuum system would be a continuous extrusion welded together with no bellows but with rigid supports to constrain thermal stresses. A similar technique is used to build very long welded railroad tracks. The beam impedance will improve without bellows. The stainless steel chambers in the straight sections will have to be changed to a lower resistance material to reduce the resistive wall effect for the LER.

Injection must be a continuous process because the beam lifetimes are short. Taking the SLAC site, the beams would come from the damping ring and linac complex. The SLAC system was built to provide about 1×10^{11} electrons per pulse at 120 Hz and about half that rate for positrons. The damping ring cavity RF frequency will be changed from 714 MHz to 476 MHz. In the damping rings, the particle bunches will be distributed uniformly over about half the circumference (35 m) in about 30 bunches. The other half of the ring circumference is used by the injection and extraction kicker rise times. The linac can operate at 120 Hz. The electron injection rate

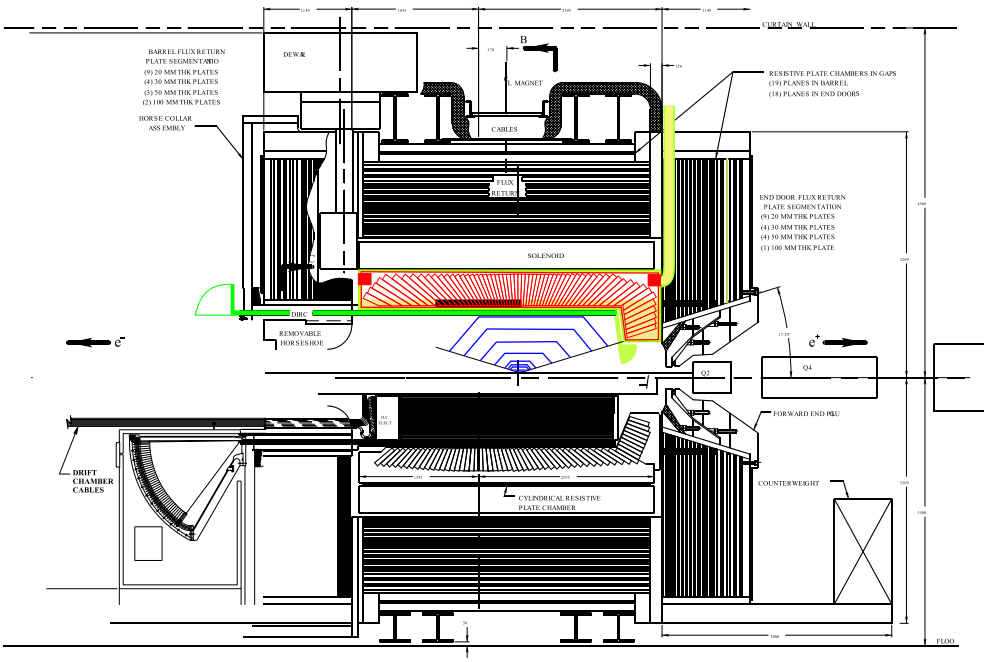

Figure 1: Elevation view of an upgraded *BABAR* detector designed for a 10^{36} collider. The upper half shows the new components, the lower half, the existing detector.

would likely be 80 Hz, the positron injection rate 20 Hz and the remaining 20 Hz used for positron production. Injection losses can cause detector problems. However, the damped injected beam will have transverse emittances smaller than the stored beam emittances. The linac bunch length and energy spread are well matched to the stored bunches, promising a relatively clean injection process. As some injection collimation will likely be needed, however, the injection efficiencies were assumed to be 75%.

4 Super*BABAR*

Doing a precision experiment at a 10^{36} asymmetric B Factory requires a new or upgraded detector to cope with backgrounds and radiation levels. Studies at Snowmass indicate that this is a tractable problem. There appears to be a feasible upgrade path from the existing *BABAR* detector, which is sketched in Fig. 1. This approach would retain the existing 1.5 T superconducting solenoid and flux return, as well as the instrumented flux return detectors, which will be upgraded over the next several years. The electromagnetic calorimeter would be based on scintillation light from liquid xenon, the vertex measurement and tracking would be done by a combination of two pixel detector layers and approximately seven double-sided silicon strip layers. The DIRC particle identification system would be rebuilt to do away with the large

water-filled stand-off box, which is a large source of background. R&D efforts on liquid xenon scintillation calorimetry and on a new readout scheme for the DIRC are getting underway.

A straightforward extension of the open trigger approach traditionally employed in experiments appears to be quite practical. Techniques for detector readout pioneered for the new generation of experiments at the Tevatron and LHC appear to be generally applicable to a 10^{36} storage ring, allowing unbiased triggering on essentially all events of interest.

5 Conclusion

In summary, the physics case for a 10^{36} asymmetric B Factory is quite strong. The program has many unique aspects and is complementary to the programs at hadronic machines. The details of machine and detector design are far from mature, but both machine and detector appear to present reasonable challenges. Undoubtedly, developments in both theory and experiment over the next several years will sharpen our vision and allow a clearer determination of the importance of pushing flavor physics investigations to this new level in rare decays and precision measurements.

References

[1] *Physics at a* 10^{36} *Asymmetric B Factory*, SLAC-PUB-8970, Aug. 2001. Proceedings of the 2001 DPF Snowmass Summer Study on the Future of Particle Physics.

[2] M. Gronau and D. London, *Phys. Rev. Lett.* **65**, 3381 (1990).

[3] M. Gronau and D. Wyler, *Phys. Lett.* **B265**, 172, (1991).

[4] A. Soffer, *Phys. Rev.* **D60**, 54032 (1999).

[5] S. Petrak, *Proceedings of the 4th International Conference on B Physics and CP Violation*, Ise (2001).

[6] J. Seeman, *Initial Parameters for a* 10^{36} $cm^{-2}s^{-1}$ *Luminosity B Factory*, SLAC-PUB-8787, March 2001. J. Seeman, *Higher Luminosity B Factories*, Proceedings of 2001 IEEE Particle Accelerator Conference,(PAC 2001) Chicago , 305.

[7] M. Sullivan, private communication.

[8] B. Parker *et al.*, *Superconducting Magnets for use inside the HERA ep Interaction Regions*, Proceedings of 1999 IEEE Particle Accelerator Conference,(PAC 1999) New York , 308.

May 18, session 1.

Session Chair: K. Abe

Neutrino and Kaon Physics

Rare Kaon Decays: Progress and Prospects

D. Bryman

Rare Kaon Decays: Progress and Prospects

Douglas Bryman
Department of Physics and Astronomy
University of British Columbia
6224 Agricultural Road, Vancouver, B.C. V6T 1Z1, Canada

1 Introduction

There is a large overlap in the current physics motivation for investigating B-meson and K-meson decays. The much newer and heavier b quark opens many possibilities for studying interesting decay channels with fascinating phenomenologies of mixing, oscillations, and CP violation. In the past year the promise of revealing the origin of CP violation has begun to be realized in pioneering experimental studies at e^+e^- colliders. The asymmetries observed in $B \to \Psi K_S$ decays by BABAR and BELLE provide the first conclusive evidence for CP violation outside the neutral K system.

K decays, a much older game, have long been a gold mine of surprising information at the forefront of particle physics. K decay experiments opened the doors to quark mixing and CP violation. In the intervening years, the effort to establish consistency with the Standard Model (SM) description involving direct CP violation was a protracted battle. Nevertheless, KTEV[1] and NA48[2] finally agreed on evidence for direct CP violation through consistent non-zero values of ϵ'/ϵ in $K \to \pi\pi$ decays. However, as with many approaches to CP violation involving K and B decays, the underlying short distance physics is not easy to get at due to complications associated with strong interactions including penguin diagram processes.

The CP-violating asymmetry in $B \to \Psi K_S$ decays which determines $sin(2\beta)$, and the ratio of B_s/B_d mixing (x_s/x_d) which yields $|\frac{V_{ts}}{V_{td}}|$ stand out as theoretically unambiguous quantities, relatively free from strong interaction uncertainties. Together they can cleanly determine the apex of the usual unitary triangle giving a powerful test of the consistency of the SM. $sin(2\beta)$ is becoming known to increasing precision as discussed at this conference and there is optimism that B_s mixing will be measured in Run II at the Tevatron, although extracting $|V_{td}|$ is subject to some uncertainty due to SU(3)-breaking effects.

During the past few years the state-of-the-art in rare K decays has reached single event sensitivities of 10^{-12} in experiments at the Brookhaven National Laboratory (BNL) Alternating Gradient Synchrotron (AGS). BNL E871 reported 6200 events of $K_L^0 \to \mu^+\mu^-$ decay at the 10^{-8} level[3] and 4 events of $K_L^0 \to e^+e^-$ at 10^{-11}[4]. Two

events were observed by BNL E787 with the kinematically incomplete $K^+ \to \pi^+ \nu\overline{\nu}$ signature at the 10^{-10} level[5]. These successes have opened up the possibility of fully accessing the "dynamic duo" of $K^+ \to \pi^+ \nu\overline{\nu}$ and $K_L^0 \to \pi^0 \nu\overline{\nu}$ which offer the best possibilities for obtaining high quality information on short distance physics, complementary and comparable in precision to the leading approaches using B mesons.

The observation of $K^+ \to \pi^+ \nu\overline{\nu}$ by E787 is consistent with the SM expectation. To fully explore the possibility of new physics or to make a precise measurement of the t-d quark coupling $|V_{td}|$, a new measurement has just commenced. E949 at the BNL AGS is designed to obtain sensitivity an order of magnitude below the SM prediction. Later in the decade, the CKM experiment[6] at Fermilab will begin to pursue $K^+ \to \pi^+ \nu\overline{\nu}$ at even higher precision.

The K sector can also yield the single most incisive measurement in the study of CP violation through a measurement of the branching ratio for $K_L^0 \to \pi^0 \nu\overline{\nu}$ decay. Within the SM context, this is a unique quantity which directly measures the area of the CKM unitarity triangles *i.e.* the physical parameter that characterizes all CP violation phenomena, or the height of the triangle shown in Fig. 1. The quest to observe $K_L^0 \to \pi^0 \nu\overline{\nu}$ is beginning in earnest with a pilot experiment at KEK (E391A) and the new KOPIO experiment at BNL. The measurements of $B(K^+ \to \pi^+ \nu\overline{\nu})$ and

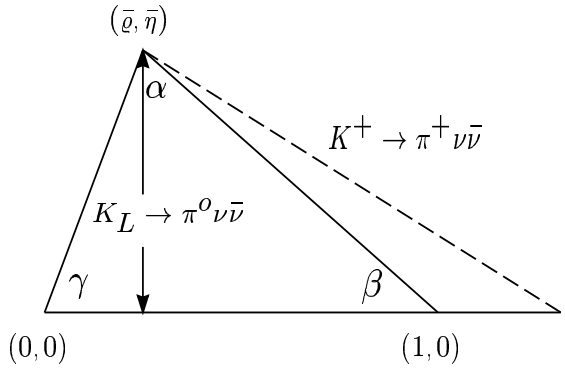

Figure 1: The unitarity triangle.

$B(K_L^0 \to \pi^0 \nu\overline{\nu})$ will result in a complete picture of SM CP violation in the K system and a comparison with comparably precise measurements anticipated from the B sector will be possible.

Other areas of current activity in the field of rare K decays include studies of radiative processes relevant to Chiral Perturbation Theory (CHPT) and searches for exotic reactions.

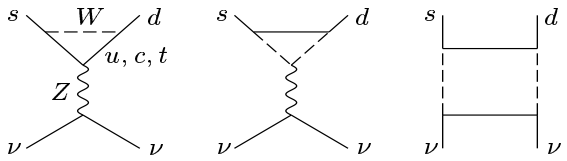

Figure 2: The leading electroweak diagrams inducing $K \to \pi\nu\overline{\nu}$ decays. For $K_L^0 \to \pi^0\nu\overline{\nu}$ only the top quark contributes.

2 THEORY OF $K \to \pi\nu\overline{\nu}$

While clean extraction of SM parameters from K decay observables like ϵ'/ϵ is presently precluded due to non-perturbative strong interaction uncertainties, $K^+ \to \pi^+\nu\overline{\nu}$ and $K_L^0 \to \pi^0\nu\overline{\nu}$ do not suffer from these maladies. In $K^+ \to \pi^+\nu\overline{\nu}$ and $K_L^0 \to \pi^0\nu\overline{\nu}$ decays, which arise at the one loop level in the SM as shown in Fig. 2, hadronic effects are well known from measurements of the similar decays K$\to\pi e\nu$ related by isospin[7]. The presence of the top quark in the loops makes these decays very sensitive to V_{td} [8] and the simple final states allow unusually precise calculations to be made. Small QCD corrections have been calculated to next-to-leading-logarithmic order [9]. Long distance effects are negligible in comparison with short distance effects. $K^+ \to \pi^+\nu\overline{\nu}$ is expected to occur with a branching ratio of $0.72 \pm 0.21 \times 10^{-10}$[10] with a purely theoretical uncertainty of about 7% due to a charm quark contribution to the loops.

$K_L^0 \to \pi^0\nu\overline{\nu}$ decay is unique in that it is completely dominated by direct CP violation [11]. Since K_L^0 is predominantly a coherent, CP odd superposition of K^0 and $\overline{K}^0$, only the imaginary part of $V_{ts}^* V_{td}$ survives in the amplitude. The lack of a significant charm quark contribution reduces the intrinsic theoretical uncertainty to $\mathcal{O}(2\%)$. Since the value of the sine of the Cabibbo angle is well known, $Im(V_{ts}^* V_{td})$ is equivalent to the Jarlskog invariant, $\mathcal{J} \equiv -Im(V_{ts}^* V_{td} V_{us}^* V_{ud}) = -\lambda(1-\frac{\lambda^2}{2}) Im(V_{ts}^* V_{td})$. $\mathcal{J}$ is equal to twice the area of any of the six possible unitarity triangles [12]. Since theoretical uncertainties are extremely small, measurement of $B(K_L^0 \to \pi^0\nu\overline{\nu})$ will provide the standard against which all other measures of CP violation will be compared, and even small deviations from the expectation derived from SM predictions or from other measurements, *e.g.* in the B sector, will unambiguously signal the presence of new physics. In the SM context the branching ratio for $K_L^0 \to \pi^0\nu\overline{\nu}$ is given by[13]

$$B(K_L^0 \to \pi^0\nu\overline{\nu}) = 1.8 \cdot 10^{-10} \left(\frac{Im(V_{ts}^* V_{td})}{\lambda^5}\right)^2 X^2(x_t) = 1.8 \cdot 10^{-10} \eta^2 A^4 X^2(x_t), \qquad (1)$$

where $X(x_t)$ is a kinematic function of the top quark mass. The branching ratio for $K_L^0 \to \pi^0\nu\overline{\nu}$ is expected to lie in the range $(2.6 \pm 1.2) \cdot 10^{-11}$. A clean measure of the height of the unitary triangle, η, is provided by the $K_L^0 \to \pi^0\nu\overline{\nu}$ branching ratio. All other parameters being known, Eq. 1 implies that the relative error of η is half

that of a measurement of $B(K_L^0 \to \pi^0 \nu\overline{\nu})$. Thus, for example, a 15% measurement of $B(K_L^0 \to \pi^0 \nu\overline{\nu})$ can, in principle, determine η to 7.5%.

Most forms of new physics [14, 15, 10] postulated to augment or supersede the SM have implications for B($K \to \pi\nu\overline{\nu}$). In minimal supersymmetry and in some multi-Higgs doublet models [16], the extraction of $\sin 2\alpha$ and $\sin 2\beta$ from CP asymmetries in B decays would be unaffected. Such effects might then show up in a comparison with $K_L^0 \to \pi^0 \nu\overline{\nu}$, where, e.g., charged Higgs contributions modify the top quark dependent function in $B(K_L^0 \to \pi^0 \nu\overline{\nu})$. In other new physics scenarios, such as supersymmetric flavor models [17], the effects in $K \to \pi\nu\overline{\nu}$ tend to be small, while there can be large effects in the B (and also the D) system. In these models the rare K decays are the only clean way to measure the true CKM parameters. Examples of new physics scenarios that show large deviations from the SM in $K \to \pi\nu\overline{\nu}$ are provided by some extended Higgs models, in topcolor-assisted technicolor models [18], in left-right symmetric models [19], in models with extra quarks in vector-like representations [15], lepto-quark exchange [15], and in 4-generation models [20]. The confirmation of a relatively large value for ϵ'/ϵ has focussed attention on the contributions of flavor-changing Z-penguin diagrams in generic low-energy supersymmetric extensions of the SM [13]. Such diagrams can interfere with the weak penguins of the SM, and either raise or reduce the predicted $B(K_L^0 \to \pi^0 \nu\overline{\nu})$ by considerable factors. The effects of SUSY and other non-SM approaches on the K and B system generally turn out to be different and apparent discrepancies between measurements of SM quantities would be indications of new physics.

3 Measurement of $K^+ \to \pi^+ \nu\overline{\nu}$

The final results from BNL E787 reported recently[5] were based on observations of decays of 5.9×10^{12} K mesons at rest. Measurement of the $K^+ \to \pi^+ \nu\overline{\nu}$ decay involves only the π^+ track and π^+ decay products and was accomplished with an efficiency of 2×10^{-3}. The efficiency is relatively small because of the necessity to suppress similar background processes by up to 10 orders of magnitude. Major background sources include the two-body decays $K^+ \to \mu^+ \nu_\mu$ and $K^+ \to \pi^+ \pi^0$, pions scattered from the beam, and K^+ charge exchange (CEX) reactions resulting in decays $K_L^0 \to \pi^+ l^- \overline{\nu}_l$, where $l = e$ or μ. In order to make an unambiguous measurement of $B(K^+ \to \pi^+ \nu\overline{\nu})$, the sum of all backgrounds was suppressed to the estimated level of $0.15^{+0.05}_{-0.04}$ events. The background suppression procedures and estimates were subjected to extensive verification, and a signal-to-background function was created to evaluate potential $K^+ \to \pi^+ \nu\overline{\nu}$ candidates.

The combined result for E787 data taken between 1995 and 1998 is shown in Fig. 3, the range vs. kinetic energy of events surviving all other cuts. In Fig. 3 the box represents the signal region in which two events appear. A likelihood ratio

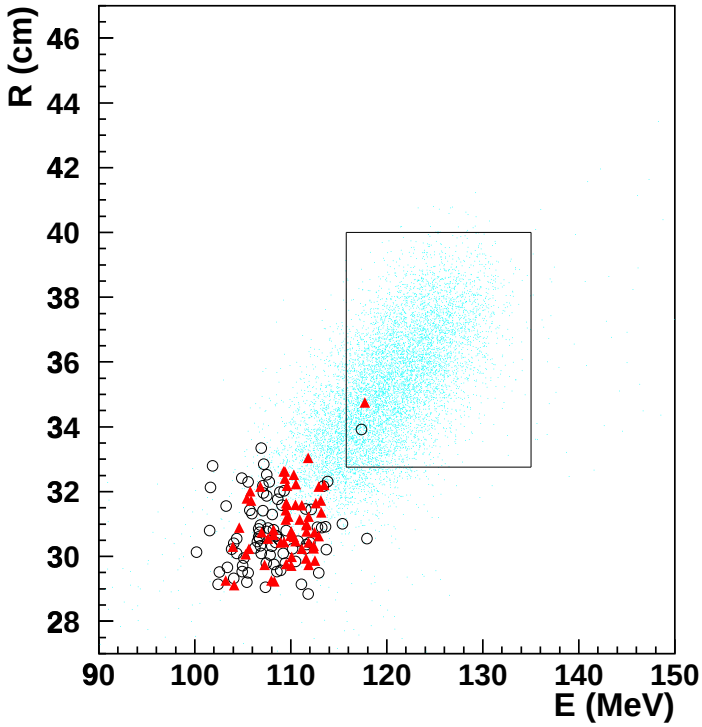

Figure 3: Range vs. energy plot of the E787 final sample for $K^+ \to \pi^+ \nu\overline{\nu}$. The circles are for the 1998 data and the triangles are for the 1995-97 data set. The group of events around $E = 108$ MeV is due to the $K^+ \to \pi^+\pi^0$ background. The simulated distribution of expected events from $K^+ \to \pi^+ \nu\overline{\nu}$ is indicated by dots.

technique[21] was used to determine the best estimate of the branching ratio. Based on two observed events and the expected background levels, the result is $B(K^+ \to \pi^+\nu\overline{\nu}) = 1.57^{+1.75}_{-0.82} \times 10^{-10}$. This result is consistent with the SM prediction. The estimated probability for the observation to be due entirely to background is at the level of 0.02% [21]. D'Ambrosio and Isidori[10] have illustrated the impact of the current E787 results on the measurements of SM quark mixing and CP violation parameters and discussed the possibilities for identifying new physics.

The follow-on experiment E949 is an improved version of E787. Upgrades included enhancements to the photon detection system, and improvements to the DAQ system, beam counters, tracking chamber electronics, monitoring systems, among others. E949 is aiming for a single event sensitivity of approximately 10^{-11}, an order of magnitude below the SM level. It began data-taking in early 2002.

In the longer term future, the proposed CKM experiment[6] at Fermilab shown schematically in fig. 4 seeks another order of magnitude in sensitivity, i.e. 10^{-12}.

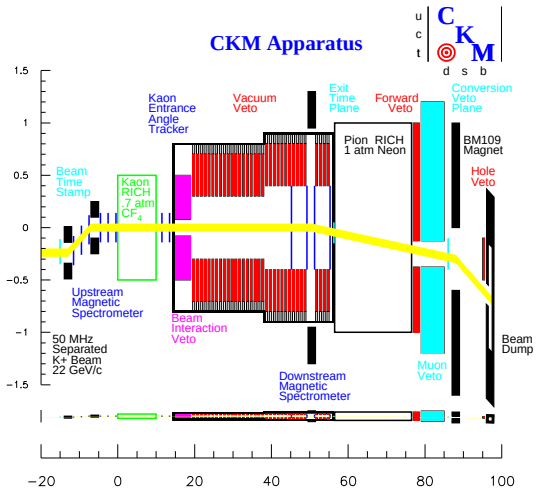

Figure 4: Layout of the proposed CKM experiment at Fermilab.

CKM uses particle identification based on ring imaging Cerenkov detectors along with momentum measurements to suppress backgrounds. At the SM level, a signal of approximately 95 events with a signal/noise ratio $S/N = 7$ is sought.

4 Prospects for Measuring $K_L^0 \to \pi^0 \nu\overline{\nu}$

The experimental challenges of studying B($K_L^0 \to \pi^0 \nu\overline{\nu}$) are comparable to those encountered in the measurement of $K^+ \to \pi^+ \nu\overline{\nu}$. There are similar competing decays, particularly $K_L^0 \to \pi^0\pi^0$, that also yield π^0s but with branching ratios that are millions of times larger. Interactions between neutrons and kaons in the neutral beam with residual gas in the decay volume can also result in emission of single π^0s, as can the decays of hyperons which might occur in the decay region. The current experimental limit $B(K_L^0 \to \pi^0 \nu\overline{\nu}) < 5.9 \times 10^{-7}$ [22] was a by-product of the KTeV experiment at Fermilab.

To definitively measure $K_L^0 \to \pi^0 \nu\overline{\nu}$, a detection technique must be developed that provides maximum possible redundancy for this kinematically unconstrained decay, that has an optimum system for insuring that the observed π^0 is the only detectable particle emanating from the K_L^0 decay, and that has multiple handles for identifying possible small backgrounds that might simulate the desired mode.

A first step at a dedicated search for $K_L^0 \to \pi^0 \nu\overline{\nu}$ is commencing soon at KEK with experiment E391a which aims for a sensitivity of $10^{-10} - 10^{-9}$. This experiment

uses a narrowly collimated "pencil" neutral beam[23] along with a high acceptance hermetic detector. E391a will test the limits of reliance on photon detection efficiency to suppress the major backgrounds and may lead to a proposal at the emerging Japanese Hadron Facility.

The new KOPIO experiment at BNL is scoped to reach a sensitivity more than an order of magnitude below the SM prediction, i.e. 10^{-12}, aiming for at least 50 events of $K_L^0 \to \pi^0 \nu\overline{\nu}$ with $S/N > 2$. KOPIO, which is presently in the R&D and design phase, employs a low momentum time-structured K_L^0 beam to allow determination of the incident kaon momentum by time-of-flight. This intense beam, with its special characteristics, can be provided by the BNL AGS. Utilizing low momentum also permits a detection system for the π^0 decay photons that yields a fully constrained reconstruction of the π^0's mass, energy, and, momentum. The system for vetoing extra particles is well understood. These features which are similar to those employed successfully in the E787 measurement of $K^+ \to \pi^+ \nu\overline{\nu}$ provide the necessary redundancy and checks.

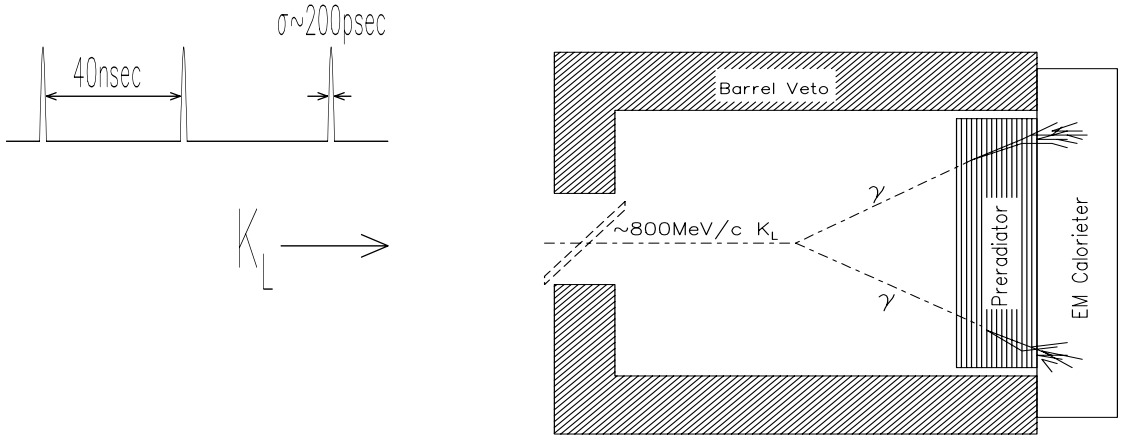

Figure 5: Elements of the KOPIO concept : a pulsed primary beam produces low energy kaons whose time-of-flight reveals their momentum when the π^0 from $K_L^0 \to \pi^0 \nu\overline{\nu}$ decay is reconstructed.

Figure 5 shows a simplified representation of the beam and detector concept for KOPIO. Photons from $K_L^0 \to \pi^0 \nu\overline{\nu}$ decay are observed in a two-stage endcap detector comprised of a fine-grained preradiator with angular resolution approximately 25 mr for photons of 250 MeV. It is followed by a shashlyk-type electromagnetic calorimeter. The preradiator-calorimeter combination is expected to have an energy resolution of $\sigma_{\rm E}/{\rm E} < 0.03/\sqrt{{\rm E(GeV)}}$. The entire decay region is surrounded by efficient charged particle and photon detectors.

5 Other Rare K Decays

Considering the obvious difficulty of measuring $K_L^0 \to \pi^0 \nu\overline{\nu}$ there is still interest in studying $K_L^0 \to \pi^0 e^+ e^-$ to obtain information on direct CP violation. However this decay presents formidable experimental and theoretical challenges. The direct CP-violating component which is due to diagrams similar to those for $K_L^0 \to \pi^0 \nu\overline{\nu}$ is estimated to occur at a branching ratio of 4×10^{-12}. There are potentially important competing effects from CP-conserving amplitudes, CP-violating amplitudes due to mixing, and backgrounds from similar decay signatures like $K_L^0 \to \gamma\gamma e^+ e^-$[24].

The present limit is $\mathrm{B}(K_L^0 \to \pi^0 e^+ e^-) < 5.1 \times 10^{-10}$[25]. The NA48 collaboration has recently reported a result on the branching ratio and shape of the spectrum for $K_L^0 \to \pi^0\gamma\gamma$ which can be used to limit the CP-conserving component of $K_L^0 \to \pi^0 e^+ e^-$[26]. A total of 2558 $K_L^0 \to \pi^0\gamma\gamma$ events were observed with a background estimated to be 3.2% giving the results $\mathrm{B}(K_L^0 \to \pi^0\gamma\gamma) = 1.36 \pm 0.03_{stat} \pm 0.03_{syst} \pm 0.03_{norm} \times 10^{-6}$ and the vector coupling constant $a_v = -0.46 \pm 0.03_{stat} \pm 0.04_{syst}$. [1] Using these results and a limit on the rate in the region $m_{\gamma\gamma} < m_{\pi^0}$, NA48 presented an estimate for the CP-conserving component of $\mathrm{B}(K_L^0 \to \pi^0 e^+ e^-)_{CPC} = 4.7^{+2.2}_{-1.8} \times 10^{-13}$, suggesting that it may not dominate in the measurement of CP-violating effects in $K_L^0 \to \pi^0 e^+ e^-$. However, there is also a dispersive amplitude which is not reliably calculated which could be of comparable importance[24].

The NA48 experiment has now been upgraded to NA48/1[28]. Improvements made to the detectors and beam lines will enable experiments with 100x (or greater) intensities to achieve single event sensitivities to rare decays at the 10^{-10} level. NA48/1 plans to study many processes including $K_S^0 \to \pi^0 l^+ l^-$ (which can be used to limit the contribution to indirect CP violation in $K_L^0 \to \pi^0 e^+ e^-$), $K_S^0 \to 3\pi$, and time-dependent CP-violating effects in $K_{L,S}^0 \to \pi\pi\gamma^*$ decays. In addition, semi-leptonic and radiative neutral hyperon decays will be investigated.

6 Summary and Prospects

Rare kaon decay experiments underway or planned for the BNL AGS, Fermilab and KEK aim to study the extraordinary decays $K^+ \to \pi^+ \nu\overline{\nu}$ and $K_L^0 \to \pi^0 \nu\overline{\nu}$. BNL E787 has presented evidence for $K^+ \to \pi^+ \nu\overline{\nu}$ at the 10^{-10} level based on the observation of two clean events leading the way for BNL E949 and CKM at Fermilab which seek one and two orders of magnitude greater sensitivities. The proposed KOPIO measurement of $B(K_L^0 \to \pi^0 \nu\overline{\nu})$ will allow a determination of the imaginary part of $V_{ts}^* V_{td}$ giving the fundamental CP-violating parameter of the SM, in a uniquely clean manner. Since the measurement of $B(K^+ \to \pi^+ \nu\overline{\nu})$ determines $|V_{ts}^* V_{td}|$, a complete derivation of the

[1] Comparable measurements reported by the KTEV collaboration[27] gave $\mathrm{B}(K_L^0 \to \pi^0\gamma\gamma) = 1.68 \pm 0.10 \times 10^{-6}$ and $a_v = -0.72 \pm 0.05 \pm 0.06$.

unitarity triangle is facilitated. The parameters derived from the K decays will be compared to high precision data expected to come from the B sector allowing for incisive searches for new physics.

New results on several other rare K decays have recently become available from NA48 ($K_L^0 \to \pi^0\gamma\gamma$), the HYPER-CP collaboration ($K^\pm \to \pi^\pm\mu\mu$)[29] and KLOE at DAPHNE ($K_S^0 \to \pi e\nu$)[30] shedding light on issues in CP violation and Chiral Perturbation Theory (CHPT). Other new results on exotic processes have been presented recently by BNL E787 ($K^+ \to \pi^+ a$[31] and $K^+ \to \pi^+\gamma$[32]) and new results on lepton flavor violating decays and other processes are anticipated from E865 at BNL and KTEV/E799 at Fermilab.

At CERN and DAPHNE, additional rare radiative decays of K_L and K_S are being vigorously pursued along with many other studies relevant to tests of CP/CPT violation and CHPT by the upgraded NA48/1 experiment and by KLOE.

7 Acknowledgements

I would like to thank L. Littenberg for comments on the manuscript.

References

[1] A. Alavi-Harati *et al. Phys. Rev. Lett* **83**, 22 (1999).

[2] V. Fanti *et al.*, Phys. Lett.**B465** 335 (1999).

[3] D. Ambrose *et al.*, *Phys. Rev. Lett* .**84** 1389 (2000).

[4] D. Ambrose *et al.*, *Phys. Rev. Lett.* **81** 4309 (1998).

[5] S. Adler *et al.*, *Phys. Rev. Lett.* **88**, 041803 (2002); S. Adler *et al.*, *Phys. Rev. Lett.* **84**, 3768 (2000); S. Adler *et al.*, *Phys. Rev. Lett.* **79**, 2204 (1997).

[6] P. Cooper, *Nucl. Phys. Proc. Suppl.* **99** 121 (2001).

[7] W.J. Marciano and Z. Parsa, *Phys. Rev.* **D53**, R1 (1996).

[8] A.J. Buras and R. Fleischer, in *Heavy Flavours II*, World Scientific, eds. A.J. Buras and M. Linder, 65-238 (1997); G. Buchalla and A.J. Buras, *Nucl. Phys.* **B400**, 225 (1993); G. Buchalla and A.J. Buras, *Nucl. Phys.* **B548**, 309 (1999).

[9] G. Buchalla and A.J. Buras, *Nucl. Phys.* **B412**, 106 (1994).

[10] G. D'Ambosio and G. Isidori, hep-ph/0112135 (2002).

[11] L. Littenberg, *Phys. Rev.* **D39**, 3322 (1989).

[12] C. Jarlskog and R. Stora, *Phys. Lett.* **B 208**, 268 (1988).

[13] A.J. Buras, G. Colangelo, G. Isidori, A. Romanino and L. Silvestrini, *Nucl. Phys.* **B566**, 3 (2000); A. J. Buras, P. Gambino, M. Gorbahn, S. Jager, and L. Silvestrini, hep-ph/0007313.

[14] M. Leurer, *Phys. Rev. Lett.* **71**, 1324 (1993); S. Davidson, D. Bailey, and B. Campbell, *Z. Phys.* **C61**, 613 (1994); A.J. Buras, A. Romanino, and L.Silvestrini, *Nucl. Phys.* **B520**, 3 (1998): G-C. Cho, hep-ph/9804327, KEK-TH-568, Apr 1998; T. Goto, Y. Okada, and Y. Shimizu, hep-ph/9804294, KEK-TH-567, Apr 1998; G. Couture and H. König, *Z. Phys.* **C69**, 167 (1996).

[15] Y. Grossman and Y. Nir, *Phys. Lett.* **B398**, 163 (1997).

[16] G. Bélanger, C.G. Geng and P. Turcotte, *Phys. Rev.* **D46**, 2950 (1992); C.E. Carlson, G.D. Dorata and M. Sher, *Phys. Rev.* **D54**, 4393 (1996) hep-ph/9606269.

[17] Y. Nir and M. Worah, *Phys. Lett.* **B423**, 319 (1998).

[18] Z. Xiao, C. Li and K. Chao, *Eur. Phys. J.* **C10**, 51 (1999).

[19] Y. Kiyo, T. Morozumi, P. Parada, M.N. Rebelo, and M. Tanimoto, *Prog. Theor. Phys.* **101**, 671 (1999).

[20] T. Hattori, T. Hasuike, and S. Wakaizumi, *Phys. Rev.* **D60**, 113008 (1999).

[21] T. Junk, Nucl. Instr. Meth. **A434**, 435 (1999).

[22] A. Alavi-Harati *et al. Phys. Rev.* **D61**, 072006 (2000).

[23] H. Watanabe, Thesis, Saga University (2002).

[24] L. Littenberg and G. Valencia, see http://pdg.lbl/gov (2002).

[25] A. Alavi-Harati *et al.*, *Phys. Rev. Lett.***86**, 397 (2001).

[26] A. Lai *et al.*, hep-ex/0205010 (2002).

[27] A. Alavi-Harati *et al.*, *Phys. Rev. Lett.* **83**, 917 (1999).

[28] R. Sacco, Rencontres de Moriond (2002), to be pub.

[29] H. K. Park *et al.*, *Phys. Rev. Lett.* **88** 111801 (2002).

[30] A. Aloisio *et al.*, *Phys. Lett.* **B535**, 37 (2002).

[31] S. Adler *et al.*, hep-ex/0201037, *Phys. Lett. B* (to be pub.) (2002).

[32] S. Adler *et al.*, *Phys. Rev.* **D88**, 052009 (2002).

May 18, session 2.

Session Chair: S. Olsen

Theoretical developments in V_{cb} and V_{ub}

$\mathcal{F}(1)$ for $B \to D^* l \nu$ from Lattice QCD

A. S. Kronfeld

B Decays

B to charmonium - mini-summary

F. Fang

$\mathcal{F}(1)$ for $B \to D^* l\nu$ from Lattice QCD

Andreas S. Kronfeld, Paul B. Mackenzie, James N. Simone
Fermi National Accelerator Laboratory
Batavia, Illinois 60510, USA

Shoji Hashimoto
High Energy Accelerator Research Organization (KEK)
Tsukuba 305-0801, JAPAN

Sinéad M. Ryan
School of Mathematics, Trinity College
Dublin 2, IRELAND

We would like to determine $|V_{cb}|$ from the exclusive semi-leptonic decay $B \to D^* l\nu$. The differential decay rate is

$$\frac{d\Gamma}{dw} = \frac{G_F^2}{4\pi^3}(w^2-1)^{1/2} m_{D^*}^3 (m_B - m_{D^*})^2 \mathcal{G}(w) |V_{cb}|^2 |\mathcal{F}_{B\to D^*}(w)|^2, \tag{1}$$

where $w = v \cdot v'$ and $\mathcal{G}(1) = 1$. At zero recoil ($w = 1$) heavy-quark symmetry requires $\mathcal{F}_{B\to D^*}(1)$ to be close to 1. So, $|V_{cb}|$ is determined by dividing measurements of $d\Gamma/dw$ by the phase space and well-known factors, and extrapolating to $w \to 1$. This yields $|V_{cb}|\mathcal{F}_{B\to D^*}(1)$, and $\mathcal{F}_{B\to D^*}(1)$ is taken from "theory." To date models [1] or a combination of a rigorous inequality plus judgment [2] have been used to estimate $\mathcal{F}_{B\to D^*}(1) - 1$. In this work [3] we calculate $\mathcal{F}_{B\to D^*}(1)$ with lattice gauge theory, in the so-called quenched approximation, but the uncertainty from quenching is included in the error budget.

The "form factor" $\mathcal{F}_{B\to D^*}(w)$ is a linear combination of several form factors of the matrix elements $\langle D^*|\mathcal{V}^\mu|B\rangle$ and $\langle D^*|\mathcal{A}^\mu|B\rangle$. At zero recoil all form factors but h_{A_1} are suppressed by phase space, so

$$\mathcal{F}_{B\to D^*}(1) = h_{A_1}(1) = \langle D^*(v)|\mathcal{A}^\mu|B(v)\rangle, \tag{2}$$

which should be "straightforward" to calculate in lattice QCD. But a brute force calculation of $\langle D^*|\mathcal{A}^\mu|B\rangle$ would not be interesting: similar matrix elements like $\langle 0|\mathcal{A}^\mu|B\rangle$ and $\langle \pi|\mathcal{V}^\mu|B\rangle$ have 15–20% errors [4, 5].

Thus, we have to involve heavy-quark symmetry from the outset: if we can focus on $h_{A_1} - 1$, we have a chance of success, because a 20% error on $h_{A_1} - 1$ is interesting: $0.2 \times 0.1 = 0.02$. There are three specific obstacles to overcome: (i) statistical uncertainties, (ii) normalization uncertainties in the lattice axial vector current, and (iii) how to

treat heavy quarks since $m_b a \not\ll 1$. The first two need computational insight; the last two theoretical insight. In the last several years, we have developed tools to attack these problems [6, 7, 8, 9, 10, 11].

At zero recoil heavy-quark symmetry implies [12, 13]

$$h_{A_1}(1) = \eta_A \left[1_{\text{Isgur-Wise}} + 0_{\text{Luke}} + \delta_{1/m^2} + \delta_{1/m^3}\right] \tag{3}$$

where η_A is a short-distance coefficient of HQET, and the δ_{1/m^n} contain long-distance matrix elements. The structure of the $1/m_Q^n$ corrections is

$$\delta_{1/m^2} = -\frac{\ell_V}{(2m_c)^2} + \frac{2\ell_A}{(2m_c)(2m_b)} - \frac{\ell_P}{(2m_b)^2} \tag{4}$$

$$\delta_{1/m^3} = -\frac{\ell_V^{(3)}}{(2m_c)^3} + \frac{\ell_A^{(3)}\Sigma + \ell_D^{(3)}\Delta}{(2m_c)(2m_b)} - \frac{\ell_P^{(3)}}{(2m_b)^3} \tag{5}$$

where $\Sigma = 1/(2m_c) + 1/(2m_b)$ and $\Delta = 1/(2m_c) - 1/(2m_b)$. One must make sure to calculate η_A and the ℓs in the same renormalization scheme.

Lattice gauge theory with Wilson fermions has the same heavy-quark symmetries as continuum QCD, for all $m_Q a$. It therefore admits a description with HQET, provided $m_Q \gg \Lambda$ [7, 8, 9, 10]. In this description, HQET matrix elements, such as the ℓs in Eqs. (4) and (5), are essentially the same as for continuum QCD. So, one needs some quantities with small statistical and normalization errors, whose heavy-quark expansion contains the ℓs. Then, one calculates the short-distance part in perturbation theory [6, 14], extracts the ℓs from a fit, and reconstitutes $h_{A_1}(1)$.

In our work on the $B \to D$ form factor [11], we found that certain ratios have the desired low level of uncertainty:

$$\frac{\langle D|\overline{c}\gamma^4 b|B\rangle\langle B|\overline{b}\gamma^4 c|D\rangle}{\langle D|\overline{c}\gamma^4 c|D\rangle\langle B|\overline{b}\gamma^4 b|B\rangle} = \left\{\eta_V^{\text{lat}}\left[1 - \ell_P\Delta^2 - \ell_P^{(3)}\Delta^2\Sigma\right]\right\}^2, \tag{6}$$

$$\frac{\langle D^*|\overline{c}\gamma^4 b|B^*\rangle\langle B^*|\overline{b}\gamma^4 c|D^*\rangle}{\langle D^*|\overline{c}\gamma^4 c|D^*\rangle\langle B^*|\overline{b}\gamma^4 b|B^*\rangle} = \left\{\eta_V^{\text{lat}}\left[1 - \ell_V\Delta^2 - \ell_V^{(3)}\Delta^2\Sigma\right]\right\}^2, \tag{7}$$

$$\frac{\langle D^*|\overline{c}\gamma^j\gamma_5 b|B\rangle\langle B^*|\overline{b}\gamma^j\gamma_5 c|D\rangle}{\langle D^*|\overline{c}\gamma^j\gamma_5 c|D\rangle\langle B^*|\overline{b}\gamma^j\gamma_5 b|B\rangle} = \left\{\check{\eta}_A^{\text{lat}}\left[1 - \ell_A\Delta^2 - \ell_A^{(3)}\Delta^2\Sigma\right]\right\}^2. \tag{8}$$

For lattice gauge theory, the heavy-quark expansions in Eqs. (6)–(8) have been derived in Ref. [8], leaning heavily on Refs. [15]. The one-loop expansions of η_V^{lat} and $\check{\eta}_A^{\text{lat}}$ are in Ref. [10]. Thus, these ratios yield all terms in δ_{1/m^3} except $\ell_D^{(3)}$.

We wish to obtain the $1/m_Q^2$ corrections to the double ratios, but the lattice action and currents do not normalize all such terms correctly. HQET reveals several sources of such contributions, in a systematic way [15, 8]. The most crucial are the $1/m_Q^2$ corrections to the currents, which enter the double ratios as follows:

$$\frac{[1 - \lambda(X_b/m_b^2 - 1/m_c m_b + X_c/m_c^2)]^2}{[1 - \lambda(2X_c - 1)/m_c^2][1 - \lambda(2X_b - 1)/m_b^2]} = 1 - \lambda\left(\frac{1}{m_c} - \frac{1}{m_b}\right)^2, \tag{9}$$

where λ is proportional to λ_1 or λ_2, and X_Q/m_Q^2 indicates incorrect normalization. The correct normalization of the $1/m_c m_b$ terms is built into the current we used. The cancellation of the others is a key feature of the double ratios. Other contributions either vanish or are correctly normalized to order α_s [8]. This, and other matching uncertainties of order α_s^2 and $(\overline{\Lambda}/m_Q)^3$, are put into the error budget.

Fig. 1(a) shows the heavy-quark mass dependence from Ref. [3]. As expected, ℓ_V is the largest of the $1/m_Q^2$ matrix elements. Because of the fit, the value of ℓ_V is highly correlated with that of $\ell_V^{(3)}$, but the physical combination is better determined.

We have also studied the dependence of the calculation on the mass of the light spectator quark, over the range $0.4 \le m_q/m_s \le 1$. As seen in Fig. 1(b), there is a slight linear dependence on m_π^2, which is proportional to m_q. The points are correlated, so the trend is significant. The main effect of extrapolating in m_π^2 is to increase the statistical error. In addition, there must be a pion loop contribution [16], which is mistreated in the quenched approximation. We treat the omission of this effect as a systematic error.

After putting everything back together again, we find [3]

$$\mathcal{F}_{B\to D^*}(1) = 0.913^{+0.024}_{-0.017} \pm 0.016^{+0.003+0.000+0.006}_{-0.014-0.016-0.014}, \tag{10}$$

where the uncertainties stem, respectively, from statistics and fitting, HQET matching, lattice spacing dependence, the chiral extrapolation, and the effect of the quenched approximation. In Fig. 2(a) we compare our result for $\mathcal{F}_{B\to D^*}(1)$ against the estimate based on the quark model [1], and on the sum rule [17]. The defects are as follows: The quark model omits some dynamics (more than quenching), and it is not clear that it gives the ℓs in the same scheme as η_A. The sum rule has an incalculable contribution from excitations with $(M - m_{D^*})^2 < \mu^2$, which can only be estimated.

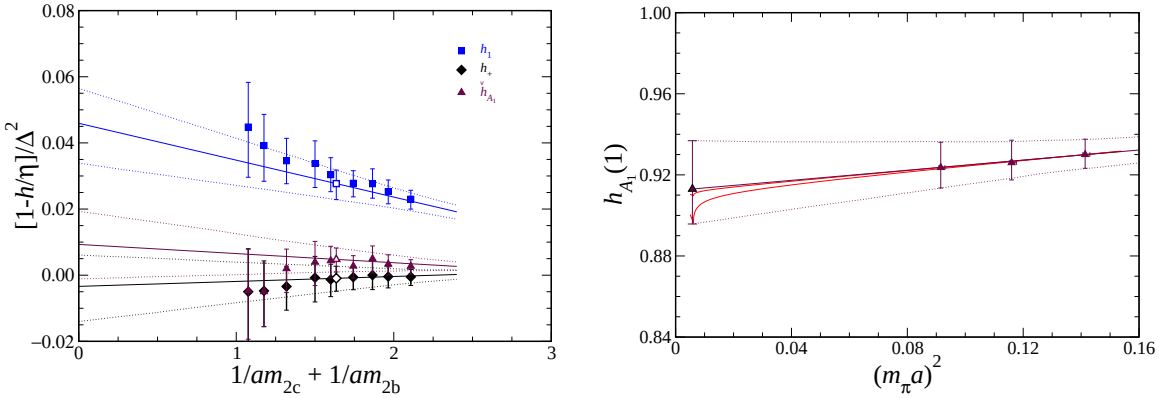

Figure 1: (a) Heavy-quark mass dependence of the double ratios. (b) Chiral extrapolation of $h_{A_1}(1)$.

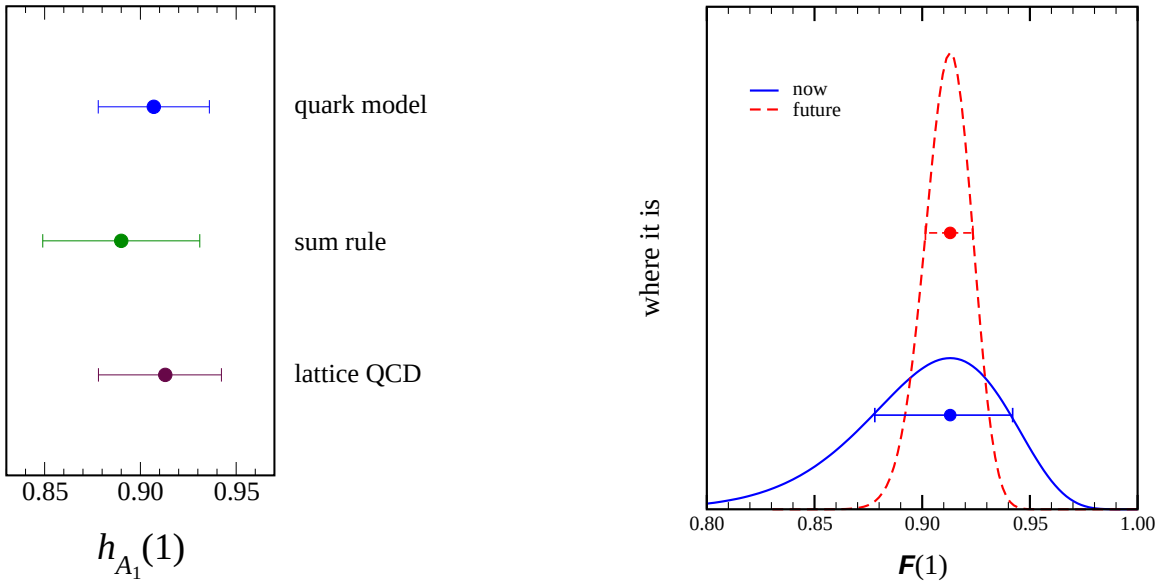

Figure 2: (a) Comparison of methods. (b) Simple Ansatz for more (and less) likely values, now and in the future.

The present lattice result is in quenched approximation, but the error from quenching is the last error bar in Eq. (10).

For using this result in a global fit to the CKM matrix, it is useful to have some idea what values of theoretical quantities are more (or less) likely. A flat distribution would be incorrect, because the first error in Eq. (10) is essentially statistical, and the others are under some control. Also, one cannot rule out a tail for lower values; they are just unlikely. Finally, we know that $\mathcal{F}_{B\to D^*}(1) \leq 1$ [2]. A simple formula that captures these features is the Poisson distribution

$$P(x) = Nx^7 e^{-7x}, \quad x = \frac{1 - \mathcal{F}_{B\to D^*}(1)}{0.087}. \tag{11}$$

In the future one could reduce the uncertainty by a factor of 3, as sketched in Fig. 2(b), and one could provide a distribution stemming from the Monte Carlo calculation, and properly propagated through the systematic analysis.

We thank Aida El-Khadra for helpful discussions. High-performance computing was carried out on ACPMAPS; we thank past and present members of Fermilab's Computing Division for designing, building, operating, and maintaining this supercomputer, thus making this work (ACPMAPS' last) possible. Fermilab is operated by Universities Research Association Inc., under contract with the U.S. Department of Energy. SH is supported in part by the Grants-in-Aid of the Japanese Ministry of Education under contract No. 11740162.

References

[1] M. Neubert, Phys. Lett. B **338**, 84 (1994) [arXiv:hep-ph/9408290].

[2] M. Shifman, N. G. Uraltsev, and A. Vainshtein, Phys. Rev. D **51**, 2217 (1995) [arXiv:hep-ph/9405207]; **52**, 3149(E) (1995); I. Bigi, M. Shifman, N. G. Uraltsev, and A. Vainshtein, Phys. Rev. D **52**, 196 (1995) [arXiv:hep-ph/9405410].

[3] S. Hashimoto, A. S. Kronfeld, P. B. Mackenzie, S. M. Ryan and J. N. Simone, arXiv:hep-ph/0110253, to appear in Phys. Rev. D.

[4] A. Duncan *et al.*, Phys. Rev. D **51**, 5101 (1995) [arXiv:hep-lat/9407025]; A. X. El-Khadra *et al.*, Phys. Rev. D **58**, 014506 (1998) [arXiv:hep-ph/9711426].

[5] A. X. El-Khadra *et al.*, Phys. Rev. D **64**, 014502 (2001) [arXiv:hep-ph/0101023].

[6] G. P. Lepage and P. B. Mackenzie, Phys. Rev. D **48**, 2250 (1993) [arXiv:hep-lat/9209022].

[7] A. X. El-Khadra, A. S. Kronfeld, and P. B. Mackenzie, Phys. Rev. D **55**, 3933 (1997) [arXiv:hep-lat/9604004].

[8] A. S. Kronfeld, Phys. Rev. D **62**, 014505 (2000) [arXiv:hep-lat/0002008].

[9] J. Harada, S. Hashimoto, K. I. Ishikawa, A. S. Kronfeld, T. Onogi, and N. Yamada, Phys. Rev. D **65**, 094513 (2002) [arXiv:hep-lat/0112044].

[10] J. Harada, S. Hashimoto, A. S. Kronfeld, and T. Onogi, Phys. Rev. D **65**, 094514 (2002) [arXiv:hep-lat/0112045].

[11] S. Hashimoto, A. X. El-Khadra, A. S. Kronfeld, P. B. Mackenzie, S. M. Ryan, and J. N. Simone, Phys. Rev. D **61**, 014502 (2000) [arXiv:hep-ph/9906376].

[12] N. Isgur and M. B. Wise, Phys. Lett. B **232**, 113 (1989); **237**, 527 (1990).

[13] M. E. Luke, Phys. Lett. B **252**, 447 (1990).

[14] S. J. Brodsky, G. P. Lepage, and P. B. Mackenzie, Phys. Rev. D **28**, 228 (1983).

[15] A. F. Falk and M. Neubert, Phys. Rev. D **47**, 2965 (1993) [arXiv:hep-ph/9209268]; T. Mannel, Phys. Rev. D **50**, 428 (1994) [arXiv:hep-ph/9403249].

[16] L. Randall and M. B. Wise, Phys. Lett. B **303**, 135 (1993); M. J. Savage, Phys. Rev. D **65**, 034014 (2002) [arXiv:hep-ph/0109190].

[17] N. Uraltsev, in *At the Frontier of Particle Physics: Handbook of QCD*, edited by M. Shifman (World Scientific, Singapore, 2001) [arXiv:hep-ph/0010328].

B to charmonium - mini-summary

Fang Fang
Department of Physics and Astronomy
University of Hawaii at Manoa
Hawaii, USA

1 Introduction

I will try to summarize recent experimental results on B to charmonium decays. Decays of B meson to final states include charmonium play an important role in the study of CP violation at B-factories. The decay modes $B_{CP}\to J/\psi K_S$, $\psi(2S)K_S$, $\chi_{c1}K_S$, $\eta_c K_S$, $J/\psi K_L$ and $J/\psi K^{*0}(K^{*0}\to K_S\pi^0)$ have been used for $\sin 2\phi_1$ measurements [1] [2] [3] [4] [5]. These two-body decay modes are dominated by the color suppressed $b\to c$ transition. Other CP eigenstates of the neutral B meson, e.g. $J/\psi\rho^0$, may also be useful for the CP measurements. Meanwhile, the branching fractions for the $B\to$*charmonium* decays can provide valuable information on their decay mechanism.

2 Non-factorizable decay modes

In the factorization approximation, the production of χ_{c0} and χ_{c2} are not allowed by angular momentum and vector-current conservation. However, these decays can occur if factorization is broken by an exchange of soft gluons between the quarks.

2.1 Observation of $B^+\to\chi_{c0}K^+$

Using a data sample containing 31.3 million $B\overline{B}$ events collected at the $\Upsilon(4S)$ resonance with the Belle detector at the KEKB asymmetric e^+e^- collider, the Belle collaboration has made the first observation of $B^+\to\chi_{c0}K^+$ [6].

The χ_{c0} candidates are reconstructed from $\chi_{c0}\to\pi^+\pi^-$ and K^+K^-. Two kinematic variables, the beam-constrained mass, $M_{\rm bc}=\sqrt{E^2_{\rm beam}-\vec{P}^2_{\rm recon}}$, and energy difference $\Delta E=E_{\rm recon}-E_{\rm beam}$ in the $\Upsilon(4S)$ center of mass frame, are formed to isolate the signal. Here $E_{\rm beam}$, $E_{\rm recon}$ and $\vec{P}_{\rm recon}$ are the beam energy, the reconstructed energy and the reconstructed momentum of the signal candidate, respectively. Figure 1 shows the invariant masses of $\pi^+\pi^-$ and K^+K^-. The peaks near 3.4

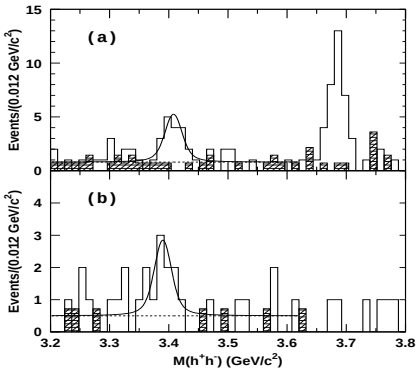

Figure 1: The (a) $\pi^+\pi^-$ and (b) K^+K^- invariant mass spectra. Open histograms correspond to events from the B signal region, and hatched histograms correspond to events from the ΔE sidebands. The curves are results of fits [6].

GeV/c^2 are identified as the χ_{c0} meson. The peak position in the K^+K^- spectrum is shifted. This could be explained by the interference of $B^+\to\chi_{c0}K^+$ with the non-resonant $B^+\to K^+K^+K^-$. The peak at 3.69 GeV/c^2 in the $\pi^+\pi^-$ spectrum is due to $B^+\to\psi(2S)K^+$, $\psi(2S)\to\mu^+\mu^-$ with the muons misidentified as pions.

Using the $\chi_{c0}\to\pi^+\pi^-$ decay channel, the ratio of branching fractions is found to be:

$$\frac{\mathcal{B}(B^+\to\chi_{c0}K^+)}{\mathcal{B}(B^+\to J/\psi K^+)} = 0.60^{+0.21}_{-0.18} \pm 0.05 \pm 0.08,$$

where the first error is statistical, the second is systematic, and the third is due to the uncertainty in the branching fraction for $\chi_{c0}\to\pi^+\pi^-$. The branching fraction is measured to be

$$\mathcal{B}(B^+\to\chi_{c0}K^+) = (6.0^{+2.1}_{-1.8} \pm 1.1) \times 10^{-4},$$

which is comparable to those for $B^+\to J/\psi K^+$ and $B^+\to\chi_{c1}K^+$ decays. The $\chi_{c0}\to K^{*0}K^-\pi^+$ decay channel has been also studied and the results are in good agreement with those determined from $\chi_{c0}\to\pi^+\pi^-$. The statistical significance of the signal is 6σ when these two channels are combined. This measurement indicates a significant non-factorizable contribution in B to charmonium decays.

2.2 Observation of $B\to\chi_{c2}X$

The Belle collaboration has also observed χ_{c2} production in B-meson decay [7]. The analysis is based on a data sample containing 31.9 million $B\overline{B}$ events collected at the $\Upsilon(4S)$ resonance with the Belle detector at the KEKB asymmetric e^+e^- collider.

The χ_{c2} candidates are reconstructed via $J/\psi\gamma$, $J/\psi\to l^+l^-$. The photon energy resolution is studied using $D^{*0}\to D^0\gamma$ decay. The σ_E/E_γ is $(2.61\pm0.04)\%$ around 400

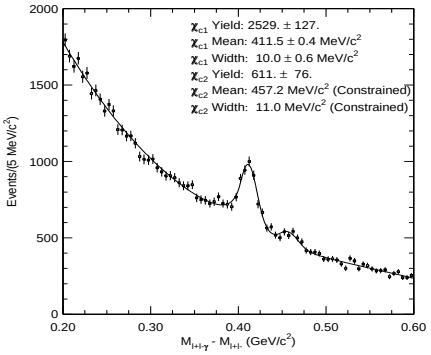

Figure 2: The distribution of the mass difference between the χ_c and the J/ψ candidates events [7].

MeV. The good photon energy resolution leads to a clear separation between the χ_{c2} peak and the lager χ_{c1} peak as shown in Fig. 2. To extract signal yields, the distribution is fit to two Crystal Ball line shapes and a third-order Chebyshev polynomial for the background. The continuum subtracted yield for $B \to \chi_{c2}$ is 607^{+76}_{-94} events. The branching fraction for $B \to \chi_{c2} X$ is $(1.80^{+0.23}_{-0.28} \pm 0.26) \times 10^{-3}$. The branching fraction for $B \to \chi_{c1} X$ is also measured. The momentum spectrum of χ_{c2} does not show a significant contribution from two body $B \to \chi_{c2} K$, in contrast to the momentum spectrum for $B \to \chi_{c1}$.

3 Other exclusive decay modes

3.1 $B^0 \to J/\psi \pi^+ \pi^-$

The BaBar collaboration has measured the branching fraction for the $B \to J/\psi \pi^+ \pi^-$ decay [8]. The data set contains approximately 56 million $B\overline{B}$ pairs produced at the $\Upsilon(4S)$ resonance with the BaBar detector at the PEP-II asymmetric e^+e^- collider. The $B \to J/\psi \pi^+ \pi^-$ decay mode includes $J/\psi \rho^0$ and the non-resonant $J/\psi \pi^+ \pi^-$ components. The invariant mass of the two pions, $M(\pi^+\pi^-)$, is plotted in Fig. 3. The signal yield is obtained by an unbinned maximum likelihood fit performed on the invariant mass distribution. The branching fraction for $B^0 \to J/\psi \pi^+ \pi^-$ is measured to be $(5.0 \pm 0.7 \pm 0.6) \times 10^{-5}$. It is about 20 times smaller than the branching fraction for $B^0 \to J/\psi K^0$ because of the Cabibbo and color suppression of $B \to J/\psi \pi^+ \pi^-$.

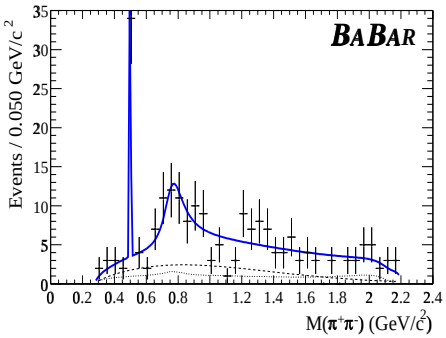

Figure 3: Distribution of the invariant mass M($\pi^+\pi^-$) for the B candidates. The solid line is the result of the unbinned likelihood fit. The dotted (dashed) line represents the background from non-J/ψ (inclusive-J/ψ) events. [8].

3.2 $B \to J/\psi K^*$

The $J/\psi K^*$ system has three helicity states and hence is a mixture of the CP-even and CP-odd eigenstates. The full angular analysis can determine the CP mix, which must be known to measure sin2ϕ_1 when the decay $B^0 \to J/\psi K^{*0}$, $K^{*0} \to K_S\pi^0$ is used. The angular analysis also provides a test of the validity of the factorization hypothesis for the B meson decays with charmonium.

The branching fractions for $B^+ \to J/\psi K^{*+}$ and $B^0 \to J/\psi K^{*0}$, where $K^{*+} \to K^+\pi^0$, $K_S\pi^+$ and $K^{*0} \to K^+\pi^-, K_S\pi^0$, are listed in Table 1 for comparison [9] [10]. The results are all in good agreement. Fig. 4 also shows evidence for the decay $B^0 \to J/\psi K_2^{*0}(1430)$. Some excess is observed in the region between 1.1 GeV/c^2 to 1.3 GeV/c^2 in these measurements. Its source is not fully understood.

The decay amplitudes of $B \to J/\psi K^*$ are measured in the transversity frame [11] by fitting the angular distributions in Fig. 5. The results from various experiments are compared in Table 2 [9] [12] [10]. They are consistent. The value of $|A_\perp|^2$, which corresponds to the CP-odd eigenstate, shows that CP-even component dominates in the $B^0 \to J/\psi K^{*0}$, $K^{*0} \to K_S\pi^0$ decay. The parameter $arg(A_\parallel)$ should be 0 or π in the factorization limit. It is shifted from π in all four measurements. However, the shift is not yet statistically significant enough to draw a conclusion.

3.3 $B \to \eta_c K^{(*)}$

The decay $B \to \eta_c K$ has the same quark level diagram as $B \to J/\psi K$. However, unlike J/ψ, η_c decays hadronically rather than leptonically with rates of a few percent or less for each channel. The decay modes $B^0 \to \eta_c K^0$, $\eta_c \to K_S^0 K^-\pi^+$ and $K^+K^-\pi^0$ have been used to measure sin2ϕ_1. Other decay channels of the η_c may also be useful for

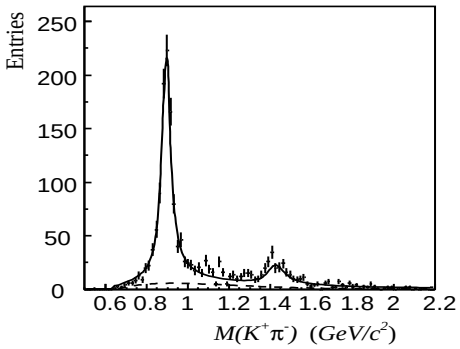

Figure 4: The $K^+\pi^-$ invariant mass distribution from Belle. The solid line is a fit to two Breit-Wigner functions corresponding to $K^*(892)$ and $K_2^*(1430)$ with a background function (dashed line).

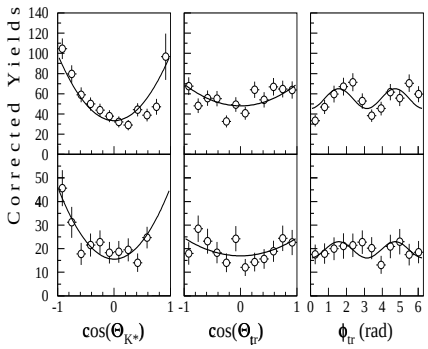

Figure 5: The background-subtracted angular distributions for the channels without (top) and without (bottom) a π^0. The curves correspond to the fit [10].

the CP measurements.

BaBar has measured the branching fractions of $B^+ \to \eta_c K^+$ and $B^0 \to \eta_c K^0$ [13] using a data sample containing 22.7 million $B\overline{B}$ pairs. The η_c is reconstructed in the decay modes: $K_S^0 K^- \pi^+$, $K^+ K^- \pi^0$, and $2(K^+ K^-)$. They observed statistically significant B meson signals in the $K_S^0 K^- \pi^+$ and $K^+ K^- \pi^0$ channels. They also observed exclusive η_c signals.

Belle has measured the branching fraction of $B^+ \to \eta_c K^+$ and $B^0 \to \eta_c K^0$ using a data sample containing 31.3 million $B\overline{B}$ pairs. The η_c is reconstructed in the decay modes: $K_S^0 K^- \pi^+$, $K^+ K^- \pi^0$, $K^{*0} K^- \pi^+$ and $p\overline{p}$. We observed statistically significant B meson signals in $K_S^0 K^- \pi^+$, $K^+ K^- \pi^0$, $K^{*0} K^- \pi^+$ and in the $p\overline{p}$ channel. Fig. 6 shows the invariant mass of η_c for events in the M_{bc} and ΔE signal region. Fitting to a Breit-Wigner convolved with the resolution determined from MC, we find a intrinsic

Experiment	$\mathcal{B}(B^0 \to J/\psi K^{*0})$ $(\times 10^{-3})$	$\mathcal{B}(B^+ \to J/\psi K^{*+})$ $(\times 10^{-3})$
CLEO	$1.32 \pm 0.15 \pm 0.17$	$1.41 \pm 0.20 \pm 0.24$
BaBar	$1.24 \pm 0.05 \pm 0.09$	$1.37 \pm 0.09 \pm 0.11$
Belle	$1.29 \pm 0.05 \pm 0.13$	$1.28 \pm 0.07 \pm 0.14$

Table 1: The measured branching fractions for $B^+ \to J/\psi K^{*+}$ and $B^0 \to J/\psi K^{*0}$.

Exp.	$\lvert A_0 \rvert^2$	$\lvert A_\perp \rvert^2$	$arg(A_\parallel)$ (rad)	$arg(A_\perp)$ (rad)
CLEO	$0.52 \pm 0.07 \pm 0.04$	$0.16 \pm 0.08 \pm 0.04$	$3.00 \pm 0.37 \pm 0.04$	$-0.11 \pm 0.46 \pm 0.03$
CDF	$0.59 \pm 0.06 \pm 0.01$	$0.13^{+0.12}_{-0.09} \pm 0.06$	$2.2 \pm 0.5 \pm 0.1$	$-0.6 \pm 0.5 \pm 0.1$
BaBar	$0.60 \pm 0.03 \pm 0.02$	$0.16 \pm 0.03 \pm 0.01$	$2.50 \pm 0.20 \pm 0.08$	$-0.17 \pm 0.16 \pm 0.07$
Belle	$0.62 \pm 0.02 \pm 0.03$	$0.19 \pm 0.02 \pm 0.03$	$2.83 \pm 0.19 \pm 0.08$	$-0.09 \pm 0.13 \pm 0.06$

Table 2: The decay amplitudes in $B \to J/\psi K^*$. The first errors are statistical and the second systematic.

width $\sigma(\eta_c) = 29 \pm 8$ MeV and a mass of $M(\eta_c) = 2979.6 \pm 2.3$ MeV. The errors are statistical only. The results are consistent with world averages [14] and the CLEO result [15].

The B branching fractions are quoted for the $\eta_c \to K^0_S K^- \pi^+$ and $\eta_c \to K^+ K^- \pi^0$ modes only. The $\eta_c \to K^0_S K^- \pi^+$ mode is the most precisely and reliably measured mode, while the branching fraction for the $\eta_c \to K^+ K^- \pi^0$ mode is related by isospin. The results are consistent with the CLEO results [16] but more precise as shown in Table 3.

Experiment	$\mathcal{B}(B^0 \to \eta_c K^0)$ $(\times 10^{-3})$	$\mathcal{B}(B^+ \to \eta_c K^+)$ $(\times 10^{-3})$
CLEO	$1.09^{+0.55}_{-0.42} \pm 0.12 \pm 0.31$	$0.69^{+0.26}_{-0.21} \pm 0.08 \pm 0.20$
BaBar	$1.06 \pm 0.28 \pm 0.11 \pm 0.33$	$1.50 \pm 0.19 \pm 0.15 \pm 0.46$
Belle	$1.23 \pm 0.23^{+0.12}_{-0.16} \pm 0.38$	$1.25 \pm 0.14^{+0.10}_{-0.12} \pm 0.38$

Table 3: The measured branching fractions for $B^+ \to \eta_c K^+$ and $B^0 \to \eta_c K^0$. The last errors come from the uncertainty in the η_c branching fraction

Belle has observed the decay mode $B^0 \to \eta_c K^{*0}$ for the first time. The K^{*0} is reconstructed in the $K^- \pi^+$ channel and the η_c in the $K^0_S K^- \pi^+$ mode. To remove the $B\overline{B}$ background, we apply vetoes to events consistent with $J/\psi \to K^0_S K \pi$, $\chi_{c1} \to K^0_S K \pi$ and $D_s \to K^+ K^- \pi$. A fit to the M_{bc} spectrum yields a signal of 33.7 ± 6.7 events with a statistical significance of 7.7σ. The branching fraction for $B^0 \to \eta_c K^{*0}$ is found to be $(1.62 \pm 0.32^{+0.24}_{-0.34} \pm 0.50) \times 10^{-3}$. The ratio $R_{\eta_c} = \mathcal{B}(B^0 \to \eta_c K^{*0}) / \mathcal{B}(B^0 \to \eta_c K^0)$ is

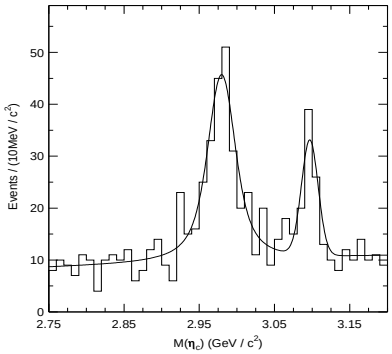

Figure 6: Candidate $M(\eta_c)$ invariant mass distribution for events in the M_{bc} and ΔE signal region. Signals at the η_c and J/ψ from $B \to \eta_c K$ and $B \to J/\psi K$ decays are visible.

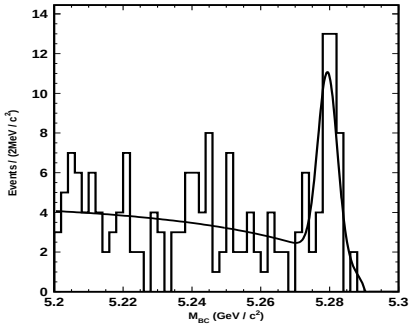

Figure 7: The M_{bc} distribution of $B^0 \to \eta_c K^{*0}$ candidates.

measured to be $1.33 \pm 0.36^{+0.29}_{-0.40}$. This result is somewhat higher than the theoretical prediction of Gourdin, Keum and Pham of 0.78 [17].

3.4 Exclusive $B \to J/\psi$, $\psi(2S)$ and χ_{c1}

Table 4 lists branching fractions for two-body B meson decays to J/ψ, $\psi(2S)$ and χ_{c1} with a kaon or pion [14] [18] [19] [20] [21] [22]. They are in good agreement with previous measurements but more precise. The decay modes $B^0 \to \chi_{c1} K^{*0}$, $B^+ \to J/\psi K_1^+(1270)$ and $B^0 \to J/\psi K_1^0(1270)$ have been observed for the first time.

Decay mode	Previous ($\times 10^{-4}$)	BaBar ($\times 10^{-4}$)	Belle ($\times 10^{-4}$)
$B^- \to J/\psi K^-$	10.0 ± 1.0	$10.1 \pm 0.3 \pm 0.5$	$10.1 \pm 0.3 \pm 0.8$
$B^0 \to J/\psi K^0$	9.6 ± 0.9	$8.3 \pm 0.4 \pm 0.5$	$7.7 \pm 0.4 \pm 0.7$
$B^- \to J/\psi K_1^-(1270)$			$18.0 \pm 3.4 \pm 3.9$
$B^0 \to J/\psi K_1^0(1270)$			$13.0 \pm 3.4 \pm 3.1$
$B^- \to \psi(2S) K^-$	5.8 ± 1.0	$6.4 \pm 0.5 \pm 0.8$	$6.7 \pm 0.6 \pm 0.7$ (a)
			$5.7 \pm 0.5 \pm 0.8$ (b)
$B^0 \to \psi(2S) K^0$	5.0 ± 1.3	$6.9 \pm 1.1 \pm 1.1$	$6.0 \pm 1.1 \pm 0.7$ (a)
			$7.2 \pm 1.1 \pm 1.1$ (b)
$B^- \to \chi_{c1} K^-$	10.0 ± 4.0	$7.5 \pm 0.8 \pm 0.8$	$6.1 \pm 0.6 \pm 0.6$
$B^0 \to \chi_{c1} K^0$	$3.9^{+1.9}_{-1.4}$	$5.4 \pm 1.4 \pm 1.1$	$3.1 \pm 0.9 \pm 0.4$
$B^0 \to \chi_{c1} K^{*0}$		$4.8 \pm 1.4 \pm 0.9$	
$B^- \to J/\psi \pi^-$	0.51 ± 0.15	0.39 ± 0.09	$0.52 \pm 0.07 \pm 0.07$
$B^0 \to J/\psi \pi^0$	$0.25^{+0.11}_{-0.09}$	$0.20 \pm 0.06 \pm 0.02$	$0.24 \pm 0.06 \pm 0.02$

Table 4: Measured branching fractions. (a) $\psi(2S) \to l^+ l^-$ (b) $\psi(2S) \to J/\psi \pi^+ \pi^-$.

4 Observation of $\eta_c(2S)$ meson

The $\eta_c(2S)$ meson is still not experimentally well established. The Crystal Ball group reported a possible evidence for the $\eta_c(2S)$ meson with a mass of 3594 ± 5 MeV [23]. The result has not been confirmed by the subsequent experiments.

Using a data set that contains 44.1 million $B\overline{B}$ pairs, Belle has searched for the $\eta_c(2S)$ meson produced via the exclusive decays $B^+ \to \eta_c(2S) K^+$ and $B^0 \to \eta_c(2S) K^0$ where $\eta_c(2S) \to K_S K^- \pi^+$. To remove backgrounds from $B \to D(D_s) X$ and $B \to K^*(890) K$ decays, D, D_s and K^* vetoes are applied. The M_{bc} and ΔE distributions are plotted for twenty five $M_{K_S K \pi}$ bins. Clear B meson signals are seen in the bins corresponding to the η_c and near the expected mass of the $\eta_c(2S)$. The signal yields extracted from the simultaneous fits to the M_{bc} and ΔE distributions are plotted in Fig. 8. A clear peak is seen around 3.65 GeV/c^2 and identified as $\eta_c(2S)$. The distribution is fit to two Breit-Wigner functions for the η_c and $\eta_c(2S)$ respectively, a Gaussian for the J/ψ, and a second-order polynomial for the non-resonant contribution. These functions are convolved with a Gaussian resolution function determined from MC. The fit value for the mass is $3654 \pm 6 \pm 8$ MeV/c^2. The 90% confidence level upper limit for the intrinc width is 55 MeV/c^2. The results are consistent with expectations of heavy-quark potential models. The ratio of product branching fractions for the η_c

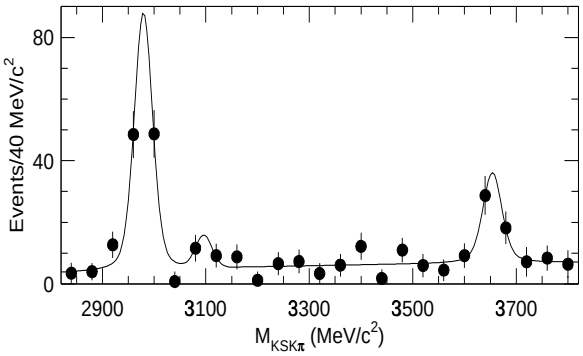

Figure 8: The signal yields for each $K_S K\pi$ bin. The curve is the result of the fit.

and $\eta_c(2S)$ is also measured to be

$$\frac{\mathcal{B}(B\to\eta_c(2S)K)\mathcal{B}(\eta_c(2S)\to K_S K^-\pi^+)}{\mathcal{B}(B\to\eta_c K)\mathcal{B}(\eta_c\to K_S K^-\pi^+)} = 0.38 \pm 0.12 \pm 0.05.$$

5 Summary

With the large $B\overline{B}$ data sets accumulated at the B-factories, we have improved the measurements of the branching fractions for the decays $B\to J/\psi K^{(*)}$, $B\to\psi(2S)K$, $B\to\chi_{c1}K$ and $B\to J/\psi\pi$. The decays modes $B^0\to\chi_{c1}K^{*0}$, $B^+\to\chi_{c0}K^+$, $B\to\chi_{c2}X$, $B^0\to\eta_c K^{*0}$ and $B\to J/\psi K_1(1270)$ have been observed for the first time. The branching fractions for the non-factorizable decays $B^+\to\chi_{c0}K^+$ and $B\to\chi_{c2}X$ are comparable to the factorizable decays $B^+\to J/\psi K^+$ and $B\to\chi_{c1}X$. Belle has observed the $\eta_c(2S)$ meson. Its properties are consistent with expectations of the heavy-quark potential models.

References

[1] B. Aubert *et al.* [BABAR Collaboration], Phys. Rev. Lett. **87**, 091801 (2001)

[2] K. Abe *et al.* [Belle Collaboration], Phys. Rev. Lett. **87**, 091802 (2001)

[3] B. Aubert *et al.* [BABAR Collaboration], hep-ex/0201020.

[4] K. Abe *et al.* [Belle Collaboration], hep-ex/0202027, submitted to Phys. Rev. D.

[5] B. Aubert *et al.* [BABAR Collaboration], hep-ex/0203007.

[6] K. Abe *et al.* [Belle Collaboration], Phys. Rev. Lett. **88**, 031802 (2002)

[7] K. Abe *et al.* [Belle Collaboration], hep-ex/0202028, submitted to Phys. Rev. Lett. .

[8] B. Aubert *et al.* [BABAR Collaboration], hep-ex/0203034.

[9] C. P. Jessop *et al.* [CLEO Collaboration], Phys. Rev. Lett. **79**, 4533 (1997)

[10] B. Aubert *et al.* [BABAR Collaboration], Phys. Rev. Lett. **87**, 241801 (2001)

[11] I. Dunietz, H. R. Quinn, A. Snyder, W. Toki and H. J. Lipkin, Phys. Rev. D **43**, 2193 (1991).

[12] T. Affolder *et al.* [CDF Collaboration], Phys. Rev. Lett. **85**, 4668 (2000)

[13] B. Aubert *et al.* [BABAR Collaboration], hep-ex/0203040.

[14] D. E. Groom *et al.* [Particle Data Group Collaboration], Eur. Phys. J. C **15**, 1 (2000).

[15] G. Brandenburg *et al.* [CLEO Collaboration], Phys. Rev. Lett. **85**, 3095 (2000)

[16] K. W. Edwards *et al.* [CLEO Collaboration], Phys. Rev. Lett. **86**, 30 (2001)

[17] M. Gourdin, Y. Y. Keum and X. Y. Pham, Phys. Rev. D **51**, 3510 (1995)

[18] S. J. Richichi *et al.* [CLEO Collaboration], Phys. Rev. D **63**, 031103 (2001)

[19] K. Abe *et al.* [Belle Collaboration], KEK-PREPRINT-2001-66, BELLE-CONF-0101, Aug 2001.

[20] K. Abe *et al.* [Belle Collaboration], Phys. Rev. Lett. **87**, 161601 (2001)

[21] B. Aubert *et al.* [BABAR Collaboration], Phys. Rev. D **65**, 032001 (2002)

[22] B. Aubert *et al.* [BABAR Collaboration], Phys. Rev. D **65**, 091101 (2002).

[23] C. Edwards *et al.*, Phys. Rev. Lett. **48**, 70 (1982).

May 18, session 3.

Session Chair: G. W. S. Hou

Radiative B Decays

Radiative B Decays — an Experimental Overview

Edward H. Thorndike
University of Rochester
Rochester, NY 14627, USA
CLEO Collaboration

1 Introduction

I'll give an informal, personal review of the status and direction of experiments on radiative B decays — $b \to s\gamma$ and $b \to d\gamma$. Let's start by listing the observables.

- the branching fractions for exclusive $b \to s\gamma$ decays, eg. $B \to K^*(892)\gamma$
- the branching fraction for the inclusive decay $b \to s\gamma$ (actually $B \to X_s\gamma$)
- the CP asymmetry in the inclusive decay and in exclusive decays:
  $a_{CP} \equiv (\Gamma(b \to s\gamma) - \Gamma(\overline{b} \to \overline{s}\gamma))/(\Gamma(b \to s\gamma) + \Gamma(\overline{b} \to \overline{s}\gamma))$
- the photon energy spectrum in inclusive decays $B \to X_s\gamma$
- in principle, all the same observables for $b \to d\gamma$

(In multibody final states, such as $B \to K\pi\pi\gamma$, there are additional observables, constructed from the particle momenta. I do not consider these observables here.)

What can each of these observables teach us? The branching fractions for exclusive $b \to s\gamma$ decays are the easiest of the observables, and CLEO's observation [1] of $B \to K^*(892)\gamma$ back in 1993 was the first penguin seen. But while that exclusive decay was fine for the 'existence proof', the rates for exclusive decays are not useful for searching for New Physics, because form factors are poorly known.

In contrast, the branching fraction for the inclusive decay $B \to X_s\gamma$ (X_s a sum over all final states containing an s quark), is ideal for revealing or limiting New Physics. Forbidden at tree level by GIM, the process proceeds via penguin diagrams. In the Standard Model, the loop contains $W^{\pm}$ and t, both heavy, and so New Physics penguins with, eg., squarks and winos in the loop, would give comparable contributions. Further, as a result of very hard theoretical work, the rate for $b \to s\gamma$ can be reliably calculated, both within the Standard Model and with New Physics.

CP asymmetries are very small in the Standard Model, 1% or less. They can reach 10 - 20 % in some New Physics proposals. The asymmetry for the inclusive

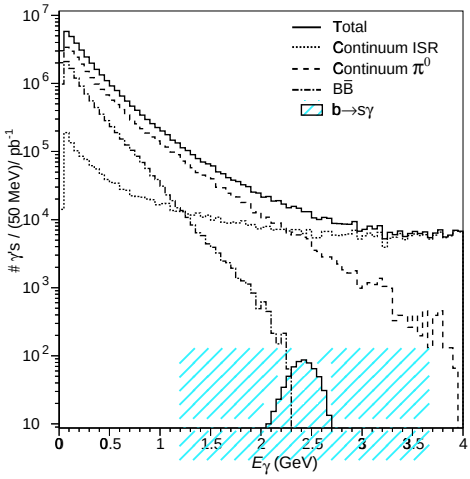

Figure 1: Photon energy spectrum expected from $b \to s\gamma$, other B decay processes, and from the continuum under the $\Upsilon(4S)$.

process is more reliably calculated than that for an exclusive process, but if a large CP asymmetry is found in either, that will be clear evidence of New Physics.

In contrast to branching fractions, the photon energy spectrum in $B \to X_s\gamma$ is very insensitive to New Physics. The basic process, $b \to s\gamma$, is a two-body decay, and hence gives a line in the b quark rest frame, broadened a bit by gluon bremsstrahlung. The photon energy spectrum for $B \to X_s\gamma$ thus depends on the mass and Fermi momentum of the b quark within the B meson. From the spectrum one can learn the B light cone shape function, useful for obtaining $|V_{ub}|$ from the endpoint lepton yield in $b \to u\ell\nu$. Also, the spectrum helps determine HQET OPE expansion parameters, needed for obtaining a precision value of $|V_{cb}|$ from the $b \to c\ell\nu$ inclusive rate.

The initial interest in $b \to d\gamma$ will be in determining $|V_{td}|$ from the rates for exclusive decays $B \to \rho\gamma$, $B \to \omega\gamma$. But here one must watch out for long distance effects and for additional CKM factors from c- and u-quark loops.

The experimental problems in studying radiative B decays are illustrated in Fig. 1. There one sees the photon energy spectrum expected from radiative B decays, from other B decay processes, and from the continuum under $\Upsilon(4S)$ – photons from initial state radiation and from decay of hadrons (dominantly from $\pi^0 \to \gamma\gamma$). While $b \to s\gamma$ can be distinguished from other B decay processes by measuring the yield above 2.2 GeV, the contribution from the continuum – two orders of magnitude larger than the signal – is a major challenge. Techniques for suppressing the continuum background are a MUST. With such techniques, and the power of full B reconstruction, exclusive decay modes stand out above the continuum background. For the inclusive process $B \to X_s\gamma$, it is essential to measure and subtract the continuum background, by

running below the $\Upsilon(4S)$.

While $b \to s\gamma$ can be separated from other B decay processes by considering only the yield above 2.2 GeV, that approach is inadequate for the precision of today's $b \to s\gamma$ inclusive branching fraction measurements, and also for obtaining a useful photon spectrum. For these, one must go down to at least 2.0 GeV, understanding and removing the substantial yield from other B decay processes between 2.0 and 2.2 GeV.

In subsequent sections I discuss branching fractions for exclusive $b \to s\gamma$ decays; the branching fraction for the inclusive $b \to s\gamma$ decay; CP asymmetries; the photon energy spectrum; $b \to d\gamma$ decays. In Section 7, I summarize and give conclusions.

2 Branching Fractions for Exclusive $b \to s\gamma$ Decays

CLEO's 1993 observation [1] of eight $B^0 \to K^{*0}\gamma$ events and five $B^+ \to K^{*+}\gamma$ events was based on 1.4 fb^{-1} of 4S luminosity. With an order of magnitude more luminosity, CLEO [2], BaBar [3], and Belle [4] now all have 10-20% measurements of both charged and neutral decays. Results are given in Table 1. Agreement among measurements is good. Branching fractions for charged and neutral decays agree well.

	$B^0 \to K^{*0}\gamma$	$B^+ \to K^{*+}\gamma$
CLEO '93[1]	$4.0 \pm 1.7 \pm 0.8$	$5.7 \pm 3.1 \pm 1.1$
CLEO '00[2]	$4.55 \pm 0.70 \pm 0.34$	$3.76 \pm 0.86 \pm 0.28$
BaBar '02[3]	$4.23 \pm 0.40 \pm 0.22$	$3.83 \pm 0.62 \pm 0.22$
Belle(prelim)[4]	$4.08 \pm 0.34 \pm 0.26$	$4.92 \pm 0.57 \pm 0.38$
Average	$4.21 \pm 0.25 \pm 0.26$	$4.32 \pm 0.38 \pm 0.30$

Table 1: $B \to K^*\gamma$ branching fractions (10^{-5})

In addition to $K^*(892)$, CLEO [2] and Belle [5, 4] have observed $B \to K_2^*(1430)\gamma$, with branching fractions of $1.66 \pm 0.56 \pm 0.13 \times 10^{-5}$ and $1.50 \pm 0.56 \pm 0.12 \times 10^{-5}$, in good agreement and of comparable accuracy. Belle has also [5] observed $B^+ \to K^+\pi^-\pi^+\gamma$ ($2.4 \pm 0.5 \pm 0.3 \times 10^{-5}$), and deduced substructures $B^+ \to K^{*0}\pi^+\gamma$ ($2.0 \pm 0.65 \pm 0.2 \times 10^{-5}$), $B^+ \to K^+\rho^0\gamma$ ($1.0 \pm 0.5 \pm 0.25 \times 10^{-5}$). There is no evidence of a nonresonant component, with upper limit $\mathcal{B}(B^+ \to K^+\pi^-\pi^+\gamma)NR < 0.9 \times 10^{-5}$.

3 Branching Fraction for Inclusive $b \to s\gamma$ Decay

For a study of the inclusive process $B \to X_s\gamma$, lacking the discrimination that comes from full B reconstruction, continuum suppression is very important. In the 'first

observation of inclusive' analysis, CLEO [6] used two approaches. The first was to choose several (eight) "shape variables", each with some power to discriminate between $b \to s\gamma$ signal and continuum background (either ISR or γ's from hadrons), and combine them into a single variable using a neural net. (This was CLEO's first use of a neural net, and I was initially very negative about the approach. Its success made me a convert.)

The second approach, dubbed "pseudoreconstruction", at first sight appears just like full reconstruction. Events containing a high energy photon are searched for combinations of particles that satisfy $B \to X_s\gamma$. For X_s, we try one kaon ($K^\pm$ or $K^0_s \to \pi^+\pi^-$), and 1 to 4 pions (of which at most one may be a π^0). The measure of "satisfying $B \to X_s\gamma$" is closeness of M and E to the proper values, as given by $\chi^2_B \equiv (E - E_{beam})^2/\sigma^2_E + (M - M_B)^2/\sigma^2_M$. A $\chi^2_B < 20$ is deemed an acceptible pseudoreconstruction. What makes this "pseudoreconstruction", rather than full reconstruction, is our lack of concern as to whether we "have all the pieces right." True $B \to X_s\gamma$ events are much more likely to pseudoreconstruct than are continuum background events, and this remains true with one or two mis-chosen pions. Further, $\cos\theta_{tt}$, the cosine of the angle between the thrust axis of the particles that pseudoreconstruct and the thrust axis of the rest of the event, is strongly peaked for the jet-like continuum events, but isotropic for signal events. (I was initially *very* dubious about this technique, fearing that it would be very sensitive to the choice of model for $B \to X_s\gamma$, but this proved not to be the case.)

In CLEO's 1995 publication [6], we performed two separate analyses, one using shape variables with a neural net, the other using pseudoreconstruction. We then averaged the two branching fractions so obtained. In CLEO's latest publication [7], we did a fully integrated analysis. For all events with a high energy photon, we obtained a combined shape variable parameter from the neural net (8 inputs, 1 output). For the subset of events that had a pseudoreconstruction with $\chi^2_B < 20$, we obtained two additional discriminating parameters, χ^2_B and $|\cos\theta_{tt}|$. For the subset that contained a lepton (e or μ), we used the energy of the lepton and the angle between lepton and high energy photon as additional discriminating parameters. Armed with these discriminating parameters (sometimes only 1, sometimes 3, sometimes 5), we determined the probability that an event with a high energy photon was $b \to s\gamma$ rather than continuum background, and assigned it a weight according to that probability.

The distribution in weights so obtained *vs.* photon energy is shown in Fig. 2. The upper panel shows On-resonance and scaled Off-resonance data. The success of the continuum suppression is apparent, in that the continuum background is now a mere factor of 4 larger than the signal, rather than the two orders of magnitude in Fig. 1.

The lower panel in Fig. 2 shows the yield in weights *vs.* photon energy after the continuum background has been subtracted, using Off-resonance data. There one sees clear evidence for $b \to s\gamma$ in the 2.2 - 2.6 GeV range, and also the increasing importance of the other B decay processes below 2.2 GeV.

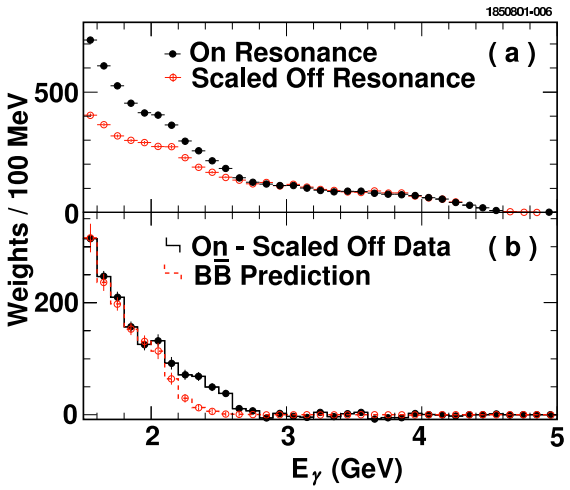

Figure 2: CLEO's [7] photon energy spectrum: (a) On resonance and scaled Off resonance; (b) On minus scaled Off, and prediction for $B\overline{B}$ processes other than $b \to s\gamma$ and $b \to d\gamma$.

In its first measurement [6], CLEO placed a cut on photon energy at 2.2 GeV, using theoretical models to account for the fraction of $b \to s\gamma$ rate below 2.2 GeV, and accepting a systematic error for this model dependence. In the recent measurement [7], by making a strenuous effort to understand background from B decay processes, CLEO lowered its photon energy cut to 2.0 GeV, thereby accepting ~90% of the rate, and reducing the systematic error from model dependence. To be competitive, future measurements will have to accept photons down to at least 2.0 GeV.

In addition to CLEO's two published measurements, there have been measurements by ALEPH [8] and Belle [9]. All four results are shown in Fig. 3. Difficult as the measurement is at the $\Upsilon(4S)$, it seems to me to be near impossible at the Z^0, and ALEPH's efforts must be characterized as heroic. Their result is consistent with the $\Upsilon(4S)$ measurements, but their error is twice that of the recent CLEO measurement. The Belle measurement, based on only 6 fb^{-1}, and with the now no-longer-acceptible 2.2 GeV photon energy cut, should be viewed as a warmup exercise.

The Standard Model theoretical expectation, as given most recently by Buras *et al.* [10], is also shown in Fig. 3. It should be mentioned that there have recently been questions raised [11] as to the appropriate value of m_c/m_b to use in the calculation. Buras *et al.* have used $m_c/m_b = m_c^{\overline{MS}}(\mu)/m_b^{1S} = 0.22$, while earlier work used $m_c/m_b = m_c^{pole}/m_b^{pole} = 0.29$, and obtained a branching fraction lower by 0.25×10^{-4}. My impression is that the theoretical community is not of a single mind as to the appropriate value of m_c/m_b to use, and so the SM theory value might come down by 10%. In any case, experiment and SM theory are in fine agreement.

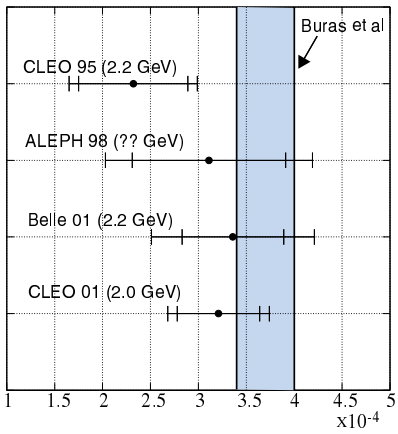

Figure 3: Measurements of the branching fraction for the inclusive process $b \to s\gamma$, by CLEO in 1995 [6], ALEPH [8], Belle [9], and CLEO in 2001 [7]. The Standard Model prediction of Buras *et al.* [10] is also shown .

4 CP Asymmetries

There have been measurements of the CP asymmetry in $B \to K^*(892)\gamma$ by CLEO [2], BaBar [3], and Belle [4], and a measurement of the CP asymmetry in $B \to X_s\gamma$ plus $B \to X_d\gamma$ inclusive by CLEO [12]. The *sign convention*, to my knowledge so far used in all measurements of B CP asymmetries, is b quark minus $\overline{b}$ quark (B^- minus B^+, $\overline{B}^0$ minus B^0). For the cases at hand, that means $a_{CP} \equiv (\Gamma(b \to s\gamma) - \Gamma(\overline{b} \to \overline{s}\gamma)/(\Gamma(b \to s\gamma) + \Gamma(\overline{b} \to \overline{s}\gamma)$, and similarly with the exclusive decays.

Results for the exclusive decays are shown in Table 2. CLEO's inclusive result, a combination of $b \to s\gamma$ and $b \to d\gamma$, is $(0.965a(b \to s\gamma) + 0.02a(b \to d\gamma)) = -0.079 \pm 0.108 \pm 0.022$. All these results, including the average of the three exclusive measurements, are consistent with zero, the Standard Model expectation.

	$a_{CP}(B \to K^*\gamma)$
CLEO '00[2]	$+0.08 \pm 0.13 \pm 0.03$
BaBar '02[3]	$-0.044 \pm 0.076 \pm 0.012$
Belle(prelim)[4]	$+0.032 \pm 0.069 \pm 0.020$
Average	$+0.009 \pm 0.048 \pm 0.018$

Table 2: $B \to K^*\gamma$ CP asymmetries

5 The Photon Energy Spectrum

As can be seen from Fig. 2, in order to obtain the photon energy spectrum for the inclusive $B \to X_s\gamma$ process, to photon energies of 2.0 GeV and below, one must understand backgrounds from B decay processes. Unlike those from continuum processes, these cannot be directly measured. CLEO [7] has proceeded as follows.

The dominant component of the background, accounting for 90%, is photons from $\pi^0 \to \gamma\gamma$ and $\eta \to \gamma\gamma$ that have escaped the π^0 and η vetoes. These backgrounds are determined by measuring π^0 (η) yields, treating the π^0 (η) as if it were a γ, applying all cuts and determining the event weight, just as in the $b \to s\gamma$ analysis. Monte Carlo is then used to determine the π^0 (η) veto inefficiency.

Photons from other sources are small by comparison to those from π^0 and η, and with modest efforts to have the Monte Carlo event generator accurate, one can (CLEO does) trust the Monte Carlo. Processes considered include $\omega \to \pi^0\gamma$, $\eta' \to \rho^0\gamma$, radiative ψ decay, $\rho \to \pi\gamma$, $a_1 \to \pi\gamma$, final state radiation. In addition to the dominant $b \to c$ decays, $b \to u$ processes and $b \to sg$ processes were considered.

Neutral hadrons, in particular antineutrons and K-longs, by interacting in the calorimeter, cause high energy clusters, above 1.5 GeV. Their contribution to the B decay background was determined by fitting the lateral distribution of the shower (E9/E25, for those familiar with this notation).

CLEO's observed laboratory frame photon energy spectrum for On-resonance minus scaled Off-resonance minus B backgrounds (the $b \to s\gamma$ plus $b \to d\gamma$ signal) is shown in Fig. 4.

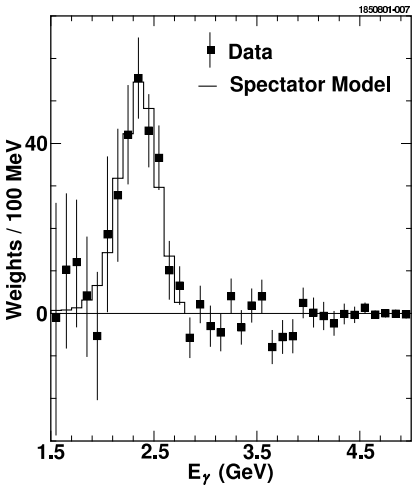

Figure 4: CLEO's [7] observed laboratory frame photon energy spectrum for On minus scaled Off minus B backgrounds, the putative $b \to s\gamma$ plus $b \to d\gamma$ signal.

From the measured spectrum CLEO has obtained first and second moments, in the B rest frame, for $E_\gamma^{restframe} > 2.0$ GeV, finding

$\langle E_\gamma \rangle = 2.346 \pm 0.032 \pm 0.011$ GeV, and

$\langle (E_\gamma - \langle E_\gamma \rangle)^2 \rangle = 0.0226 \pm 0.0066 \pm 0.0020$ GeV^2.

HQET plus OPE allows inclusive observables to be written as double expansions, in powers of α_s and $1/M_B$. The parameter $\overline{\Lambda}$ enters at order $1/M_B$, λ_1 and λ_2 enter at $1/M_B^2$, and six more parameters, ρ_1, ρ_2 and $\mathcal{T}_1 - \mathcal{T}_4$ at $1/M_B^3$. Using expressions in the $\overline{MS}$ renormalization scheme, to order $1/M_B^3$ and order $\alpha_s^2\beta_0$, CLEO obtains $\overline{\Lambda} = 0.35 \pm 0.08 \pm 0.10$ GeV from the first moment. The expression for the second moment converges slowly in $1/M_B$, and CLEO did not extract parameters from it.

To lowest order in Λ_{QCD}/M_B, the hadron level $B \to X_s\gamma$ photon energy spectrum is given by a convolution of the parton level $b \to s\gamma$ photon energy spectrum with the $b \to lightquark$ light cone shape function of the B meson [13]. Again to lowest order in Λ_{QCD}/M_B, the same shape function describes $B \to X_u\ell\nu$, i.e., the hadron level $B \to X_u\ell\nu$ lepton energy spectrum is given by a convolution of the parton level $b \to u\ell\nu$ lepton energy spectrum with the same shape function [14]. CLEO has thus used their measured $B \to X_s\gamma$ photon energy spectrum to determine (to some accuracy) the light cone shape function, and from this predicted the fraction of the $B \to X_u\ell\nu$ lepton energy spectrum that lies above some cut near the endpoint. This, combined with a measurement of the $B \to X_u\ell\nu$ yield above that cut gives the total $B \to X_u\ell\nu$ yield, and that in turn gives $|V_{ub}|$ [15]. Corrections enter at next order in Λ_{QCD}/M_B, and these are currently the subject of active investigation [16, 17, 18].

6 $b \to d\gamma$

So far there is nothing on inclusive $b \to d\gamma$. On exclusive $b \to d\gamma$, there are upper limits on $B^+ \to \rho^+\gamma$, $B^0 \to \rho^0\gamma$, and $B^0 \to \omega\gamma$. From isospin and SU(3) considerations, one expects $\mathcal{B}(B^+ \to \rho^+\gamma) = 2 \times \mathcal{B}(B^0 \to \rho^0\gamma) = 2 \times \mathcal{B}(B^0 \to \omega\gamma)$. Upper limits, from CLEO [2], Belle [19], and BaBar [20], are given in Table 3. The BaBar limit is by far the best. Since CLEO's first observation of $B \to K^*(892)\gamma$ was based on 1.4 fb^{-1}, and since $B^+ \to \rho^+\gamma$ is expected to be 20 times smaller than $B \to K^*\gamma$, one can anticipate an observation by BaBar and/or Belle in the near future.

From their limit, BaBar [20] obtains $[(1-\rho)^2 + \eta^2]^{1/2} < 1.6$. This limit, while not an improvement in the limit on $|V_{td}|$ over that obtained from the limit on $B_s - \overline{B}_s$ mixing, provides nice confirmation. But, I should repeat the warning that, as accuracy improves, one needs to watch out for long distance effects, and for contributions from c- and u-quark loops, carrying other CKM factors.

	B pairs (Million)	Branching Fraction Upper Limits (10^{-6})		
		$\mathcal{B}(B^+ \to \rho^+\gamma)$	$2 \times \mathcal{B}(B^0 \to \rho^0\gamma)$	$2 \times \mathcal{B}(B^0 \to \omega\gamma)$
CLEO '00[2]	9.7	13	34	18
Belle '01[19]	11	10	21	—
BaBar(prelim)[20]	63	2.8	3.0	—

Table 3: Upper limits on $B^+ \to \rho^+\gamma$, $B^0 \to \rho^0\gamma$, and $B^0 \to \omega\gamma$ branching fractions

7 Summary and Conclusions

$b \to s\gamma$ Exclusive Branching Fractions
These are no longer of great fundamental interest. However, by identifying a larger fraction of the makeup of $B \to X_s\gamma$ decays, one will reduce some systematic errors on the branching fraction for the inclusive process $b \to s\gamma$. Belle has made progress on this front. Perhaps more important, their observation of $B \to K\pi\pi\gamma$ lays the groundwork for looking at correlations among the momentum vectors of the decay products, providing a way to "measure" the helicity of the photon.

$b \to s\gamma$ Inclusive Branching Fraction
Experiment agrees well with the predictions of the Standard Model, and places strong restrictions on New Physics. But there is really only one good measurement, CLEO's. BaBar and Belle need to get to work on this one. They will need to accept photons down to 2.0 GeV or lower – 2.2 GeV is no longer good enough. They will also need to take sufficient data at beam energies below the $\Upsilon(4S)$, as the continuum subtraction *must* be done with *data*.

CP Asymmetries
So far there is no hint of a non-zero value. Present limits place weak restrictions on some New Physics models. There is *plenty* of room for improvements, with BaBar and Belle's large data samples, before systematic error limitations set in. Asymmetry measurements for the *inclusive* decay are desirable (BaBar, Belle?).

Photon Energy Spectrum
CLEO's photon energy spectrum has helped provide a precise determination of $|V_{cb}|$ from the inclusive semileptonic decay branching fraction, and (more important) a good determination of $|V_{ub}|$ from the lepton endpoint yield in $b \to u\ell\nu$, with *quantifiable errors*. Measurements of the spectrum will be key for future determinations of $|V_{ub}|$ from inclusive $b \to u\ell\nu$. Improved measurements of the spectrum are highly desirable.

$b \to d\gamma$ Searches
So far there is nothing on inclusives, and only upper limits on exclusives. These limits are not yet an improvement in the limit on $|V_{td}|$ over that provided by the limit on $B_s - \overline{B}_s$ mixing. But with data samples of 100 fb^{-1}, BaBar and Belle should see

$B \to \rho\gamma$. Stay tuned.

I have benefitted from interactions with my many CLEO collegues. Particular thanks are due to Dan Cronin-Hennessy for his assistance in preparing this talk and writeup.

References

[1] R. Ammar *et al.* (CLEO), Phys. Rev. Lett. **71**, 674 (1993). $K^*\gamma$ discovery

[2] T. E. Coan *et al.* (CLEO), Phys. Rev. Lett. **84**, 5283 (2000).

[3] B. Aubert *et al.* (BaBar), Phys. Rev. Lett **88**, 101805 (2002).

[4] A. Ishikawa (Belle), XXXVIIth Rencontres de Moriond, March 10, 2002.

[5] S. Nishida *et al.* (Belle), hep-ex/0205025.

[6] M. S. Alam *et al.* (CLEO), Phys. Rev. Lett. **74**, 2885 (1995).

[7] S. Chen *et al.* (CLEO), Phys. Rev. Lett. **87**, 251807 (2001).

[8] R. Barate *et al.* (ALEPH), Phys. Lett. **B 429**, 169 (1998).

[9] K. Abe *et al.* (Belle) Phys. Lett. B **511**, 151 (2001).

[10] A. Buras, A. Czarnecki, M. Misiak, and J. Urban, hep-ph/0203135.

[11] P. Gambino and M. Misiak, hep-ph/0104034.

[12] T. E. Coan *et al.* (CLEO), Phys. Rev. Lett. **86**, 5661 (2001).

[13] A. L. Kagan and M. Neubert, Eur. Phys. J. C **7**, 5 (1999).

[14] F. De Fazio and M.Neubert, JHEP **06**, 017 (1999).

[15] A. Bornheim *et al.* (CLEO), Phys. Rev. Lett. **88**, 231803 (2002).

[16] C. Bauer, M. Luke, and T. Mannel, hep-ph/0205150.

[17] A.Leibovich, Z. Ligeti, and M. Wise, hep-ph/0205148.

[18] M. Neubert, private communication.

[19] Y. Ushiroda (Belle), hep-ex/0104045.

[20] H. Tanaka (BaBar), XXXVIIth Rencontres de Moriond, March 2002.

$B \to X_s \ell^+ \ell^-$ at Belle

Katsumi Senyo
Department of Physics
Nagoya University
Nagoya, 464-8602 JAPAN

1 Introduction

The electroweak penguin mediated $B \to X_s \ell^+ \ell^-$ decay is a good probe to study beyond the Standard Model physics at low energy. The effect of new physics could be observed as corrections to the branching fraction, di-lepton invariant mass spectrum, and to the Wilson coefficients such as C_9, C_{10}, and a phase of C_7 [1-10]. Experimentally, the exclusive $B \to K \ell^+ \ell^-$ decay was observed by the Belle collaboration for the first time [11] and has also recently confirmed by the BABAR collaboration [12]. We present here a preliminary result on a search for the inclusive $B \to X_s \ell^+ \ell^-$ decay, which can be calculated more reliably than exclusive decay modes.

2 Analysis

The data sample used in this analysis consists of 43 fb^{-1} of e^+e^- collisions at the $\Upsilon(4S)$ resonance collected by the Belle detector [13] at the KEKB storage ring.

The signal is identified as $X_s \ell^+ \ell^-$, where X_s is defined to be a $K^\pm$ or K_S accompanying 0 to 4 pions including one π^0 at most, and $\ell^+ \ell^-$ is an oppositely charged electron or muon pair. Charged tracks are required to originate from the interaction point and be well identified by the Belle particle identification devices. Electrons are identified using the ratio between the energy deposited in the electromagnetic calorimeter and the measured track momentum(E/p). Electrons are required to have momenta above 0.5 GeV/c. Muon candidates are required to reach the iron flux return and have momenta greater than 1.0 GeV/c. The muon identification efficiency is about 80 to 85 % with a fake rate of 1 to 2 %. Charged hadrons are identified by the combined response of aerogel counters, time of flight, and dE/dx measured in the drift chamber. For charged kaons, we have an efficiency of 85 to 90% and a pion fake rate that is less than 10%. Candidate π^0's are identified from pairs of photons with energy deposits of at least 50 MeV and an invariant mass within 10 MeV/c^2 of the nominal π^0 mass.

Events with leptons from charmonia, such as J/ψ and ψ' are vetoed if the dilepton mass lies around the nominal charmonia masses.

Background from $q\overline{q}$ continuum events is suppressed by requiring the ratio of the second to zeroth Fox-Wolfram moments $R_2 \equiv H_2/H_0 < 0.35$ and $|\cos\theta_{thrust}| < 0.85$, where θ_{thrust} is the angle between the thrust axis of the B candidate and that of the rest of the event. The $|\cos\theta_{thrust}|$ distribution of continuum events peaks at 1 while that of signal events is flat.

To reduce backgrounds further and select the best candidate in an event, we introduce four kinematic variables: the angles between the K and $\ell^+(\theta_{K\ell^+})$, and the K and $\ell^-(\theta_{K\ell^-})$, the B flight direction(θ_B), and the energy difference$(\Delta E = E_B - E_{beam})$. If the K meson and $\ell^+\ell^-$ pair originated from a photon or Z boson; since these are emitted in opposite directions, the sum of $\cos\theta_{K\ell^+}$ and $\cos\theta_{K\ell^-}$ should be negative for the signal. The polar angle of B flight direction has a $1-\cos^2\theta_B$ distribution while background is flat. The signal ΔE distribution peaks at zero.

A likelihood ratio LR is determined by parameterizing distributions of three kinematic variables with Monte Carlo simulation for both the signal and background. It is expressed as $LR = p_{sig}/(p_{sig} + p_{BG})$, where p_{sig} and p_{BG} are probability density functions for the signal and background distributions, respectively. An LR selection requirement is chosen to maximize the figure of merit $S/\sqrt{S+N}$ in the signal region where S is the expected signal yield assuming the SM prediction and N is the number of expected background events.

The invariant mass of the X_s must satisfy $M_{X_s} < 2.1$ GeV/c^2 in order to reject combinatorial background.

After the application of all selection requirements, the reconstruction efficiencies are estimated by Monte Carlo simulation based on the inclusive model in the recent paper by Ali *et al.*,[1] and based on the exclusive $B\to K\ell^+\ell^-$ and $B\to K^*\ell^+\ell^-$ model by Greub *et al.*,[2]. The nominal reconstruction efficiencies are determined to be 3.6 % for $B\to X_s e^+e^-$ and 3.8 % for $B\to X_s\mu^+\mu^-$.

Most of the background is combinatorial background from B and D decays. The background is determined by fitting the distribution of beam constrained mass M_{bc}. The beam constrained mass is expressed as $M_{bc} = \sqrt{(E_{beam})^2 - (p_B)^2}$, where p_B is the B candidate's center-of-mass momentum vector and E_{beam} is the center-of-mass energy of B meson, respectively. In this distribution, the signal peaks at the B meson mass and is fitted by a Gaussian function while the combinatorial background is parameterized by a phase space function with a kinematic threshold (the ARGUS function).

Background from $B\to X_s\pi^+\pi^-$ decay can make a small contribution to the signal peak in the M_{bc} distribution when both the π^+ and π^- are misidentified as muons. The muon misidentification rate is determined to be 1 to 2 % in the laboratory momentum range $p_\mu > 1.0$GeV/c. To estimate the contamination in the signal region, a $B\to X_s\pi^+\pi^-$ sample is selected by applying all the signal selection requirements ex-

cept for the muon identification. The yield is multiplied by the momentum dependent fake rate for each pion. This $B \to X_s \pi^+ \pi^-$ background is estimated to be 2.4 events and subtracted from the yield of the signal fit.

3 Results and discussion

Figure 1 shows the M_{bc} distribution for $B \to X_s e^+ e^-$, $B \to X_s \mu^+ \mu^-$, and for the combined $B \to X_s \ell^+ \ell^-$ samples, respectively. The $B \to X_s e^\pm \mu^\mp$ sample is used to check the background parameterization. The fit results, signal yields, branching fractions, and statistical significances are shown in Table 1.

Systematic uncertainties in this measurement are listed in Table 2. The largest contribution to the systematic uncertainty is the decay modeling for $B \to X_s e^+ e^-$ and $B \to X_s \mu^+ \mu^-$ decays.

We measure the inclusive $B \to X_s \ell^+ \ell^-$ decay branching fraction for the first time with a statistical significance of greater than 4σ. Preliminary results for branching fractions are $\mathcal{B}(B \to X_s \mu^+ \mu^-) = (8.9^{+2.3+1.6}_{-2.1-1.7}) \times 10^{-6}$ and $\mathcal{B}(B \to X_s \ell^+ \ell^-) = (7.1^{+1.6+1.4}_{-1.6-1.2}) \times 10^{-6}$, where the first error is statistical and the second is systematic.

The branching fractions and upper limits determined by this study agree well with theoretical predictions in the SM framework. We expect that both the theoretical and experimental errors will decrease so that theories based on SM can be tested with precision measurements in the near future.

The M_{X_s} and dilepton invariant mass plots are shown in Figures 2 and 3, respectively. The M_{X_s} distribution extends beyond the K and K^* mass region. The dips around 3.1GeV/c^2 and 3.7GeV/c^2 in the $M_{\ell\ell}$ distribution are due to J/ψ and ψ' vetoes. The experimental and theoretical uncertainties are expected to improve as more data is accumulated. Precision measurements can be done for SM and beyond SM predictions.

In summary, evidence for the inclusive $B \to X_s \ell^+ \ell^-$ decay has been presented for the first time. The experimental and theoretical uncertainties are expected to decrease with time. Precision measurements can be done in near future that test the Standard Model and Beyond the Standard Model predictions.

References

[1] A. Ali, E. Lunghi, C. Greub, and G. Hiller, hep-ph/0112300.

[2] C. Greub, A. Ioannissian and D. Wyler, Phys. Lett. **B346**,149(1995).

[3] F. Borzumati and C. Greub, Phys. Rev. **D58**, 074004(1998);F. Borzumati and C. Greub, Phys. Rev. **D59**, 057501(1999); M. Ciuchini, G. Degrassi, P. Gambino and G. F. Giudice, Nucl. Phys. **B527**, 21(1998).

Mode	#signal	B.F.($\times 10^{-6}$)	Signif.
$X_s e^+ e^-$	$16.6^{+8.0+3.9}_{-7.3-3.8}$	< 11.0	2.1
$X_s \mu^+ \mu^-$	$30.7^{+7.9+5.4}_{-7.4-3.8}$	$8.9^{+2.3+1.6}_{-2.1-1.7}$	4.4
$X_s \ell^+ \ell^-$	$47.6^{+11.0+9.6}_{-10.4-8.0}$	$7.1^{+1.6+1.4}_{-1.6-1.2}$	4.8

Table 1: Preliminary results for $B \to X_s e^+ e^-$, $X_s \mu^+ \mu^-$, and combined $X_s \ell^+ \ell^-$. Significance is extracted from the statistical error only. Only a 90% confidence level upper limit is shown for the $B \to X_s e^+ e^-$ process.

Source	$X_s e^+ e^-$	$X_s \mu^+ \mu^-$
Tracking	8.1 %	8.0 %
Kaon ID	1.9 %	2.0 %
Pion ID	0.8 %	0.8 %
Lepton ID	3.6 %	4.4 %
K_S detection	2.1 %	1.5 %
π^0 detection	2.0 %	1.6 %
MC stat.	3.9 %	4.1 %
Decay model	$^{+14\%}_{-9\%}$	$^{+16\%}_{-12\%}$
Total	$^{+18\%}_{-14\%}$	$^{+19\%}_{-16\%}$

Table 2: Systematic uncertainty summary.

[4] T. Besmer, C. Greub and T. Hurth, CERN-TH-2001-136, BUTP-01-12, ZU-TH-15-01, hep-ph/0105292; M. Ciuchini, G. Degrassi, P. Gambino and G. F. Giudice, Nucl. Phys. **B534**, 3(1998), C. Bobeth, M. Misiak and J. Urban, Nucl. Phys. **B567**, 153(2000); F. Borzumati, C. Greub, T. Hurth an D. Wyler, Phys. Rev. **D62**, 075005(2000).

[5] T.Gotou, Y. Okada and Y. Shimizu, KEK-TH-611, hep-ph/9908499.

[6] A. Ali, G. F. Giudice and T. Mannel, Z. Phys. **C67**, 417(1995); A. Ali, T. Mannel and T. Morozumi, Phys. Lett. **B273**, 505(1991); W. Jaus and D. Wyler, Phys. Rev. **D41**, 3405(1990).

[7] A. Ali, P. Ball, L. T. Handoko and G. Hiller, Phys. Rev. **D61**, 074024(2000).

[8] D. Melikhov and N. Nikitin, Phys. Lett. **B410**, 290(1997).

[9] A. Ali, G. Hiller, L. T. Handoko and T. Morozumi, Phys. Rev. **D55**, 4105(1997).

[10] F. Kruger and L. M. Sehgal, Phys. Lett. **B380**, 199(1996).

[11] K. Abe, *et al.,*(Belle Collaboration), Phys. Rev. Lett. **88**, 021801(2002).

[12] J. Walsh (BABAR Collaboration), presented at Flavor Physics and CP Violation(FPCP) at Philadelphia, 2002.

[13] A. Abashian *et al.,*(Belle Collaboration), Nucl. Instr. and Meth. **A479**, 117 (2002).

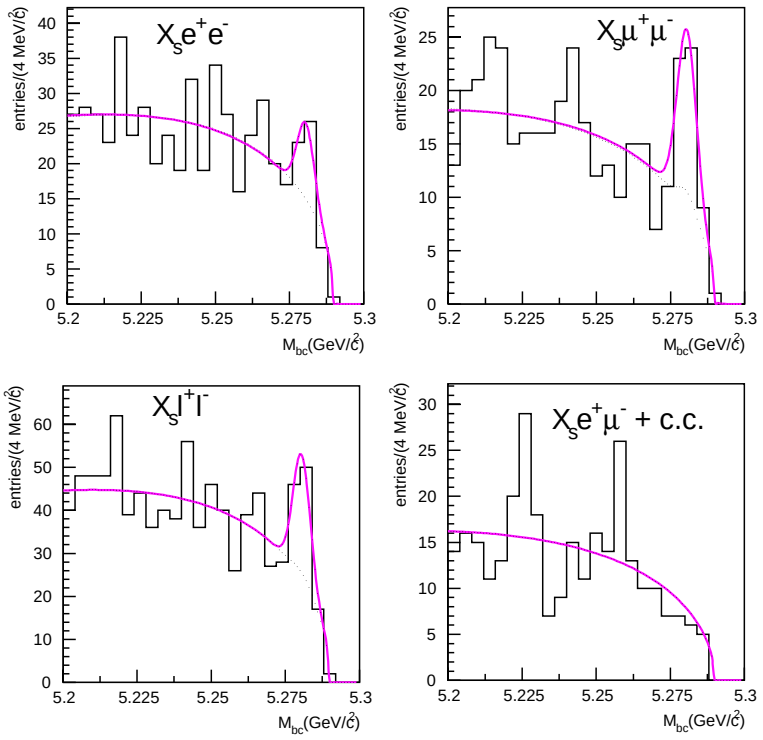

Figure 1: M_{bc} distributions and fit results. Top-left: $X_s e^+ e^-$ candidates, top-right: $X_s \mu^+ \mu^-$ candidates, bottom-left: $X_s \ell^+ \ell^- = (X_s e^+ e^-) + (X_s \mu^+ \mu^-)$ candidates, and bottom-right: $X_s e^\pm \mu^\mp$ to estimate combinatorial background. The significance is determined from the statistical error only.

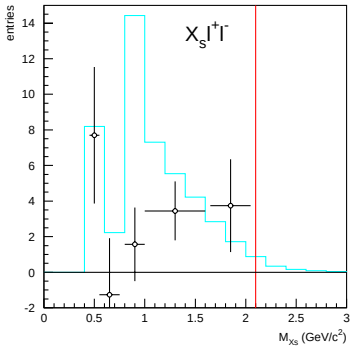

Figure 2: Comparison of the M_{X_s} distribution for data and MC.

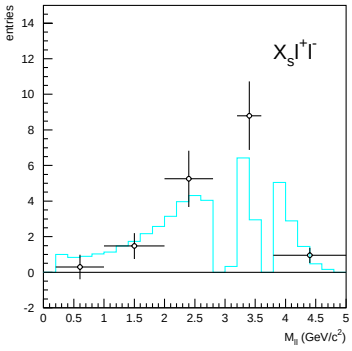

Figure 3: Comparison of the $M_{\ell\ell}$ distribution for data and MC.

BABAR Results on the Decays $B \to K\ell^+\ell^-$ and $B \to K^*\ell^+\ell^-$

John J. Walsh
(on behalf of the BABAR Collaboration)
Istituto Nazionale di Fisica Nucleare
Sezione di Pisa
john.walsh@pi.infn.it

Abstract

We present preliminary results on a search for the rare decays $B \to K\ell^+\ell^-$ and $B \to K^*\ell^+\ell^-$ performed with the *BABAR* experiment at the PEP-II B Factory. The data set consists of approximately 60 million $\Upsilon(4S) \to B\overline{B}$ decays. We obtain the results:

$$\mathcal{B}(B \to K\ell^+\ell^-) = (0.84^{+0.30+0.10}_{-0.24-0.18}) \times 10^{-6}$$
$$\mathcal{B}(B \to K^*\ell^+\ell^-) < 3.5 \times 10^{-6} \text{ at } 90\% \text{ C.L.} \quad (1)$$

1 Introduction

The flavor-changing neutral current decays $B \to K\ell^+\ell^-$ and $B \to K^*\ell^+\ell^-$ (where ℓ is understood to be an electron or a muon) proceed primarily via the one-loop diagrams, known as penguin and box diagrams. The Standard Model branching ratios are predicted to be quite small, on the order of 10^{-7} to 10^{-6} [1, 2]. However, significant enhancements to the branching ratios are obtained when considering extensions to the Standard Model, such as super-symmetry [1, 2]. Indeed, these channels are very interesting due to their sensitivity to New Physics.

The decay modes considered for this analysis are eight in number: $B^+ \to K^+\ell^+\ell^-$, $B^0 \to K^0_S\ell^+\ell^-$, $B^+ \to K^{*+}\ell^+\ell^-$ and $B^0 \to K^{*0}\ell^+\ell^-$, where $K^{*0} \to K^+\pi^-$, $K^{*+} \to K^0_S\pi^+$, $K^0_S \to \pi^+\pi^-$, and ℓ is either an e or μ. Charge-conjugate modes are implied throughout this paper. The results contained herein are preliminary.

The data set used to in the analysis consists of 56.4 fb^{-1} of on-peak data, corresponding to about 60 million $B\overline{B}$ pairs produced. We do not discuss the *BABAR* apparatus here, details can be found in reference [3].

Two primary kinematic variables are used to extract the signal from the background. The energy substituted mass, $m_{ES}\sqrt{E^{*2}_{\rm b} - (\sum_i \mathbf{p}^*_i)^2}$ and $\Delta E = \sum_i \sqrt{m_i^2 + \mathbf{p}^{*2}_i} - E^*_{\rm b}$, where $E^*_{\rm b}$ is the beam energy in the e^+e^- rest (c.m.) frame, $\mathbf{p}^*_i$ is the c.m. momentum of daughter particle i in the B meson candidate, and m_i is the mass of particle i. Signal events have m_{ES} near the B meson mass (resolution is about 2.5 MeV)

and ΔE near zero (resolution is channel dependent). The analysis was conducted "blind", meaning that event selection criteria were optimized on simulated events, without looking at the data or the sidebands used to measure the background rates. Only after the all selection criteria were established were the data actually examined.

2 Analysis Strategy

The basic analysis strategy can be summarized rather succinctly. Kaon and lepton candidates are appropriately combined to form $K\ell^+\ell^-$ or $K^*\ell^+\ell^-$ candidates. Backgrounds are suppressed by designing explicit vetoes or combined variables that discriminate signal from background. Extensive use of control samples allows us to determine our efficiency for the signal directly from the data and to perform general quality checks of our simulation. Finally, the signal yield is extracted from a two-dimensional fit in the m_{ES} vs. ΔE plane. We now discuss in more detail these various steps in the analysis.

Candidates are reconstructed selecting pairs of opposite charge leptons and combining them with identified kaons. Electron-positron pairs that are consistent with $\gamma \to e^+e^-$ are explicitly vetoed. For $K^* \to K\pi$ decays, the pion candidate is required to be inconsistent with the kaon hypothesis. The invariant mass of the reconstructed K^* is required to be within 75 MeV/c^2 of the mean $K^*(892)$ mass. K^0_s candidates are reconstructed from oppositely charge tracks that form a good vertex displaced from the primary vertex by at least 1 mm.

Obtaining sufficient suppression of the background is essential when search attempting to measure such small branching ratios. We now discuss the different types of background source and the techniques employed to suppress them.

Continuum backgrounds Backgrounds from the continuum are suppressed using event shape variables, *e.g.*, ratio of second and zeroth Fox-Wolfram moments. The variables are optimally combined employing the Fisher Discriminant technique. Further details of the continuum suppression may be found in [4].

$B\overline{B}$ backgrounds Another composite variable, based on likelihood ratios, uses the lepton and B vertex probabilities and the missing energy in the event to discriminate against backgrounds coming from $B\overline{B}$ events. $E_{\rm miss}$ is particularly useful, since most of this background comes from semileptonic B decays, which usually have large missing energy.

Decays to charmonium A significant background comes from the decays $B \to J/\psi(\to \ell^+\ell^-)K^{(*)}$ and $B \to \psi(2S)(\to \ell^+\ell^-)K^{(*)}$, which have the same topologies as the signal events. Figure 1 shows the rather complex veto region employed to remove these events. The veto was designed not only to reject candidates candidates with $M_{\ell\ell}$ near the J/ψ mass, but also candidates where one of the leptons has radiated a

photon or has otherwise been poorly measured. In such cases, there is a correlation between $M_{\ell\ell}$ and ΔE, which accounts for the diagonal bands observed in the figure.

Peaking Backgrounds There is a small contribution from backgrounds that peak in the signal region such as $B \to D(\to K\pi)\pi$, where both pions are misidentified as muons. Events compatible with this hypothesis are vetoed and the small contribution surviving the veto is accounted for in the extraction of the signal.

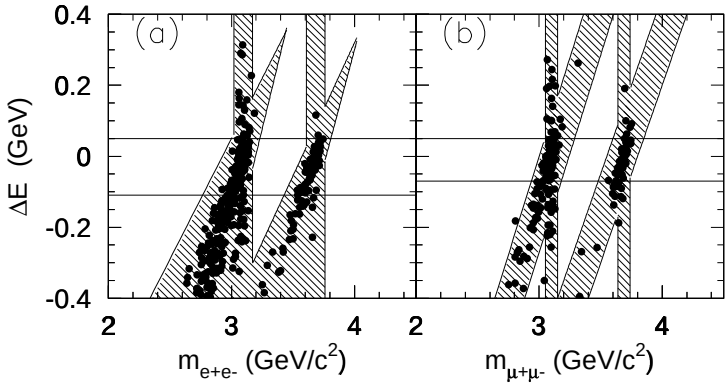

Figure 1: Regions in the ΔE- $M_{\ell\ell}$ plane employed to remove decays containing charmonium, (a) $B \to K^{(*)}e^+e^-$ decays and (b) $B \to K^{(*)}\mu^+\mu^-$ decays. Events falling in the hatched regions are removed from the analysis. The dots are simulated $B \to KJ/\psi$ decays.

An important part of the analysis is the extensive use of control samples to validate our simulation and to derive our signal efficiency directly from the data. The most important control sample is comprised of charmonium decays, $B \to J/\psi(\to \ell^+\ell^-)K^{(*)}$ and $B \to \psi(2S)(\to \ell^+\ell^-)K^{(*)}$, that have been vetoed with the criteria discussed above. The J/ψ control sample has been used extensively to validate the Monte Carlo as well as to verify the efficiency for the signal obtained from the simulation. Combining all channels, the ratio of the efficiency obtained from the control sample to that obtained from the Monte Carlo is found to be 0.99 ± 0.02. Additional control samples constructed from $Ke\mu$ combinations as well as combinations that fall far from the signal region (the Grand Sideband) in the m_{ES}-ΔE plane have also been used as checks on the simulation.

3 Results

The signal and background yields are obtained for each channel by performing a maximum likelihood fit in the region defined by $m_{ES} > 5.2$ GeV/c^2 and $|\Delta E| < 0.25$ GeV. The signal shapes, including radiation effects and correlations between ΔE and

m_{ES}, are taken from simulation. The background shape is a 2-dimensional "Argus" function, with two parameters which are determined directly from the fit. A small peaking background component is included in the background shape. The fit results are shown in Figure 2, which shows the projections of the fits onto the m_{ES} and ΔE axes. The fit yields for each mode are presented in Table 1.

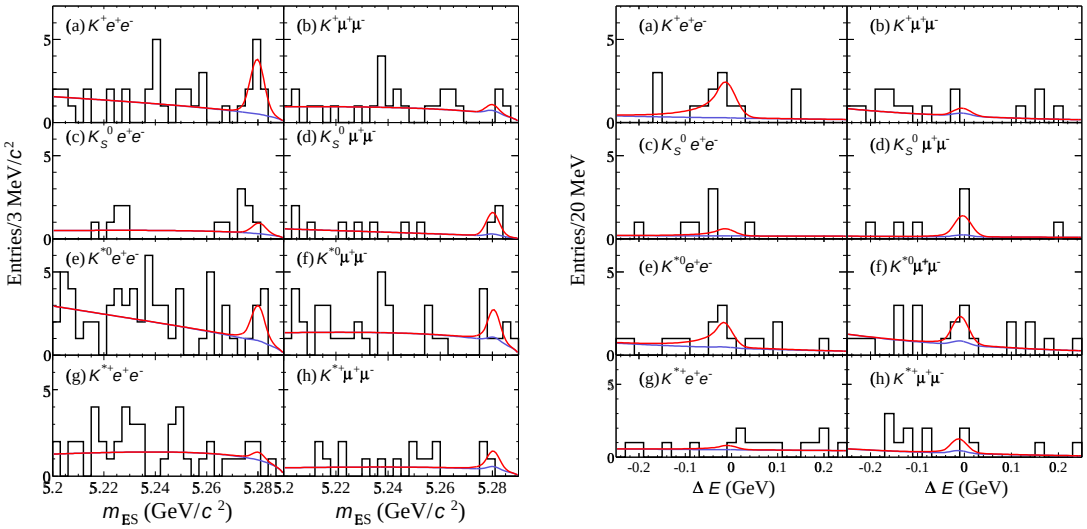

Figure 2: Projections of the two-dimensional fit, m_{ES} (left) and ΔE (right). The fit results are shown (both total fit and background contribution) are shown overlaid on the data.

Systematic uncertainties are divided into two categories, uncertainties on the efficiency, which are multiplicative in nature, and uncertainties on the yields from the fit procedure. The values are given, for each mode, in Table 1 in the columns labeled $(\Delta\mathcal{B}/\mathcal{B})_\epsilon$ and $(\Delta\mathcal{B})_{\rm fit}$, respectively. The dominant uncertainties on the efficiency arise from the uncertainty on the charged tracking efficiency and from the theoretical model dependence of the efficiency. The main contributions to $(\Delta\mathcal{B})_{\rm fit}$ come from uncertainties on the signal and background shapes in the fitting function.

The fit has all been performed combining the $K\ell^+\ell^-$ and $K^*\ell^+\ell^-$ modes together, with the results:

$$\begin{aligned}\mathcal{B}(B \to K\ell^+\ell^-) &= (0.84^{+0.30+0.10}_{-0.24-0.18}) \times 10^{-6} \\ \mathcal{B}(B \to K^*\ell^+\ell^-) &= (1.89^{+0.84}_{-0.72} \pm 0.31) \times 10^{-6} \end{aligned} \quad (2)$$

The theoretical constraint $\mathcal{B}(B \to K^*e^+e^-)/\mathcal{B}(B \to K^*\mu^+\mu^-) = 1.2$ from [1] has been employed for the combined fit.

Mode	Signal yield	Eff. bkgd	ϵ (%)	$(\Delta\mathcal{B}/\mathcal{B})_\epsilon$ (%)	$(\Delta\mathcal{B})_{\rm fit}$ (10^{-6})	$\mathcal{B}$ (10^{-6})
$B^+ \to K^+e^+e^-$	$9.6^{+4.6}_{-3.3}$	1.9	17.1	± 6.8	$^{+0.11}_{-0.23}$	$0.91^{+0.42+0.13}_{-0.32-0.24}$
$B^+ \to K^+\mu^+\mu^-$	$0.8^{+2.5}_{-1.3}$	1.2	9.9	± 6.8	± 0.10	$0.13^{+0.37}_{-0.23} \pm 0.10$
$B^0 \to K^0e^+e^-$	$1.8^{+2.8}_{-1.3}$	1.1	18.1	± 8.0	± 0.35	$0.47^{+0.69}_{-0.39} \pm 0.35$
$B^0 \to K^0\mu^+\mu^-$	$2.9^{+2.7}_{-1.5}$	0.4	10.3	± 7.8	± 0.22	$1.34^{+1.16}_{-0.78} \pm 0.25$
$B^0 \to K^{*0}e^+e^-$	$7.3^{+4.7}_{-3.5}$	3.4	10.2	± 7.7	± 0.48	$1.66^{+1.08}_{-0.83} \pm 0.50$
$B^0 \to K^{*0}\mu^+\mu^-$	$4.6^{+4.2}_{-2.9}$	2.3	6.6	± 9.3	± 0.39	$1.68^{+1.57}_{-1.09} \pm 0.42$
$B^+ \to K^{*+}e^+e^-$	$1.5^{+4.0}_{-2.0}$	4.9	9.8	± 9.7	$^{+1.04}_{-1.06}$	$1.07^{+2.86+1.04}_{-1.51-1.06}$
$B^+ \to K^{*+}\mu^+\mu^-$	$2.8^{+3.5}_{-2.0}$	1.5	5.4	± 11.1	± 1.82	$3.68^{+4.39}_{-2.88} \pm 1.86$

Table 1: Results from the fits to individual modes. The columns are, from left to right: fitted signal yield; the contribution of the background to the error on the signal yield, expressed as an effective background yield; the signal efficiency, ϵ (not including the branching fractions for K^*, K^0, and K^0_S decays); the systematic error on the selection efficiency, $(\Delta\mathcal{B}/\mathcal{B})_\epsilon$; the systematic error from the fit, $(\Delta\mathcal{B})_{\rm fit}$; the branching fraction central value ($\mathcal{B}$); and the 90% C.L. upper limit on the branching fraction, including systematic uncertainties.

We have investigated the signal significance of the combined fit using a toy Monte Carlo technique and conclude that the $K\ell^+\ell^-$ signal is statistically significant at $> 5\sigma$ level. If systematic uncertainties are included, the significance remains above 4σ. The $K^*\ell^+\ell^-$ channel has a statistical significance of about 3.5σ and we choose to set an upper limit for that mode:

$$\mathcal{B}(B \to K^*\ell^+\ell^-) < 3.5 \times 10^{-6} \text{ at } 90\% \text{ C.L.}$$

4 Conclusions

We have analyzed the decay modes $B \to K\ell^+\ell^-$ and $B \to K^*\ell^+\ell^-$ in the *BABAR* experiment, with a data set of approximately 60 million $B\overline{B}$ events, and obtain the following results:

$$\begin{aligned} \mathcal{B}(B \to K\ell^+\ell^-) &= (0.84^{+0.30+0.10}_{-0.24-0.18}) \times 10^{-6} \\ \mathcal{B}(B \to K^*\ell^+\ell^-) &< 3.5 \times 10^{-6} \text{ at } 90\% \text{ C.L.} \end{aligned} \quad (3)$$

These results are compatible with *BABAR*'s previous $K\ell^+\ell^-/K^*\ell^+\ell^-$ results (upper limits for both modes) [4] at the few percent level and is consistent with Belle's recently published result [5].

All results presented in this paper are preliminary.

Acknowledgements

I would like to thank Prof. Nigel Lockyer and the other organizers of the *Flavor Physics-CP Violation Conference* for a very interesting and enjoyable conference.

References

[1] A. Ali *et al.*, Phys. Rev. D **61**, 074024 (2000); P. Colangelo *et al.*, Phys. Rev. D **53**, 3672 (1996); D. Melikhov, N. Nikitin, and S. Simula, Phys. Rev. D **57**, 6814 (1998).

[2] T.M. Aliev *et al.*, Phys. Lett. B **400**, 194 (1997); T.M. Aliev, M. Savci, and A. Özpineci, Phys. Rev. D **56**, 4260 (1997); G. Burdman, Phys. Rev. D **52**, 6400 (1995); C. Greub, A. Ioannissian, and D. Wyler, Phys. Lett. B **346**, 149 (1995); J.L. Hewett and J.D. Wells, Phys. Rev. D **55**, 5549 (1997); C.Q. Geng and C.P. Kao, Phys. Rev. D **54**, 5636 (1996); and references therein.

[3] *BABAR* Collaboration, B. Aubert *et al.*, Nucl. Instrum. Methods **A479**, 1 (2002).

[4] *BABAR* Collaboration, B. Aubert *et al.*, hep-ex/0201008, to be published in Phys. Rev. Lett. (2002).

[5] Belle Collaboration, K. Abe *et al.*, Phys. Rev. Lett. **88**, 021801 (2002).

Probing New Physics with $b \to s\gamma$ decays

Dan Pirjol
Department of Physics, UCSD
9500 Gilman Drive
La Jolla, CA 92093

Abstract

In the Standard Model, the photon emitted in $b \to s\gamma$ decays is predicted to be left-handed polarized. We discuss the types of New Physics which can produce a deviation from this prediction, focusing on the Minimal Supersymmetric Standard Model. A new method is proposed for testing these predictions, which makes use of angular correlations in exclusive $B \to K^{**}(\to K\pi\pi)\gamma$ decays.

Rare radiative $b \to s\gamma$ decays have been extensively investigated both as a probe of the flavor structure of the Standard Model and for their sensitivity to any new physics beyond the SM. The present experimental average of the $B \to X_s\gamma$ inclusive rate $Br(B \to X_s\gamma) = (3.22 \pm 0.40) \times 10^{-4}$ [1] agrees well with the Standard Model prediction, to next-to-leading order in perturbation theory $Br(B \to X_s\gamma) = (3.54 \pm 0.49) \times 10^{-4}$ (corresponding to a pole mass ratio $m_c/m_b = 0.25 \pm 0.06$) [2]. In addition to the rather well predicted inclusive branching ratio, there is a unique feature of this process within the SM which drew only moderate theoretical attention and which has not yet been tested. Namely, the emitted photons are left-handed in radiative B^- and $\overline{B}^0$ decays and are right-handed in B^+ and B^0 decays. In the SM the photon in $b \to s\gamma$ is predominantly left-handed, since only left chiral quarks couple to the W into loops.

This prediction holds in the SM to within a few percent, up to corrections of order Λ/m_b, for exclusive and inclusive decays. On the other hand, in certain extensions of the Standard Model, an appreciable right-handed component can be induced in $b \to s\gamma$ decays. While measurements of the inclusive radiative decay rate agree with SM calculations, no evidence exists so far for the helicity of the photons in these decays.

In view of its popularity as a model of New Physics, we will focus the discussion below on the Minimal Supersymmetric Standard Model (MSSM) [3] (an alternative source of nonstandard photon helicity is the left-right symmetric model [4]). In addition to the $t - W^\pm$ penguin loop, which is responsible for the $b \to s\gamma$ decay in the Standard Model, the MSSM allows for new contributions. These come from loops

containing at least one charged particle, and include the top-charged Higgs contribution $t-H^{\pm}$, stop-chargino $\tilde{t}-\tilde{\chi}^{\pm}$ and sbottom-neutralino/gluino contributions $\tilde{\chi}^0-\tilde{b}$, $\tilde{g}-\tilde{b}$.

The flavor structure of the MSSM is not determined by symmetries and is generated by the soft SUSY breaking terms which can introduce many arbitrary parameters. They are severely constrained in models with minimal flavor violation (MFV), where the only source of flavor violation is the usual CKM matrix. The most general form of the squark mass matrices in the super-CKM basis can be written as (see, e.g., [5])

$$\mathcal{M}_U^2 = \begin{pmatrix} M_{U_{LL}}^2 & M_{U_{LR}}^2 \\ M_{U_{LR}}^{2\dagger} & M_{U_{RR}}^2 \end{pmatrix}, \qquad \mathcal{M}_D^2 = \begin{pmatrix} M_{D_{LL}}^2 & M_{D_{LR}}^2 \\ M_{D_{LR}}^{2\dagger} & M_{D_{RR}}^2 \end{pmatrix} \tag{1}$$

The 3×3 submatrices $M_{U_{ij}}^2$ and $M_{D_{ij}}^2$ are given in terms of the quark mass matrices and soft SUSY breaking terms $M_{\tilde{U}_{L,R}}^2$, $M_{\tilde{D}_{L,R}}^2$ and A_U, A_D defined as usual by

$$\mathcal{L}_{soft} = -\sum_{\tilde{Q}=\tilde{U}_L,\tilde{D}_L} \tilde{Q}^\dagger M_{\tilde{Q}_L}^2 \tilde{Q} - \tilde{U}^\dagger M_{\tilde{U}_R}^2 \tilde{U} - \tilde{D}^\dagger M_{\tilde{D}_R}^2 \tilde{D} + \tilde{Q} A_U H_U \tilde{U} + \tilde{Q} A_D H_D \tilde{D}\,. \tag{2}$$

In MFV models the matrices A_U, A_D, $M_{\tilde{U}_R}^2$ and $M_{\tilde{D}_R}^2$ must be diagonal. Usually, this is taken to imply that the only contribution to $b\to s\gamma$ in MFV-MSSM is the top-charged Higgs diagram, which has the same chiral structure as the SM. In such a situation, the photon in $b\to s\gamma$ is again left-handed.

It was pointed out in [6] that MFV models actually allow nontrivial flavor violation in the squark sector. The matrices $M_{\tilde{U}_L}^2$ and $M_{\tilde{D}_L}^2$ are connected by SU(2) gauge invariance as $M_{\tilde{D}_L}^2 = V_{CKM}^\dagger M_{\tilde{U}_L}^2 V_{CKM}$, which implies that a diagonal, but not proportional to the unit matrix $M_{\tilde{D}_L}^2$, can give a non-diagonal structure for $M_{\tilde{U}_L}^2$ (and vice versa). This allows the chargino-up squark and neutralino/gluino-up squark contributions to $b\to s\gamma$. The latter graphs can occur with a helicity flip along the gluino line, which can produce a right-handed photon component in $b\to s\gamma$.

Relaxing the MFV constraints on the flavor structure (the so-called unconstrained MSSM) generally leaves the new physics contributions to $b\to s\gamma$ be dominated by the gluino graph, which can easily introduce a right-handed photon component. Data on the total $B\to X_s\gamma$ branching ratio set very stringent constraints on the allowed squark mass matrices [7]. An extreme way of satisfying such constraints in a generic MSSM has been proposed in [8], where it is suggested that the MSSM graphs exactly cancel the SM contribution to the left-handed penguin amplitude, in such a way that the right-handed amplitude precisely reproduces the observed rate. A measurement of the photon helicity in $b\to s\gamma$ will clearly help decide which of these possibilities (if any) is realized in Nature.

Several ways were suggested to look for signals of physics beyond the SM through photon helicity effects in $B \to X_s\gamma$. In the first suggested method [9] the photon helicity is probed through mixing-induced CP asymmetries. The sensitivity to the polarization comes from interference between B^0 and $\overline{B}^0$ decay amplitudes into a common state of definite photon polarization. However, measuring asymmetries at a level of a few percent, as expected in the SM, require an order of 10^9 B mesons which might not be available at the existing B factories for some time. In a second scheme one studies angular distributions in $B \to \gamma(\to e^+e^-)K^*(\to K\pi)$, where the photon can be virtual [10] or real, converting in the beam pipe to an electron-positron pair [12]. The efficiency of this method is comparable to that of the previous method. A somewhat different method was proposed in [11] and makes use of angular correlations in both exclusive and inclusive $\Lambda_b \to X_s\gamma$ decays.

We discuss in the following a method [13, 14, 15] for measuring the photon polarization using angular correlations in the strong decay products of a K resonance in $B \to K_{\rm res}\gamma$. Denoting with $A_{R,L}(\vec{p}_i)$ the amplitude for the strong decay of a $K_{\rm res}$ at rest in a spin state $|j, m = \pm 1\rangle$ into a final state $|f\rangle$ containing hadrons with momenta $\vec{p}_i$, one could ask what is the condition for a nonvanishing asymmetry $|A_R(\vec{p}_i)| \neq |A_L(\vec{p}_i)|$. This is a typical 'motion-reversal' asymmetry of the form

$$a_{i\to f}^{T-odd} \equiv |T_{i\to f}|^2 - |T_{P\bar{i}\to P\bar{f}}|^2 \tag{3}$$

where $\bar{i}$, $\bar{f}$ are motion-reversed states, changing the momenta and spins $(\vec{p}_i, s_i) \to (-\vec{p}_i, -s_i)$, and P is the parity operator. Since parity is conserved in strong interactions, one can replace $|T_{P\bar{i}\to P\bar{f}}| = |T_{\bar{i}\to\bar{f}}|$ on the right-hand side (this is equivalent to $|A_{R,L}(\vec{p}_i)| = |A_{R,L}(-\vec{p}_i)|$). T-invariance (or equivalently CP invariance) of the strong interactions gives $|T_{\bar{i}\to\bar{f}}| = |T_{f\to i}|$. Using this together with the unitarity condition $T^*_{i\to f} - T_{f\to i} = -i\sum_k T^*_{i\to k}T_{f\to k} \equiv -i\alpha_{i\to f}$ into (3) gives that the left/right asymmetry can be written as

$$a_{i\to f}^{T-odd} = 2{\rm Im}\,(T_{i\to f}\alpha_{i\to f}) - |\alpha_{i\to f}|^2\,. \tag{4}$$

If all decay amplitudes are real then $\alpha_{i\to f} = 0$ which shows that a nonvanishing asymmetry requires nontrivial final state interactions.

Furthermore, 2-body final states (e.g. $K\pi$) cannot produce an asymmetry because it is impossible to form a quantity which is odd under motion reversal from just two vectors $\vec{q}$ (photon momentum in the $K_{\rm res}$ frame) and $\hat{n}$ (the direction parameterizing the final state $|K(\hat{n})\pi(-\hat{n})\rangle$.

A nonvanishing asymmetry can be realized however in 3-body strong decays $K_{\rm res} \to K\pi\pi$. Such decays are realized for the lowest excitations of the K with quantum numbers $J^P = 1^-, 1^+, 2^+$, some of which have been recently observed to be produced in rare radiative decays. Both Belle and CLEO measured recently the decay $B \to K_2^*(1430)\gamma$ with a branching ratio of $(1.50^{+0.58+0.11}_{-0.53-0.13}) \times 10^{-5}$ and $(1.66^{+0.59}_{-0.53} \pm$

$0.13) \times 10^{-5}$, respectively [16]. Similar branching ratios are expected from theoretical estimates for decays into $K_1(1400)$ and $K_1(1270)$ [17].

These states decay strongly to 3-body final $K\pi\pi$ states. Neglecting a small non-resonant contribution, these decays are dominated by interference of a few channels

$$K^+_{\rm res} \to \left\{ \begin{array}{c} K^{*+}\pi^0 \\ K^{*0}\pi^+ \\ \rho^+ K^0 \end{array} \right\} \to K^0\pi^+\pi^0\,, \qquad K^0_{\rm res} \to \left\{ \begin{array}{c} K^{*+}\pi^- \\ K^{*0}\pi^0 \\ \rho^- K^+ \end{array} \right\} \to K^+\pi^-\pi^0\,. \tag{5}$$

The different channels $K^*\pi$ are related by isospin symmetry and contribute with a relative strong phase which can be parameterized in terms of Breit-Wigner forms. The $K_1(1400)$ decays predominantly to $K^*\pi$ in a mixture of S and D waves, with a branching ratio of 95% [18]. To a good approximation one can neglect the D wave component, which allows a parameter-free computation of the asymmetry. The smaller D-wave component and the $K\rho$ contribution can be also included using the measurements of the partial wave amplitudes and phases measured by the ACCMOR Collaboration [19].

The most convenient way of presenting the result for the polarization sensitive observable is in terms of an angular distribution in the rest frame of the resonance $K_{\rm res}$. Introducing the angle θ between the opposite of the photon momentum $-\vec{q}$ and the normal to the $K\pi\pi$ decay plane defined as $\vec{p}_{\rm slow} \times \vec{p}_{\rm fast}$, where $\vec{p}_{\rm slow}$ and $\vec{p}_{\rm fast}$ are the momenta of the slower and faster pions, this is given by [15]

$$\begin{aligned} \frac{{\rm d}^2\Gamma}{{\rm d}s\,{\rm d}\cos\tilde{\theta}} &= |c_1|^2 \left\{ 1 + \cos^2\tilde{\theta} + 4P_\gamma R_1 \cos\tilde{\theta} \right\} \\ &+ |c_2|^2 \left\{ \cos^2\tilde{\theta} + \cos^2 2\tilde{\theta} + 12 P_\gamma R_2 \cos\tilde{\theta}\cos 2\tilde{\theta} \right\} + |c_3|^2 B_{K_1^*}(s) \sin^2\tilde{\theta} \\ &+ \left\{ c_{12}\frac{1}{2}(3\cos^2\tilde{\theta} - 1) + P_\gamma c'_{12} \cos^3\tilde{\theta} \right\}\,, \end{aligned} \tag{6}$$

where the first three terms are produced by decays through $K_{\rm res}$ resonances with $J^P = 1^+, 2^+$ and 1^-, and the last terms come from $1^+ - 2^+$ interference. The hadronic parameters $R_{1,2}$ can be computed with relatively small model dependence as explained above, which gives [14, 15] $R_1 = 0.22 \pm 0.03$, $R_2 = 0.01 - 0.05$. Thus, measurements of the angular distribution (6) can be used to extract the photon polarization parameter P_γ.

Assuming an exclusive B branching ratio into $K_1(1400)\gamma$ of 0.7×10^{-5} and assuming that the final states in (5) are detected through $K^+\pi^-\pi^0$ and $K_S\pi^+\pi^0$ implies that about 2×10^7 $B\overline{B}$ pairs are required to measure 80 $K\pi\pi\gamma$ events which should be sufficient for a 3σ confirmation of a left-handed photon in $b\to s\gamma$ decay. Such a measurement should be feasible at the existing B factories in the near future.

It is a pleasure to thank Michael Gronau, Yuval Grossman and Anders Ryd for an enjoyable collaboration.

References

[1] CLEO Collaboration, Phys. Rev. Lett. **87**, 251807 (2001); ALEPH Collaboration, Phys. Lett. B**429**, 169 (1998); BELLE Collaboration, Phys. Lett. B**511**, 151 (2001).

[2] M. Misiak, hep-ph/0106050, proceedings of the XXXVIth Rencontres de Moriond, Les Arcs, March 10-17, 2001, and references therein; A. Ali, C. Greub, G. Hiller and E. Lunghi, hep-ph/0112300.

[3] For a review of B physics in SUSY models, see S. Bertolini, F. Borzumati and A. Masiero, *B Decays*, second edition, ed. S. Stone, World Scientific, 1994, p. 620.

[4] K. Fujikawa and A. Yamada, Phys. Rev. D49, 5890 (1994); K. S. Babu, K. Fujikawa and A. Yamada, Phys. Lett. B333, 196 (1994); P. Cho and M. Misiak, Phys. Rev. D49, 5894 (1994). For a review of B physics in LR models, see M. Gronau, *B Decays*, second edition, ed. S. Stone, World Scientific, 1994, p. 644.

[5] M. Misiak, S. Pokorski and J. Rosiek, in *Heavy Flavors II*, edited by A. J. Buras and M. Lindner, hep-ph/9703442.

[6] C. Bobeth, T. Ewerth, F. Krüger and J. Urban, hep-ph/0204225.

[7] F. Borzumati, T. Hurth, C. Greub and D. Wyler, Phys. Rev. D**62**, 075005 (2000); T. Besmer, C. Greub and T. Hurth, Nucl. Phys. B609, 359 (2001).

[8] L. Everett, G. L. Kane, S. Rigolin, L. T. Wang and T. T. Wang, JHEP 0201, 02 (2002).

[9] D. Atwood, M. Gronau and A. Soni, Phys. Rev. Lett. **79**, 185 (1997).

[10] D. Melikhov, N. Nikitin and S. Simula, Phys. Lett. B**442**, 381 (1998); F. Krüger, L. Sehgal, N. Sinha and R. Sinha, Phys. Rev. D**61**, 114028 (2000); C. S. Kim, Y. G. Kim, C. D. Lü and T. Morozumi, Phys. Rev. D**62**, 034013 (2000).

[11] T. Mannel and S. Recksiegel, Acta Phys. Polonica B**28**, 2489 (1997); G. Hiller and A. Kagan, Phys. Rev. D**65**, 074038 (2002).

[12] Y. Grossman and D. Pirjol, JHEP **6**, 29 (2000).

[13] T. Islam and A. Weinstein, CLEO Internal Note, July 1999 (unpublished).

[14] M. Gronau, Y. Grossman, D. Pirjol and A. Ryd, Phys. Rev. Lett. 88, 051802 (2002).

[15] M. Gronau and D. Pirjol, hep-ph/0205065.

[16] CLEO Collaboration, Phys. Rev. Lett. **84**, 5283 (2000); Babar Collaboration, Phys. Rev. Lett. **88**, 101805 (2002); Belle Collaboration, A. Ishikawa, talk at the XXVII Recontres de Moriond on Electroweak Interactions and Unified Theories, Les Arcs, 2002.

[17] A. Ali, T. Ohl and T. Mannel, Phys. Lett. B**298**, 195 (1993); S. Veseli and M. G. Olsson, Phys. Lett. B**367**, 309 (1996).

[18] Particle Data Group, D. E. Groom *et al.*, Eur. Phys. J. C**15**, 1 (2000).

[19] C. Daum *et al.*, Nucl. Phys. B**187**, 1 (1981).

May 18, session 4.

Session Chair: J. Appel

Charm Physics II

Charm Semileptonic Decays

Jim Wiss
Department of Physics
University of Illinois
Urbana, IL,61801, USA

I discuss new data on charm semileptonic decay concentrating on two topics involving the decay $D^+ \to K^-\pi^+\mu^+\nu$. The first topic is the observation of interference in this decay by the FOCUS collaboration[1]. The second are new measurements of branching ratio of $D^+ \to \overline{K}^{*0}\ell^+\nu_\ell$ relative to $D^+ \to K^-\pi^+\pi^+$ from CLEO[2] and FOCUS. Fig. 1 shows the $D^+ \to \overline{K}^{*0}\ell^+\nu_\ell$ signals of these two groups.

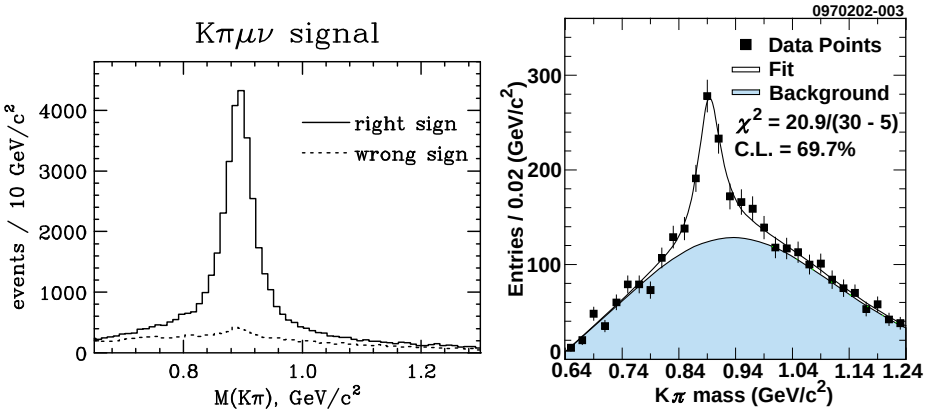

Figure 1: $D^+ \to K^-\pi^+\mu^+\nu$ signal. (left) The FOCUS right-sign and wrong-sign samples are shown. The wrong-sign-subtracted yield is 31 254 events. (right) A partial sample of $D^{*+} \to \pi^0 D^+ \to \pi^0(\overline{K}^{*0}e^+\nu)$ from CLEO. This is the sample form one of their bins in the $D^* - D$ mass difference.

1 Interference in $D^+ \to K^-\pi^+\mu^+\nu$

In our attempts to fit for the form factors controlling the decay $D^+ \to \overline{K}^{*0}\mu^+\nu$, we discovered a large, unexpected asymmetry in the $\cos\theta_V$ distribution shown in Fig. 2. This asymmetry was very strong for events with a $m_{K\pi}$ mass below the pole and weak for events above the pole. It was possible to understand the forward-backward

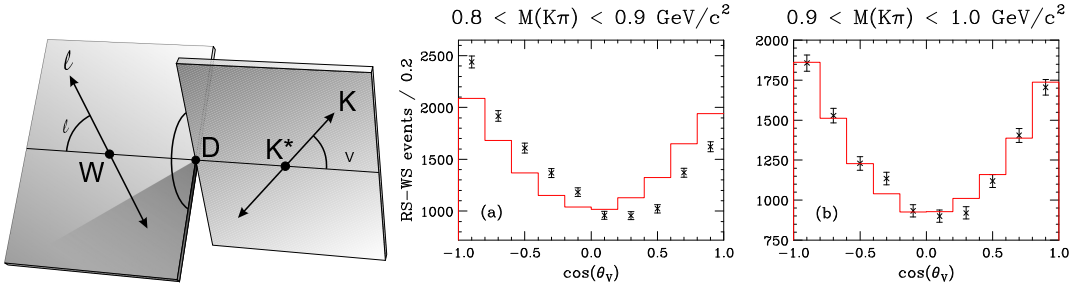

Figure 2: (left) Definition of the three decay angles: $\cos\theta_{\rm V}$ is the decay angle of the kaon in the $\overline{K}^{*0}$ frame, $\cos\theta_\ell$ is the angle of the charged lepton in the virtual W^+ frame. χ is the acoplanarity angle between the two decay planes. (right) Event distribution in $\cos\theta_{\rm V}$, split between samples below and above 0.9 GeV/c^2. The points with error bars are (wrong-sign subtracted) FOCUS data and the solid histogram is a Monte Carlo simulation with efficiency and known charm backgrounds but no interference.

asymmetry in $\cos\theta_{\rm V}$ using the simple model summarized by Eqn. 1. Using the notation of [3], we write the decay distribution (in the zero charged lepton mass limit) for $D^+ \to K^-\pi^+\mu^+\nu$ in terms of the three helicity basis form factors: H_+ , H_0 , H_-. We have taken the standard amplitude and added an interfering s-wave amplitude with a constant modulus and phase ($A\ \exp(i\delta)$) that interferes with the $\overline{K}^{*0}$ Breit-Wigner ($\mathrm{B}_{K^{*0}}$) in the one place allowed by angular momentum conservation.

$$\frac{d^5\Gamma}{dm_{K\pi}\ dq^2\ d\cos\theta_{\rm V}\ d\cos\theta_\ell\ d\chi} \propto q^2 \left| \begin{array}{l} (1+\cos\theta_\ell)\sin\theta_{\rm V} e^{i\chi}\mathrm{B}_{K^{*0}} H_+ \\ -(1-\cos\theta_\ell)\sin\theta_{\rm V} e^{-i\chi}\mathrm{B}_{K^{*0}} H_- \\ -2\sin\theta_\ell(\cos\theta_{\rm V}\mathrm{B}_{K^{*0}} + Ae^{i\delta})H_0 \end{array} \right|^2 \qquad (1)$$

Assuming the s-wave amplitude is small (or the effect would have been discovered already) it will be primarily observable through three interference terms:
$8\cos\theta_{\rm V}\sin^2\theta_\ell A\Re\left(e^{-i\delta}\mathrm{B}_{K^{*0}}\right)H_0^2$, $-4(1+\cos\theta_\ell)\sin\theta_\ell\sin\theta_{\rm V}\ A\Re\left(e^{i(\chi-\delta)}\mathrm{B}_{K^{*0}}\right)H_+H_0$, and $+4(1-\cos\theta_\ell)\sin\theta_\ell\sin\theta_{\rm V}\ A\Re\left(e^{-i(\chi+\delta)}\mathrm{B}_{K^{*0}}\right)H_-H_0$. Only the first of these terms will survive averaging over the acoplanarity, χ. This was the term responsible for creating the $\cos\theta_{\rm V}$ asymmetry shown in Fig. 2 since it is proportional to $\cos\theta_{\rm V}$. If we further weight our wrong-sign subtracted, azimuthally averaged data by $\cos\theta_{\rm V}$, this is the only term that will survive in the full decay amplitude (given our nearly uniform angular acceptance). It will have a distinct dependence on the $m_{K\pi}$ mass: $\Re\left(e^{-i\delta}\mathrm{B}_{K^{*0}}\right)$, as well as on $\cos\theta_\ell$: $(1-\cos^2\theta_\ell)$.

Figure 3 shows two $\cos\theta_{\rm V}$-weighted, wrong sign subtracted distributions for $K\pi\mu\nu$. The left plot is the asymmetry weighted $m_{K\pi}$ distribution which should resemble

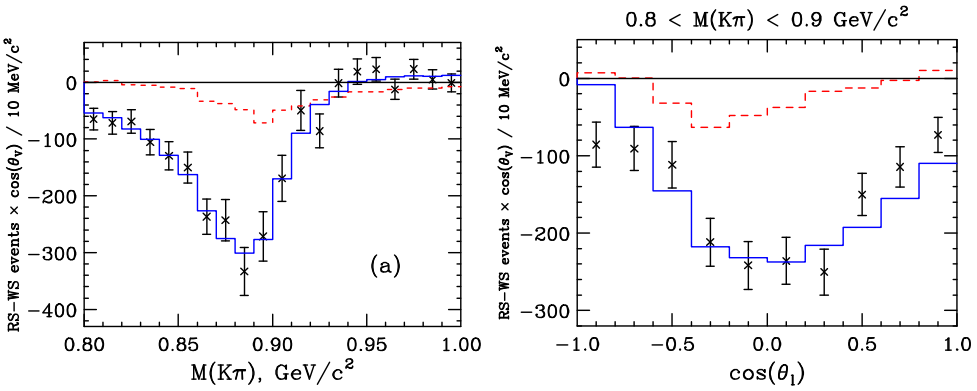

Figure 3: (left) The $\cos\theta_V$-weighted distribution in $K\pi$ invariant mass. The data are the points with error bars. The dashed (red) histogram have no s-wave amplitude (null hypothesis). The solid (blue) histogram includes an s-wave amplitude of 0.36 $\exp(i\pi/4)$ GeV^{-1}. (right) The $\cos\theta_V$-weighted distribution in $\cos\theta_V$ compared to the null (red) and amplitude (blue) simulations.

$\Re\left(e^{-i\delta}\mathrm{B}_{K^{*0}}\right)$. For $\delta = 0$, $\Re\left(e^{-i\delta}\mathrm{B}_{K^{*0}}\right)$ is odd function of $m_{K\pi}$ - $m_{K^{*0}}$, while for $\delta = \pi/2$ this form is even in $m_{K\pi}$ - $m_{K^{*0}}$. The data strongly resembles the expected plot for $\delta = \pi/4$. The right half of Fig. 2 is the asymmetry weighted $\cos\theta_\ell$ distribution with masses in the region $0.8 < m_{K\pi} < 1.0$ GeV/c^2. It resembles the expected parabola in $\cos\theta_\ell$ with some modulation due to acceptance and resolution.

In the absence of the s-wave interference, all acoplanarity dependent terms in the $D^+ \to \overline{K}^{*0}\mu^+\nu$ decay intensity are functions of $\cos\chi$ and $\cos 2\chi$. The s-wave interference includes additional acoplanarity dependent s-wave terms of the form:
$+4(1-\cos\theta_\ell)\sin\theta_\ell \sin\theta_V\, A\Re\left(e^{-i(\chi+\delta)}\mathrm{B}_{K^{*0}}\right) H_- H_0$ which brings in a $\sin\chi$ dependence thereby breaking $\chi \leftrightarrow -\chi$ symmetry. Figure 4 shows the wrong-sign subtracted χ distribution separately for D^+ and D^- events in the range $0.8 < m_{K\pi} < 1.0$ GeV/c^2 Initially we were surprised by the inconsistency between the D^+ and D^- acoplanarity until we realized that there is a sign change in the χ convention between the particle and antiparticle. After applying the correct convention, the D^+ and D^- distributions become consistent, and the odd χ contributions brought in through the s-wave interference become very evident. Why has the s-wave interference in $D^+ \to \overline{K}^{*0}\ell^+\nu_\ell$ never been reported before, given that it has been a process studied for nearly twenty years by several experiments? One answer is that an amplitude of this strength and form creates a very minor modulation to the $m_{K\pi}$ spectrum as shown in Figure 4. Another reason is that this effect is much more evident when one divides the data above and below the $\overline{K}^{*0}$ pole. Finally, the FOCUS data set has significantly more clean $D^+ \to K^-\pi^+\mu^+\nu$ events than previously published data.

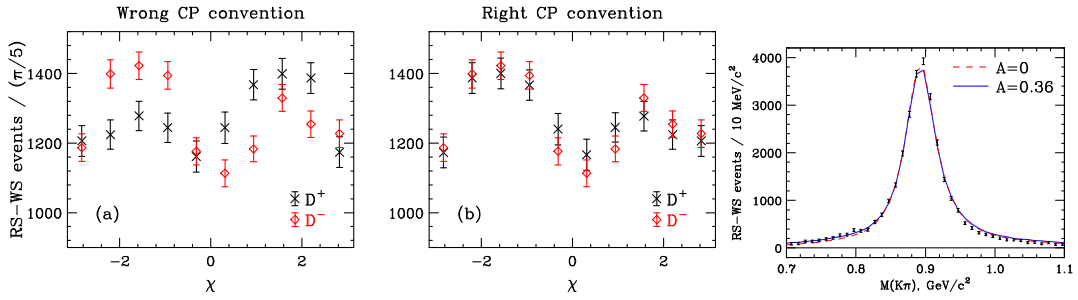

Figure 4: (left) The wrong-sign subtracted acoplanarity distribution separated by charm. The "x" points are for the D^+ while the "diamond" points are for the D^-. (a) compares the distributions without the required change in the χ convention as discussed above. (b) compares the distributions with the correct χ sign convention change. (right) The $m_{K\pi}$ mass distribution in data (with error bars) compared to our null hypothesis (red) and s-wave (blue) Monte Carlos. The two predicted $m_{K\pi}$ spectra are nearly identical.

2 New Measurements of $\frac{\Gamma(D^+\to\overline{K}^{*0}\ell^+\nu_\ell)}{\Gamma(D^+\to K^-\pi^+\pi^+)}$

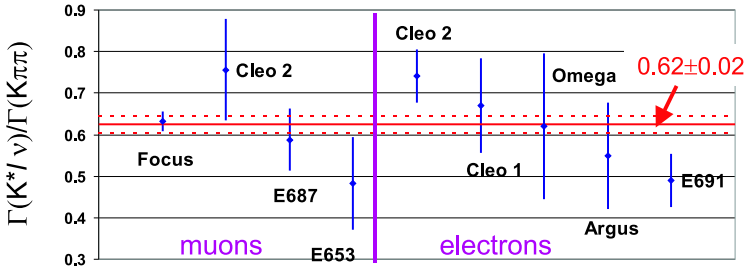

Figure 5: Summary of measurements on $\frac{\Gamma(D^+\to\overline{K}^{*0}\ell^+\nu_\ell)}{\Gamma(D^+\to K^-\pi^+\pi^+)}$. The muon data, on the left, has been scaled by a factor of 1.05 to compare to the electron data. Our preliminary FOCUS point is plotted first. The new CLEO2 electron plot is the first "electron" point. I also show an informal weighted average of these measurements including our preliminary FOCUS point.

The CLEO Collaboration has made a new measurement of $\frac{\Gamma(D^+\to\overline{K}^{*0}\ell^+\nu_\ell)}{\Gamma(D^+\to K^-\pi^+\pi^+)} = 0.74\pm 0.04 \pm 0.05$ that is somewhat higher than previous measurements and significantly higher than the previous high precision measurement by E691 as shown in Fig. 5. The new CLEO measurement can be interpreted as helping to resolve an old problem

with theory theory over-predicting the $\Gamma\left(D^+ \to \overline{K}^{*0}\ell^+\nu_\ell\right)$ by a rough factor of two.

FOCUS is in the process of making a new measurement of $D^+ \to \overline{K}^{*0}\mu^+\nu$ using a Monte Carlo that includes the s-wave interference described above. Our preliminary number is $\frac{\Gamma(D^+\to\overline{K}^{*0}\ell^+\nu_\ell)}{\Gamma(D^+\to K^-\pi^+\pi^+)} = 0.60\pm0.01$ with a systematic error expected to be roughly twice the statistical error. After multiplying this relative muon branching ratio by 1.05 to compare to the electron branching ratio[4], our preliminary number lies about 1.6 σ below the new CLEO number.

To summarize: I presented evidence for an s-wave interference with the dominant $D^+ \to \overline{K}^{*0}\mu^+\nu$ contribution to $D^+ \to K^-\pi^+\mu^+\nu$ decay. This interference creates a strong ($\approx 20\%$) forward-backward asymmetry in the $\overline{K}^{*0}$ decay angular distribution, but creates very minimal distortion to the $K^-\pi^+$ mass distribution. The dependence of the asymmetry on the $m_{K\pi}$ suggests that it has a phase of 45^o near the $\overline{K}^{*0}$ pole and amplitude that is roughly 7% of the Breit-Wigner amplitude at the pole mass in the H_0 helicity contribution.

CLEO recently published branching ratio of $D^+ \to \overline{K}^{*0}\ell^+\nu_\ell$ relative to $D^+ \to K^-\pi^+\pi^+$ that was somewhat higher than the previous world average and would help resolve a discrepancy with theoretical predictions. A preliminary number from FOCUS with better precision than previously reported is 1.6 σ lower than this CLEO number.

We can look forward to new measurements of the $D^+ \to \overline{K}^{*0}\mu^+\nu$ form factors, the $D_s^+ \to \phi\mu\nu/\phi\pi$ and their form factors, studies of the q^2 dependence of the $D^0 \to K^-\mu^+\nu$ form factor, and Cabibbo suppressed ratios such as $D^+ \to \rho\mu\nu/\overline{K}^{*0}\mu\nu$ and $D^0 \to \pi^-\mu^+\nu/K^-\mu^+\nu$.

I am grateful to the FOCUS Collaboration and organizers of this excellent conference.

References

[1] FOCUS Collaboration (J.M. Link et al.). FERMILAB-PUB-02-054-E, Mar 2002. 14pp. e-Print Archive: hep-ex/0203031

[2] CLEO Collaboration, Measurement of the $D^+ \to \overline{K}^{*0}\ell^+\nu_\ell$ Branching Fraction Mar 20, 2002 hep-ex/0203030

[3] J.G. Korner and G.A. Schuler, Z. Phys. C 46 (1990) 93.

[4] Particle Data Group, J. Bartels *et al.*,, Eur. Phys. J. C**15** (2000) 490.

D^0-$\overline{D^0}$ mixing

Alexey A. Petrov
Department of Physics and Astronomy
Wayne State University
Detroit, MI 48201

1 Introduction

One of the most important motivations for studies of $D^0 - \overline{D}^0$ mixing is the possibility of observing a signal from new physics which can be separated from the one generated by the Standard Model (SM) interactions. The $D^0 - \overline{D}^0$ mixing proceeds extremely slowly, which in the Standard Model is usually attributed to the absence of superheavy quarks destroying GIM cancelations [1]. The low energy effect of new physics particles can be naturally written in terms of a series of local operators of increasing dimension generating $\Delta C = 2$ transitions. These operators, as well as the one loop Standard Model effects, generate contributions to the effective operators that change D^0 state into $\overline{D}^0$ state leading to the mass eigenstates

$$|D_{_2^1}\rangle = p|D^0\rangle \pm q|\overline{D}^0\rangle, \tag{1}$$

where the complex parameters p and q are obtained from diagonalizing the $D^0 - \overline{D}^0$ mass matrix. The mass and width splittings between these eigenstates are parameterized by

$$x \equiv (m_2 - m_1)/\Gamma, \quad y \equiv (\Gamma_2 - \Gamma_1)/(2\Gamma), \tag{2}$$

where $m_{1,2}$ and $\Gamma_{1,2}$ are the masses and widths of $D_{1,2}$ and the mean width and mass are $\Gamma = (\Gamma_1 + \Gamma_2)/2$ and $m = (m_1 + m_2)/2$. Since y is constructed from the decays of D into physical states, it should be dominated by the Standard Model contributions, unless new physics significantly modifies $\Delta C = 1$ interactions.

Presently, experimental information about the $D^0 - \overline{D}^0$ mixing parameters x and y comes from the time-dependent analyses that can roughly be divided into two categories. First, more traditional studies look at the time dependence of $D \to f$ decays, where f is the final state that can be used to tag the flavor of the decayed meson. The most popular is the non-leptonic doubly Cabibbo suppressed decay (DCSD)

$D^0 \to K^+\pi^-$. Time-dependent studies allow one to separate the DCSD from the mixing contribution $D^0 \to \overline{D}^0 \to K^+\pi^-$,

$$\Gamma[D^0(t) \to K^+\pi^-] = e^{-\Gamma t}|A_{K^-\pi^+}|^2 \times \left[R + \sqrt{R}R_m(y'\cos\phi - x'\sin\phi)\Gamma t + \frac{R_m^2}{4}(y^2+x^2)(\Gamma t)^2\right], \quad (3)$$

where R is the ratio of DCS and Cabibbo favored (CF) decay rates and $q/p = R_m e^{i\phi}$. Since x and y are small, the best constraint comes from the linear terms in t that are also *linear* in x and y. A direct extraction of x and y from Eq. (3) is not possible due to unknown relative strong phase δ of DCS and CF amplitudes [2], as $x' = x\cos\delta + y\sin\delta$, $y' = y\cos\delta - x\sin\delta$. This phase can be measured independently [3]. The corresponding formula can also be written for $\overline{D}^0$ decay with $x' \to -x'$ and $R_m \to R_m^{-1}$ [4].

Second, D^0 mixing can be measured by comparing the lifetimes extracted from the analysis of D decays into the CP-even and CP-odd final states. This study is also sensitive to a *linear* function of y via

$$\frac{\tau(D\to K^-\pi^+)}{\tau(D\to K^+K^-)} - 1 = y\cos\phi - x\sin\phi\left[\frac{R_m^2-1}{2}\right]. \quad (4)$$

Time-integrated studies of the semileptonic transitions are sensitive to the *quadratic* form $x^2 + y^2$ and at the moment are not competitive with the analyses discussed above. The construction of a new tau-charm factory at Cornell will introduce other time-independent methods that are sensitive to a linear function of y [5].

The current experimental upper bounds on x and y are on the order of a few times 10^{-2}, and are expected to improve significantly in the coming years. To regard a future discovery of nonzero x or y as a signal for new physics, we would need high confidence that the Standard Model predictions lie well below the present limits. As was recently shown [6], in the Standard Model x and y are generated only at second order in $SU(3)$ breaking,

$$x\,,\, y \sim \sin^2\theta_C \times [SU(3)\text{ breaking}]^2\,, \quad (5)$$

where θ_C is the Cabibbo angle. Therefore, predicting the Standard Model values of x and y depends crucially on estimating the size of $SU(3)$ breaking. Although y is expected to be determined by Standard Model processes, its value nevertheless affects significantly the sensitivity to new physics of experimental analyses of D mixing [4].

2 Theoretical Expectations

Theoretical predictions of x and y within and beyond the Standard Model span several orders of magnitude (see Ref. [7]). Roughly, there are two approaches, neither of which

give very reliable results because m_c is in some sense intermediate between heavy and light. The "inclusive" approach is based on the operator product expansion (OPE). In the $m_c \gg \Lambda$ limit, where Λ is a scale characteristic of the strong interactions, ΔM and $\Delta\Gamma$ can be expanded in terms of matrix elements of local operators [8]. Such calculations yield $x, y < 10^{-3}$. The use of the OPE relies on local quark-hadron duality, and on Λ/m_c being small enough to allow a truncation of the series after the first few terms. The charm mass may not be large enough for these to be good approximations, especially for nonleptonic D decays. An observation of y of order 10^{-2} could be ascribed to a breakdown of the OPE or of duality, but such a large value of y is certainly not a generic prediction of OPE analyses. The "exclusive" approach sums over intermediate hadronic states, which may be modeled or fit to experimental data [9]. Since there are cancellations between states within a given $SU(3)$ multiplet, one needs to know the contribution of each state with high precision. However, the D is not light enough that its decays are dominated by a few final states. In the absence of sufficiently precise data on many decay rates and on strong phases, one is forced to use some assumptions. While most studies find $x, y < 10^{-3}$, Refs. [9] obtain x and y at the 10^{-2} level by arguing that $SU(3)$ violation is of order unity, but the source of the large $SU(3)$ breaking is not made explicit.

In what follows we first prove that $D^0 - \overline{D}^0$ mixing arises only at *second* order in $SU(3)$ breaking effects. The proof is valid when $SU(3)$ violation enters perturbatively. This would not be so, for example, if D transitions were dominated by a single narrow resonance close to threshold [6, 10]. Then we argue that reorganization of "exclusive" calculation by explicitly building $SU(3)$ cancellations into the analysis naturally leads to values of $y \sim 1\%$ if only one source of $SU(3)$ breaking (phase space) is taken into account.

The quantities M_{12} and Γ_{12} which determine x and y depend on matrix elements $\langle \overline{D}^0 | \, \mathcal{H}_w \mathcal{H}_w \, | D^0 \rangle$, where $\mathcal{H}_w$ denote the $\Delta C = -1$ part of the weak Hamiltonian. Let D be the field operator that creates a D^0 meson and annihilates a $\overline{D}^0$. Then the matrix element, whose $SU(3)$ flavor group theory properties we will study, may be written as

$$\langle 0 | \, D \, \mathcal{H}_w \mathcal{H}_w \, D \, | 0 \rangle \, . \tag{6}$$

Since the operator D is of the form $\bar{c}u$, it transforms in the fundamental representation of $SU(3)$, which we will represent with a lower index, D_i. We use a convention in which the correspondence between matrix indices and quark flavors is $(1, 2, 3) = (u, d, s)$. The only nonzero element of D_i is $D_1 = 1$. The $\Delta C = -1$ part of the weak Hamiltonian has the flavor structure $(\overline{q}_i c)(\overline{q}_j q_k)$, so its matrix representation is written with a fundamental index and two antifundamentals, H_k^{ij}. This operator is a sum of irreps contained in the product $3 \times \overline{3} \times \overline{3} = \overline{15} + 6 + \overline{3} + \overline{3}$. In the limit in which the third generation is neglected, H_k^{ij} is traceless, so only the $\overline{15}$ and 6 representations

appear. That is, the $\Delta C = -1$ part of $\mathcal{H}_w$ may be decomposed as $\frac{1}{2}(\mathcal{O}_{\overline{15}} + \mathcal{O}_6)$, where

$$\begin{aligned}
\mathcal{O}_{\overline{15}} &= (\bar{s}c)(\bar{u}d) + (\bar{u}c)(\bar{s}d) + s_1(\bar{d}c)(\bar{u}d) + s_1(\bar{u}c)(\bar{d}d) \\
&\quad - s_1(\bar{s}c)(\bar{u}s) - s_1(\bar{u}c)(\bar{s}s) - s_1^2(\bar{d}c)(\bar{u}s) - s_1^2(\bar{u}c)(\bar{d}s)\,, \\
\mathcal{O}_6 &= (\bar{s}c)(\bar{u}d) - (\bar{u}c)(\bar{s}d) + s_1(\bar{d}c)(\bar{u}d) - s_1(\bar{u}c)(\bar{d}d) \\
&\quad - s_1(\bar{s}c)(\bar{u}s) + s_1(\bar{u}c)(\bar{s}s) - s_1^2(\bar{d}c)(\bar{u}s) + s_1^2(\bar{u}c)(\bar{d}s)\,,
\end{aligned} \tag{7}$$

and $s_1 = \sin\theta_C$. The matrix representations $H(\overline{15})^{ij}_k$ and $H(6)^{ij}_k$ have nonzero elements

$$\begin{aligned}
H(\overline{15})^{ij}_k: \quad & H_2^{13} = H_2^{31} = 1\,, && H_2^{12} = H_2^{21} = s_1\,, \\
& H_3^{13} = H_3^{31} = -s_1\,, && H_3^{12} = H_3^{21} = -s_1^2\,, \\
H(6)^{ij}_k: \quad & H_2^{13} = -H_2^{31} = 1\,, && H_2^{12} = -H_2^{21} = s_1\,, \\
& H_3^{13} = -H_3^{31} = -s_1\,, && H_3^{12} = -H_3^{21} = -s_1^2\,.
\end{aligned} \tag{8}$$

We introduce $SU(3)$ breaking through the quark mass operator $\mathcal{M}$, whose matrix representation is $M^i_j = \mathrm{diag}(m_u, m_d, m_s)$ as being in the adjoint representation to induce $SU(3)$ violating effects. We set $m_u = m_d = 0$ and let $m_s \neq 0$ be the only $SU(3)$ violating parameter. All nonzero matrix elements built out of D_i, H^{ij}_k and M^i_j must be $SU(3)$ singlets.

We now prove that $D^0 - \overline{D}^0$ mixing arises only at second order in $SU(3)$ violation, by which we mean second order in m_s. First, we note that the pair of D operators is symmetric, and so the product D_iD_j transforms as a 6 under $SU(3)$. Second, the pair of $\mathcal{H}_w$'s is also symmetric, and the product $H^{ij}_k H^{lm}_n$ is in one of the reps which appears in the product

$$\begin{aligned}
\left[(\overline{15} + 6) \times (\overline{15} + 6)\right]_S &= (\overline{15} \times \overline{15})_S + (\overline{15} \times 6) + (6 \times 6)_S \\
&= (\overline{60} + \overline{24} + 15 + 15' + \overline{6}) + (42 + 24 + 15 + \overline{6} + 3) + (15' + \overline{6})\,.
\end{aligned} \tag{9}$$

A direct computation shows that only three of these representations actually appear in the decomposition of $\mathcal{H}_w\mathcal{H}_w$. They are the $\overline{60}$, the 42, and the $15'$ (actually twice, but with the same nonzero elements both times). So we have product operators of the form (the subscript denotes the representation of $SU(3)$)

$$DD = \mathcal{D}_6\,, \qquad \mathcal{H}_w\mathcal{H}_w = \mathcal{O}_{\overline{60}} + \mathcal{O}_{42} + \mathcal{O}_{15'}\,. \tag{10}$$

Since there is no $\overline{6}$ in the decomposition of $\mathcal{H}_w\mathcal{H}_w$, there is no $SU(3)$ singlet which can be made with $\mathcal{D}_6$, and no $SU(3)$ invariant matrix element of the form (6) can be formed. This is the well known result that $D^0 - \overline{D}^0$ mixing is *prohibited by $SU(3)$ symmetry*. Now consider a single insertion of the $SU(3)$ violating spurion $\mathcal{M}$. The combination $\mathcal{D}_6\mathcal{M}$ transforms as $6 \times 8 = 24 + \overline{15} + 6 + \overline{3}$. There is still no invariant to be made with $\mathcal{H}_w\mathcal{H}_w$, thus $D^0 - \overline{D}^0$ mixing is *not induced at first order in $SU(3)$*

breaking. With two insertions of $\mathcal{M}$, it becomes possible to make an $SU(3)$ invariant. The decomposition of $\mathcal{D}\mathcal{M}\mathcal{M}$ is

$$6 \times (8 \times 8)_S = 6 \times (27 + 8 + 1) = (60 + \overline{42} + 24 + \overline{15} + \overline{15}' + 6) + (24 + \overline{15} + 6 + \overline{3}) + 6 \,. \quad (11)$$

There are three elements of the 6×27 part which can give invariants with $\mathcal{H}_w \mathcal{H}_w$. Each invariant yields a contribution to $D^0 - \overline{D}^0$ mixing proportional to $s_1^2 m_s^2$. Thus, $D^0 - \overline{D}^0$ mixing arises only at *second order* in the $SU(3)$ violating parameter m_s.

We now turn to the contributions to y from on-shell final states, which result from every common decay product of D^0 and $\overline{D}^0$. In the $SU(3)$ limit, these contributions cancel when one sums over complete $SU(3)$ multiplets in the final state. The cancellations depend on $SU(3)$ symmetry both in the decay matrix elements and in the final state phase space. While there are $SU(3)$ violating corrections to both of these, it is difficult to compute the $SU(3)$ violation in the matrix elements in a model independent manner. Yet, with some mild assumptions about the momentum dependence of the matrix elements, the $SU(3)$ violation in the phase space depends only on the final particle masses and can be computed. We estimate the contributions to y solely from $SU(3)$ violation in the phase space. We find that this source of $SU(3)$ violation can generate y of the order of a few percent.

The mixing parameter y may be written in terms of the matrix elements for common final states for D^0 and $\overline{D}^0$ decays,

$$y = \frac{1}{\Gamma} \sum_n \int [\mathrm{P.S.}]_n \, \langle \overline{D}^0 | \, \mathcal{H}_w \, |n\rangle \langle n| \, \mathcal{H}_w \, |D^0\rangle \,, \quad (12)$$

where the sum is over distinct final states n and the integral is over the phase space for state n. Let us now perform the phase space integrals and restrict the sum to final states F which transform within a single $SU(3)$ multiplet R. The result is a contribution to y of the form

$$\frac{1}{\Gamma} \langle \overline{D}^0 | \, \mathcal{H}_w \Big\{ \eta_{CP}(F_R) \sum_{n \in F_R} |n\rangle \rho_n \langle n| \Big\} \mathcal{H}_w \, |D^0\rangle \,, \quad (13)$$

where ρ_n is the phase space available to the state n, $\eta_{CP} = \pm 1$ [6]. In the $SU(3)$ limit, all the ρ_n are the same for $n \in F_R$, and the quantity in braces above is an $SU(3)$ singlet. Since the ρ_n depend only on the known masses of the particles in the state n, incorporating the true values of ρ_n in the sum is a calculable source of $SU(3)$ breaking.

This method does not lead directly to a calculable contribution to y, because the matrix elements $\langle n|\mathcal{H}_w|D^0\rangle$ and $\langle \overline{D}^0|\mathcal{H}_w|n\rangle$ are not known. However, CP symmetry, which in the Standard Model and almost all scenarios of new physics is to an excellent approximation conserved in D decays, relates $\langle \overline{D}^0|\mathcal{H}_w|n\rangle$ to $\langle D^0|\mathcal{H}_w|\overline{n}\rangle$. Since $|n\rangle$

and $|\overline{n}\rangle$ are in a common $SU(3)$ multiplet, they are determined by a single effective Hamiltonian. Hence the ratio

$$y_{F,R} = \frac{\sum_{n\in F_R}\langle \overline{D}^0|\,\mathcal{H}_w|n\rangle\rho_n\langle n|\mathcal{H}_w\,|D^0\rangle}{\sum_{n\in F_R}\langle D^0|\,\mathcal{H}_w|n\rangle\rho_n\langle n|\mathcal{H}_w\,|D^0\rangle} = \frac{\sum_{n\in F_R}\langle \overline{D}^0|\,\mathcal{H}_w|n\rangle\rho_n\langle n|\mathcal{H}_w\,|D^0\rangle}{\sum_{n\in F_R}\Gamma(D^0\to n)} \qquad (14)$$

is calculable, and represents the value which y would take if elements of F_R were the only channel open for D^0 decay. To get a true contribution to y, one must scale $y_{F,R}$ to the total branching ratio to all the states in F_R. This is not trivial, since a given physical final state typically decomposes into a sum over more than one multiplet F_R. The numerator of $y_{F,R}$ is of order s_1^2 while the denominator is of order 1, so with large $SU(3)$ breaking in the phase space the natural size of $y_{F,R}$ is 5%. Indeed, there are other $SU(3)$ violating effects, such as in matrix elements and final state interaction phases. Here we assume that there is no cancellation with other sources of $SU(3)$ breaking, or between the various multiplets which occur in D decay, that would reduce our result for y by an order of magnitude. This is equivalent to assuming that the D meson is not heavy enough for duality to enforce such cancellations. Performing the computations of $y_{F,R}$ [6], we see that effects at the level of a few percent are quite generic. Our results are summarized in Table 1. Then, y can be formally constructed from the individual $y_{F,R}$ by weighting them by their D^0 branching ratios,

$$y = \frac{1}{\Gamma}\sum_{F,R} y_{F,R}\Big[\sum_{n\in F_R}\Gamma(D^0\to n)\Big]\,. \qquad (15)$$

However, the data on D decays are neither abundant nor precise enough to disentangle the decays to the various $SU(3)$ multiplets, especially for the three- and four-body final states. Nor have we computed $y_{F,R}$ for all or even most of the available representations. Instead, we can only estimate individual contributions to y by assuming that the representations for which we know $y_{F,R}$ to be typical for final states with a given multiplicity, and then to scale to the total branching ratio to those final states. The total branching ratios of D^0 to two-, three- and four-body final states can be extracted from Ref. [11]. Rounding to the nearest 5% to emphasize the uncertainties in these numbers, we conclude that the branching fractions for PP, $(VV)_{s\text{-wave}}$, $(VV)_{d\text{-wave}}$ and $3P$ approximately amount to 5%, while the branching ratios for PV and $4P$ are of the order of 10% [6].

We observe that there are terms in Eq. (15), like nonresonant $4P$, which could make contributions to y at the level of a percent or larger. There, the rest masses of the final state particles take up most of the available energy, so phase space differences are very important. One can see that y on the order of a few percent is completely natural, and that anything an order of magnitude smaller would require significant cancellations which do not appear naturally in this framework. Cancellations would be expected only if they were enforced by the OPE, or if the charm quark were heavy

Final state representation		$y_{F,R}/s_1^2$	$y_{F,R}$ (%)
PP	8	-0.0038	-0.018
	27	-0.00071	-0.0034
PV	8_A	0.032	0.15
	8_S	0.031	0.15
	10	0.020	0.10
	$\overline{10}$	0.016	0.08
	27	0.04	0.19
$(VV)_{s\text{-wave}}$	8	-0.081	-0.39
	27	-0.061	-0.30
$(VV)_{p\text{-wave}}$	8	-0.10	-0.48
	27	-0.14	-0.70
$(VV)_{d\text{-wave}}$	8	0.51	2.5
	27	0.57	2.8
$(3P)_{s\text{-wave}}$	8	-0.48	-2.3
	27	-0.11	-0.54
$(3P)_{p\text{-wave}}$	8	-1.13	-5.5
	27	-0.07	-0.36
$(3P)_{\text{form-factor}}$	8	-0.44	-2.1
	27	-0.13	-0.64
$4P$	8	3.3	16
	27	2.2	11
	$27'$	1.9	9.2

Table 1: Values of $y_{F,R}$ for some two-, three-, and four-body final states.

enough that the "inclusive" approach were applicable. The hypothesis underlying the present analysis is that this is not the case.

3 Conclusions

We proved that if $SU(3)$ violation may be treated perturbatively, then $D^0 - \overline{D}^0$ mixing in the Standard Model is generated only at second order in $SU(3)$ breaking effects. Within the exclusive approach, we identified an $SU(3)$ breaking effect, $SU(3)$ violation in final state phase space, which can be calculated with minimal model dependence. We found that phase space effects alone provide enough $SU(3)$ violation to induce $y \sim 10^{-2}$. Large effects in y appear for decays close to D threshold, where an analytic expansion in $SU(3)$ violation is no longer possible.

Indeed, some degree of cancellation is possible between different multiplets, as would be expected in the $m_c \to \infty$ limit, or between $SU(3)$ breaking in phase space and in matrix elements. It is not known how effective these cancellations are, and the most reasonable assumption in light of our analysis is that they are not significant enough to result in an order of magnitude suppression of y, as they are not enforced by any symmetry arguments. Therefore, any future discovery of a D meson width difference should not by itself be interpreted as an indication of the breakdown of the Standard Model.

It is my pleasure to thank S. Bergmann, E. Golowich, Y. Grossman, A. Falk, Z. Ligeti, and Y. Nir for collaboration on this and related projects.

References

[1] A. Datta, D. Kumbhakar, Z. Phys. C**27**, 515 (1985); A. Petrov, Phys. Rev. D**56**, 1685 (1997).

[2] A. F. Falk, Y. Nir and A. A. Petrov, JHEP **9912**, 019 (1999).

[3] M. Gronau, Y. Grossman and J. L. Rosner, Phys. Lett. B **508**, 37 (2001); J. P. Silva and A. Soffer, Phys. Rev. D **61**, 112001 (2000). E. Golowich and S. Pakvasa, Phys. Lett. B **505**, 94 (2001).

[4] S. Bergmann, Y. Grossman, Z. Ligeti, Y. Nir, A. Petrov, Phys. Lett. B **486**, 418 (2000).

[5] D. Atwood and A. A. Petrov, arXiv:hep-ph/0207165.

[6] A. F. Falk, Y. Grossman, Z. Ligeti and A. A. Petrov, Phys. Rev. D **65**, 054034 (2002).

[7] H. N. Nelson, in *Proc. of the 19th Intl. Symp. on Photon and Lepton Interactions at High Energy LP99* ed. J.A. Jaros and M.E. Peskin, arXiv:hep-ex/9908021.

[8] H. Georgi, Phys. Lett. B297, 353 (1992); T. Ohl, G. Ricciardi and E. Simmons, Nucl. Phys. B403, 605 (1993); I. Bigi and N. Uraltsev, Nucl. Phys. B **592**, 92 (2001), for a recent review see A. A. Petrov, *Proc. of 4th Workshop on Continuous Advances in QCD*, Minneapolis, Minnesota, 12-14 May 2000, arXiv:hep-ph/0009160.

[9] J. Donoghue, E. Golowich, B. Holstein and J. Trampetic, Phys. Rev. D33, 179 (1986); L. Wolfenstein, Phys. Lett. B164, 170 (1985); P. Colangelo, G. Nardulli and N. Paver, Phys. Lett. B242, 71 (1990); T.A. Kaeding, Phys. Lett. B357, 151 (1995).

[10] E. Golowich and A. A. Petrov, Phys. Lett. B **427**, 172 (1998).

[11] D. E. Groom *et al.* [Particle Data Group Collaboration], Eur. Phys. J. C **15**, 1 (2000).

Program

Program for FPCP 2002

Wednesday Evening May 15th

Reception for Registration

6:00-8:00 Bodek Lounge, Houston Hall, Penn Campus (Light Refreshments)

Thursday Morning May 16th
Logan Hall Room 17 (center of campus)

8:00-8:25 Pastries, coffee, and tea
8:30-8:40 Welcome – N. Lockyer (Penn)
8:40-8:45 Conference Proceedings – R. Oldeman (Penn)
8:45-8:55 Introduction – A. I. Sanda (Nagoya) and K. Schubert (Dresden)

Present status of CKM parameters [35 min]

Session Chair: S. Smith (Princeton)

9:00-9:25 An experimentalist's review of the CKM parameters – A. Hoecker (LAL-Orsay) [25 min]

Indirect CP violation [160 min]

9:35-9:55 $\sin 2\beta$ from BABAR – S. Rahatlou (UCSD) [20 min]

10:00-10:25 *Break (beverages provided)*

10:30-10:50 $\sin 2\phi_1$ from BELLE – M. Hazumi (KEK) [20 min]

10:55-11:10 Theory: New physics in $B \to J/\Psi K^*$ – R. Sinha (Madras) [15 min]
11:15-11:30 Theory: New physics in $B \to J/\Psi K^*$ – T. Mannel (Karlsruhe) [15 min]

11:35-1:50 *Break for Lunch (not provided)*

Thursday Afternoon May 16th
Logan Hall Room 17

Session Chair: A. I. Sanda (Nagoya)

2:00-2:20 $\sin 2\phi_2$ from BELLE – E. Won (Seoul) [20 min]
2:25-2:45 $\sin 2\alpha$ from BABAR – P. Dauncey (Imperial College) [20 min]
2:50-3:05 Theory: Penguin pollution in $B \to \pi\pi$ – N. Sinha (Madras) [15 min]

Recent results in theories of hadronic B decay [80 min]

Recent results from the theories of hadronic B decays:

3:10-3:25 QCD factorization – M. Beneke (Aachen) [15 min]
3:30-3:45 Charming penguins – M. Ciuchini (Rome) [15 min]

3:50-4:10 *Break (beverages provided)*

Session Chair: G. Bonneaud (Paris)

4:15-4:30 PQCD – H. N. Li (National Taiwan University) [15 min]
4:35-4:50 Soft-collinear effective theory (SCET) – I. Stewart (Washington) [15 min]

Experimental Results from the Tevatron and LEP [75 min]

4:55-5:15 Status of CDF – R. Hughes (Ohio State) [20 min]
5:20-5:40 Status of D0 – R. Van Kooten (Indiana) [20 min]
5:45-6:05 New results on B_s mixing from LEP – S. Armstrong (CERN) [20 min]

Evening Entertainment in Amado Recital Hall Irvine Auditorium

8:00-8:30 Reception (beverages provided)
8:30-10:00 Musical Trio: Time 4 Three (Curtis Institute)

Friday Morning May 17th
Logan Hall Room 17

8:00-8:25 Pastries, coffee, and tea

Session Chair: V. Luth (SLAC)

8:30-8:55 Cosmology – A. Kusenko (UCLA/BNL) [25 min]

Branching Ratios and Direct CP Violation [60 min]

9:00-9:25 Review of BR and DCPV results for Quasi 2-body – A. Bondar (BINP) [25 min])
9:30-9:55 Review of rare two-body B decays (e.g., $K\pi$) – R. Bartoldus (Iowa) [25 min]

Theory: New ideas about CP in B decays and CKM determination [40 min]

10:00-10:15 New methods for getting at α and γ – D. Atwood (Iowa State) [15 min]
10:20-10:35 New method for measuring α using $B \to K^*\overline{K}^*$ D. London (Montreal) [15 min]

10:40-11:10 *Break (beverages provided)*

Recent Hot Results from B Factories [80 min]

Session Chair: K. Schubert (Dresden)

11:15-11:30 BABAR New results on rare charmless decays: $B\to\eta'(K, K^*)$ and $B\to h^+h^-h^+$ – V. Shelkov (LBNL) [15 min]
11:35-11:50 BABAR New results on rare leptonic B decays – V. Halyo (SLAC) [15 min]
11:55-12:10 BELLE $B\to Khh$ – A. Garmash (KEK) [15 min]
12:15-12:30 BELLE $B\to\omega K$ $B\to\eta' K$ – K. F. Chen (NTU) [15 min]

12:30-1:50 *Break for Lunch (not provided)*

Friday Afternoon May 17th
Logan Hall Room 17

Charm Physics I [110 min]

Session Chair: J. Appel (FNAL)

2:00-2:25 Theory: Review of charm physics – G. Burdman (LBNL) [25 min]

2:30-2:45 Charm Lifetimes and $D^0\overline{D^0}$ Mixing – P. Pakhlov (ITEP) [15 min]
2:50-3:05 Spectroscopy from Heavy Flavor Decay – I. Bediaga (Brazil) [15 min]
3:10-3:25 Charm Baryons – J. Yelton (Florida) [15 min]
3:30-3:45 New Results on Rare Charm Decays – W. Johns (Vanderbilt) [15 min]

3:50-4:25 *Break (beverages provided)*

Future Experiments in Heavy Flavor Physics [80 min]

Session Chair: M. Artuso (Syracuse)

4:30-4:45 CLEO-c – I. Shipsey (Purdue) [15 min]
4:50-5:05 LHCb – G. Carboni (Rome 2) [15 min]
5:10-5:25 BTeV – J. C. Wang (Syracuse) [15 min]
5:30-5:45 Super B Factory – D. Hitlin (Caltech) [15 min]

Banquet at University Museum

6:00-7:00 Reception
7:00-10:30 Banquet (After dinner speaker: Anthropologist Professor Alan Mann)

Saturday Morning May 18th
Logan Hall Room 17

8:00-8:25 Pastries, coffee and tea

Neutrino and Kaon Physics [70 min]

Session Chair: K. Abe (KEK)

8:30-9:00 CP violation in the neutrino sector – B. Kayser (Fermilab)[30 min]
9:05-9:35 Kaon Physics – D. Bryman (British Columbia) [30 min]

9:40-10:20 *Break (beverages provided)*

Theoretical Developments in V_{cb} and V_{ub} [50 min]

Session Chair: S. Olsen (Hawaii)

10:25-10:40 $\mathcal{F}(1)$ from lattice QCD – A. Kronfeld (Fermilab) [15 min])
10:45-11:10 Theory for V_{ub} determination – M. Luke (Toronto) [25 min]

B Decays [80 min]

11:15-11:35 Open Charm decays ($B \to D\overline{D}, D^*D$ etc.) mini summary – Y. Kolomensky (Berkeley/LBNL) [20 min]
11:40-12:00 $B\to$ Charmonium mini summary – F. Fang (Hawaii) [20 min]
12:05-12:30 V_{ub}, V_{cb} from semileptonic decays mini summary – K. Ecklund (Cornell) [25 min]

12:30-1:50 *Break for Lunch (not provided)*

Saturday Afternoon May 18th
Logan Hall Room 17

Radiative B Decays [85 min]

Session Chair: G. W. S. Hou (NTU)

2:00-2:20 $b \to s\gamma$ and $b \to d\gamma$ mini review – E. Thorndike (Rochester) [20 min]
2:25-2:40 $B \to Kl^+l^-$ from BELLE – K. Senyo (Nagoya) [15 min]
2:45-3:00 $B \to Kl^+l^-$ from BABAR – J Walsh (Pisa) [15 min]
3:05-3:20 Theory: New Physics with $b \to s\gamma$ decays – D. Pirjol (UCSD) [15 min]

3:25-4:00 *Break (beverages provided)*

Charm Physics II [60 min]

Session Chair: H. Jawahery (Maryland)

4:00-4:15 Review of CP in D Decays – M. Selen (Illinois) [15 min]
4:20-4:35 Semileptonic Charm Decays– J. Wiss (Illinois) [15 min]
4:40-4:55 Theory: D^0-$\overline{D^0}$ mixing – A. Petrov (Wayne State) [15 min]

Conference Summary and Adieu [55 min]

5:00-5:40 Conference Summary – R. Patterson (Cornell) [40 min]
5:45-5:55 FPCP 2003 in Paris – G. Bonneaud (Paris) [10 min]

End of Conference

Sunday May 19th

10:30-3:30 Barnes Foundation (Timed tickets provided to those that have registered)

Participants

FPCP Participants

Kazuo Abe	KEK
Hiroaki Aihara	University of Tokyo
Jeffrey Appel	Fermilab
Stephen Armstrong	CERN
Marina Artuso	Syracuse University
David Atwood	Iowa State University
Rainer Bartoldus	University of Iowa
Ignacio Bediaga	Centro Brasileiro de Pesquisas Fisicas
Martin Beneke	RWTH Aachen
Steven Blusk	Syracuse University
Alexander Bondar	Budker Institute of Nuclear Physics
Gerard Bonneaud	Ecole Polytechnique Paris France
Chaouki Boulahouache	Syracuse University
Tom Browder	University of Hawaii
Douglas Bryman	University of British Columbia
Gustavo Burdman	Lawrence Berkeley National Laboratory
Karen Byrum	Argonne National Lab
Giovanni Carboni	Università di Roma "Tor Vergata" and CERN
Alessandro Cerri	Lawrence Berkeley National Laboratory
Lali Chatterjee	Institute of Physics Publishing
Chuan Hung Chen	Institute of Physics, Academia Sinica, Taipei
Chunhui Chen	University of Pennsylvania
Kai-Feng Chen	National Taiwan University
Hai-Yang Cheng	Academia Sinica
Marco Ciuchini	INFN - Sezione di Roma III
Erdenebayar Dambasuren	Syracuse University
Paul Dauncey	Imperial College, London, UK
Dongsheng Du	Inst. of High Energy Phys., Chinese Academy of Sciences
Karl Ecklund	Cornell University
Gerald Eigen	University of Bergen
Sandrine Emery	CEA-Saclay DAPNIA/SPP (FRANCE)
Harold Evans	Columbia University
Fang Fang	University of Hawaii
Alexei Garmach	High Energy Accelerator Research Organization (KEK)
Larry Gladney	University of Pennsylvania
Qinghua Guo	University of Pennsylvania
Junji Haba	KEK
Kristian Hahn	Penn
Valerie Halyo	SLAC
Masashi Hazumi	KEK
Joel Heinrich	University of Pennsylvania
David Hitlin	Caltech

Andreas Höcker	Laboratoire de l'Accèlérateur Linéaire (LAL) - Orsay
George W.S. Hou	National Taiwan University
Minxin Huang	University of Pennsylvania
Richard Hughes	Ohio State University
Toru Iijima	Nagoya University
Hassan Jawahery	University of Maryland
Will Johns	Vanderbilt University
Matthew Jones	University of Pennsylvania
Junhai Kang	University of Pennsylvania
Paul Karchin	Wayne State University
Boris Kayser	Fermilab
Paul Keener	University of Pennsylvania
Alexander Khodjamirian	University of Karlsruhe, Germany
Yury Kolomensky	LBNL/UC Berkeley
Walter Kononenko	University of Pennsylvania
Joseph Kroll	University of Pennsylvania
Andreas Kronfeld	Fermilab
Takeshi Kurimoto	Toyama University
Alexander Kusenko	UCLA
Christopher Kyba	University of Pennsylvania
Paul Langacker	University of Pennsylvania
Jens-Soeren Lange	Frankfurt University
David Lange	Lawrence Livermore National Laboratory
Urs Langenegger	Stanford Linear Accelerator Center
Hsiang-nan Li	Academia Sinica
Tao Liu	University of Pennsylvania
Nigel Lockyer	University of Pennsylvania
David London	Universite de Montreal
Cai-Dian Lu	Institute of High Energy Physics, Beijing
Michael Luke	University of Toronto
Vera Luth	SLAC
Thomas Mannel	University of Karlsruhe
Takuya Morozumi	Hiroshima University
Isamu Nakamura	University of Pennsylvania
Raja Nandakumar	Syracuse University
Rolf Oldeman	University of Pennsylvania
Stephen L. Olsen	University of Hawaii
Pavel Pakhlov	ITEP
Ioannis Papadimitriou	University of Pennsylvania
Ritchie Patterson	Cornell University
Manfred Paulini	Carnegie Mellon University
Alexey Petrov	Wayne State University
Jonatan Piedra	Instituto de Fisica de Cantabria
Dan Pirjol	University of California at San Diego
Kevin Pitts	University of Illinois

Soeren Prell	Universiy of California at San Diego
Shahram Rahatlou	UC San Diego
Michael Roney	University of Victoria
Yoshihide Sakai	KEK, IPNS
A. I. Sanda	Nagoya University
Klaus R. Schubert	Technicsche Universitat Dresden
Marie-Helene Schune	LAL-Orsay
Gino Segre	University of Pennsylvania
Lalit Sehgal	Inst.of Theor.Physics, RWTH Aachen
Mats Selen	University of Illinois at Urbana-Champaign
Walter Selove	University of Pennsylvania
Katsumi Senyo	Faculty of Science, Nagoya University
Marjorie Shapiro	Lawrence Berkeley National Lab
Vivek Sharma	UC San Diego
Vasilii Shelkov	Lawrence Berkeley National Laboratory
Ian Shipsey	Purdue University
Dennis Silverman	Univ. of California, Irvine
Nita Sinha	Institute of Mathematical Sciences, India
Rahul Sinha	Institute of Mathematical Sciences, India
Stewart Smith	Princeton University
Iain Stewart	University of Washington
Sheldon Stone	Syracuse University
Hong Sungho	University of Pennsylvania
Edward H. Thorndike	University of Rochester
Toru Tsuboyama	KEK, High Energy Accelerator Research Organization
Fumihiko Ukegawa	University of Tsukuba, Japan
Joerg Urban	Technical University Munich, Institut fuer Theoretische Physik
Yutaka Ushiroda	KEK
Denys Usynin	University of Pennsylvania
Rick Van Kooten	Indiana University
Ivan Vila	Instituto de Fisica de Cantabria
John Walsh	INFN - Sezione di Pisa
Jianchun Wang	Syracuse University
Brig Williams	University of Pennsylvania
Peter Wilson	Fermilab
Jim Wiss	University of Illinois (Urbana)
Peter Wittich	University of Pennsylvania
Eunil Won	Seoul National University
Douglas Wright	LLNL
Masanori Yamauchi	KEK
Kwei-Chou Yang	Department of Physics, Chung Yuan Christian University
Shimizu Yasuhiro	Nagoya University
John Yelton	University of Florida
Shin-Shan Yu	University of Pennsylvania